INOWAS Book Series

DISSERTATION

Miguel Alonzo Moreno Gómez

Development of an Integrated Methodology
to Estimate Groundwater Vulnerability to
Pollution in Karst Areas

Beiträge zu Abfallwirtschaft / Altlasten – Volume 112

Development of an Integrated Methodology to Estimate Groundwater Vulnerability to Pollution in Karst Areas

Dissertation

Development of an Integrated Methodology to Estimate Groundwater Vulnerability to Pollution in Karst Areas

Miguel Alonzo Moreno Gómez

Editor

Prof. Dr.-Ing. habil. Christina Dornack

Development of an Integrated Methodology to Estimate Groundwater Vulnerability to Pollution in Karst Areas

DISSERTATION

for the award of the degree of

Doctor Ingenieur

(Dr. -Ing)

submitted to

the Faculty of Environmental Sciences

of the Technische Universität Dresden

by

M.Sc. Miguel Alonzo Moreno Gómez

Born on the 14th of May, 1978 in Progreso, Yucatan, Mexico

Statement of authorship – Individual thesis

I hereby declare that I have written this final thesis independently and have listed all used sources and aids. I am submitting this thesis for the first time as a piece of assessed academic work. I understand that attempted deceit will result in the failing grade "not sufficient" (5.0).
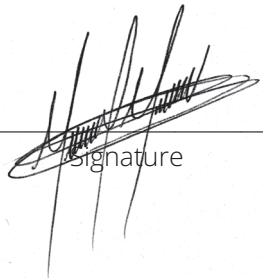
Last name: Moreno Gómez
Name: Miguel Alonzo
Student number: 3926046

_____05.08.2020_____
Date

_____
Signature

Abstract

Groundwater is a very important resource since water volumes stored underground are much larger compared with those located at the surface, such as rivers and lakes. Aquifers supply a high percentage of freshwater for human consumption as well as supplying economic activities like industry, agriculture, and livestock production. Among them, karst aquifers stand out due to their special hydrologic characteristics and behaviour.

In karst aquifers, infiltration occurs faster in comparison with unconsolidated aquifers, due to high permeability features at the surface like dolines, karren, epikarst, and swallow holes that allow precipitating water to recharge the aquifer at higher rates. Nevertheless, these characteristics also increase the aquifer's susceptibility to being affected by pollution generated by anthropogenic practices.

With a low natural pollutant degradation capacity, karst systems mostly experience problems related with water quality rather than water quantity. At present, this represents a significant challenge because a high percentage of the world population is settled on karst areas and is solely dependent upon karst aquifers to fulfil their necessary water supply.

A good example to represent this case is the Yucatan Peninsula. The Peninsula is a transboundary limestone platform, covering parts of Mexico, Belize, and Guatemala, whose characteristics do not allow surface streams to generate. Therefore, the karstic aquifer provides water for nearly 4.5 million inhabitants within Mexican territory; this estimation excludes water volumes used for economic activities. The anthropogenic impacts over this karst aquifer have generated problems for water intended for human consumption, furthered by weak environmental regulations that allow the disposal of wastewater without adequate treatment. In the Mexican state of Yucatan, roughly 10% of the population has access to public sewer services where wastewater is treated. Additionally, the use of fertilizers and pesticides is not regulated in agricultural areas, while pig farming is an increasing activity, which fails to keep the necessary standards for the proper disposal of pig slurry.

Similar situations can be found around the world, thus the development of plans and strategies to preserve karst groundwater quality that aim to find a balance between resource protection and regional development is increasingly necessary. One important tool emerged to support decisions regarding groundwater protection: the groundwater vulnerability concept. However, due to the hydrologic differences among detritus and karst aquifers, the vulnerability concept, which was first promoted for the former aquifer type, necessitated the development of a specialized vulnerability method to consider the natural characteristics of karst landscapes.

Nevertheless, due to the high heterogeneity and anisotropy present in karst systems several methodologies to estimate karst groundwater vulnerability have arisen. Current methodologies are theoretical approximations to differentiate areas where an assumed pollutant particle, released at the surface, is more likely to reach the aquifer due to the natural characteristics of the area. These methods have shown themselves to be useful in defining protection areas and in highlighting regions in which further studies can be performed. However, the high subjectivity and exclusion of anthropogenic influences as part of the analysis is a drawback for these methods.

In order to estimate karst groundwater vulnerability for current and future scenarios, an integrated approach is highly necessary. Since most of the methods focus solely on the travel time of a theoretical pollutant from the surface towards groundwater or to a spring, inclusion of pollutants residence time and concentration as parameters to estimate vulnerability is of the uttermost importance. To reach this goal, it is necessary to investigate current intrinsic-based methods in terms of their applicability and regional congruence in order to highlight advantages and probable misclassifications among them and to propose improvements.

Pollutant residence time and concentration can be estimated from modelling, which can highlight areas where pollution can represent a problem due to anthropogenic practices, such as wastewater disposal and water extraction fields influencing groundwater flow. Other problems to be contemplated are the data availability and the variable processes by which areas are classified as vulnerable or not. Evaluation of multiple criteria to define degrees of vulnerability is complicated, since several factors, such as subjectivity, data quality, scale, and regional conditions, will always be present.

This work presents the results from the application of eight karst groundwater vulnerability methods to the Yucatan karst and outcomes from solute transport. Important considerations are explained in order to improve the workflow for intrinsic groundwater vulnerability assessment. Possible parameters, to be included as part of vulnerability analysis, are evaluated by modelling, demonstrating the importance of anthropogenic impacts for current vulnerability scenarios. Results obtained in this research are displayed as the basis for an Integrated Karst Aquifer Vulnerability (IKAV) method proposed as an alternative for vulnerability studies.

Zusammenfassung

Grundwasser ist eine sehr wichtige Ressource, da die unterirdisch gespeicherten Wasservolumina viel größer sind als diejenigen an der Oberfläche, wie Flüsse und Seen. Aquifere liefern einen hohen Prozentsatz an Frischwasser für den menschlichen Verzehr und für wirtschaftliche Aktivitäten wie Industrie, Landwirtschaft und Viehzucht. Unter ihnen werden Karstgrundwasserleiter aufgrund ihrer besonderen hydrologischen Eigenschaften und ihres Verhaltens hervorgehoben.

Im Karst erfolgt die Infiltration im Vergleich zu nicht konsolidierten Grundwasserleitern durch hochpermeable Merkmale wie Dolinen, Karren, Epikarst und Schlucklöcher schneller, sodass Niederschlagswasser den Grundwasserleiter schneller wieder aufladen kann. Diese Eigenschaften erhöhen jedoch auch die Anfälligkeit des Grundwasserleiters für Verschmutzungen durch anthropogene Handlungen. Karstsysteme haben von Natur aus eine geringe Fähigkeit, um Schadstoffe abzubauen und daher meistens Probleme im Zusammenhang mit der Wasserqualität anstelle der Wassermenge. Dies ist zu einem großen Problem geworden, da ein hoher Prozentsatz der Weltbevölkerung in Karstgebieten angesiedelt und ausschließlich von Karstgrundwasserleitern abhängig ist, um ihren Bedarf an Wasserversorgung zu decken.

Ein gutes Beispiel für diesen Fall ist die Halbinsel Yucatan, die sich über Teile Mexikos, Guatemala und Belize erstreckt. Die Halbinsel ist eine Kalksteinplattform, deren natürliche Eigenschaften die Erzeugung von Oberflächenströmen nicht zulassen. Daher versorgt der Karstgrundwasserleiter auf mexikanischer Seite fast 4,5 Millionen Einwohner mit Wasser, ohne das für wirtschaftliche Aktivitäten verwendete Wasservolumen zu berücksichtigen.

Die anthropogenen Einflüsse auf diesen Karstgrundwasserleiter haben Probleme für den menschlichen Wasserverbrauch verursacht, da schwache Umweltvorschriften die Entsorgung von Abwasser ohne angemessene Behandlung ermöglichen. Nur etwa 10% der Bevölkerung haben Zugang zu öffentlichen Abwassersystemen, in denen Abwasser behandelt wird. Die Verwendung von Düngemitteln und Pestiziden ist in landwirtschaftlichen Gebieten nicht geregelt, während die Schweinehaltung zunimmt, wobei die erforderlichen Standards und eine ordnungsgemäße Entsorgung der Schweinegülle nicht eingehalten wird. Ähnliche Situationen gibt es auf der ganzen Welt, weshalb Pläne und Strategien zur Erhaltung der Karstgrundwasserqualität entwickelt werden müssen, um ein Gleichgewicht zwischen Ressourcenschutz und regionaler Entwicklung zu finden. Ein wichtiges Instrument zur Unterstützung von Entscheidungen zum Grundwasserschutz ist das Grundwasservulnerabilitätskonzept.

Aufgrund der hydrologischen Unterschiede zwischen Lockergesteins- und Karstgrundwasserleitern machte für das Vulnerabilitätskonzept, das ursprünglich für den Lockergesteinsgrundwasserleiter entwickelt wurde, die Entwicklung spezieller Methoden erforderlich, um die natürlichen Eigenschaften von Karst zu berücksichtigen. Das Ziel der gegenwärtigen Methoden sind theoretische Annäherungen zur Unterscheidung von Gebieten, in denen aufgrund der natürlichen Eigenschaften des Gebiets eine Verschmutzung wahrscheinlicher ist. Diese Methoden haben sich als nützlich erwiesen, um Schutzgebiete zu definieren und Regionen hervorzuheben, um weitere Studien durchzuführen. Die hohe Subjektivität und der Ausschluss anthropogener Einflüsse in der Analyse stellen jedoch einen Nachteil dieser Methoden dar.

Um die Vulnerabilität von Karstgrundwasser für aktuelle und zukünftige Szenarien abzuschätzen, ist ein integrierter Ansatz dringend erforderlich. Da sich die meisten Methoden ausschließlich auf die Laufzeit eines theoretischen Schadstoffs von der Oberfläche zum Grundwasser oder zu einer Quelle konzentrieren, ist die Berücksichtigung der Verweilzeit des Schadstoffs im Grundwasserleiter und der Schadstoffkonzentration von größter Bedeutung. Um dies zu integrieren, ist es notwendig, aktuelle Methoden hinsichtlich ihrer Anwendbarkeit und regionalen Kongruenz zu untersuchen und damit Vorteile und wahrscheinliche Fehlklassifizierungen unter ihnen hervorzuheben und Verbesserungen vorzuschlagen.

Die Verweilzeit des Schadstoffs im Grundwasserleiter und die Schadstoffkonzentration können anhand der Modellierung geschätzt werden. Dabei werden Bereiche hervorgehoben, in denen die Verschmutzung aufgrund anthropogener Handlungen, wie Abwasserentsorgung und Wassergewinnungsfelder die den Grundwasserfluss beeinflussen, ein Problem darstellen können. Weitere zu berücksichtigende Faktoren sind die Datenverfügbarkeit und der Prozess zur Klassifizierung der Vulnerabilität von Bereichen.

Die Bewertung mehrerer Kriterien zur Definition des Grads der Vulnerabilität ist kompliziert, da immer mehrere Faktoren wie Subjektivität, Datenqualität, Umfang und regionale Bedingungen vorliegen. Diese Arbeit stellt die Ergebnisse der Anwendung von acht Karstgrundwasser-Vulnerabilitätsmethoden vor, die für den Karst von Yucatan durchgeführt wurden, sowie die Ergebnisse des Transports gelöster Stoffe. Wichtige Überlegungen werden erläutert, um den Workflow für die Bewertung der Grundwasservulnerabilität zu verbessern. Als Alternative wird die Grundlage für eine neue theoretische integrierte Karst-Aquifer-Vulnerabilitätsmethode (IKAV) vorgeschlagen.

Resumen

Los acuíferos son un recurso muy importante ya que los volúmenes de agua almacenados en el subsuelo son inmensos en comparación con ríos y lagos. Los acuíferos abastecen agua para el consume humano y actividades económicas como la industria, agricultura y ganadería. Entre ellos, los acuíferos kársticos destacan debido a sus muy especiales características hidrológicas.

En áreas kársticas, la precipitación pluvial se infiltra rápidamente a través del subsuelo debido a la alta permeabilidad que presentan las dolinas, el karren (pavimento de caliza con surcos erosionados), el epikarst y los sumideros, los cuales permiten mayores tasas de recarga para el acuífero. Sin embargo, estas características incrementan la susceptibilidad de dichos acuíferos a ser afectados por contaminantes generados por múltiples prácticas antropogénicas ya que cuentan con una baja capacidad natural de atenuación. Los sistemas kársticos mayormente experimentan problemas relacionados con la calidad del agua. Esto representa un problema enorme, el cual debe ser afrontado ya que el número habitantes viviendo en áreas kársticas es considerable, dependiendo de dichos acuíferos para subsistir.

Como ejemplo de lo mencionado, tenemos el caso de la Península de Yucatán. La Península es una plataforma trasfronteriza de caliza cuyas características orográficas y kársticas no permiten la generación de corrientes de agua superficiales. Este acuífero kárstico es la fuente principal de abastecimiento para cerca de 4.5 millones de habitantes en el área correspondiente a México; esto, sin incluir los volúmenes destinados para actividades económicas. Los impactos antropogénicos en el acuífero han generado problemas para el consumo del agua ya que las leyes ambientales, no tan estrictas, permiten la descarga de aguas residuales sin tratamiento previo. Aproximadamente, solo un 10% de la población cuenta con servicios de drenaje donde las aguas residuales son dirigidas hacia plantas de tratamiento. El uso de fertilizantes y plaguicidas en la agricultura no está regulado mientras que la creciente industria porcina no cumple adecuadamente con el tratamiento necesario para sus desechos.

Situaciones similares ocurren globalmente, haciendo necesario el desarrollo de planes y estrategias para preservar la calidad del agua en acuíferos kársticos y encontrar un balance entre la protección del recurso y el desarrollo económico. Una herramienta importante de soporte en la toma de decisiones para el cuidado y preservación de los acuíferos es el concepto de vulnerabilidad. Sin embargo, debido a las diferencias hidrológicas entre acuíferos detríticos y kársticos, ya que el concepto de vulnerabilidad se desarrolló pensando en el primero, ha hecho necesaria la creación de metodologías especializadas considerando las características naturales del karst.

Siendo los sistemas kársticos altamente heterogéneos y anisotrópicos, han dado como resultado la creación de múltiples métodos para estimar la vulnerabilidad de dichos acuíferos. La mayoría de los métodos existentes son aproximaciones teóricas para diferenciar áreas en las cuales la contaminación es más probable debido a sus características naturales. Estos métodos han demostrado su utilidad para definir áreas para ser protegidas y enfocar estudios posteriores. Sin embargo, la alta subjetividad y la exclusión de las influencias antropogénicas como parte del análisis representan algunas desventajas de su aplicación.

Para estimar la vulnerabilidad de los acuíferos kársticos, ya sea de escenarios presentes o futuros, un enfoque integral es altamente necesario. En vista de que los métodos existentes se enfocan únicamente el tiempo que le llevaría a un contaminante teorético universal llegar al acuífero desde la superficie, incorporar el tiempo de residencia y la concentración de un contaminante en un punto específico del acuífero es extremadamente importante. Para alcanzar esta meta, es necesario investigar los métodos existentes, evaluar su aplicabilidad y congruencia con las características regionales para destacar las ventajas, desventajas y posibles clasificaciones erróneas entre ellos y por lo tanto proponer mejoras.

Resumen

El tiempo de residencia de un contaminante en el acuífero y su concentración puede ser estimada por medio de modelos de flujo y transporte, incluyendo prácticas antropogénicas como la descarga de aguas residuales y la extracción de agua para localizar áreas donde la contaminación puede representar un mayor problema. Otros problemas del proceso para estimar la vulnerabilidad son la disponibilidad de datos y el subjetivo proceso para clasificar áreas como vulnerables o no.

La evaluación de múltiples criterios para definir grados de vulnerabilidad es complicada ya que factores como la subjetividad, la calidad de los datos, la escala y las condiciones regionales siempre tendrán cierto efecto sobre los resultados. Este trabajo presenta los resultados de la aplicación de ocho métodos para estimar la vulnerabilidad de acuíferos kársticos y los resultados de un modelo de transporte de solutos en el karst Yucateco. También se presentan algunas consideraciones importantes para mejorar la estimación de la vulnerabilidad. La base para un nuevo modelo integrado para la vulnerabilidad de acuíferos kársticos (IKAV por sus siglas en Ingles) es presentado como una alternativa para dichos estudios.

Acknowledgements

"Zorro, if you are going to do something, do it well and give the best of you, but if not, it is better not to try"

J.M.M.N.

Content

Acronyms

Abbreviations

°C	degrees Celsius
asl	above sea level
ADV	Advection package
AET	actual evapotranspiration
AHP	Analytical Hierarchy Process
AI	artificial intelligence
APLIE	water abundance (A); protection cover (P); land use (L); infiltration conditions (I); groundwater exploitation (E)
APLIS	altitude (A); protective cover (P); lithology (L); infiltration landforms (I); slope (S)
ASTER	Advanced Spaceborne Thermal Emission and Reflection Radiometer
BTN	Basic Transport package
Ca^{2+}	calcium ion
$CaCO_3$	calcium carbonate
$CaMg(CO_3)_2$	calcium magnesium carbonate
Cc	coefficient of circularity
CFP	Conduit Flow Process
CHD	Time-Variant Specified Head package
CICESE	Ensenada Centre for Scientific Research and Higher Education, Baja California
CLICOM	Climate Computing project
cm	centimetres
CO_2	carbon dioxide
CONAGUA	National Water Commission
COP	concentration of flow (C); overlying layers (O); precipitation (P)
CR	consistency ratio
DEM	digital elevation model
DOC	dissolved organic carbon
DRASTIC	depth to groundwater (D); recharge (R); aquifer media (A); soils (S); topography (T); impact of the vadose zone (I); hydraulic conductivity (C)
DRISTPi	depth to groundwater (D); recharge (R); impact of the vadose zone (I); soils (S); topography (T); preferential infiltration (Pi)
DSP	Dispersion package
eFC	effective field capacity
EPIK	epikarst (E); protective cover (P); infiltration (I); karstification (K)
EPM	equivalent porous medium
FAO	Food and Agriculture Organization of the United Nations
FAVA	Florida Aquifer Vulnerability Assessment
GCG	Generalized Conjugate Gradient Solver
GDEM	Global Digital Elevation Model
GIS	Geographic Information System
GUI	graphical user interface

Acronyms

H_2O	water
HCO_3^-	bicarbonate ion
HOB	Head Observation package
IADI	Iterative Alternating Direction Implicit
INEGI	National Institute of Statistics and Geography
inh/km^2	inhabitants per square kilometre
IQR	interquartile range
IVAKY	Vulnerability Index of the Yucatan Karst Aquifer
IZDAN	infiltration conditions (I); protective cover (Z); rock type and thickness (D); karstification (A); groundwater table (N)
JAPAY	Yucatan Drinking Water and Sewage Council
KARSTIC	karstification (K); aquifer media (A); recharge (R); soils (S); topography (T); impact of the vadose zone (I); hydraulic conductivity (C)
KAVA	Karst Aquifer Vulnerability Assessment
KAVI	Karst Aquifer Vulnerability Index
km	kilometres
km^2	square kilometres
LEPT	Lithology (L); sinkhole distribution based on elevation (E); protective cover by soils presence (P); topography as slope (T)
lps	litres per second
m	metres
m/d	metres per day
m/s	metres per second
m^2	square metres
m^3	cubic metres
m^3/d	cubic metres per day
MCA	methods congruence analysis
MCDA	Multi-criteria Decision Analysis
MDTA	multi-depth threshold approach
mg/L	milligrams per litre
Mg^{2+}	magnesium ion
mm	millimetres
mm/y	millimetres per year
Mm^3/y	millions of cubic metres per year
MMA	Merida metropolitan area
MT3DMS	Modular 3-Dimensional Transport model with multi-Species structure
NO_3^-	nitrate
PaPRIKa	protection of aquifers (Pa); protective layers (P); aquifer rock type and structure (R); infiltration conditions (I); karstification (Ka)
PCA	parameter congruence analysis
PET	potential evapotranspiration
pH	potential of Hydrogen
PI	protective layers (P); Infiltration conditions (I)
PRESK	protective role of topography and vegetation (P); rock type and structure (R); epikarst (E); soil cover (S); karstification (K)
Q_1	first quartile
Q_2	median

Q$_3$	third quartile
RCH	Recharge package
REKS	rock hydraulic properties (R); epikarst (E); karstification (K); soils (S)
REV	representative elemental volume
RISKE	aquifer rock type and structure (R); infiltration condition as slope (I); soil texture and thickness (S); karstification (K); epikarst (E)
RMSE	root mean square error
RSG	Reference Soil Groups
SA	Slovene Approach
SAGARPA	Ministry of Agriculture, Livestock, Rural Development, Fishing and Food
SARH	Secretariat of Agriculture and Hydraulic Resources
SMN	National Meteorological Service
SRTM	Shuttle Radar Topography Mission
SSM	Sink & Source Mixing package
UCS	Unique Condition Sub-area
UNESCO	United Nations Educational, Scientific and Cultural Organization
USDA	United States Department of Agriculture
USGS	United States Geological Survey
UTM	Universal Transverse Mercator
UZF	Unsaturated Flow Zone package
VULK	Vulnerability and Karst
VURAAS	Vulnerability and Risk Assessment for Alpine Aquifer Systems
WEL	Well package
WGS	World Geodetic System
WHO	World Health Organization
WOKAM	World Karst Aquifer Mapping
WRB	World Reference Base
WWTP	plants for wastewater treatment

Symbols

h	potentiometric head [L]
K	hydraulic conductivity [L/T]
K_{xx}	hydraulic conductivity (horizontal, x axis) [L/T]
K_{yy}	hydraulic conductivity (horizontal, y axis) [L/T]
K_{zz}	hydraulic conductivity (vertical, z axis) [L/T]
S	travel path length [L]
S_i	Sensitivity [-]
S_s	specific storage [L^{-1}]
t	time [T]
V_i	vulnerability index [-]
W	volumetric flux [L^3 / T · L^2]
W_i	variation index [-]
$\partial h/\partial l$	hydraulic gradient [-]
ηe	effective porosity [-]

List of figures

List of tables

1 Introduction

Groundwater is an important resource supplying freshwater for human consumption and economic activities like agriculture, livestock production, and industry. Some estimations designate groundwater as accounting for 97% of the available freshwater worldwide (Lvovitch, 1973). Similar percentages of freshwater volumes are presented by Freeze and Cherry (1979) who estimated 95% of the global budget as groundwater, 3.5% as surface water bodies, and the remaining 1.5% was designated to soil moisture. These estimations do not include ice bodies which account for nearly 75% of the global freshwater budget in general terms (Healy et al., 2007; Schneider et al., 2011). Such percentages highlight groundwater stores as larger reservoirs of freshwater, in terms of volume, than those located at the surface like lakes and rivers (Shiklomanov, 1993). This also highlights the relevance of groundwater and the importance of using this resource in a sustainable way to provide water in sufficient volumes to future generations. However, in current scenarios around the world, groundwater is threatened due to the increasing anthropogenic influence, which negatively affects this natural resource in terms of quantity and quality.

Groundwater does not only play an important role for the improvement of communities in terms of welfare, economics, or development, it is also a key element in the hydrologic cycle, influencing the environment, flora, and fauna. Groundwater occupies a three-dimensional space below the surface where significant volumes of freshwater are stored, depending on the geologic characteristics, in pores or fissures. These underground systems are denominated as aquifers and can be further classified according to their hydrostatic pressure (confined, unconfined) or according to the lithology and water-filled spaces (detritus, fissured, or karstic).

Karst aquifers are an important source of freshwater because they supply approximately 20% to 25% of the global population as estimated by Ford and Williams (2007). Despite the fact that karst aquifers commonly hold substantial groundwater budgets, due to a fast infiltration of rainwater through fissures, cracks, and swallow holes, these characteristics also increase the risk for such aquifers to be polluted. In detritus aquifers, water experiences longer infiltration times to reach the water table; in this case, soils and biota are able to attenuate pollution at some degree by physical, chemical, or biological processes. This does not occur in karst areas since the parent material, being mostly soluble rocks like limestone or dolostone, does not allow considerable soil formation. Therefore, karst landscapes are mostly characterized as areas with thin or absent soil layers. Lack of soils, in addition to karst features like dolines, karren, and swallow holes, allow a fast infiltration regime making karst aquifers more susceptible to pollution scenarios.

Due to their natural characteristics, karst aquifers mostly face problems related to water quality instead of water quantity. Therefore, specific strategies to protect karst aquifers from pollution are necessary. Groundwater vulnerability maps are important decision supporting tools for the management and preservation of groundwater resources. Vulnerability maps are a visual interpretation of different levels of vulnerability estimated from multiple arrays of natural features overlying the aquifer. Outcomes derived from these tools support decisions regarding urban planning, protective measures and water supply strategies. They also help to maintain a balance between the exploitation of natural resources and ecological changes (Malík and Švasta, 1999).

Methodologies to estimate how vulnerable to pollution a given aquifer is have been developed during the last few decades. These methodologies mostly follow a multi-parameter approach where a range of values are assigned according to the multiple characteristics of the unsaturated and saturated zones. These characteristics are also weighted to highlight their relevance in allowing water movement from the surface towards the underlying aquifer. Generally, the process to estimate groundwater vulnerability is a combination of Geographic Information System (GIS) software and Multi-criteria Decision Analysis (MCDA), such as the Analytical Hierarchy Process (AHP), that work to define a ranking among parameters and weights (if applicable) for each evaluated feature.

However, due to the natural characteristics of karst aquifers, methodologies to estimate vulnerability of unconsolidated aquifers are not applicable to karst landscapes. From the necessity to evaluate karst groundwater vulnerability, including the hydrological behaviour of the multiple karst features, many methodologies have been proposed, tested, and applied in several karst areas around the world. There are some "classic" methods which have been taken as the basis for the development of other methodologies. Countless adaptations appear constantly in literature, due to the high heterogeneity of karst, variability of hydrological response, and data availability.

The existence of several methods focusing on the same goal creates uncertainty regarding the selection of a single method to be applied on a given karst area. When multiple methods are applied over the same karst area uncertainty increases further. Attempts to do so have demonstrated a mismatch between outcomes categorizing vulnerability, thereby complicating the decision about which method to apply for vulnerability studies in areas of interest. Most importantly, the majority of current methodologies do not include other important processes in the analysis, such as pollution residence time or pollutant concentration in a given section of the aquifer, but focus solely on the travel time of a particle from the surface towards the groundwater or to a spring.

1.1 Motivation

The groundwater vulnerability concept has demonstrated itself as a valuable decision support tool for groundwater management. The application of this concept and the results obtained, displayed as two-dimensional vulnerability maps, help decision makers to delineate protection areas to prevent pollution of water sources and minimize environmental damage. Vulnerability maps are also beneficial for sustainable development strategies indicating areas where some activities could be located, representing a minor risk for pollution. Nevertheless, there are still some conceptual problems related to groundwater vulnerability estimation.

Current groundwater vulnerability methods solely evaluate the travel time of a theoretical and unalterable pollutant particle to define the "likeliness" of the aquifer to be polluted, based on how the natural characteristics of the area influence its movement. Factors affecting this type of vulnerability analysis are the high subjectivity and personal interpretation of some karst features from hydrological or hydrogeological points of view. Although karst areas around the world can demonstrate similar characteristics, no standardization exists, with a focus on vulnerability analysis, to classify their behaviour according to degrees of karstification in relation with feature development or hydrological response. Additionally, the necessary data to apply some of the current methodologies is sometimes not available for the potential areas of interest.

Pollutant residence time and pollutant concentration at a given point in the aquifer are not included as part of the intrinsic groundwater vulnerability assessment. Despite the fact that the evaluation of two or more criteria as part of the same analysis is complicated, an integrated approach, contemplating the aforementioned parameters, is highly necessary in order to deal with real pollution scenarios. Therefore, inclusion of the anthropogenic influence over karst aquifers is of the uttermost importance.

Nowadays, many karst areas are already affected by anthropogenic practices, such as extraction wellfields, wastewater disposal, leakage from sewers, and agriculture practices among others (Parise et al., 2004; Parise et al., 2008). Thus, it is necessary to estimate the movement and concentration of pollutants in order to designate areas, communities, or water extraction fields as vulnerable or otherwise for current and future scenarios. A good example of an endangered karst aquifer is the Yucatan Peninsula; a transboundary karst aquifer covering parts of Mexico, Belize and Guatemala. Population and economic activities on the Mexican side of the Peninsula are not as high when compared with other areas of Mexico. Nevertheless, the low coverage of sewer systems and the unrestricted use of permeable artisanal septic tanks for wastewater disposal, have created pollution conditions that threaten the aquifer (Marín et al., 2000).

In the sub-surface of Merida, an urban area with high population density located in the Mexican state of Yucatan, a pollution plume has been detected at the upper part of the aquifer, restricting the use of shallow water extraction wells inside this urban area (Marín et al., 2000). The same condition, but presumably at different levels, is expected in the sub-surface of other urban settlements. In addition to this problem, farm, poultry, and cattle-related activities fail to fulfil national and state regulations for the disposal of wastewater, thereby further increasing the potential of groundwater degradation (Pacheco, 1994; Pacheco and Cabrera, 1997; Pacheco et al., 2002).

Given the limitations of the current vulnerability concept and the current pollution scenarios in karst areas, an integrated process to estimate groundwater vulnerability, coupling the effects of natural protection, pollutant residence time, and pollutant concentration as parameters to evaluate the influence of anthropogenic activities is necessary. Anthropogenic influence and the characteristic regional features make the Yucatan karst an interesting area to apply and analyse groundwater vulnerability methods and to perform solute transport analysis.

To deal with current pollution scenarios, it is very important to re-evaluate the influence on vulnerability of various natural characteristics under different conditions and to define an overall criterion to designate vulnerability classes according to natural and anthropogenic parameters. Some of the characteristics that an integrated karst aquifer vulnerability workflow must include are: the possibility to estimate groundwater vulnerability with available data, the capacity to match regional characteristics, and the inclusion of any anthropogenic influence.

1.2 Objectives

This work aims to introduce the basis for a new conceptual approach to evaluate groundwater vulnerability in karst terrains from an integrated point of view. Coupling outcomes of intrinsic vulnerability maps with those from solute transport investigations it is expected that areas where groundwater could represent a potential danger due to anthropogenic practices will be more accurately defined. However, given the high subjectivity presented by the intrinsic vulnerability concept steps to minimize such subjectivity, previous to its implementation as part of an integrated approach, must be included.

To reach this goal, it is necessary to evaluate the congruence between the current intrinsic methodologies in order to identify potential mistaken evaluations. It is also necessary to investigate anthropogenic activities and their negative effects to be included in the analysis. The herein proposed methodology intends to change the current view of vulnerability studies from an intrinsic point of view into an integrated approach, where the response of the natural system is affected, to some extent, by anthropogenic activities.

In order to achieve the goal of this work, the following steps will be taken:

- To investigate current intrinsic groundwater vulnerability methodologies applied around the world, with the aim to compare results from different karst areas and the advantages and limitations of the applied methods.

- To analyse outcomes of selected intrinsic groundwater vulnerability methods from their application in a proposed karst area, with the aim to define the most influential parameters for the different vulnerability classifications.

- To statistically compare intrinsic vulnerability outcomes and analyse the vulnerability match among the different methodologies (methods congruence analysis), in order to highlight subjective considerations of each method.

- To estimate the agreement of the different vulnerability classes with regional features, or attributes rating, of the study area (parameters congruence analysis), in order to analyse possible modifications for parameters, attributes values, and weights.

- To apply solute transport studies, in order to estimate pollutants behaviour, selecting areas with high pollutant concentrations and evaluate the time it takes from pollutant release points to targets.

- To define a theoretical process to classify vulnerability areas based on numerical model outcomes, drinking water standards, and anthropogenic practices in the area of interest.

- To develop an integrated methodology for karst groundwater vulnerability estimation coupling results from GIS-based analysis and solute transport.

In order to fulfil the objectives presented here, a research structure was created in order to obtain a solid base to develop an integrated strategy. The structure of this thesis is divided into six chapters; three of them are correspondent to the application of the aforementioned steps including their own methodology. A summarized workflow containing the objectives of this work is presented in Figure 1.1.
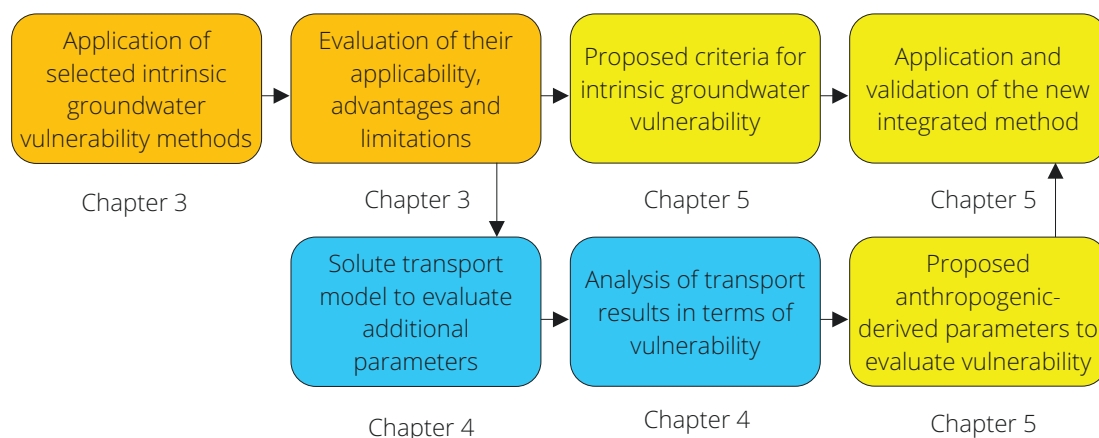
Figure 1.1: Simplified workflow and the objectives of this research.

Despite the study area being the same for the GIS-based estimation of vulnerability and the numerical model, the chapter focusing on the applicability of intrinsic groundwater vulnerability methods (chapter 3) describes solely the relevant natural features that are necessary to create intrinsic groundwater vulnerability maps. The chapter including the numerical model (chapter 4) focuses on regional data that describes the anthropogenic influences (e.g., extraction rates, generated wastewater volumes, etc.) required to reach the goal of the chapter. Parts of this research have been previously published in scientific journals; when necessary, the journals will be mentioned at the beginning of the corresponding chapter.

1.3 Thesis structure

Chapter 1: A brief introduction about groundwater, karst, and vulnerability is presented. It includes the motivation and objectives of this research. The structure of this work and descriptions of each chapter are also presented here.

Chapter 2: Important hydrological and hydrogeological characteristics, karst development processes, and features found in karst landscapes are explained. The importance of karst aquifers and their hydrological behaviour are presented to highlight the conditions promoting the possible infiltration of pollutants through the system. The groundwater vulnerability concept is studied in detail, highlighting important considerations to be analysed. A broad description of current methodologies for groundwater vulnerability focusing on karst terrains is given. In this chapter the problems and limitations of the current intrinsic groundwater vulnerability approaches are also discussed.

Chapter 3: The most relevant natural characteristics of the study area are presented. Utilized data and results of the selected vulnerability methods from their application on the study area are evaluated. Multiple analysis procedures are carried out to investigate the relevance of single parameters, rates, and weights assigned to them. The spatial match between methods, vulnerability classes and regional characteristics is also investigated. This section highlights misleading theoretical considerations of some natural features with regard to vulnerability analysis. Alternative points of view are suggested to improve the intrinsic groundwater vulnerability analysis.

Chapter 4: In this section, the anthropogenic influence within the study area is presented in detail in order to have a broad view regarding the current pollution scenario. Previous groundwater models of the area are shown to demonstrate the influence of regional hydrogeological features affecting groundwater flow. Development of the necessary database and the utilized software are introduced. Relevant hydrological considerations for the model are explained together with the multiple anthropogenic conditions, which were settled upon as parameters for the numerical model. Outcomes are discussed in terms of vulnerability, thus leading to the proposition of characteristics to be considered as estimators to be included into a theoretical workflow.

Chapter 5: This chapter merges results from the GIS-based and numerical models. An integrated methodology to estimate karst groundwater vulnerability is presented. The criteria and steps to develop an integrated vulnerability analysis are explained at detail. The proposed method is tested and compared with previous methodologies. Improvements and drawbacks regarding data availability, scale and regionalization are also analysed.

Chapter 6: Here, the scientific innovations and the fulfilled goals are discussed. Considerations and further steps are proposed.

2 Karst landscapes

A karst area is defined by Ford and Williams (2007) as "a terrain with distinctive hydrology and landforms that arise from a combination of high rock solubility and a well-developed secondary porosity". Karst mostly develops in carbonate rocks like limestone, dolostone, and marble, which possess high solubility due to their calcium carbonate ($CaCO_3$) composition. Karst can also appear in evaporites formed by anhydrite or gypsum minerals, but their dissolution rates and conditions are divergent from those taking place over carbonates (Klimchouk, 1996; Andrejchuk and Klimchouk, 2002; Zhang et al., 2013).

According to the previous definition of karst, rock solubility is not the only factor for karst evolution. As fissures are the pathways by which precipitation enters into the system, both conditions are necessary for karst to develop. When water acts over soluble rocks with a considerable fracture density, the dissolution process enlarges such fissures, which eventually evolve into cracks, conduits, and other larger karst expressions. This mechanism is identified as "karstification" and it is a ceaseless process, therefore, karst must also be considered as a continuously evolving system.

Water is the triggering element for dissolution in carbonates (van Beynen, 2011). However, to effectively dissolve carbonate minerals the water must be acidic. Karstification starts in the atmosphere where water absorbs carbon dioxide (CO_2) in small amounts. The acidity of the precipitation is still not high enough to act upon the carbonates. However, during infiltration, the water acidity increases by absorbing even more CO_2 that was stored in soils from the decay of organic forms. Soils can contain high quantities of CO_2 but its budget depends largely on soil texture, depth, climate, and the flora and fauna of the region. The interaction of acidic water with carbonates is derived from chemical erosion, denoted as:

$$CaCO_3 + H_2O + CO_2 \Leftrightarrow Ca^{2+} + 2HCO_3^- \tag{1}$$

or

$$CaMg(CO_3)_2 + 2H_2O + 2CO_2 \Leftrightarrow Ca^{2+} + 4HCO_3^- + Mg^{2+} \tag{2}$$
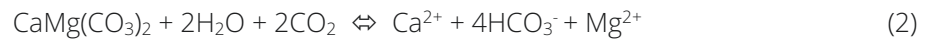
where (1) and (2) are the dissolution reactions for the minerals calcite (the most stable polymorph of $CaCO_3$) and dolomite, a calcium magnesium carbonate ($CaMg(CO_3)_2$), respectively. Calcite is the main mineral found in marble rock and limestone while dolomite is the mineral mostly found in dolostone. Equations (1) and (2) display the chemical dissolution promoted by water (H_2O) and CO_2 upon these minerals, releasing carbonate (Ca^{2+}), magnesium (Mg^{2+}), and bicarbonate (HCO_3^-) ions. The reaction in (1) also applies to rocks composed of carbonate minerals like aragonite, a different form of calcium carbonate. Table 2.1 displays other rocks, besides limestone and dolostone, which are able to undergo karstification.

Table 2.1: Rocks that experience karstification and examples from literature.

Rock/mineral	Rock type	Formation	Example
Chalk, $CaCO_3$	Sedimentary	Marine sediments (algae, skeletons) deposited mostly during the Cretaceous.	The Berkshire karst, United Kingdom (Schürch and Buckley, 2002).
Marble, $CaCO_3$	Metamorphic	Recrystallization of carbonates by heat and pressure.	The Menderes Massif, Turkey (Şimşek et al., 2015).
Gypsum, $CaSO_4 \cdot 2H_2O$	Sedimentary	From a continuous evaporation-soaking process in sediments containing calcium and sulphate.	The Gypsum karst, western Ukraine (Andrejchuk and Klimchouk, 2001).
Halite, NaCl	Sedimentary	Evaporation of salty waters in arid climates.	Mount Sedom, shore of the Dead Sea, Israel (Frumkin, 1994).

The high heterogeneity of karst, and the multiple conditions for their formation, have promoted multiple classifications categorizing karst in relation to their activity, drainage, landforms, or the type of water acting upon them (Table 2.2).

Table 2.2: Some karst classifications and examples from literature. Table based on information from Quinlan (1978), Klimchouk and Ford (2000), and Ford and Williams (2007).

Classification	Characteristics	Example
Paleokarst	Buried karst; decoupled from the current system; inert.	The Kaskaskia paleokarst, northern Rocky Mountains, USA (Palmer and Palmer, 1995).
Exhumed karst	Former Paleokarst which has been reintegrated into the current system; active.	The Balouta exhumed karst, las Médulas, Spain (Redondo-Vega et al., 2015).
Relic karst	Karst experiencing hydrological conditions different from those of its formation.	Adriatic shelf offshore, Apulian Coast, Italy (Taviani et al., 2012).
Hyperkarst	Karst which dissolution is triggered solely by meteoric water.	Nakanai Mountains, New Britain, Papua New-Guinea (Audra et al., 2011).
Hypokarst	Karst which dissolution is triggered by fossil or magmatic water.	Konya Closed Basin, Anatolia, Turkey (Bayari et al., 2009).
Pseudo-karst	Karst-like features formed from processes other than dissolution.	Silvermine Kalk Bay Mountain, Western Cape, South Africa (Marker and Swart, 1995).

Dissimilar flow patterns taking place at variable zones inside the karst system seem to influence characteristics and sequences of karst dissolution features (Gutiérrez et al., 2019). An example of this is found in cases like epigene and hypogene genesis. Epigene refers to karst areas where the surface and sub-surface are well connected and dissolution is triggered by meteoric waters. Hypogene karst (per ascensum) originates when meteoric water, moving upwards from lower formations, generates dissolution (Florea, 2015; Hong et al., 2016; Klimchouk, 2017).

Karstification is a relatively long-term process that modifies the surface and sub-surface through the dissolution of carbonates, or any other soluble rock, creating complex forms. Karst has been the focus of countless research since the work of Cvijić (1893), who linked the complicated hydrology in karst to the multiple landforms and conduit systems that influence the aquifer response.

For the purpose of this work, karst will refer solely to landscapes and their sub-surface (saturated and unsaturated) where dissolution processes have created typical karst features, affecting infiltration and groundwater flow patterns, without further distinction related to characteristics displayed in Table 2.1 and Table 2.2.

2.1 Karst intrinsic features

Evolution of the exclusive features of karst landscapes and their aquifers emerge primarily from carbonate dissolution and processes derived therefrom (e.g., subsidence, collapse). However, from a broader perspective, such evolution is related to a more complicated interplay of several conditions such as hydrological, geological, climatic, and biological factors (Stokes et al., 2010).

Depending upon their location within the karst three-dimensional system, karst features are classified either as exokarstic or endokarstic; the former embraces karst landforms developed at the surface or near surface, while the latter consists of those features developed in the sub-surface where groundwater flow also influences karstification, thereby corroding conduits of considerable diameter.

Exokarst features cover a wide range of scales, varying from millimetres (mm) to metres (m), and are divided into small scale (1×10^{-3} to 1×10^{-2} m) and large scale ($> 1 \times 10^{-2}$ m). Some exokarst features are commonly taken as indications of karst development in the sub-surface. Nevertheless, underground karst systems can exist without karst surface expressions (Ford and Williams, 2007).

Karst features are considered either as input, through-put, or output components of the karst system. The function of the majority of exokarst features is to facilitate the movement of surface water towards the aquifer, whilst others act as a connection between input and output points. Some of the most prominent karst features are briefly described in the coming sections in order to better understand their role in the karst vulnerability analysis.

2.1.1 Dolines

Dolines (also known as sinkholes or cenotes) are circular depressions commonly found in carbonate and evaporite landscapes. They range in diameter from a couple of metres to hundreds, with depths varying in a similar range. Doline formation is caused by multiple mechanisms like subsidence, collapse, and dissolution, acting at different stages of the doline formation (Jennings, 1971; Williams, 1972b; White, 1988). The profile shapes of dolines are also variable depending on the lithological structure and the overall mechanisms acting on its evolution; they can be cylindrical, conical or saucer-shaped among others.

Dolines act as small catchments concentrating autogenic runoff, enhancing infiltration at their base, thereby increasing rock dissolution under the doline base rather than in the doline rim. However, doline formation largely depends on the connection between small passages at the surface, like fissures or cracks (in the order of millimetres of diameter), and larger sub-surface features like conduits or caves. Dolines can be divided into two main categories, according to the mechanism of its formation, as solution dolines or collapse dolines (Figure 2.1).
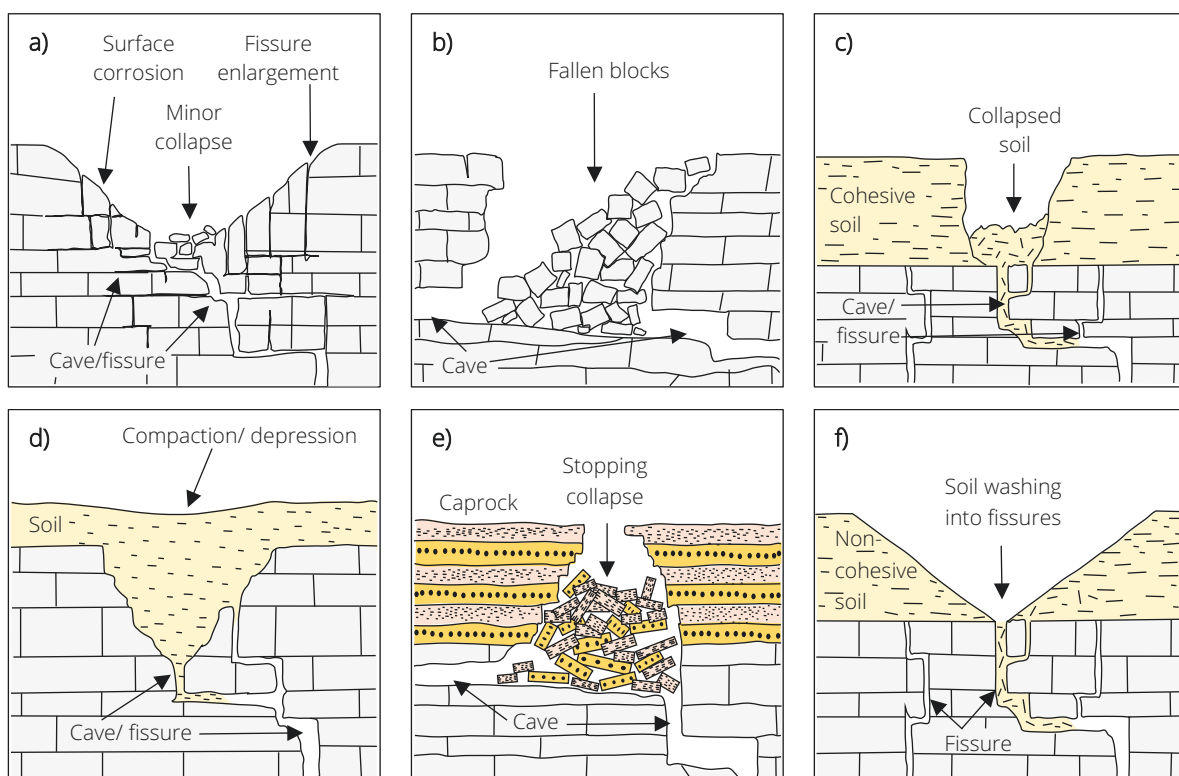
Figure 2.1: Doline classification according to Ford and Williams (2007). In a), solution doline; in b), collapse doline; in c), dropout doline; in d), buried doline; in e), caprock doline; in f), suffusion doline. Image digitalized from Waltham and Lu (2007).

Solution dolines evolve when runoff concentrates on exposed bedrock openings, causing a long-term dissolution of the surrounding surface area. This continuous process gradually enlarges the radius of influence of the opening, generating a slight slope in a funnel-like shape. As the area concentrating flow increases so does the doline. However, for this type of dolines, other factors also influence their formation, such as soil cover, the climatic location of the karst area, and its topography. Multiple morphometric studies have been applied in karst areas around the world, aiming to investigate origin and evolution of dolines (Williams, 1972a; Jennings, 1975; Bondesan et al., 1992). From data collected at different karst regions of Europe, Péntek et al. (2007) subclassify solution dolines; from statistical analysis, dolines were catalogued according to the widening area (rim and/or base) and depth.

Collapsed dolines are formed when the roof of underground cavities of considerable size fail to support the overlying material (Waltham and Lu, 2007). Characteristics of this type of doline are their step sides and the collapsed material inside. Collapse can occur abruptly when the dissolution has considerably weakened the upper part of the underground openings. Another scenario promoting collapsed dolines is related to overall karst development; as karstification increases, underground conduit systems are able to transport more volumes of water at faster rates. This situation leads to a decrease in the water table. Therefore, hydrostatic pressure supporting cavity rooves (or buoyancy support) is minimized, allowing collapse. Collapse can occur either in exposed or covered bedrock. Nevertheless, the latter is mostly triggered by sub-surface dissolution and a loss of buoyancy support rather than dissolution at the surface.

A doline can also appear after subsidence of unconsolidated sediments at the surface (dropout, suffusion, and buried dolines). These dolines are also called "alluvial dolines". A gradual downward displacement of sediments (or suffusion), via enlarged fractures and conduits, triggers the appearance of alluvial dolines. The shape of these dolines is controlled by the unconsolidated material's cohesiveness. An extensive study by Sauro (2016), highlights important characteristics of dolines, their evolutionary aspects, and problems with classifying them.

Solution dolines act as low-scale drainage basins, conveying water towards the lowest doline point where a connection with a vertical shaft usually exists. The hydrology of other doline types is highly dependent on their shape and cover. When a collapsed doline presents steep sides, the area of influence (or doline catchment area) is minimal, therefore, such dolines are inactive and do not provide a representative hydrological function. Their point infiltration capacity, connectivity with the sub-surface, and their function as a natural by-pass between the surface and sub-surface put dolines as key features for karst related studies.

2.1.2   Karren

Karren (or Lapiaz) are a variety of dissolution landforms of small to medium scale developed at the surface of soluble rocks like limestone, gypsum, or halite outcrops. These karst landforms appear mostly as linear furrows or channels with separations ranging from millimetres to metres, creating a rugged surface in a diverse array of patterns. In terms of the scale, karren landforms are divided as micro-karren and karren; the former includes karst expressions in the range of millimetres while the latter considers larger features ranging from centimetres (cm) to metres. However, the term "karren" is sometimes used to generally describe all kinds of micro-features appearing in exposed limestone (Ginés, 2009a).

According to White (1988), karren evolve from the action of precipitation over rock outcrops, where water flows perpendicular to the surface, sculpting small dissolution channels. Karren can develop even when soil cover is present; when located in a depositional zone and covered by sediments, karren is denoted as crypto-lapiaz (Salomon et al., 1995). Karren classification is very extensive. Various authors consider multiple factors when organizing karren, including scale, area of extension, weathering processes, and topography among others. Across the literature, multiple definitions for karren are found, since their characteristics are highly variable.

Ginés (2009a) suggests a general classification for karren landforms considering scale and complexity, dividing karren into karrenfields, assemblages, and elementary features. Elementary karren features can be categorized by their distinctive forming factors. Therefore, karren landforms can be divided according to their size or scale, or by the solution agent acting upon the soluble outcrops. Many karren can display similar patterns but differ in size by one or two orders of magnitude (Figure 2.2).
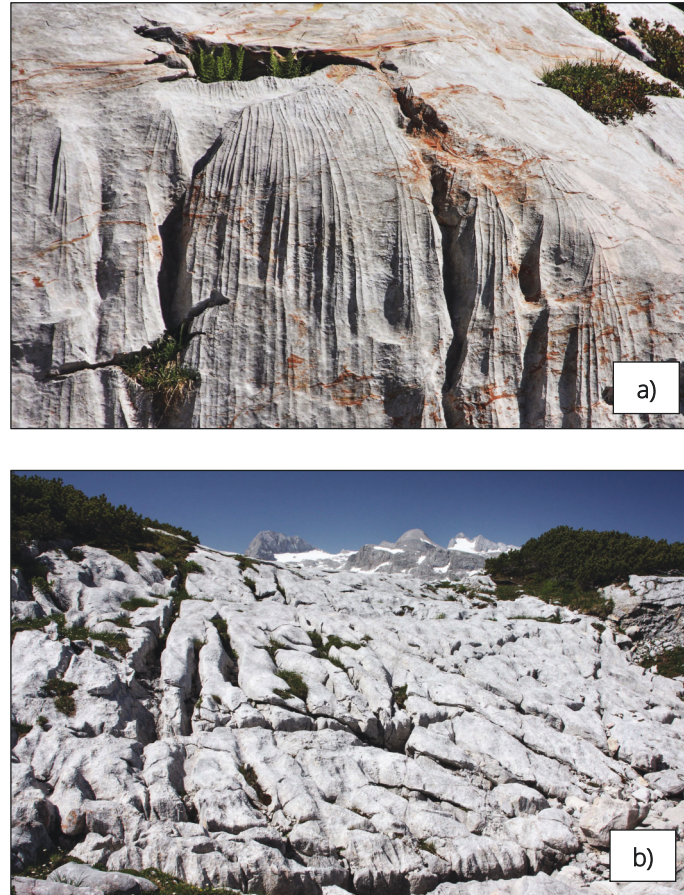
Figure 2.2: Examples of karren landforms. In a), small-scale karren landforms (Rillenkarren) in the range of millimetres caused by dissolution of limestone along the preferential runoff flow lines; in b), a system of clints and grikes in the order of centimetres. Both images were taken in the Krippenstein-Heilbronner Kreuz area in Austria. Photos are courtesy of Martin Mergili, 2012.

Water is the solvent agent in karren formation, however, water can be either precipitation falling directly from the atmosphere or water in solid phase overlying the earth surface, promoting rock dissolution when it takes liquid form. It is important to highlight the use of different names for the same karren features according to the German or English denominations. Many karren elementary features are not displayed in Table 2.3 since individual types of karren are too numerous to be mentioned. Solution bevels (Ausgleichsflächen), cockling patterns, funnel karren (Trichterkarren) and undercut runnels (Hohlkarren) are some other karren types found in the literature. For more detailed descriptions regarding karren genesis, broader classification schemes, and the occurrence of karren around the world, the works of Bögli (1980), Ginés (2004), and Veress (2010) are highly recommended.

Some karren features are related with near sub-surface karst zones where infiltrating water can be either stored or conducted downward by vertical shafts. Therefore, the hydrological functioning of karren is relevant to this work as water is guided through the sub-surface. Features, such as grikes and subsoil tubes, act as important drains, transporting water towards point infiltrating features like dolines or even directly to rivers (Ford and Williams, 2007).

Table 2.3: Characteristics of some karren elementary features. Table modified after Ginés (2009a).

Karren forms	Scale	Solution agent	Characteristics
Borings	< 1 mm	Bio-karstic	Solution by cyanobacteria, fungi or algae (Viles, 2009).
Rillensteine (Microrills)	1 mm - 1 cm	Tiny water films	Tiny channels of variable patterns (Laudermilk and Woodford, 1932).
Rainpits (Solution pits)	1 cm - 10 cm	Storm showers	Cup shaped features commonly clustered (Ginés and Lundwerg, 2009).
Rillenkarren (Solution flutes)	1 cm - 1 m	Direct rainfall	Solutional furrows, nearly straight, closely arranged (Glew and Ford, 1980).
RInnenkarren (Solution runnels)	1 m - 10 m	Channelled water flow	Variety of linear channels of greater size than Rillenkarren (Veress et al., 2015).
Wandkarren (Wall karren)	10 m - 100 m	Channelled water flow	Straight channels on nearly vertical walls (Veress, 2009).
Mäanderkarren (Mandering runnels)	1 m - 100 m	Channelled water flow or ice-snow melt	Winding shape channels (Veress and Tóth, 2004).
Kamenitzas (Solution pans)	10 cm - 1 m	Standing water	Semi-circular shallow depressions containing soils or algae (Cucchi, 2009).
Trittkarren (Heelsteps)	10 cm - 1 m	Sheet wash water flow	Steps in small dip angle (Ginés, 2009b).
Kluftkarren (Grikes)	1 m - 10 m	Infiltration	Linear widened fissures (Goldie, 2009).
Bodenkarren (Sub-soil tubes)	10 cm - 10 m	Soil percolating water	Developed from concentrated flow of water along the contact with the soil (Slabe and Liu, 2009).

When elementary karren features start to integrate, larger areas dominated by karren arise as intermediate assemblages of complex landforms (Bögli, 1980). A karrenfield is then defined as the area formed by many individual karren (Ford and Williams, 2007). In a karrenfield, karst is commonly exposed at the surface but can be partially covered by soils. The extension of karrenfields ranges in scale from square metres (m^2) to square kilometres (km^2). Some well-known examples of karrenfields are the limestone pavements of the British Isles and the stone forest of Lunan in China.

A karrenfield acts as an extensive autogenic recharge area where precipitation is vertically transported towards the sub-surface. Therefore, karren is associated with the epikarst (see section 2.1.4). As a result of the large, two-dimensional extension of such fields and their link with the epikarst, karrenfields could play a more significant role regarding infiltration than depression features.

2.1.3   Poljes

Poljes (also named karst fields or karst valleys) are large scale, closed depressions of fertile land occurring in karst areas (Bonacci, 2013). Poljes are basins characterized by a nearly flat area of alluvial deposits, commonly from the Neogene and Quaternary periods, accumulated on the surface. Poljes are surrounded by elevated areas with steep slopes between the flat bottom and the elevated sides (LeGrand, 1983; Gracia et al., 2003). The flatness of polje bottoms is derived from the horizontal dissolution of carbonates, deposition of allogenic and autogenic fine sediments, or by structural consequences. They are subjected to perennial or intermittent streams feeding and flooding the area.

According to De Waele et al. (2009), the origin of karst poljes is polygenetic; tectonics and corrosion of carbonates are fundamental processes for poljes formation (Roglic, 1964). However, poljes differ in origin, extension, shape, and hydrological function. They are located in multiple karst areas of the world, especially those in Africa, America, Asia, and Europe. Nevertheless, they show a particularly acute development in Mediterranean countries (Bonacci, 2013).

According to Milanović (2004a), the Dinaric karst - a karst area located in South-Eastern Europe - holds a major concentration of karst poljes. In this karst area poljes represent 2.5% of the Dinaric karst extension. Poljes can be located at altitudes higher than 1,000 m above sea level (asl) or just a couple of metres (Sackl et al., 2014). In extent, the polje's area is variable, ranging from less than 0.5 km^2 to more than 500 km^2 (Bonacci, 2014). However, the minimum area of a karst flat terrain to be classified as polje varies among authors (compare Cvijić (1893) and Gams (1978)).

The complexity of poljes derives from their hydrological and hydrogeological attributes. Poljes can be connected to springs and swallow holes with temporal functions; they can retain water, flooding the karst plain, and hold intermittent or perennial rivers (Figure 2.3). Therefore, poljes are not a separate entity from the karst system but rather part of it, with a high influence on the karst water balance. In relation to their hydrological function, poljes can be characterized as permanently flooded (lakes), intermittently flooded (covering the whole polje area or just parts of it), or dry.
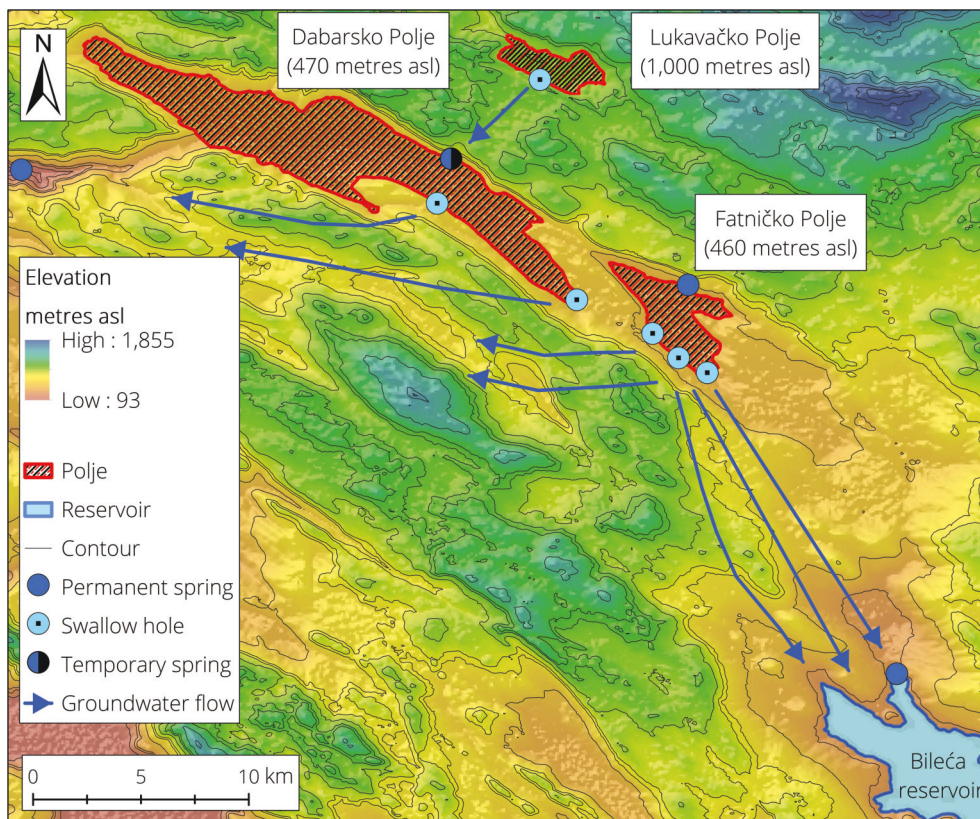
Figure 2.3: Some poljes in Bosnia & Herzegovina. Image digitalized from Bonacci (2013) utilizing the Shuttle Radar Topography Mission (SRTM) digital elevation model, version 3; resolution of 3 arc-seconds (NASA JPL, 2013).

Flooding in a polje occurs when inflow volumes are much higher than the polje's outflow capacity. However, to estimate the infiltration capacity of swallow holes draining poljes is complicated because piezometric pressures also influence their capacity and groundwater can also rise to the surface, flooding the karst valley. Flooding can be caused by these two conditions at the same time. Flooding periods commonly match cold and wet seasons with variable event duration.

Flooding is also variable on a yearly basis; measurements in the Popovo Polje, located in Bosnia and Herzegovina, have demonstrated flood durations of hundreds of days, a considerably long period in comparison with drier years when the flooding of this polje lasted just a couple of hours (Milanović, 2004b).

Bonacci (1987) proposed a polje classification in relation to their feeding and draining features. These were detailed as: closed, upstream-open, downstream-open and upstream/downstream open. The characteristics of each class are described, according to Milanović (2004a), as follows:

- Closed poljes are completely surrounded by areas of higher elevation than the flat plain. Groundwater flow and variations of the phreatic level are responsible for the occurrence of surface water.

- If water inflow occurs at the surface via a river or spring, then it is categorized as upstream-open polje.

- In contrast to the previous category, a polje is downstream-open when surface water exits the polje via swallow holes (Lukavačko Polje in Figure 2.3).

- When the input and output of surface water is simultaneously present, the upstream/downstream open polje is defined (Dabarsko Polje and Fatničko Polje in Figure 2.3).

Karst poljes are then through-put landforms connecting surface water with an aquifer, thus greatly influencing the water cycle. Ecologically speaking, poljes also support life for multiple species of flora and fauna when water levels decrease (Salathé, 2014).

2.1.4 Epikarst

Epikarst (or the subcutaneous zone) is the uppermost part of the karst landscape where rocks have experienced considerable weathering (Klimchouk, 2004). This near-surface zone holds a high porosity and a high permeability, as a product of the enhanced dissolution processes near the land's surface. Epikarst is a spatially discontinuous feature overlaying deeper massive carbonate rock zones where joints, fissures, and cracks are less dense (Jones et al., 2004).

A denuded karst could be taken as the starting stage for epikarst evolution. However, multiple internal and external factors influence epikarst's development. Despite epikarst evolution is linked mainly to dissolution, as with the genesis of other karst features, some pre-established conditions on the bedrock must be present. Since initial pathways are necessary to allow water to flow and activate dissolution, rocks must have experienced some stress and physical weathering. Therefore, precipitation, temperature, fracturing, and a soil cover supplying CO_2 are responsible for epikarst progression (Bauer et al., 2005). The multiple possible combinations between these conditions make epikarst variable, in development and behaviour, in karst areas. Evolution of the epikarst starts at the surface where size and depth of fractures gradually augment. Epikarst evolution can be delayed when fractures retain soil, organic residues, or rock debris.

The degree of epikarst development also decreases with distance from the surface since corrosion rates tend to be minimized with depth. Furthermore, the CO_2 source (the soil cover) is more distant. This leads to contrasting porosities at the upper and lower parts of the epikarst. Such porosities are estimated to be approximately 20% and 2% for the upper and lower epikarst zones, respectively. Epikarst extends from 3 to 10 m depth, however, depending on climatic and rock characteristics, epikarst can reach up to 30 m depth (Ford and Williams, 2007).

The evolution of this subcutaneous zone is also related to karren landforms (see section 2.1.2). Nevertheless, the process for this evolution is still not well understood due to the complexity of both features and their multiple forming components (Klimchouk, 2000; Williams, 2008). Epikarst collects autogenic precipitation in a diffuse way. Due to differences in permeability and porosity at its upper and lower zones the epikarst can act as a buffer, storing infiltrated water if the rate of infiltration at the surface is higher than the infiltration capacity at the bottom. However, when exposed rocks are present, an epikarst's capacity for precipitation intake is directly related with its vertical hydraulic conductivity. Whereas, when the epikarst is covered, the precipitation intake capacity is directly related to soil infiltration capacity.

According to Ford and Williams (2007), the epikarst's ability to store water (or epikarst storativity) is dependent upon three characteristics: thickness, porosity, and the inflow/outflow difference. If the epikarst storativity is high, its function is similar to that of a perched aquifer; supplying a continuous recharge during dry season. Evidence from field investigations indicates that epikarst has a major water storage role compared with the minimum storativity of the saturated zone (Perrin et al., 2003).

The stored water in the epikarst then infiltrates vertically through the rock matrix of the unsaturated zone at slow rates. Nevertheless, when strong precipitation events occur, the epikarst can be over-saturated, promoting a lateral overflow towards vertical shafts or joints, commonly located under dolines, gradually enhancing the shafts dimensions (Klimchouk, 1995). A similar statement by Clemens et al. (1999), identifies epikarst as responsible, to some extent, of conduit evolution in the saturated zone (Figure 2.4).
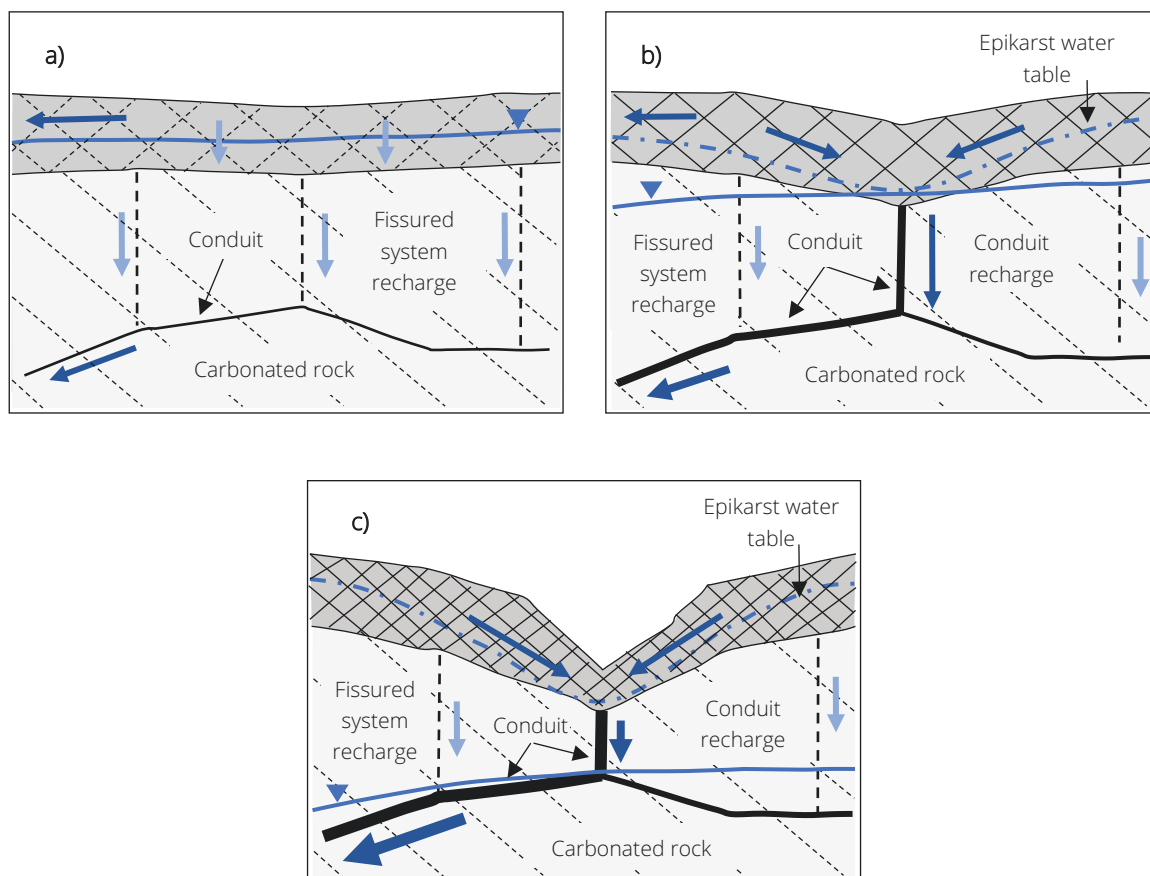
Figure 2.4: Epikarst evolution and influence on conduit and doline development. In a), epikarst's early stage of evolution; in b), epikarst's intermediate development; in c), a well-developed epikarst. Image digitalized from Bauer et al. (2005).

Spatial recharge patterns alternate due to fluctuations in water volumes stored in the epikarst, thereby allowing the diameter and length of the vertical paths to extend and the rate of percolation to accelerate. These vertical conduits are the internal outlets for epikarst overflow. Therefore, epikarst storativity is compromised if the shafts are deep and well developed because most of the epikarst water could flow directly towards the saturated zone. A conceptual model presented by Bauer et al. (2005) describes the combined evolution of the epikarst and phreatic conduits.

Epikarst promotes either diffuse percolation from its bottom or concentrated infiltration, affecting the travel time of water from the surface to the saturated zone and distributing and delaying recharge (Palmer, 1991; Ford and Williams, 2007). Hydrological and geochemical data from karst springs show evidence of the epikarst dual recharge and flow pattern by the distinctive isotopic water characteristics (Bakalowicz et al., 1974; Williams, 1983; Aquilina et al., 2006). As investigated by Emblanch et al. (1998) and Batiot et al. (2000), dissolved organic carbon (DOC) can be also used as a natural tracer to indirectly evaluate epikarst development. The existence and importance of an epikarst layer is also supported by hydrological models. The necessity of a perched aquifer to simulate the karst aquifer function has been demonstrated according to spring variability in relation with precipitation events (Király, 1975). The spring response is an indicator of the epikarst development, as a result of the direct relationship existing between epikarst maturity and the discharge response in springs; discharge peaks occur more rapidly after a precipitation event if the epikarst is well developed. Epikarst is an important karst feature because it regulates vertical infiltration at its base, which is, of course, dependent on its permeability.

Water storage provided by epikarst is of the uttermost importance for hydrological studies and further solute transport. Also, its geomorphological relation to the evolution of other karst features, such as karren, shafts, dolines, and conduits, results in the high variability found in karst systems (Klimchouk, 2000; Williams, 2008).

2.1.5   Swallow holes, conduit system and karst springs

Swallow holes (ponors, swallets) are openings at the surface where streams, mostly generated outside the karst area, flow into the sub-surface. If present, swallow holes are the main water feeding point of a conduit system, controlling the majority of the water input in karst aquifers. Water volumes entering into the karst system through these point infiltration features are relatively higher than those that are autogenously generated from the karst surface. When the inflow capacity of a swallow hole is surpassed, temporal flooding in the surrounding areas can follow, as in the case of poljes. The capacity of the swallow hole to drain a surface stream is also related to the sub-surface conditions, in particular in relation to saturation. It has been demonstrated that swallow holes' draining function is more efficient when water storage is minimal, as it happens during dry periods (Couturier and Fourneaux, 1998).

Ford and Williams (2007) distinguish two core types of swallow holes according to whether the direction of infiltration is vertical or horizontal. Surface streams feeding a swallow hole can be perennial or intermittent. Impermeable stratigraphic formations also influence the characteristics of a swallow hole (Figure 2.5). Due to the hydraulic functioning of swallow holes, dissolution acts faster over the conduits, shafts, or cracks directly connected with it. Therefore, water transport is largely influenced by the capacity and development of the conduit system. By modelling, Liedl et al. (2003) highlight that development of these preferential pathways as part of karstification is highly dependent upon multiple boundary conditions affecting the karst evolution timescale.

Due to the dimensions of conduits, turbulent flow conditions are associated with the water transport, hence, both mechanical and chemical erosion take place in conduits. With velocities at orders of magnitude higher than those displayed in fissured or porous matrix, conduits are a key feature for the system response against precipitation events. Doline development is also directly linked to underground conduit systems, therefore, areas with high doline density are highly likely to contain a well-developed network in the sub-surface.
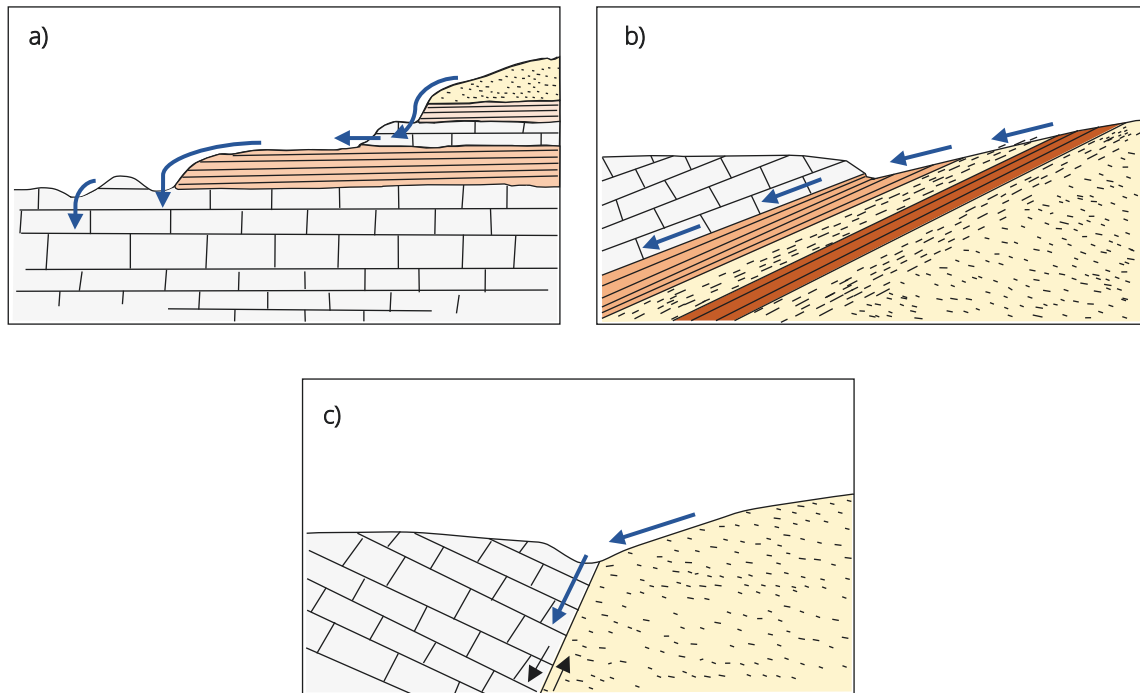
Figure 2.5: Swallow holes' infiltration by allogenic recharge. In a), less permeable layers overlying soluble rocks; in b), an uplifted impermeable lithology generates surface flow, producing river caves; in c), a swallow hole in a faulted boundary. Image digitalized from Ford and Williams (2007).

When karstification is well-developed and groundwater levels decrease, due to an enhanced transport-discharge process, conduits located above water level can become air-filled caves. Cave genesis is not only linked to dissolution, but also to other factors like climate, tectonics, and pedology. Cave classification is variable according to interpretation and the definition from multiple fields of research. A general definition states that caves are three-dimensional dissolution openings, varying in pattern, shape, and size, and are large enough for a human to enter. Palmer (1991), defines swallow holes as the main promotor of cave evolution in terms of length, estimating that 67% of cave passages are related to sinking streams.

Karst springs are natural aquifer outlets, which are related to conduit flow. Springs are the main water outputs in karst aquifers; they represent the end-point of a large system composed of interconnected conduits transporting groundwater that eventually discharges into a fluvial system or into the sea. Proposed classifications for karst springs, such as those from Bögli (1980) and Worthington (2004) were modified by Ford and Williams (2007), who included the hydrological behaviour of springs. Therefore, springs can be classified as free draining, dammed, or confined (Figure 2.6).

Free draining springs discharge water onto adjacent lower valleys by gravity. Dammed springs arise from an underground barrier, such as a less permeable lithology, sediments, or even sea water in the case of coastal aquifers, minimizing groundwater lateral flow. Finally, confined springs develop from the confinement of a karst layer where artesian conditions exist or a fault directs groundwater outflow. Spring discharge is a result of precipitation, starting at the surface, moving through a tangled geological structure formed either by a rock matrix or preferential passages towards a spring.

The spring's function is regulated by the shape and size of the main conduits and their connectivity with other karst features such as dolines and epikarst. This is reflected in the high variability of karst springs in terms of water quality and discharge volume (Bakalowicz, 2005; Kresic and Bonacci, 2009). Additionally, other characteristics, like catchment area or vegetation cover, influence spring response.
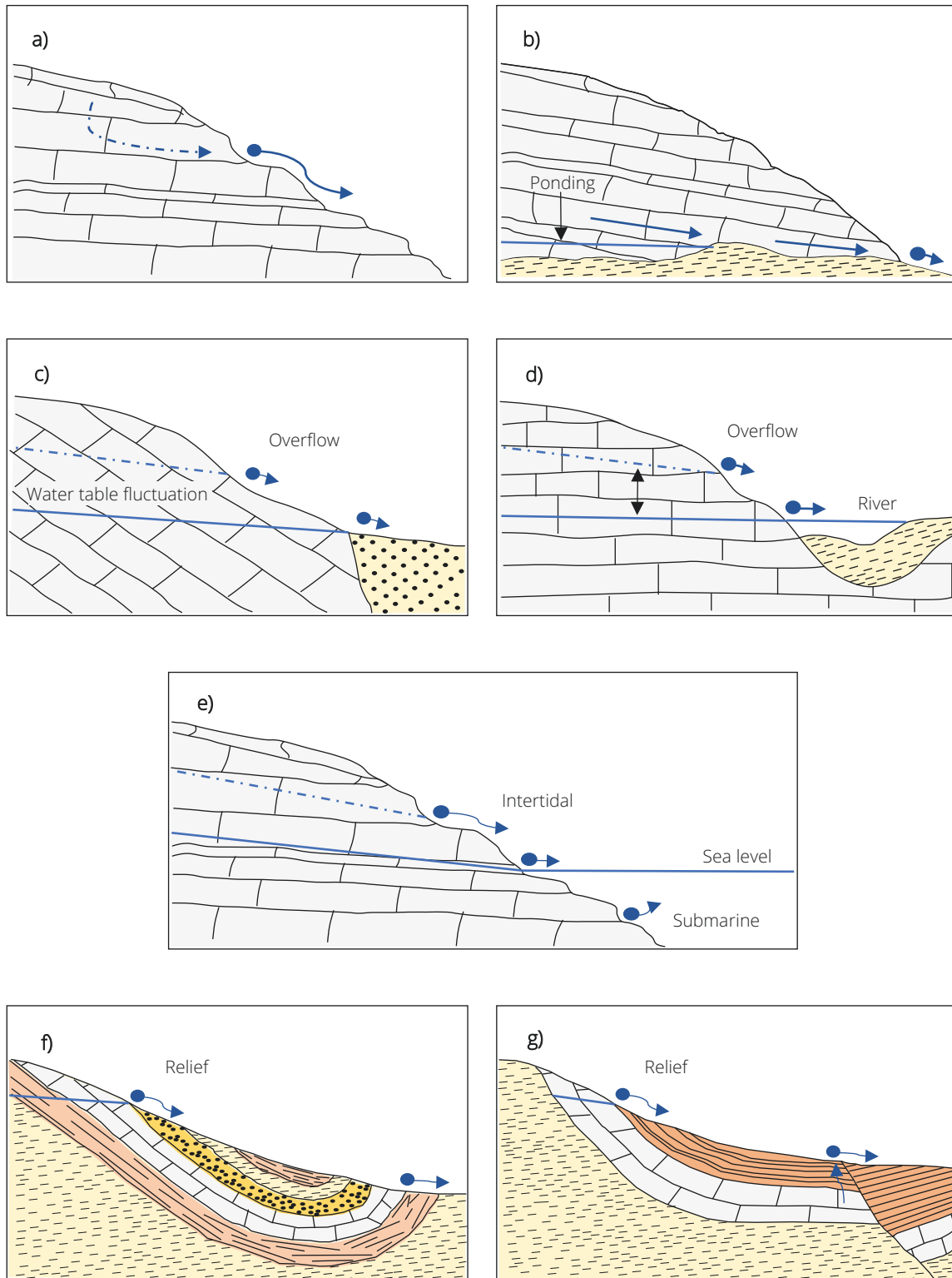
Figure 2.6: Multiple types of karst spring. In a) and b), free draining springs where gravity controls spring discharge; c), d), and e) represent dammed spring conditions; f) and g) display confined springs arising from hydrostatic pressure. Image digitalized from Ford and Williams (2007).

Models have highlighted the importance of karst springs as the most influential feature promoting karstification. The work of Clemens et al. (1997) supports this statement, which was initially proposed from field observations and theoretical results presented by Howard (1963). If some conditions are fulfilled, springs can inverse their functioning to act as swallow holes and vice versa; these springs are then called estavelles (Herak and Burdon, 1984).

2.2 Karst aquifers

In the previous section some of the most important karst characteristics and dissolution features were briefly described in terms of genesis, interconnectivity among them, and hydrological behaviour. We can, then, define karst aquifers as the three-dimensional open system where water is contained and transported at considerable volumes by intergranular pores, fissures, and conduits, where recharge occurs as both diffuse and concentrated. These different pathways, according to shape and size, are also referred to as having primary, secondary and tertiary porosity. Primary porosity is the consequence of diagenesis, while tectonic forces and weathering promote the formation of a secondary porosity (fissures, faults) where water moves more freely. The flow of water through this secondary porosity facilitates the karstification process and promotes the formation of complex systems of conduits, also referred to as tertiary porosity.

Although karst aquifers can display all three aforementioned porosities, it is the conduit system which leads the complexity and groundwater flow patterns for its association with other exokarst features. This tertiary porosity is able to transport high water volumes at considerable distances according to the size, interconnection, and extension of the conduits. Conduit flow is turbulent, in contrast with the laminar flow in the rock matrix (pores and fissures), therefore, conduits decrease the residence time of water in the aquifer, while the residence time of water in the karst matrix is longer (Kovács et al., 2005).

Differences in groundwater flow and storage between the karst matrix and conduits is, of course, dependent upon the degree of karstification, thereby enhancing the high heterogeneity and anisotropy of karst aquifers. Different water flow conditions render the use of mathematical models that are based on Darcy's law, or conventional hydrogeological approaches to be applied in karst aquifers studies, impractical, since they do not consider the implications of conduits systems (Bakalowicz, 2005).

White (2007) and Worthington (2009) pointed out the significant changes found in turbulent flow, regarding geochemistry, where solution concentrations vary spatially and quantitatively. With regard to water circulation and saturation conditions in karst, Ford and Williams (2007) have defined three hydrographic zones as vadose, epiphreatic, and phreatic. The vadose zone is the area where water circulation mostly occurs vertically; nevertheless, when an epikarst is present, lateral flow towards vertical shafts can be generated under precipitation events surpassing the epikarst's storage capacity. The epiphreatic zone is denoted by water table fluctuations, while the phreatic zone is the zone where saturation is constant and horizontal flow is dominant. Therefore, water movement in the karst system is highly dependent upon exokarst and endokarst features (Figure 2.7).

The main characteristics of karst aquifers are their high anisotropy and heterogeneity resulting from the interconnection of several characteristics. Infiltration is present either in a diffuse form or concentrated at the surface. While diffuse infiltration occurs though the soil cover and the subcutaneous zone (see section 2.1.4), some karst features, like dolines and swallow holes (see sections 2.1.1 and 2.1.5), concentrate infiltration at a given point, due to the feature's intrinsic characteristics (Goldscheider, 2015). Besides lateral inflow, water input from the surface is divided according to the catchment area type feeding the karst aquifer; vertical recharge is, therefore, denoted either as autogenic or allogenic.
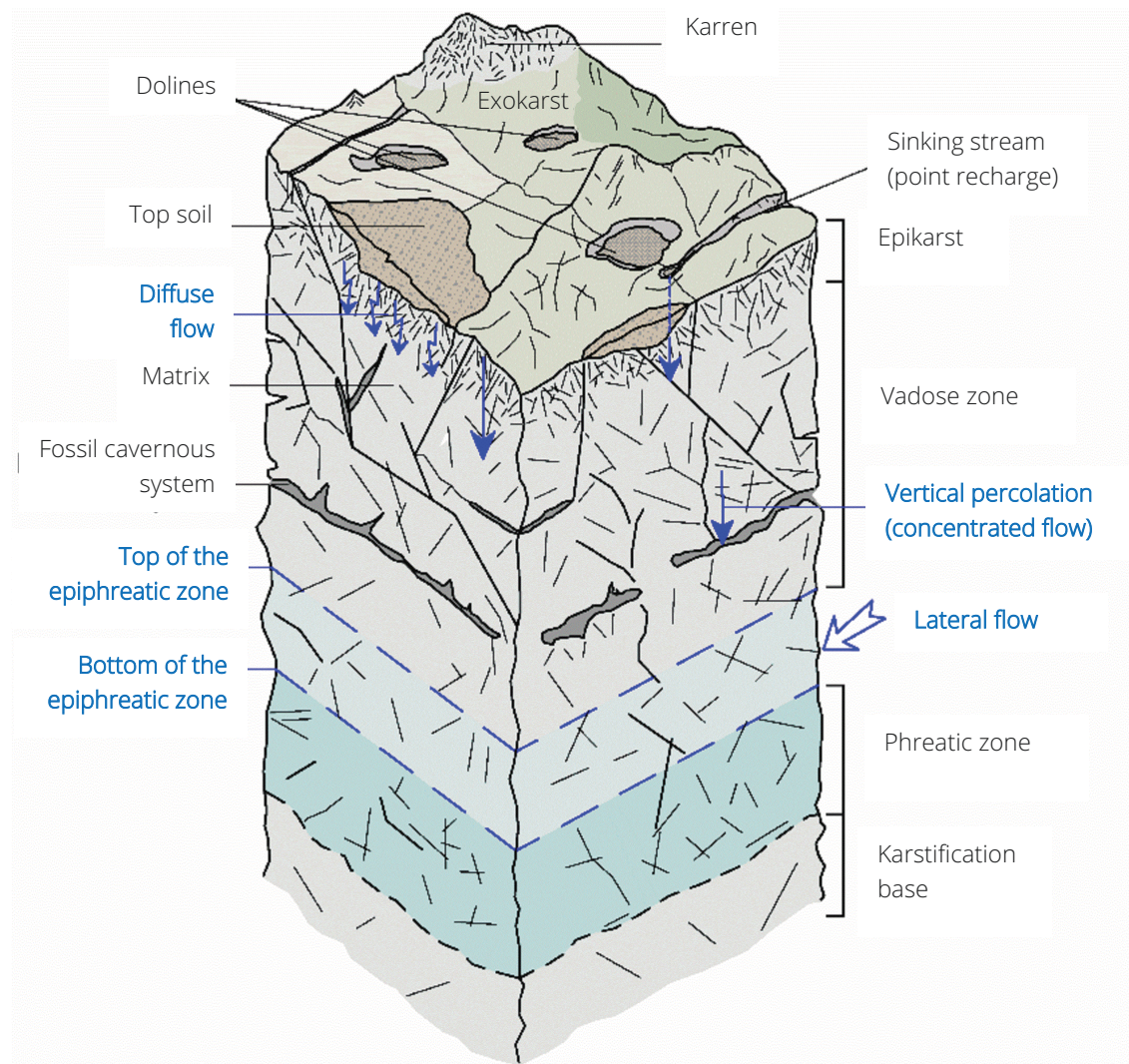
Figure 2.7: Conceptual model of an unconfined karst aquifer. Image reproduced from Stevanović (2015).

Autogenic recharge occurs when precipitation feeds a catchment area that is solely composed of karst. Although autogenic recharge is mostly considered to be a promotor of diffuse infiltration, local surface depressions, like dolines, enhance point infiltration insofar as the doline holds a good connection with the sub-surface. Allogenic recharge exists when adjacent non-karst areas generate a stream flow towards a karst landscape; in this case, recharge takes place mostly through swallow holes by direct infiltration.

Certain hydrogeochemical processes contrast with these two recharge conditions; water interacting with the secondary porosity and conduits in both recharge scenarios differ in terms of volume, therefore, considerable effects on the scale and distribution of karst evolution are derived from recharge. Due to the different porosities found in karst and their high spatial heterogeneity, the hydraulic response to recharge in karst is highly variable. A well-developed near-surface secondary porosity and karst surface features allow a fast infiltration while conduit systems transport high water volumes at high velocities. This makes karst aquifers react almost immediately to precipitation, displaying rapid changes in the groundwater table.

Karst conduits also re-establish the phreatic level according to the degree of karst development, which means a high variability. This is reflected in spring flow data, where flow variations are measured at different orders of magnitude over time (Goldscheider, 2015). Karst aquifers can then be categorized according to their productivity as low, moderate, and high; productivity is estimated from discharge, transmission, and storage, the latter being a key factor for karst aquifer regimes (Stevanović et al., 2015). Despite karst aquifers allowing a bountiful recharge due to the multiple exokarst features, storage can be diminished by a well-developed drainage system.

The heterogeneity of karst aquifers is also reflected in water quality, which fluctuates in relation to the infiltration and recharge patterns of the system. Dissolution of the carbonate rocks, as expressed in equations (1) and (2), is responsible for the high concentration of ions, such as Ca^{2+}, Mg^{2+} and HCO_3^- commonly present in karst groundwater (Jianhua et al., 2012). This high amount of dissolved Ca^{2+} and Mg^{2+} lead to a greater groundwater hardness in comparison with that from detritus aquifers (Loehnert and Papakonstantinou, 1988). Estimations for the potential of Hydrogen (pH) in karst groundwater ranges from 6.5 to 8.9, in limestone and dolomite areas (Ford and Williams, 2007).

Some estimations point out that landscapes demonstrating karstification occupy 11%–20% of the continents, excluding ice-covered areas (Stokes et al., 2010; van Beynen, 2011). However, it is important to always consider that karstification can occur in the sub-surface without exposing surface characteristics. Karst areas, and presumably karst aquifers, are located around the world in different climatic and elevation conditions as long as the prerequisites for karstification exist. Some large karst landscapes and aquifers encompass multiple countries (partly or entirely), such as the Dinaric karst or the Yucatan Peninsula.

The Dinaric karst is an area extending across multiple countries including Albania, Bosnia & Herzegovina, Croatia, Italy, Montenegro, North Macedonia, Serbia and Slovenia. The Dinaric karst covers an approximate area of 60,000 km^2, the largest karst area in Europe, reaching an elevation of 1,796 metres asl (Bonacci, 1987; Mihevc and Prelovšek, 2010). Located next to the Mediterranean Sea, the Dinaric karst is an area of temperate climate, according to the Köppen-Geiger climate classification (Peel et al., 2007).

As a comparison, the Yucatan Peninsula is a karst limestone platform of about 160,000 km^2 shared by Belize, Guatemala and Mexico. The Peninsula has a maximum elevation of approximately 250 metres asl and experiences a tropical climate (Bauer-Gottwein et al., 2011). This comparison highlights the relevance of influential characteristics among karst areas around the world. This is reflected in exokarst and endokarst development, the occurrence of which is also influenced according to the high variation of conditions.

For example, unlike the Dinaric karst, the Yucatan Peninsula does not have surface flows or karst springs at the surface due to the low relief and a regionally homogeneous, and highly fractured, lithology. Nevertheless, underwater springs are commonly found at the coastal line. Karrenfields are also not part of the Yucatan Peninsula's landscape, as occur in the Dinaric karst. While precipitation and snow melt are inflow sources for the Dinaric karst, rainwater is the only source feeding the Yucatan aquifer.

Karst areas can be categorized as well-developed karst, entirely or partially, but the karst features, lithology, and climate are different. This demonstrates that karst aquifers are not only heterogeneous and anisotropic inside a given region but also worldwide, making the task of standardization almost impossible (Figure 2.8).

With around 25% of the world population living in such areas, karst groundwater, as a source for freshwater supply, is extremely important (Ford and Williams, 2007). Therefore, management, protection strategies, and the perception of karst groundwater as a key resource for development, need to be assessed (Chen et al., 2017). Part of the work to reach this goal is to locate and classify karst areas globally; the World Karst Aquifer Mapping (WOKAM) project fulfilled this objective (Chen et al., 2017).
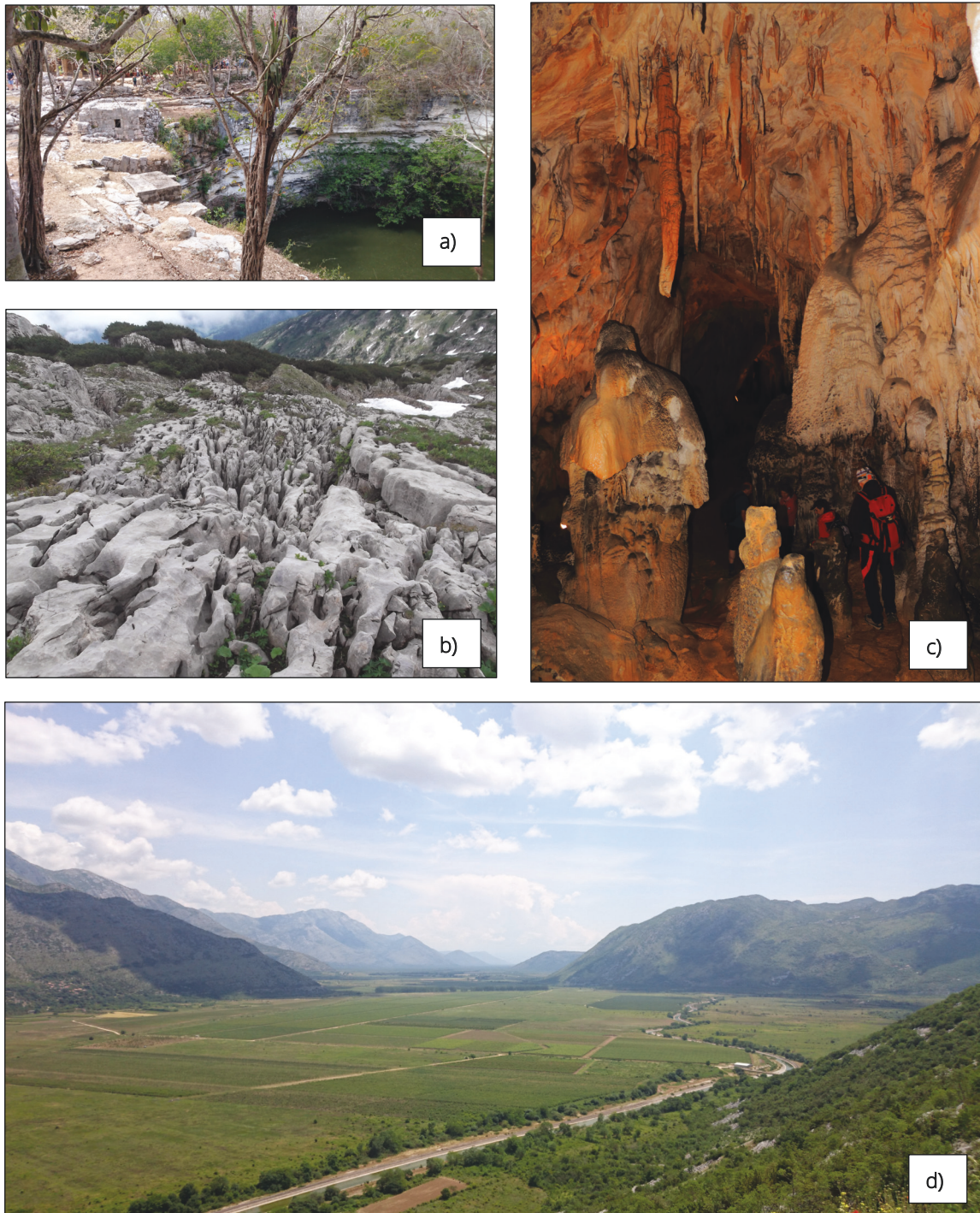
Figure 2.8: Endokarst and exokarst expressions around the world. In a) the "Sacred Cenote" at the old Mayan city of Chichen Itza in Yucatan, Mexico; in b) a karrenfield at the Schrattenkalk limestone, Gottesacker plateau, Germany/Austria; in c) the Cerovac caves in Zadar, Croatia; in d), one of the world's largest poljes, the Popovo Polje in Bosnia and Herzegovina (All photos by Miguel Moreno, except b), courtesy of Chloé Fandel, 2018).

Part of the WOKAM map, corresponding to North America, is displayed in Figure 2.9. The map illustrates the distribution of potential rocks for karstification, such as carbonates and evaporites. Such rocks are further subdivided as continuous or discontinuous depending on the rock percentage in a given area; when a given rock covers more than 65% of the outcrop area it is classified as continuous, while those representing a range of 15% to 65% are classified as discontinuous. When each one of the represented rock types is present in more than 15% of the area, the category is mixed. Although it is complicated to assess a general karstification degree, as mentioned previously, the WOKAM map highlights areas of potential karst aquifers.
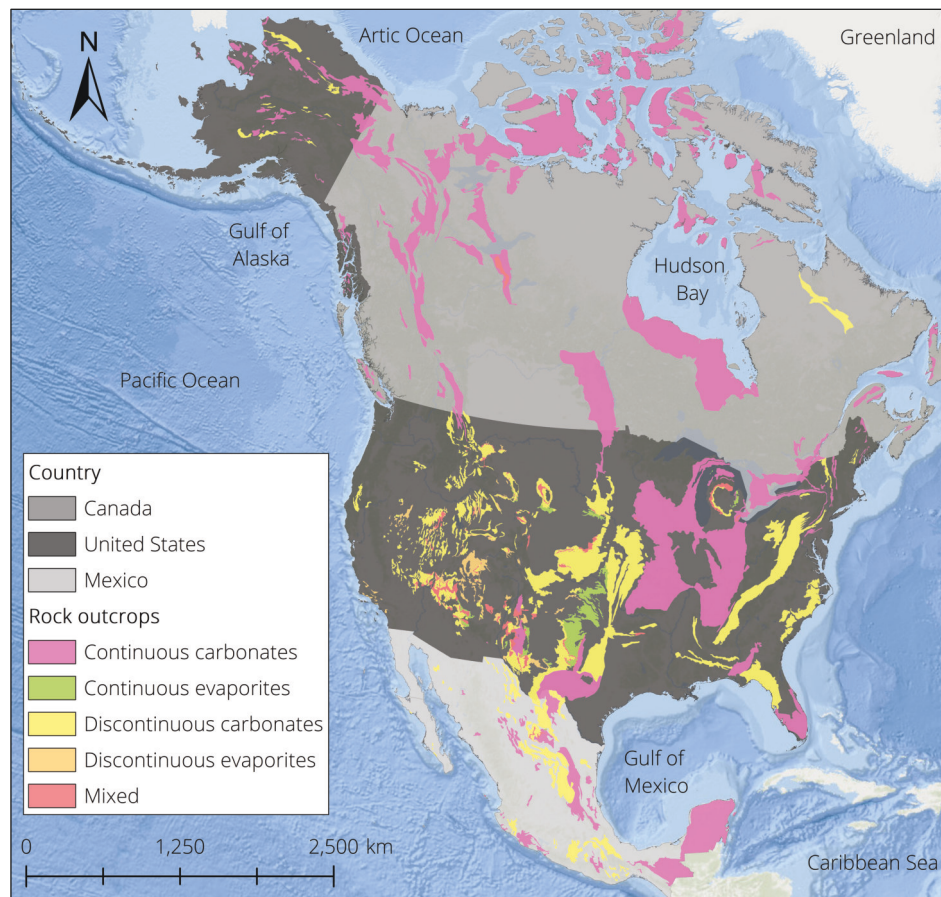
Figure 2.9: Rock outcrops in the North America continent. Map elaborated with the publicly available WOKAM shapefile (BGR, IAH, KIT and UNESCO, 2017).

Using the map, it is possible to note the importance of continuous carbonates, which are exposed at 3 million km^2 (14%) of the 23 million km^2 of the North America continent. In Mexico, continuous carbonates represent 16% of the Mexican territory, mostly in the south-east in the Yucatan Peninsula. Since karst landscapes are located all around the world and occurrence of transboundary aquifers is common, an international understanding and cooperation for a sustainable use of karst water resources is necessary.

Some of the main factors contributing to karst groundwater deterioration are uncontrolled urban sewage, effluents from industry, quarrying, and the use of caves or dolines as dumping sites (Parise et al., 2008). Besides groundwater, karst systems are also biologically important since they contain other natural resources and a rich biodiversity, which are also threatened by human impacts (Parise et al., 2004). As part of environmental strategies to face current problems affecting karst groundwater resources, climate change and population growth are key issues to be considered.

Karst features result in a high pollution risk in karst groundwater resources due to their hydrologic function, allowing a fast infiltration from the surface, with little degradation of pollutants, therefore, enabling severe human impacts over karst resources (Drew, 2017). One important concept has emerged as a tool for water managers and decision makers with the aim to focus aquifer protection on specific areas; the groundwater vulnerability assessment.

Groundwater vulnerability maps are an attempt to characterize aquifers in terms of self-protectiveness under theoretical pollution scenarios. Since the hydrological behaviour of karst aquifers differs from unconsolidated aquifers, special methodologies to estimate karst groundwater vulnerability to pollution have been developed. However, some drawbacks regarding the necessary data, applicability, and the overall vulnerability estimation are still present. The groundwater vulnerability concept and its application on karst aquifers are discussed in further sections.

2.3 Karst groundwater vulnerability to pollution

2.3.1 The groundwater vulnerability concept

The term "vulnerability" indicates the response degree of a given system to any external factor, which can negatively alter such system. As an example of this term, the human body is vulnerable (at variable levels) to the environment to which it is exposed (cold, heat, viruses, radiation), responding to said environmental conditions according to the human body's capabilities (constitution, fitness, immune system). This concept is commonly applied to natural systems to quantify the action of stressors over the environment, with the goal of developing strategies and plans to minimize the negative effects on natural resources.

Regarding aquifers, the first groundwater vulnerability definition was introduced by Albinet (1970), and several redefinitions of this term have been presented during the last few decades. With a focus on theoretical pollution scenarios, groundwater vulnerability is currently defined by Foster (1987), as "the natural characteristics, which influence, at variable levels, the sensitivity of multiple parts of an aquifer that can be affected by an imposed contaminant load". This definition is similar to that presented by Vrba and Zaporožec (1994), where groundwater vulnerability refers to the natural protection of the aquifer against human impacts. Some literature uses the term "protectiveness" as an antonym of vulnerability to indicate and evaluate (subjectively) the self-protective ability of the physical environment. Despite both terms being used interchangeably, they classify natural protection levels from an opposing point of view: the less vulnerable, the more protective an area is.

Following the previous definitions, groundwater vulnerability analyses the role of multiple natural characteristics found in a given area based on the effect exerted by such features over a theoretical pollutant particle, either delaying its movement though the system or by their influence on pollutant degradation. This type of analysis makes groundwater vulnerability assessment closely related to several disciplines, such as pedology, hydrology, meteorology, and geology among others. Groundwater vulnerability analysis results in a dimensionless, probabilistic indicator based on the natural characteristics of an area, used to highlight zones where groundwater pollution is more likely to occur. Therefore, "groundwater vulnerability outcomes must not be taken as an absolute property of the system but as a theoretical approximation" (National Research Council, 1993).

A reclassification of vulnerability, also presented by Vrba and Zaporožec (1994), distinguishes two approaches to evaluate groundwater vulnerability: intrinsic and specific. The former solely evaluates the role of intrinsic features affecting the travel time, starting at the surface, of a theoretical immutable pollutant particle. The latter adds to the intrinsic vulnerability analysis the characteristics of a specific pollutant, or group of pollutants with similar behaviours and properties, according to the changes they can undergo along its pathway.

The COST Action 620 (European Cooperation in the Field of Scientific and Technological Research) suggests the current definitions for intrinsic and specific vulnerability, according to Goldscheider, (2003), to be as follows:

- Intrinsic vulnerability focuses solely on a pollutant particle's travel time affected by the hydrological, geological and hydrogeological conditions, considering neither the pollutant type nor the pollution scenario.

- Specific vulnerability includes the properties of a pollutant and the changes that such pollutant can experience, as a complement to the intrinsic vulnerability of the area.

Intrinsic groundwater vulnerability analysis is mostly commonly used because it does not deal with the extensive data needed to evaluate the degradation processes that a pollutant experiences at different stratigraphic layers. Several methodologies to estimate the degree to which groundwater is vulnerable have been developed, following the previous definitions. Most of the methodologies are based on a conceptual groundwater vulnerability model considering three main factors: a release point, the pathway, and a target; this model has served as a theoretical base for the development of several methodologies. According to the conceptual model depicted in Figure 2.10, the pollutant release point is commonly settled at the surface. However, it can be located in the sub-surface, as is the case of leakage from sewage conduits. The pathway is directly related to the target, which is defined either as the water table, vertically located below the release point or at a given location in the aquifer, with horizontal discrepancy from the pollutant release grid in a two-dimensional map.
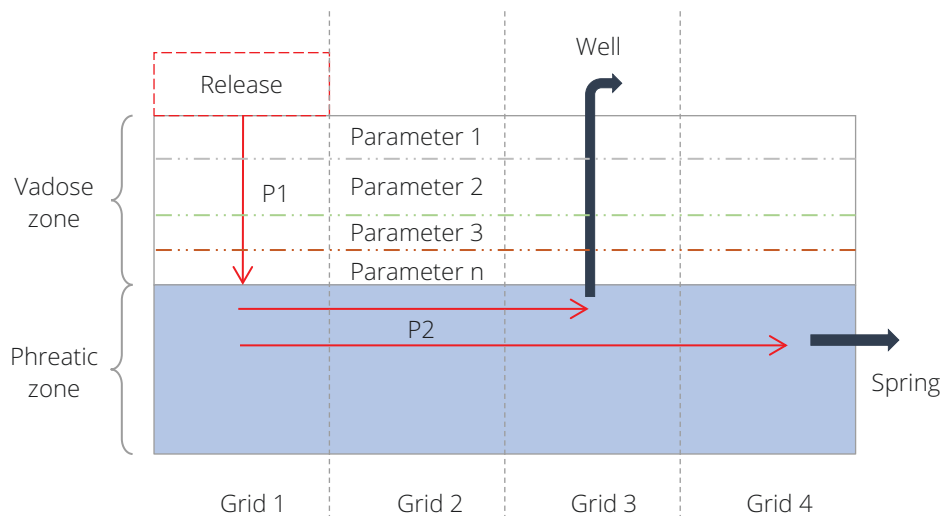
Figure 2.10: Groundwater vulnerability conceptual model.

From this conceptual model, two more concepts have arisen in relation to the target: resource vulnerability and source vulnerability. The former indicates the evaluation of the vadose zone and surface characteristics to estimate the vertical travel time of a pollutant particle until it reaches the aquifer (P1), denoting groundwater as "the resource". The latter adds some properties of the aquifer into the analysis, evaluating its influence on the horizontal movement of a pollutant particle to reach either a spring or a well (P1 + P2); both are defined as "the source". Separation of source and resource vulnerability helps to focus their application according to the problem that needs to be dealt with in a given area. While resource vulnerability is helpful to minimize environmental damage, source vulnerability aids in the delineation of protection areas to maintain acceptable standards of water quality at supply points (Kavouri et al., 2011).

Groundwater vulnerability analysis was conceived to be a helpful tool in decision making for water and environmental agencies. Spatial estimation of vulnerability can be assessed using GIS software, where raster, point, or vector data are transformed and managed to describe natural characteristics of the area of interest as map layers. Therefore, these layers in GIS represent parameters, for example, lithology, soil texture, slope, or any other natural feature according to the parameters considered by the employed method. In some cases, map layers are combined to represent their influence on a special process (e.g., slope and soil on runoff generation); this combination is denoted as a factor. Each parameter, or map layer, is subdivided into attributes, following either a discrete or a continuous approach derived from the characteristics being analysed. For example, a soil map layer can be divided according to textural classes or, by pre-defined intervals in the case of continuous data, as precipitation.

A classification process follows, where a number is assigned to each attribute to illustrate the degree of that particular characteristic influencing pollutant advection. The next step is a map layers' overlap, which is carried out in conformity with the equation proposed for the used method to obtain a numerical vulnerability index. Usually, a weight is assigned to each parameter to enhance the relevance of the natural feature, therefore affecting the index. However, not all methodologies follow the weighting concept. Vulnerability indexes obtained from overlapping are discretized in correspondence with the method-established ranges to define vulnerability classes. Assignment of representative colours highlights areas where the advection transport occurs more "easily" over time.

Vulnerability maps can be interpreted by non-experts on water related fields. Nevertheless, their development and application need some degree of knowledge about hydrogeological processes and hydrology in order to deal with the high subjectivity inherently attached to each methodology. According to the literature, the DRASTIC method, proposed by Aller et al. (1987), is the most known and applied method to estimate groundwater vulnerability. This method evaluates seven parameters, transformed into map layers to obtain a vulnerability map; this method focuses its analysis on estimating groundwater vulnerability for detritus aquifers, although, it considers some fracturing in the aquifer. A graphic representation of the groundwater vulnerability process is displayed in Figure 2.11, with an example of the DRASTIC.

Other methodologies to estimate vulnerability for this aquifer type are GOD (Foster and Hirata, 1988) and SINTACS (De Maio et al., 2001). However, other methodologies for groundwater vulnerability estimation have not been as well documented (Villumsen et al., 1982; Zaporožec, 1985; Sotornikova and Vrba, 1987). To estimate groundwater vulnerability in karst, methods for detritus aquifers are not suitable, as they do not consider the hydrological implications derived from karst features. As an example, if we consider the intrinsic features evaluated by the DRASTIC method to estimate vulnerability, as displayed in Figure 2.11, we can agree, for a karst vulnerability scenario, that parameters like depth to groundwater and impact of the vadose zone would need to be re-evaluated due to the by-passing of karst characteristics. Furthermore, slope would exert a more significant influence for point infiltration, whilst recharge volumes can be higher due to the increased infiltration capacity of karst. Nevertheless, it is necessary to point out that these considerations can also vary among different karst areas, making the evaluation or adaptation of such features even more complicated.

Despite these limitations, some of the groundwater vulnerability methods for detritus aquifers are still used to estimate vulnerability in karst areas, with the DRASTIC method being the most commonly employed for this purpose (Panagopoulos et al., 2006; Różkowski, 2007; Mimi et al., 2012). Due to the necessity to evaluate the vulnerability of karst aquifers, several methodologies have been introduced as alternatives to deal with karst areas. Figure 2.12 displays an updated timeline, highlighting the relationship among some of the current methodologies. However, it is a very ambitious task to register all of the existing vulnerability methods since their development is continuous and many are expected to be either unpublished or presented in languages other than English.

Parameter (map layer)	Parameter's attributes	Assigned rates

Depth to groundwater (D) — 0 to 10 km

- > 5 m → 7
- 3.1 - 5 m → 8
- 1.1 – 3 m → 9
- < 1 m → 10

Recharge (R) — 0 to 10 km

- < 10 mm/year → 2
- 10 - 30 mm/year → 3
- 31 – 50 mm/year → 4
- 51 - 70 mm/year → 5
- 51 - 70 mm/year → 6

Aquifer medium (A) — 0 to 10 km

- Sands, fine-grained → 3
- Sands with clay → 4
- Fluvioglacial sands → 6
- Gravel and aeolian sands → 8

Soils (S) — 0 to 10 km

- Muck soil, alluvial soil → 5
- Brown soil, black soil → 6
- Silt, peat soils → 7
- Podzolic soils → 8

Topography as slope (T) — 0 to 10 km

- 1.6 – 2 % → 8
- 1 – 1.6 % → 9
- < 1 % → 10

Impact of the vadose zone (I) — 0 to 10 km

- Mud, alluvium → 3
- Morainic clays → 4
- Fluvioglacial sands → 6
- Gravel, aeolian sands and → 8

Hydraulic conductivity (C) — 0 to 10 km

- 4 – 12 m/d → 2
- 13 – 28 m/d → 4
- 29 – 40 m/d → 6
- 41 – 80 m/d → 8

DRASTIC vulnerability index:

D(5) + R(4) + A(3) + S(2) + T(1) + I(5) + C(3)

Class	Index
Very low	< 79
Low	80 - 109
Moderate	110 - 139
High	140 - 169
Very high	> 169

DRASTIC vulnerability map — 0 to 10 km

Figure 2.11: Example of the DRASTIC method. Application in the Vistula floodplain, central Poland. Map layers and the final DRASTIC map are reproduced from Krogulec and Trzeciak (2017).
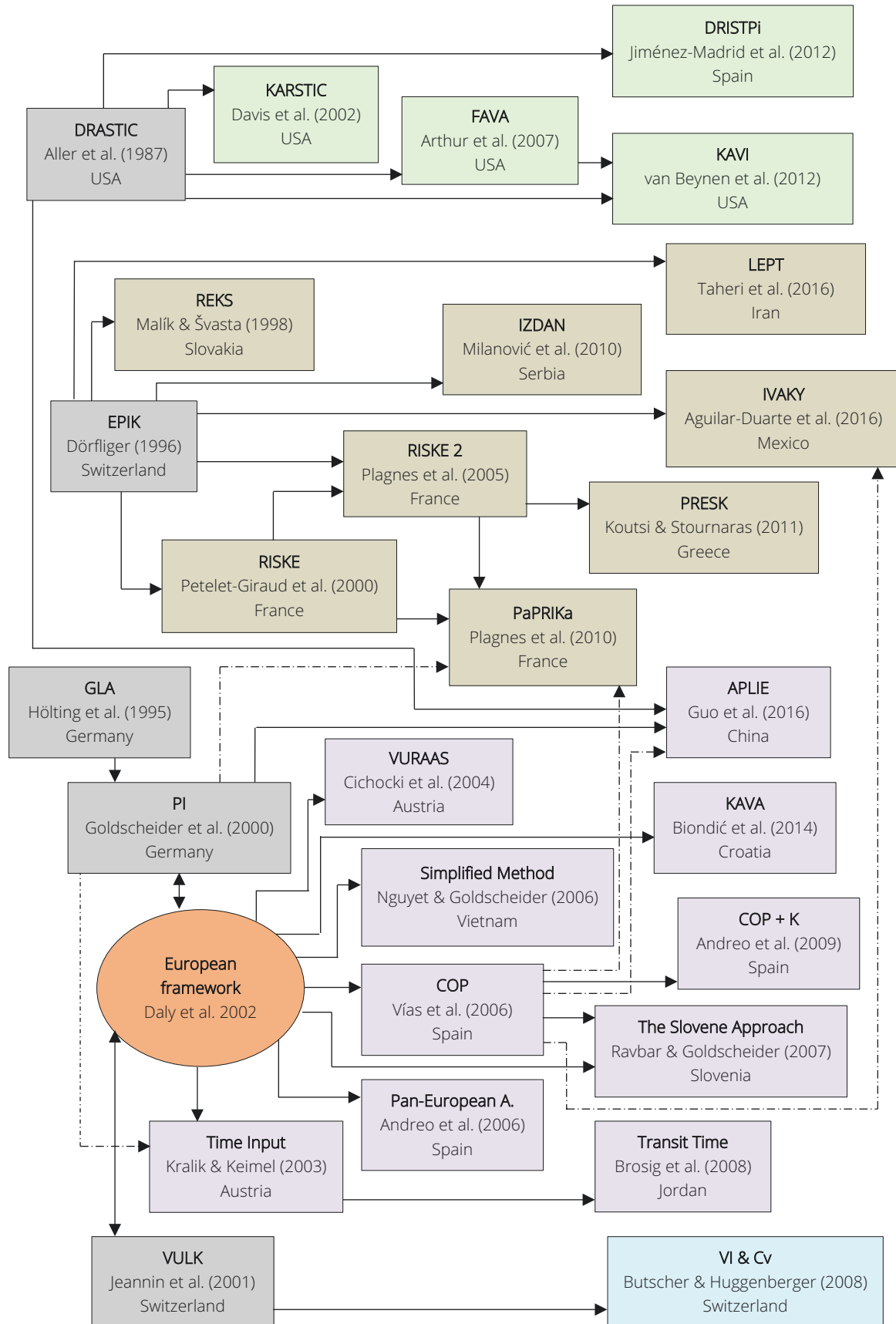
Figure 2.12: Relationship and timeline among vulnerability methods. Schematic modified after Iván and Mádl-Szőnyi (2017); base methodologies displayed in grey.

2.3.2   Methods to estimate groundwater vulnerability in karst areas

The EPIK method (Dörfliger et al., 1999) is, thus, the first documented approach, which focuses on karst and it has been taken as basis for the development of other proposed methodologies. An important period for groundwater vulnerability studies emerged from the COST Action 620, an international project whose goal was to develop a European framework for the protection of karst groundwater. This action entitled "Vulnerability and Risk Mapping for the Protection of Carbonate (Karst) Aquifers" was an international cooperation among scientist from 15 participating European countries bringing their expertise from multiple fields to elaborate a general, non-prescriptive framework to estimate intrinsic vulnerability, specific vulnerability, and risk mapping (Zwahlen et al., 2003).

With a focus on intrinsic vulnerability, several schemes to reach the same goal exist; they have been developed during the last three decades due to several aspects like the high heterogeneity and anisotropy presented by karst, differences among regulations by country, and available data of karst regions around the world.

Due to the elevated number of methodologies commented on in this section, only a brief explanation to highlight their link with the core schemes is presented. Further characteristics of the methods are displayed in Table 2.4, Table 2.5, and Table 2.6. The methods reviewed were divided according to the base method from which they were conceived, being denoted as DRASTIC, EPIK, or European framework derived. A review of the suggested literature is encouraged for a more detailed description of each method, however, section 3.2.1 introduces precise explanations for the eight selected groundwater vulnerability methods, applied and evaluated as part of this research.

2.3.2.1   DRASTIC-derived methods

The DRASTIC (Aller et al., 1987) is considered as a method for detritus aquifers. Although it incorporates the impact of karst limestone in the saturated zone, it does not include the hydrogeological response of exokarst features regarding flow concentration at the surface. To solve this problem, the KARSTIC method was proposed, including parameters representing karst development such as fissuring and karst surface expressions (Davis et al., 2002). Nevertheless, the classification of parameters such as slope, recharge, and depth of groundwater remain identical as those proposed by the DRASTIC method; a situation which can represent a misclassification for karst scenarios.

The Florida Aquifer Vulnerability Assessment (FAVA) was presented as a scalable, updatable, and flexible methodology to estimate intrinsic vulnerability of the major aquifers in Florida state (Arthur et al., 2007). This method bases its analysis on a statistical modelling technique referred to as Weights of Evidence (Bonham-Carter, 1996; Raines et al., 2000). This approach generates prediction outcomes after analysing training sites based on lithology combinations found by borehole data.

The DRISTPi method is also a derivation from DRASTIC, but has been adapted to estimate vulnerability for two scenarios: karst and non-karst areas (Jiménez-Madrid et al., 2013). One of the major modifications proposed by this method is the elimination of the two parameters defining lateral flow in the saturated zone proposed by the DRASTIC (aquifer media and hydraulic conductivity), hence, focusing on resource vulnerability. It also includes a new scenario-dependent parameter to evaluate preferential infiltration and the role of sinking streams, swallow holes, and fissuring on vulnerability estimates. Since depth to groundwater is less relevant for karst, due to its by-pass ability, the DRISTPi also redefines the attributes of this parameter according to the scenario to be evaluated.

Another methodology is the Karst Aquifer Vulnerability Index (KAVI); this method estimates specific groundwater vulnerability by the inclusion of one layer representing land use as a complement for geologic parameters (van Beynen et al., 2012). This method demonstrated a better correlation among vulnerability classes and nitrate concentrations in the studied aquifer. Since aquifers' hydraulic conductivity is one of the evaluated parameters, source specific vulnerability is the outcome from this method.

The APLIE method (Guo et al., 2016) is a combination of different methods, such as DRASTIC, COP, and PI, adapted to meet the hydrogeological settings of a karst study area in China; this method includes the evaluation of groundwater extraction as an external indicator of source vulnerability. Parameters, weights, and scope of each DRASTIC-derived method are displayed in Table 2.4.

Table 2.4: Parameters and goals of the DRASTIC-derived methods.

Method	Evaluated parameters	Equation	Vulnerability
KARSTIC	Karstification (K); aquifer media (A); recharge (R); soils by texture (S); topography by slope (T); impact of the unsaturated zone by lithology (I); aquifer hydraulic conductivity (C).	$K(10)+A(3)+R(4)+S(2)+T+I(20)+C(3)$ *	Intrinsic; source
FAVA	Soil permeability, karst features, hydraulic head difference, and aquifer thickness.	Statistically estimated (Weights of evidence)	Intrinsic; resource
DRISTPi	Depth to groundwater (D); recharge (R); impact of the unsaturated zone by lithology (I); soils by texture (S); topography by slope (T); preferential infiltration (Pi).	$D(2)+R(4)+I(5)+S(2)+T(1)+Pi(5)$ **	Intrinsic; resource
KAVI	Depth to groundwater (D); soil permeability (S); aquifer hydraulic conductivity (A); epikarst (E); land use (LU).	$D(0.15)+S(0.15)+A(0.15)+E(0.25)+LU(0.3)$	Specific; source
APLIE	Water abundance (A); protection cover (P); land use (L); infiltration conditions (I); groundwater exploitation (E).	$A(0.17)+P(0.22)+L(0.22)+I(0.30)+E(0.09)$	Intrinsic; source

* K = Combination of swallow holes and fissuring; I = Combination of lithology and depth to groundwater.
** Weight of the D parameter changes to 5 for non-karstic areas.

2.3.2.2   EPIK-derived methods

EPIK-derived methods also follow a theoretical index-based methodology where single parameters are evaluated with an assigned weight to highlight their relevance to vulnerability outcomes. Similar parameters are evaluated among these methods, however, the characteristics to assign values to parameters' attributes can be variable (Table 2.5).

The EPIK method was proposed to designate protection areas of water supply points for catchment scale; it is the first methodology that considers the hydrological behaviour of karst to improve Swiss water regulations (Dörfliger et al., 1999). One of the first EPIK adaptations is the REKS method, which was introduced as an alternative due to the lack of necessary data and regional complications to apply the EPIK method in a Slovak karst area (Malík and Švasta, 1999).

RISKE is the French analogous of the EPIK method; it evaluates the same parameters as its ancestor with slight modifications and adds the aquifer rock type, as an extra component, into the analysis (Petelet-Giraud et al., 2000). Later, this method was further modified as RISKE-2 (Plagnes et al., 2005).

Table 2.5: Parameters and goals of the EPIK-derived methods.

Method	Evaluated parameters	Equation	Vulnerability
EPIK	Epikarst (E); protective layer by soil thickness (P); infiltration conditions by slope (I); karstification (K).	E(3)+P(1)+I(3)+K(2)	Intrinsic; source
REKS	Rock hydraulic properties (R); epikarst (E); karstification (K); soils (S).	R+E+K+S	Intrinsic; resource
RISKE	Aquifer rock type and structure (R); infiltration condition by slope (I); soil texture and thickness (S); karstification (K); epikarst (E).	R(0.1)+I(0.4)+S(0.1)+K(0.2)+E(0.3)	Intrinsic; resource
PaPRIKa	Protective layers (Pa) by soils, epikarst, or unsaturated zone by lithology and structure (P); aquifer rock type and structure (R); infiltration condition by slope (I); karstification (Ka).	P(0.2)+R(0.2)+I(0.3)+Ka(0.3)	Specific; source
IZDAN	Infiltration conditions by slope (I); protective cover by soil (Z); rock type and thickness (D); karstification (A); groundwater table (N).	I(1)+Z(1.5)+D(2)+A(3)+N(2)	Intrinsic; resource
PRESK	Protective role of topography in combination with vegetation (P); rock type and structure (R); epikarst (E); soil cover by texture and thickness (S); karstification (K).	P(0.26)+R(0.09)+E(0.16)+S(0.41)+K(0.06)	Intrinsic; resource
LEPT	Lithology (L); sinkhole distribution based on elevation (E); protective cover by soil presence (P); topography by slope (T).	L(4)+E(3)+P(2)+T(1)	Intrinsic; resource
IVAKY	Geomorphology factor by karst features and elevation (K); edaphology factor by soils and relief (S); climatic factor by precipitation variability and rain periods (C).	K(0.65)+S(0.29)+C(0.05)	Intrinsic; resource

Application of RISKE in a karst area located in southern Greece resulted in the PRESK method (Koutsi and Stournaras, 2011); parameters considered by the RISKE were modified to meet local geological settings in an attempt to delineate protection zones in the study area.

PaPRIKa is another French methodology used to estimate either source or resource intrinsic vulnerability based on the geologic structure and hydraulic function of karst aquifers (Dörfliger and Plagnes, 2009). Despite it being mostly a derivation of the EPIK method, it also includes considerations of the European framework; this method has been applied for vulnerability studies in Cuba (Farfán-González and Plagnes, 2013) and the Pyrenees (Huneau et al., 2013).

As a solution to deal with sparse data in Iranian karst regions the LEPT method was presented to estimate vulnerability; this approach displays a very basic vulnerability analysis due to the lack of detailed datasets to apply any other methodology in the region (Taheri et al., 2015). Although agreement with karst regional features has been shown, its parameter classification is driven by high subjectivity.

Two more EPIK-derived methodologies, that are less frequently mentioned in the literature, are the IZDAN (Milanović et al., 2010) and IVAKY (Aguilar-Duarte et al., 2016). The former was presented as a regional option to characterize karst aquifer vulnerability in Serbia as part of regional strategic projects to improve current groundwater scenarios. The latter could be considered as a simplification of the EPIK, with considerations from the COP, developed as the regional option for the Yucatan karst utilizing three groups of parameters.

2.3.2.3   European framework-derived methods

Before presenting the methodologies of this section, it is necessary to briefly explain the scope of the European framework as a result of the COST Action 620. For this action, three working groups were created with the goal of defining a solid scheme base for the estimation of intrinsic vulnerability, specific vulnerability, and risk mapping. Work group 1 proposed parameters to be considered for intrinsic vulnerability according to their functioning, divided into three influencing factors: overlay protection, concentration of flow, and precipitation as external stressor. An additional factor related to karstification with a focus on conduit systems, which is necessary for source vulnerability assessment, was also included (Goldscheider and Popescu, 2003).

The work of the European framework regarding intrinsic vulnerability is closely related to two other contemporaneous vulnerability methods: the PI (Goldscheider, 2005) and the VULK (Jeannin et al., 2001). The PI method proposes the analysis of two factors, one for the protective function (overlying layers) and other for the by-passing conditions to evaluate how vulnerable an aquifer is. The protective function is based on the GLA method (Hölting et al., 1995), which evaluates the characteristics of layers forming the unsaturated zone. The potential by-pass is evaluated according to the surface conditions that are able to generate and concentrate flow at the surface; parameters such as slope, soil hydraulic conductivity, vegetation, and karst features are evaluated for this factor.

The VULK method estimates pollution transport, advection, and dispersion by means of breakthrough curves, considering four layers in the system (soil, subsoil, unsaturated non-karst, and unsaturated karst). This method adds one more layer (representing the saturated zone, hence, lateral flow) for resource vulnerability estimation. This analytical model maps vulnerability from a quantitative approach, being the first process-based method for vulnerability studies.

The European framework, considered mainly as a guideline, settled a base for intrinsic groundwater vulnerability mapping. It highlights the most relevant characteristics to be considered for vulnerability estimation but takes into account the necessary flexibility to achieve this objective, according to the variability of conditions, such as data, scale, geological settings and resources (Daly et al., 2002). Therefore, this framework has served as a guide to develop individual groundwater vulnerability schemes to fit all possible conditions found in European karst areas.

A common characteristic among methods derived from the European framework is the use of factors, groups of single parameters affecting distinctive conditions, hence, influencing vulnerability. As a measure to minimize subjectivity, the European framework does not utilize weights, nevertheless, the numerical index range of the factor representing flow concentration serves to denote the importance of this component (Table 2.6).

Chronologically, the approach proposed by Kralik and Keimel (2003), referred to as the Time-Input method, was the first derived from the European framework. Although its analysis focuses on mountain karst areas for the inclusion of characteristics like the dip of the bedding planes towards or away from the groundwater, it can also be used for detritus aquifers and other hydrological conditions. As its name suggests, this vulnerability analysis is carried out using infiltration values as the input, calculated after performing a water balance of the region. Then, hydraulic conductivity values of each layer forming the unsaturated zone serve as an estimator of the travel time from the surface to the water table, considering the thickness of each stratum.

Table 2.6: Parameters and goals of the European framework-derived methods.

Method	Evaluated parameters, factors	Index equation	Vulnerability
PI	P factor: topsoil (T); recharge (R); soil texture (S); lithology (B). I factor: soil hydraulic conductivity, slope, vegetation cover, and karst catchment area.	P · I	Intrinsic; source and resource
Time-input	T factor: soil hydraulic conductivity, lithology hydraulic conductivity, and thickness of each stratum. I factor: recharge from groundwater balance.	T · I	Intrinsic; resource
VURAAS	Unsaturated zone (UZ); infiltration type (A); recharge (GWN).	UZ · A · GWN	Intrinsic; resource
COP	C factor*: distance to swallow holes (Dh); distance to sinking streams (Ds); slope and vegetation (Sv); surface features (Sf). O factor: soil texture and thickness (Os); lithology and fracturing (Ol); confinement (Cn). P factor: precipitation volume (Pq); precipitation intensity (Pi).	C · O · P	Intrinsic; resource and source**
Simplified method	O factor: soil thickness and permeability. C factor: dominant flow process and catchment delimitation.	Index defined by a matrix system	Intrinsic; resource
Slovene Approach	C factor*: distance to swallow holes (Dh); distance to sinking streams (Ds); temporal variability (Tv); slope and vegetation (Sv); surface features (Sf). O factor: soil texture and thickness (Os); lithology and fracturing (Ol); confinement (Cn). P factor: rainy days (Rd); storm events (Se).	C · O · P	Intrinsic; resource and source**
Transit time	Travel path length to the final infiltration point in the valley (s); soils and lithology hydraulic conductivity (K); effective porosity (ηe); hydraulic gradient (∂h/∂l);	$s / (K/ \eta e \cdot \partial h/ \partial l)$	Intrinsic; resource
KAVA	O factor: overlaying soils (Os); overlaying karst features (Okf). I factor: Infiltration, slope and vegetation (Isv); groundwater depth (Igwd). A factor: hydrogeological and fracturing aquifer conditions (Ahg); tracing test (Att). P factor: precipitation.	(O + I + A) · P	Intrinsic; resource and source ***

* The C factor changes according to scenarios (C1= swallow hole catchment; C2= rest of the area).
** Source vulnerability is estimated by the addition of a karstification parameter.
*** For source vulnerability both Agh and Att parameters are included; for resource, only Agh.

The VURAAS method, similarly to the Time-Input method, was also developed for alpine karst areas. This approach evaluates three factors: input, infiltration, and exfiltration; the latter estimating the behaviour of the karst network, to obtain the vulnerability map (Cichocki and Zojer, 2007). VURAAS also performs risk mapping, merging both maps to obtain a final vulnerability index.

The Simplified Method proposed by Nguyet and Goldscheider (2006) is an option to perform vulnerability studies in areas where data is sparse. It requires minimum data to evaluate the function of overlying layers and flow concentration. The former segregates areas according to the permeability of the soil and its thickness in order to define the protective function. The latter analyses the dominant flow process in order to define how vulnerable different sections of the area can be. A further overlap defines vulnerability classes, which can be overlapped once more with a risk map to define protection zones.

The first application of the full European framework is presented by Andreo et al. (2006) in a test site located in Spain, where all elements proposed by the European framework were applied (intrinsic vulnerability, specific vulnerability, and risk mapping). After validation of the results from multi-tracer tests, the application of this approach demonstrates improvements in vulnerability mapping but there are still some limitations from a validation point of view.

The COP method is also derived directly from the European framework, with the goal to estimate resource intrinsic vulnerability (Vías et al., 2006). However, source intrinsic vulnerability is also assessed by the inclusion of the karst network into the analysis, thereby evolving into the COP+K method (Andreo et al., 2009).

The Slovene Approach (Ravbar and Goldscheider, 2007) is a modified COP method to fit characteristics of the Slovene karst; it adds some parameters not considered by the COP, such as temporal variability of swallow holes. The Transit-Time method defines vulnerability classes in relation with the groundwater travel time, with a special focus on the role of epikarst and high slopes promoting point infiltration (Brosig et al., 2008).

The KAVA method (Biondić et al., 2014) follows the European Framework analysing four factors: overlay protection, precipitation influence, infiltration conditions, and aquifer conditions. This method estimates source intrinsic vulnerability. The CI & Vi method (Butscher and Huggenberger, 2008) assesses intrinsic source vulnerability with a focus on karst springs by modelling the hydrological dynamics of karst in terms of the different flow characteristics.

2.4 Problems and limitations of the intrinsic vulnerability methods

Several classifications for the vulnerability methods have been presented by multiple authors according to the proposed analysis, evaluated process, statistics, or modelling used for vulnerability estimation (Magiera, 2000; Goldscheider, 2002; Dunne, 2004). Methodologies to estimate groundwater vulnerability vary in scale, scope, and concept.

A simple classification highlights three types of methodologies, being denoted as index methods, statistical methods, and process-based methods. Index methods analyse multiple natural characteristics of karst, designating numbers to reflect their influence on pollutant movement in order to obtain vulnerability classes (e.g., KARSTIC, EPIK, COP). Statistical methods utilize multiple analytical processes, such as regression analysis, weights of evidence, or simply descriptive statistics, to obtain predictions about vulnerability (e.g., FAVA). Finally, process-based methods rely on hydrological simulations to calculate water movement so that areas, where groundwater is more likely under pollution risk, can be identified (VULK and Vi & Cv).

Therefore, vulnerability can be estimated theoretically, quantitatively, semi-quantitatively, or analytically, with theoretically based methods being the most utilized. Although the availability of a large number of existing methodologies could be seen as a positive scenario when looking for alternatives, the differences among them in evaluative process, scale, and necessary data, can cause complications when trying to apply a vulnerability analysis.

Despite current methodologies being tested and validated in their respective areas of development, their application in other karst areas forever necessitates some adaptations. The continuous development of new or adapted methodologies arises to solve problems related to methods applicability in a given karst region, mainly due to the lack of available data. According to the literature review, the EPIK and COP methods seem to be the methodologies most utilized or adapted for vulnerability studies (Barrocu et al., 2007; Kovacic and Petric, 2007; Leyland and Witthüser, 2010; Tayer and Velásques, 2017; Bagherzadeh et al., 2018 among others).

The existence of multiple procedures for groundwater vulnerability assessment increases the uncertainty surrounding the methods' reliability, rendering decision making difficult in regard to which approach is more accurate to depict groundwater vulnerability for a potential area of interest. Moreover, some methods require a minimum amount of easily available data, while others need very complex information about the hydrology and hydrogeology of the area of interest. Therefore, method applicability is mainly linked to data availability.

2.4.1   Inconsistencies among intrinsic vulnerability methods

From comparisons between detritus and karst groundwater vulnerability methodologies applied in the same area, a mismatch of results regarding vulnerability outcomes has been demonstrated (Gogu et al., 2003; Vías et al., 2005). Although these differences were expected, as detritus and karst vulnerability methods differ on the hydrological and hydrogeological analysis, a mismatch was also found when vulnerability was evaluated with multiple methods focusing exclusively on karst (Figure 2.13). Several authors have reported these inconsistencies among methods regarding vulnerability classification (Ravbar and Goldscheider, 2009; Marín et al., 2012; Kavousi et al., 2018).
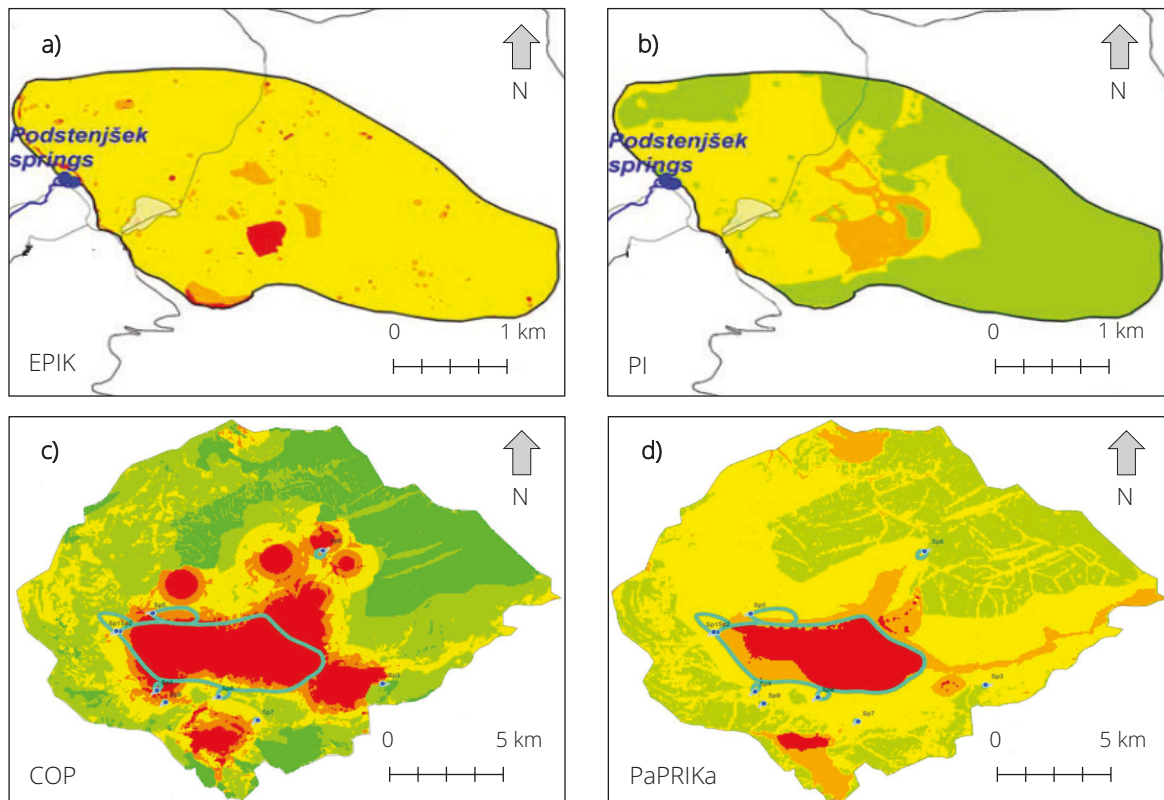
Figure 2.13: Inconsistencies in vulnerability classification among methods. In a) and b), Ravbar and Goldscheider (2009) compared results from the EPIK and PI methods in Slovenia; in c) and d), Kavousi et al. (2018) evaluated the application of the COP and PaPRIKa methods in the Dorfak karst region, Iran. Vulnerability maps are reproduced from their respective sources.

Uncertainty in karst groundwater vulnerability mapping is not only caused by the variety of existing methods complicating the selection according to appropriateness for purpose, but is also promoted though the difficulty of comparing results among the methods. Discrepancies in vulnerability estimations among methodologies derive from inconsistencies during the evaluation process. Some of the differences among the methods include the dissimilar number of used parameters, the classification and number of attributes, assigned values, and proposed weights (Figure 2.14).

When comparing Table 2.4, Table 2.5, and Table 2.6, such numerical differences are evident. Additionally, the authors' interpretation, regarding the hydrogeological behaviour of some parameters, profoundly affects groundwater vulnerability outcomes.
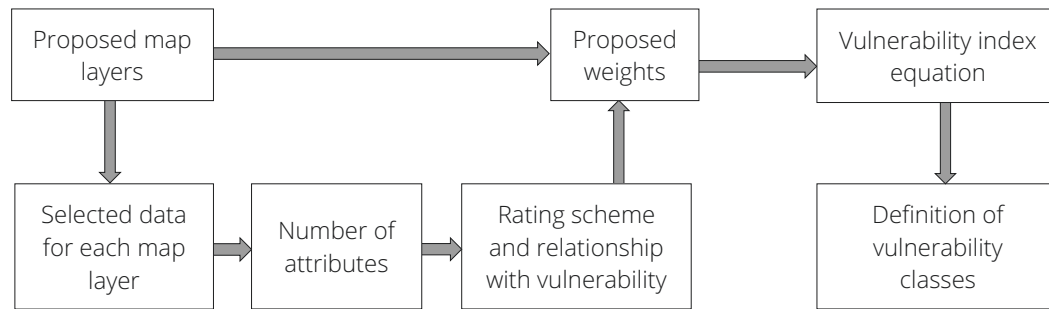
Figure 2.14: Steps to evaluate intrinsic groundwater vulnerability subject to discrepancy.

To highlight the previous statement, we can take the epikarst as an example since it is one important karst feature frequently presented as a parameter to estimate vulnerability. The effect and relevance of the epikarst for groundwater vulnerability can be ambiguous and highly subjective. If we analyse the epikarst role within the EPIK method, its effect is negative, increasing vulnerability because the allowance of infiltration through vertical shafts is expected (see Appendix A1).

An opposite point of view is found in the PaPRIKa method where epikarst is considered a protective feature, delaying infiltration and acting as a perched aquifer according to its hydrogeological function (see Appendix A4). Besides the uncertainty regarding the hydraulic function of a given parameter, the parameters' attributes classifications are also method-dependent; a situation that also leads to contradicting results.

Some of the methods meticulously state in their guidelines how attributes must be classified, mostly those attributes derived from a quantitative process such as spring flow data. Others, just briefly mention how to perform an attributes classification with ambiguous definitions and unclear classification schemes.

Either due to extremely explicit or very ambiguous definitions, uncertainties during the attributes' classification step will always be present. For example, the KARSTIC method proposes an attribute classification of high, moderate, and low for the map layer representing karstification. However, the guidelines do not specify how this characterization can be achieved. On the other hand, the PaPRIKa proposes values from spring hydrographs and chemographs in order to identify and evaluate karstification stages, according to Mangin's classification (Mangin, 1975).

In addition to the authors' intuitive interpretation about some attributes, the methods' area of development and validation is also influential. Some attributes classifications are highly dependent on the pre-established state or country guidelines. This is exemplified in Table 2.7 where two international classifications display how soil texture, as a vulnerability parameter, is affected.

Table 2.7: Differences in soil texture classification by country.

Content (%)			Soil texture classification		Assigned attribute rate	
Clay	Silt	Sand	*Germany (PI)	**USA (KARSTIC)	PI	KARSTIC
2.2	2.6	95.2	Pure Sands	Sand	25	9
16.0	19.2	64.8	Highly Loamy Sand	Sandy Loam	120	6
34.0	16.0	50.0	Clayey Sandy Loam	Sandy Clay Loam	160	4
29.5	38.5	32.0	Slightly Clayey Loam	Clay Loam	160	3
45.1	23.5	31.3	Loamy Clay	Clay	400	1

* Classification according to the German Bodenartendiagramm (soil chart).
** Classification according to the United States Department of Agriculture.

While the German soils textural diagram divides soil into thirty-one textural classes, as applied for the PI method, the KARSTIC methodology utilizes a soil classification according to the United States Department of Agriculture (USDA), classifying soils into twelve textural classes. Also, the influence of soils on vulnerability is evaluated differently for each method, either considering soil texture, thickness, a combination of both, or soil's hydraulic properties.

These are some of the inconsistencies among methodologies, which lead to contrasting results when methods are compared over the same karst area. Despite the evaluated natural characteristics being the same, their characterization differs numerically and subjectively. Currently, there is no standardization to classify either the used parameters to estimate vulnerability or the vulnerability classes. For the majority of the current groundwater vulnerability methods, the travel time from the release point to the resource or to a source, is the only evaluated characteristic used to define vulnerability. However, other parameters, which can also be influential to classify areas, cities, or wellfields as vulnerable or otherwise, are excluded from the analysis.

2.4.2 Limitations of the current intrinsic groundwater vulnerability concept

Despite maps derived from intrinsic groundwater vulnerability analysis having demonstrated their utility in protection zoning and groundwater strategy development, they do not consider the influence of anthropogenic activities. Solely analysing the travel time of a theoretical, immutable pollutant in a karst landscape, where human activities are already affecting the environment, could lead to erroneous assumptions regarding urban planning, groundwater extraction schemes, waste disposal, and other activities.

Therefore, two important characteristics that can play a fundamental role for groundwater vulnerability studies are the pollutant concentration and the residence time of such pollutants at a given point of the aquifer. Nevertheless, evaluation of multiple criteria to determine if a given source is vulnerable or not, complicates the analysis further because the judgement to identify one of these parameters as the most relevant can also be highly influenced by personal interpretation.

According to the hypothetical pollution scenarios displayed in Figure 2.15, groundwater sampling shows that the same pollutant, when released from two different locations, will affect a source (spring or well), but will display contrasting aspects. In scenario one, pollution from release point A displays a shorter travel time but a higher concentration and a longer residence time to reach the target in comparison with pollution from release point B. In this scenario, the three criteria, travel time, residence time, and concentration, suggest an undeniable worst-case scenario, derived from pollution released at point A.

In scenario two, however, pollution from both release points reaches the spring at the same time (similar travel time) but at different concentrations, while residence time is longer for pollution released at point A. Pollution scenario two reflects the uncertainty of intrinsic vulnerability methods that only estimate the travel time of a theoretical pollutant as vulnerability indicator. According to the analysis of the majority of groundwater vulnerability schemes based on the travel time of a pollutant, for scenario two, the area of influence for both release points must be categorized as a high vulnerability zone, ignoring pronounced differences in pollutant concentration and residence time.

Although the COST Action has proposed the inclusion of such parameters as vulnerability estimators, this ideal evaluation is hitherto complicated; no methodology exist to evaluate three or more different criteria to define groundwater vulnerability, consequently only one of these parameters is usually analysed. Addition of human-driven characteristics to evaluate the role of the pollutant concentration and its residence time as part of vulnerability studies is fundamental. Despite the complications, their inclusion is highly necessary in order to evaluate current scenarios where groundwater is already affected by anthropogenic practices.

Pollution scenario 1

Pollution scenario 2
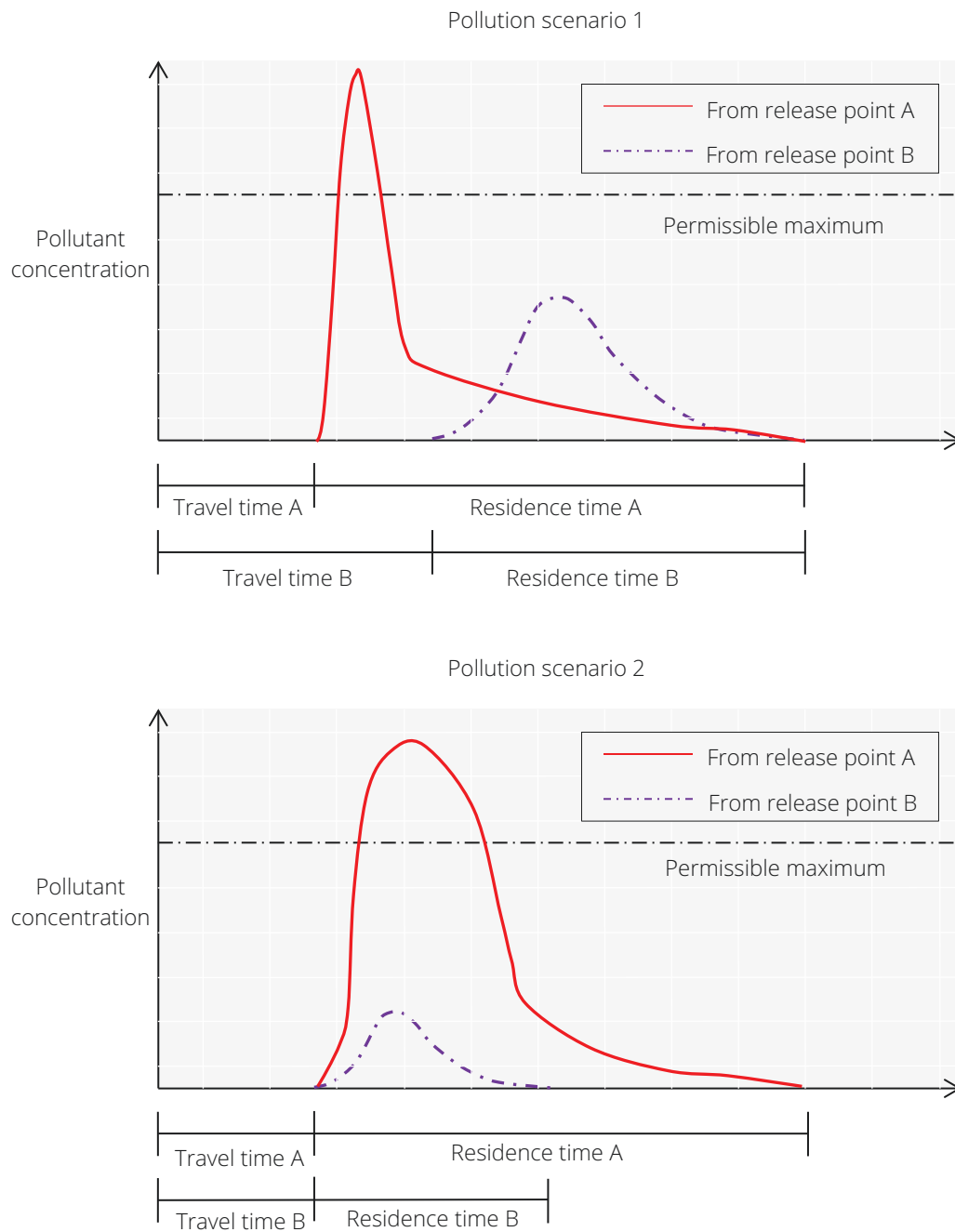
Figure 2.15: Uncertainty in evaluating travel time, residence time, and pollutant concentration. Modified after Brouyère (2003).

Before including more conditions into the analysis, it is necessary to minimize the subjectivity of current methodologies. Even though vulnerability mapping has proved to be an important tool for the management and planning of groundwater resources, their applicability is undermined by high subjectivity in the selection of a suitable method and the final vulnerability classification.

2.5 Chapter remarks and outlook

Karst aquifers are highly vulnerable to pollution given the intrinsic characteristics that allow fast infiltration of precipitation, which facilitates rapid, long-distance transport of pollutants released at the surface. Given the high heterogeneity and anisotropy in karst systems, specialized tools are necessary to develop protection strategies; one such tool is groundwater vulnerability mapping.

Although one goal of vulnerability mapping is to visually display results in an easily understandable format, data processing to classify the prescribed parameters during the evaluation processes requires specific knowledge of the hydrological and hydrogeological conditions of the study area. Since adaptations have always been needed, vulnerability assessment has remained as a continuously evolving scheme.

At present, some problems and limitations exist given the considerable number of proposed methodologies for groundwater vulnerability mapping in karst. Results usually display contrasting maps, increasing the uncertainty for the application of this tool. Additionally, the "intrinsic" approach does not consider other important parameters, such as pollutant concentration and pollutant residence time in a given section of the aquifer. These parameters can be highly beneficial for vulnerability mapping, especially in karst areas already affected by anthropogenic practices. Although an overall standardization is extremely complicated due to the high heterogeneity of karst, some steps can be modified to incorporate regional characteristics, data availability, and the anthropogenic influence over karst groundwater.

For this purpose, eight methodologies were applied as a starting point to evaluate the congruence among vulnerability maps and to study the applicability of methods in a selected study area. This was done with the goal of highlighting key parameters, to redefine their influence on resource vulnerability, and to find inconsistencies among the applied methodologies. The outcomes and analysis of the eight selected methods are presented in Chapter 3.

In order to evaluate how additional parameters can be included to consider the anthropogenic influence on groundwater vulnerability, a transport model was applied. The model was developed to represent the pollution generated from septic tanks in a highly populated karst area. The outcomes and analysis of the transport model, with focus on vulnerability estimation, are presented in Chapter 4.

3 Applicability of groundwater vulnerability methods in the Yucatan karst

This chapter is based on the following research articles:

Moreno-Gómez, M.; Pacheco, J.; Liedl, R. and Stefan, C. (2018). Evaluating the applicability of European karst vulnerability assessment methods to the Yucatan karst, Mexico. Environmental Earth Sciences 77:682.
doi: 10.1007/s12665-018-7869-5.

Moreno-Gómez, M.; Martínez-Salvador, C.; Moulahoum, A.-W.; Liedl, R.; Stefan, C. and Pacheco, J. (2019). First steps into an Integrated Karst Aquifer Vulnerability Approach (IKAV). Intrinsic groundwater vulnerability analysis of the Yucatan karst, Mexico. Water 11:1610.
doi: 10.3390/w11081610.

As presented in the previous chapter, several methodologies to estimate intrinsic groundwater vulnerability in karst have been proposed. One of the elements influencing the continuous development of vulnerability approaches arises because of the high complexity of karst systems in terms of karst development and hydrological response. When an estimation of vulnerability is needed, some decisions prior the application of one or more of the existing methods need to be taken.

The first judgement in order to perform a vulnerability analysis is the evaluation of the potential methods to be applied in the area of interest, after having defined the vulnerability type to be assessed (resource, source, intrinsic, or specific). The validation site of an existing method can be taken as a decisive aspect in regard to the purposes of a given work. For example, if we want to estimate intrinsic source vulnerability in a mountainous karst area, it is more comprehensible to consider the VURAAS method instead of the COP approach. This decision is sensible because the former method was developed and validated in an alpine karst area, while the latter deals with vulnerability in more general terms. However, despite this first filtering, several methods may still be suitable to be applied for the purposes herein or may be impractical due to data availability or scale.

With multiple methods yet possible, the next resolution focuses on method selection. It is critical to recognize that each method has its own considerations and, therefore, maintain high subjectivity regarding the hydrological behaviour and the relevance of their parameters. Although most of the methods have been tested, either in the field by tracer tests or by comparison with other methods by spatial autocorrelation, their application in a karst area, other than those where they were developed, is always a laborious effort. The high complexity of karst means that it is always necessary to include some degree of adjustment, since several aspects need to be reconsidered.

Previous studies have shown that the evaluation of two or more methodologies in the same area will always display contrasting results. Nevertheless, comparison between methods can serve to highlight important parameters to be considered in further research. Part of the analysis corresponds to map layer sensitivity, which is used as a helpful tool to investigate the degree to which each parameter influences vulnerability results. Nevertheless, either from its effect on the vulnerability index or by the study area percentage affected by a parameter removal, sensitivity serves to highlight the importance of such parameters without presenting a detailed guideline about how to perform parameter or weight adjustments based on sensitivity analysis results.

To investigate the feasibility and propose a base for a new integrated process to estimate groundwater vulnerability in karst, it is necessary to evaluate how applicable and consistent the available methods are among each other. Estimating the applicability and congruence of the existing vulnerability methods within a given study area and its regional features is a key step to better understand a parameter's role, to redefine mistaken vulnerability evaluation processes, and to highlight possible improvements in vulnerability studies.

In this work eight groundwater vulnerability methods were selected and applied to our study area; the selected methods are further explained in section 3.2.1. Since most of the current methodologies for karst groundwater vulnerability were developed and tested in European karst areas, the study area selected for this work presents a very interesting challenge due to their contrasting natural characteristics. The Mexican state of Yucatan, part of the Yucatan Peninsula, was selected to perform vulnerability studies in this research.

3.1 The Yucatan Peninsula

The Yucatan Peninsula is an emerged limestone platform with an area of 165,000 km^2. The Peninsula is located in the south-east of Mexico and includes northern parts of the Centro-American countries of Belize and Guatemala (Figure 3.1). According to Weidie (1985), the Peninsula is formed by limestone, dolomites, and evaporites with thicknesses reaching up to 1,500 m. Rocks at the surface correspond to northward sequences from the Upper Cretaceous to Holocene epochs (Butterlin, 1958; Bonet and Butterlin, 1962; López-Ramos, 1975).

The Yucatan Peninsula is defined as a karst area containing dissolution cavities near the surface and below the water table. Large conduit systems, where groundwater flow is turbulent, are present, however, no detailed mapping of conduit system extension and its connectivity exists for the whole area. Fractures and regional faults are also present in the Peninsula ranging in extent from metres to kilometres (km) and acting as preferential pathways for water flow. Other karst regional expressions are dolines, which are dispersed in the Peninsula but show dominance in areas of low relief.
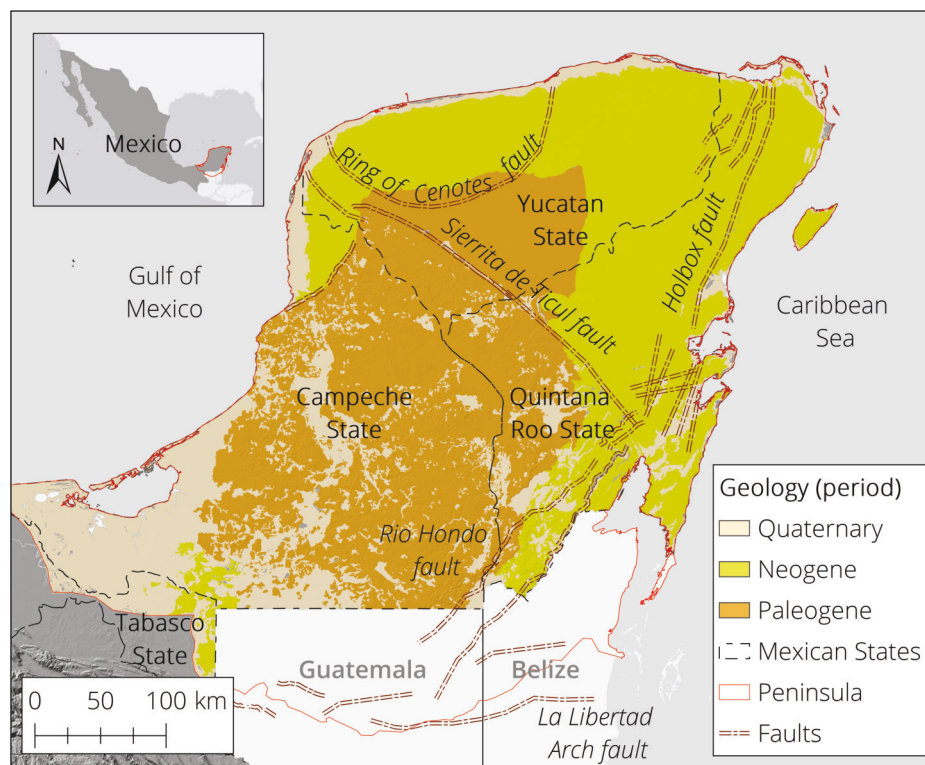
Figure 3.1: The Yucatan Peninsula's geology and regional faults. Peninsula limits according to Vinson (1962) and López-Ramos (1975) as presented by Bauer-Gottwein et al. (2011). Map elaborated from geology datasets, publicly available from the National Institute of Statistics and Geography (INEGI, 1984).

Being a coastal area, seawater intrusion is present intruding up to 110 km inland (Perry et al., 1995; Steinich and Marín, 1996). Therefore, groundwater is defined as a lens of freshwater with a variable thickness floating over saline water. The geological and topographical settings of the Peninsula do not allow runoff generation, with the exception of the southern limits where the rivers Usumacinta and Belize act as natural drains. The lack of surface streams and terrain-level springs leave groundwater as the only source for freshwater supply in the region (Marín et al., 2000).

3.1.1 Study area

The Yucatan State (hereinafter Yucatan) is one of the 31 states forming The United Mexican States and is the area of interest for this research. It covers an area of about 39,500 km^2; 2% of the Mexican territory representing around 23% of the Yucatan Peninsula. Yucatan is located in the south-east of Mexico with latitude 21° 36' north, 19° 32' south and longitude 87° 32' east, 90° 25' west. The Yucatan's geographic boundaries are the Gulf of Mexico in the north and the Mexican states of Campeche and Quintana Roo in the west and the east, respectively.

Yucatan is generally characterized by its geomorphology, defining the north as a plain with gentle slopes and a high number of depressions, while the south is denoted as an area with plains and hills where slope increases progressively (Lugo-Hubp and García, 1999). Administratively, Yucatan is divided into four hydrogeological regions: the Coastal Area, the Inner Cenote Ring, the Central Plain, and Valleys and Hills (SARH, 1989). The strata in Yucatan are mostly from the Cretaceous and Quaternary periods. The strata from the Upper Cretaceous to Oligocene epochs (Paleogene system) are located in the hill area and the southern part of Yucatan, while strata from the Miocene to Pleistocene epochs (Neogene system) are found in the Yucatan plain (López-Ramos, 1975); younger deposits from the Holocene epoch are found parallel to the coastline (see Figure 3.1).

In Figure 3.2, a digital elevation model (DEM), shows that most of the Yucatan area is a nearly flat plain where elevation is variable, ranging from centimetres along the coastline, gently increasing southward, reaching approximately 40 metres asl at the base of the Valleys and Hills region; this area is located approximately 80 km from the northern coastline (Doehring and Butler, 1974). The hill area, named "Sierrita de Ticul", reaches an elevation of 204 metres asl (Lesser and Weidie, 1988); the origin of the hill is considered to be the result of tectonic activity (Isphording, 1975).

3.1.2 Karst features in Yucatan

Yucatan is a karst area with primary and secondary porosity, whilst joints and fractures have developed a tertiary porosity consisting of conduit systems with diameters varying from centimetres to metres (Bauer-Gottwein et al., 2011). Two regional faults are located in Yucatan, the Sierrita de Ticul fault and the Cenote Ring fault. The former sets the limit between the Central Plain and the Valleys and Hills regions, whereas the latter is well-marked as the boundary of the Inner Cenote Ring (see Figure 3.1).

Fissures are also present in the region; according to public maps, fissures vary in length with minimum and maximum values of 73 m and 31 km, respectively. As displayed in Figure 3.3, a total of 926 fissures are mapped in Yucatan with an average length of about 460 m. The Valleys and Hills area and the north-eastern Central Plain are the locations that display a particularly high fissure density.

Dissolution has also created depressions, caves, and other karst features, with dolines being the most noticeable karst expressions in the area. Dolines are dispersed within Yucatan showing predominance in the Central Plain in comparison with the Valleys and Hills area and the Inner Cenote Ring. Dolines are locally named "Cenotes" when they expose phreatic water, the occurrence of which is high due to the shallow water table.

Figure 3.2: Elevation and hydrogeological division of Yucatan. Map elaborated from the Advanced Spaceborne Thermal Emission and Reflection Radiometer, Global Digital Elevation Model, version 3, resolution of 30 m (NASA, METI, AIST, Japan Spacesystems and U.S./Japan ASTER Science Team, 2019).
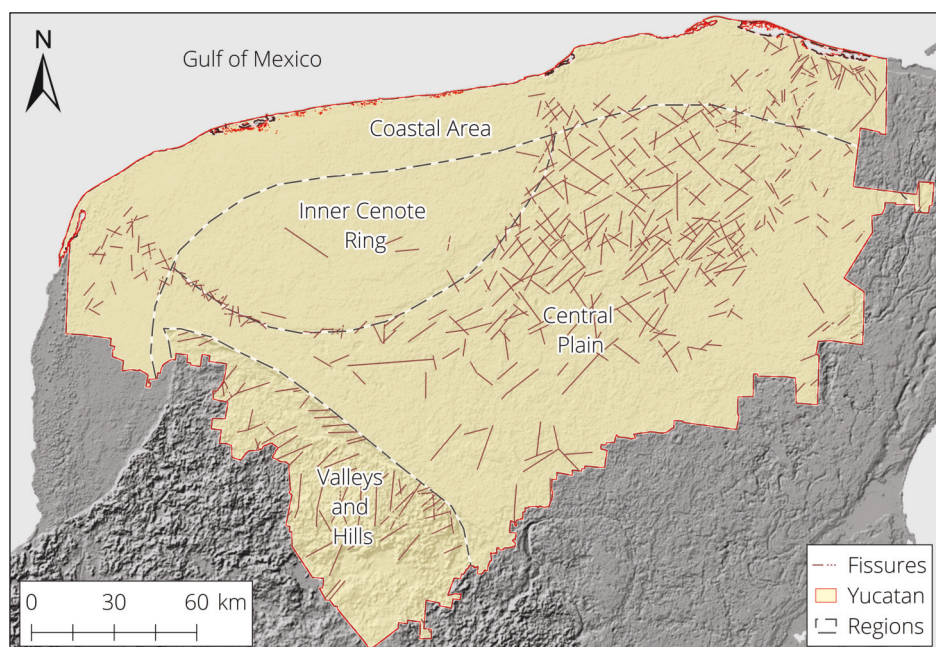
Figure 3.3: Fissures distribution in Yucatan. Map elaborated from geologic datasets, publicly available from the National Institute of Statistics and Geography (INEGI, 1984).

Doline spatial location and density is variable; distances between dolines range from several dolines within a single square kilometre to several kilometres between them (Escolero et al., 2002). Two areas are highlighted for their high doline density, according to contour maps at a scale of 1:50,000: the north-eastern Central Plain and the "Cenote Ring". In public datasets, some water bodies, subclassified as perennial or intermittent according to their temporal water exposure, are further classified as dolines by morphometry (Figure 3.4).
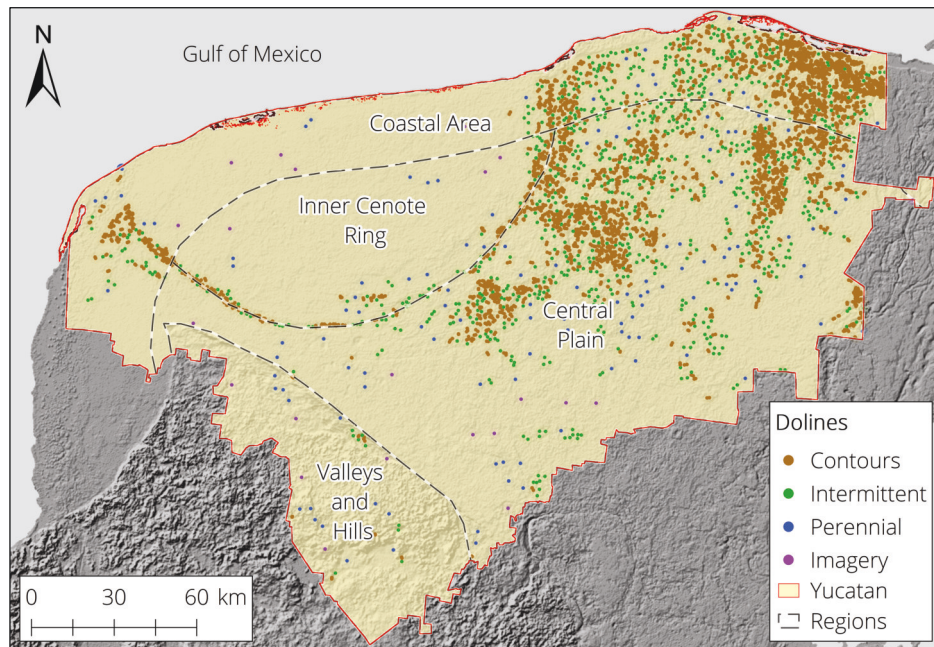
Figure 3.4: Dolines distribution in Yucatan. Doline map elaborated from topography datasets (contours) at a scale of 1:50,000, publicly available from the National Institute of Statistics and Geography (INEGI, 2015). Dolines located by imagery analysis are also included.

Doline formation in the north-eastern Central Plain is associated with cave collapse and sea level variations, where seawater has, presumably, acted as the triggering agent for the dissolution of the shallow limestone, resulting in high doline development (Hanshaw and Back, 1980; Lugo-Hubp et al., 1992).

The Cenote Ring is a semi-circular belt with high doline density showing a well-marked alignment. This belt is variable throughout its area, ranging from 5 to 20 km wide (Marín, 1990; Pope et al., 1991). The ring highlights the boundary of the Inner Cenote Ring, also named the Chicxulub impact crater; a sedimentary semi-circular area of about 180 km of diameter (Hildebrand et al., 1995). This crater is the result of an asteroid impact at the end of the Cretaceous period (Hildebrand et al., 1995; Perry et al., 1995).

Unlike the north-eastern doline field, the genesis of high doline density in the belt is not clear but their development is associated with breccia collapse or the differing lithological compaction of the sedimentary basin (Perry et al., 1995). Dolines located at the Cenote Ring can be classified as underprinting dolines according to the classification proposed by Sauro (2016). Throughout the state, the dolines' morphometric attributes show variations in their diameter ranging from 10 to 500 m and depths from 2 to 120 m (Hall, 1936; Gaona-Vizcayno et al., 1980). Other depressions exist with diameters of up to 100 m and depths reaching up to 15 m. These depressions, known as "Aguadas", act as natural rainwater ponds and have poor connectivity with the Yucatan aquifer (Gaona-Vizcayno et al., 1980).

The latest depression classification of the Yucatan area was performed based on topographic maps (contours) at 1:50,000 scale that are publicly available from the National Institute of Statistics and Geography (INEGI) through its open-source server. Applying a morphometric classification, Aguilar et al. (2016) defined 4,620 dolines, 2,021 uvalas and 76 poljes in Yucatan. However, a new semi-automatic multi-depth threshold approach (MDTA) for doline mapping, tested in a 625 km^2 area in north-eastern Yucatan, has demonstrated the underestimation of dolines by contour maps.

Moreno-Gómez et al. (2019a) presented a study where a total of 665 dolines were semi-automatically mapped using this method, with sensitivity and precision values of 85% and 71%, respectively after comparison with dolines located by visual inspection of high-resolution imagery (0.3 m resolution). Results from this study demonstrated the underestimation of dolines derived from contour maps in the MDTA study area, since the area displays just 144 dolines from contours against the 665 mapped by the MDTA; an approximated difference of one doline per square kilometre. This underestimation is expected across the whole Yucatan area. This is significant because doline mapping plays a fundamental role in several studies, such as land use planning, subsidence risk, and groundwater vulnerability (Gutiérrez et al., 2008; Fleury, 2009; Theilen-Willige et al., 2014).

3.1.3   Hydrology

Groundwater is generally shallow with hydraulic gradients gradually increasing southward. Levels are varying from centimetres at the coast to approximately 30 metres asl in the south (Figure 3.5). This low hydraulic gradient in the plain region, with values ranging from 7 to 10 mm/km, suggests a high hydraulic conductivity (Marín, 1990). A general groundwater flow model of Yucatan displays flow in a south-east to north-west direction with the Cenote Ring acting as a groundwater divide due to its higher hydraulic conductivity (Marín, 1990; Steinich and Marín, 1997). Nevertheless, the model presented by González-Herrera et al. (2002) does not support the idea of the Cenote Ring influencing groundwater flow, proposing a radial groundwater movement from inland towards the coast due to the Peninsula characteristics. A more detailed description of groundwater models, previously applied in Yucatan, is presented in section 4.3.
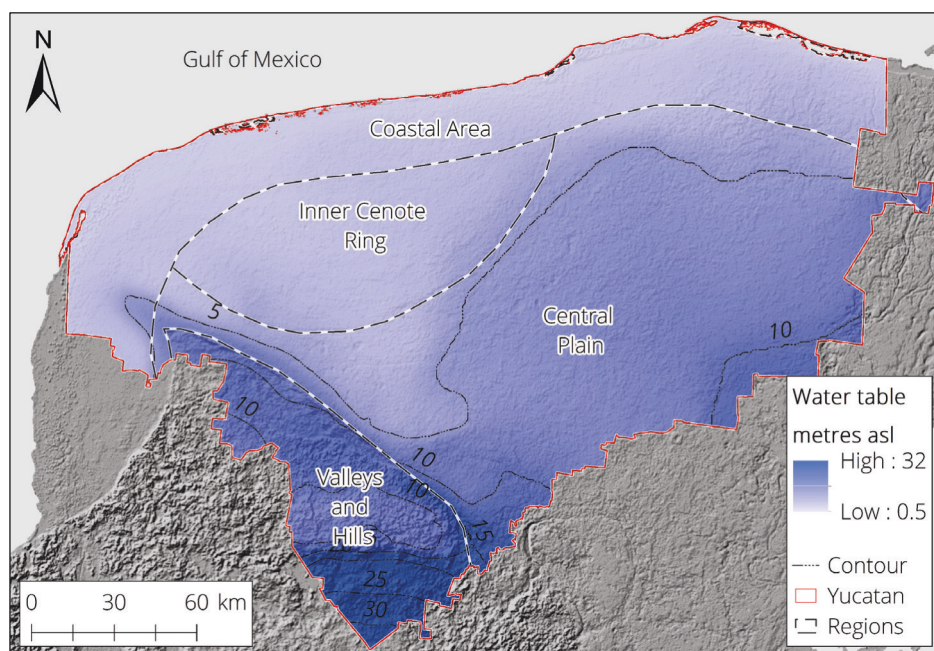
Figure 3.5: Mean groundwater elevation in Yucatan. Map elaborated from a water table contour map presented by the Ministry of Agriculture and Hydraulic Resources (SARH, 1989).

The National Water Commission (CONAGUA) has reported mean precipitation values for Yucatan ranging from 1,100 mm to 1,400 mm per year (CONAGUA, 2015a; CONAGUA, 2015b). Precipitation varies spatially, displaying a distinctive pattern; lower precipitation volumes are recorded in the north-west coastal areas where the stations' average gauge is around 400 millimetres per year (mm/y); precipitation increases in a south-easterly direction, with precipitation values of around 1,600 mm/y, as measured by stations located at the southern limits of the state (Figure 3.6).
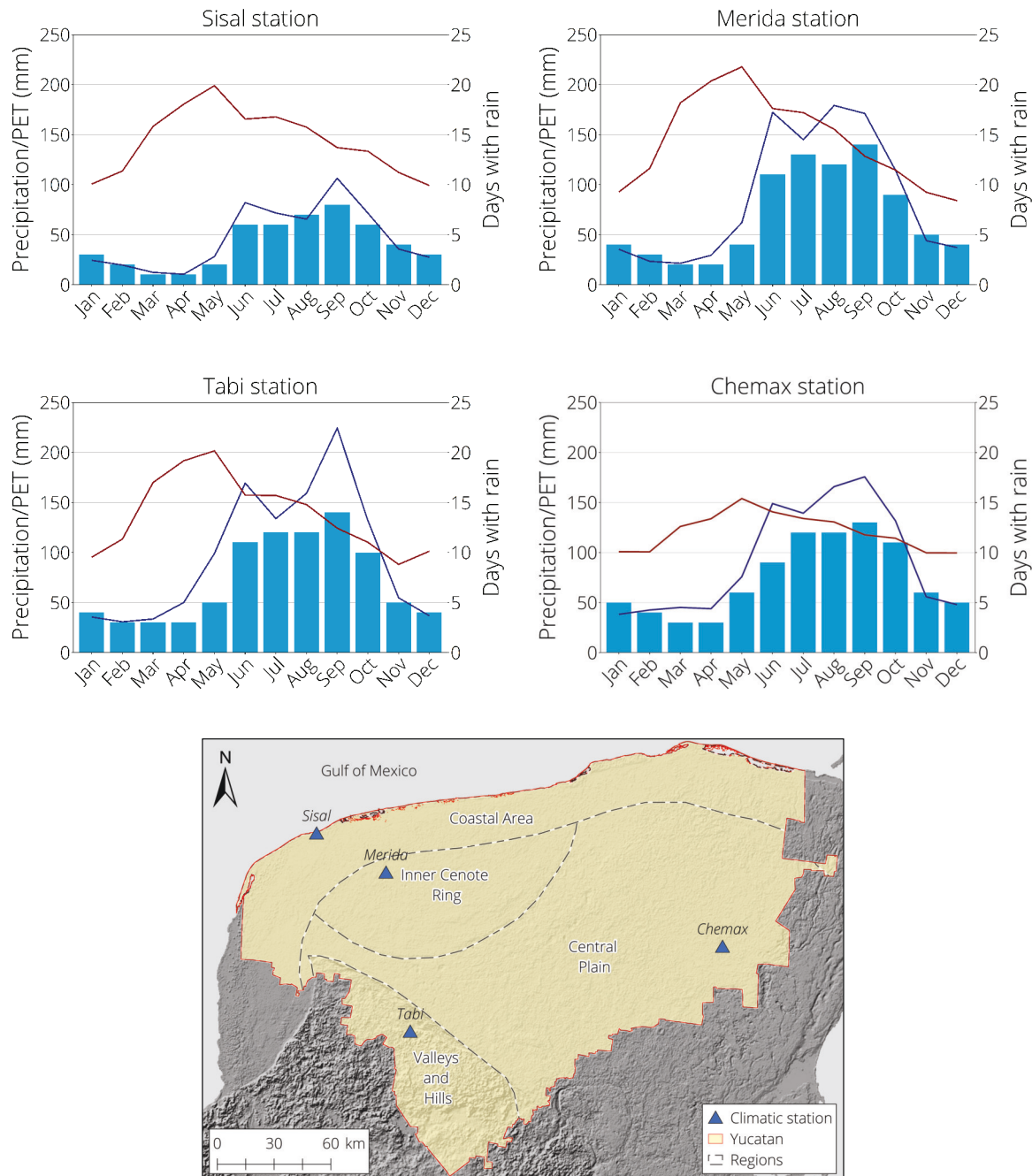
Figure 3.6: Data from climatic stations representing the four hydrological regions. Blue lines indicate precipitation and red lines potential evapotranspiration; blue bars represent days with rain. Graphics elaborated from daily climate data from the Climate Computing project (CLICOM) of the National Meteorological Service (SMN) through the Ensenada Centre for Scientific Research and Higher Education, Baja California (CICESE) web platform (SMN, 2017).

As a tropical zone, Yucatan has well marked seasonal precipitation regimes. The wet season takes place from May to October, with tropical storms supplying almost 90% of the total precipitation during this season. The dry season takes place from November to April; however, some precipitation events are present during the months of December and January. According to data gathered from 65 climatic stations dispersed across Yucatan, a regional average of 80 days of rain per year is estimated. Monthly distribution of high-precipitation days closely follows precipitation patterns of dry and wet seasons. The coast experiences less days with high precipitation and less precipitation overall than the southern areas, resulting in a regional homogeneity regarding average precipitation intensities. It is important to mention that Yucatan experiences extreme events, such as tropical storms and hurricanes, that generate huge amounts of precipitation; this also occurs seasonally from May to November.

Villasuso and Méndez (2000) estimate a mean annual regional temperature of 25 degrees Celsius (°C), reaching a minimum value of 13 °C in January and a maximum of 39 °C in August. Average potential evapotranspiration (PET) in Yucatan is estimated as 1,236 mm/y; with minimum and maximum values of 1,050 mm and 1,400 mm, respectively, as reported by water authorities (CONAGUA, 2015a; CONAGUA, 2015b). However, PET also displays a regional gradient from the north-west to the south-east, ranging from 850 to 1,600 mm/y, decreasing towards the south and the east coast (Bauer-Gottwein et al., 2011).

Actual evapotranspiration (AET) was calculated from remote sensing data to range from 350 to 2,500 mm/y (Gondwe et al., 2010). There exists spatial variability within PET and AET; the latter shows higher values near the coastline in contrast with dry zones where vegetation is sparse (Gondwe et al., 2010); high AET values are close to those of PET near the coast, where shallow water tables are expected to influence such outcomes.

Regarding the water balance of the region, estimations suggest high evapotranspiration rates ranging from 90% to 95% of precipitation. Villasuso and Méndez (2000) calculated the water balance for the entirety of the Yucatan Peninsula, defining 80% of the mean annual precipitation as evapotranspiration; the remaining 20% is accounted for by infiltration and zero runoff. Although infiltration does not occur homogeneously, no spatial discretization for infiltration was found in the literature. Due to the flat topography and considerable karstification, no surface runoff is generated and precipitating water, that is not affected by evapotranspiration, directly infiltrates, thereby recharging the aquifer.

3.1.4 Land cover

Yucatan soil maps are displayed according to edaphology since soil data, in terms of texture, is sparse. This classification takes into account soil horizon development, soil material, and other properties, with a focus on the soils' process of formation. Mexican edaphology maps are based on the current World Reference Base (WRB), which was established according to previous works presented by the Food and Agriculture Organization of the United Nations (FAO) and the United Nations Educational, Scientific and Cultural Organization (UNESCO) in 1971 (IUSS Working Group WRB, 2015). The WRB classifies soils into 32 Reference Soil Groups (RSG) according to soil conditions and soil forming factors. It also includes a second classification level, taking RSG characteristics as the foundation, with the addition of auxiliary attributes. In this work, Yucatan soil maps are displayed based solely on RSG. From the analysis of edaphology maps, Yucatan displays 12 RSG (Figure 3.7).

The main soil class in Yucatan is Leptosol, covering an area of 23,000 km^2; more than 50% of the state. Following the WRB definition, Leptosols mostly overlie rock strata, carbonates or other soils with a high stone content (gravelly soils), which are close to the surface. Therefore, Leptosols are generally shallow ($\leq$ 25 cm), thereby allowing percolation. The extent of the area over which Leptosols are present displays agreement with regional characteristics, in terms of soil thickness, since Yucatan is regionally considered, as an area with thin or absent soils with constant limestone outcrops. However, outcrops in the region are not mapped; this overestimates soils covering the whole area.
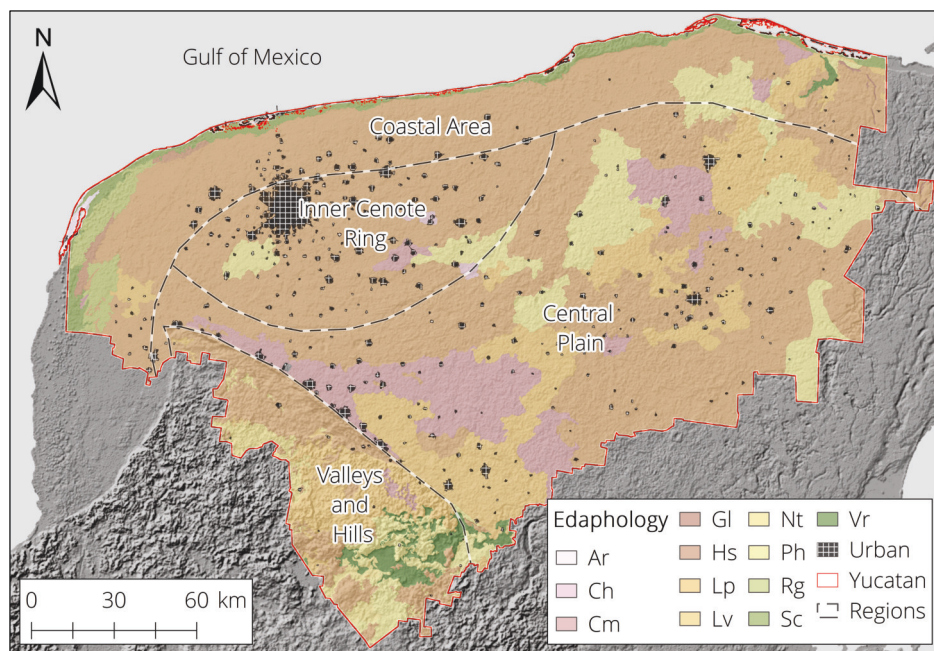
Figure 3.7: Yucatan edaphology map. Corresponding RSG are: Arenosol (Ar); Chernozem (Ch); Cambisol (Cm); Gleysol (Gl); Histosol (Hs); Leptosol (Lp); Luvisol (Lv); Nitisol (Nt); Phaeozem (Ph); Regosol (Rg); Solonchak (Sc); Vertisol (Vr). Map elaborated from edaphology datasets, publicly available from the National Institute of Statistics and Geography (INEGI, 2007).

Leptosols are mostly present on low relief areas like the Inner Cenote Ring and the Central Plain. Nonetheless, they have also been discovered, in a lower percentage, in the hill area where Luvisol is predominant. A recent study presented by Estrada-Medina et al. (2016) focuses on Yucatan Leptosols and the differences that this soil type displays in relation to edaphology and soil bacterial community. This study presents important information regarding Leptosols' characteristics in accordance with location; when located on the plains, a red Leptosol that is rich in hematite, predominates, whereas a black Leptosol is found on hills and has a higher organic matter content.

Other important soils, in regard to their spatial extent, are Luvisols, Phaeozems, and Cambisols, covering approximately 5,000 km^2, 4,000 km^2, and 3,000 km^2, respectively. Luvisols are reddish fertile soils with a high clay content reaching a thickness of up to 100 cm. They cover most of the hill area but are also found in the Central Plain, with a low presence in the Coastal Area and absent in the Inner Cenote Ring. Their hydrologic characteristics are high water retention and an elevated cation exchange capacity.

Phaeozems are located in low relief areas and part of the hill area; these soils are rich in organic matter at the top with a structure of soil particles bound by calcium ions. Phaeozems are permeable with a thickness reaching more than 100 cm, which makes them excellent soils for the cultivation of pasture and some grains such as wheat. Cambisols are also adequate soils for agriculture due to their mineral content and aggregated structure mostly formed by sandy loam; this soil type is found on the Central Plain representing 7% of the Yucatan area.

Each one of the remaining soil types have areal extents of less than 1,000 km^2. However, it is important to note that some soil types are located in specific hydrogeological regions, such as Regosols and Solonchaks, which are present near the coast. Yucatan soils have been widely studied in terms of geomorphology, geochemical, and mineralogical characteristics in the works of Bautista et al. (2004), Cabadas et al. (2010), and Bautista et al. (2011).

From land-use and vegetation maps (series V from INEGI), the main land cover characteristics of Yucatan were defined and modified according to land-use definitions used by the United States Geological Survey (USGS). A simplified version, displayed in Figure 3.8, shows the predominance of upland forest, grasslands, and lowland forest, covering approximately 60%, 18%, and 8% of the Yucatan state, respectively.
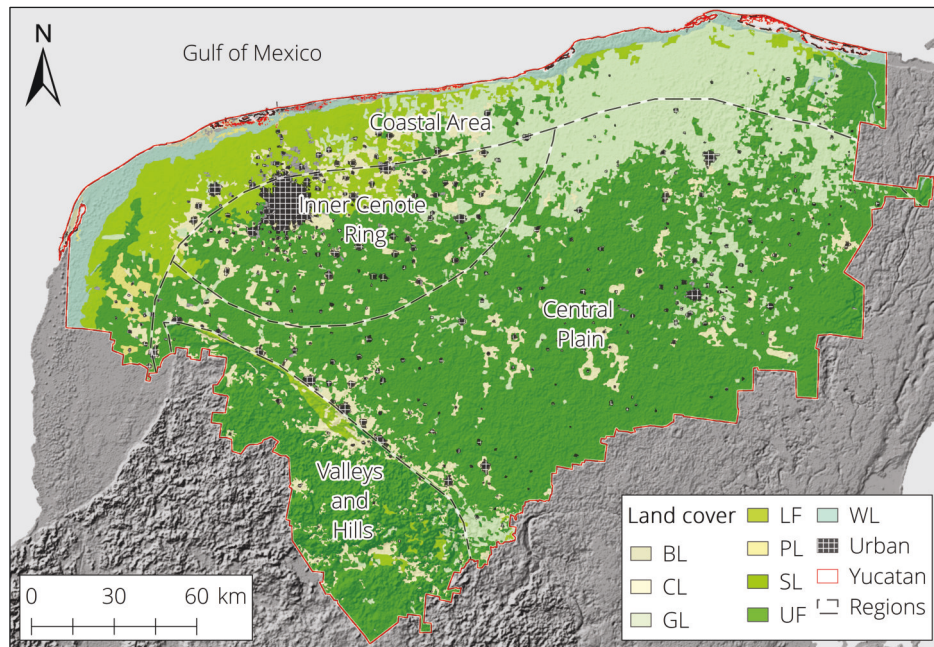
Figure 3.8: Yucatan land cover map. Categories, established by INEGI and adapted to USGS groups, correspond to: barren land (BL); cultivated land (CL); grass land (GL); lowland forest (LF); pasture land (PL); shrub land (SL); upland forest (UF); wetland (WL). Map elaborated from vegetation data sets publicly available from the National Institute of Statistics and Geography (INEGI, 2013).

Upland forests are located in areas where mean annual precipitation fluctuates from 700 to 1,600 mm/y. Foliage retention for upland forest in the region is variable, with vegetation being categorized either as evergreen or deciduous. This type of vegetation reaches heights from 15 to 30 m. Despite soils in Yucatan being generally thin, deciduous vegetation provides a good amount of organic matter to cover the soil when vegetation loses foliage.

Grasslands are mostly found in the north-east, where a combination of low slopes and thin soils are subject to seasonal flooding during the wet season. Vegetation in these areas ranges between 3 and 6 m in height and also includes halophytic vegetation in locations close to the coastline where soils have a high salt content. Lowland forest is located in the north-west, where mean annual precipitation is lower in comparison with upland forest. Vegetation in this area ranges between 2 and 5 m in height. The geomorphic characteristics for this land cover type are low slopes, that are prone to some degree of flooding during the wet season, with a well-defined dry season.

Wetlands are located along the coastline where the area is constantly flooded or soils allow water stagnation. Mangroves are present, growing up to 30 m in height. Other types of vegetation cover small portions of Yucatan, for example, shrubs or vegetation present in sand dunes.

3.2 Material and methods

3.2.1 Selected groundwater vulnerability methods

From the evaluation of current groundwater vulnerability methodologies and the available data sets of the study area obtained from multiple public sources, a filtering of applicable and non-applicable methods was performed. A total of eight groundwater vulnerability methods were selected to estimate intrinsic resource vulnerability in Yucatan, these being: EPIK, COP, PI, PaPRIKa, KARSTIC, RISKE, DRISTPi, and the Slovene Approach (hereinafter SA). Data availability was the key factor in choosing the methodologies applied here (Table 3.1).

Table 3.1: Data utilized to create map layers for the eight applicable methods in Yucatan.

Map layers	DRISTPi	KARSTIC	RISKE	SA	PaPRIKa	COP	PI	EPIK	Base data
Soil thickness			X	X	X	X	X	X	Borehole data [a]
Soil texture	X	X	X	X	X	X	X		Borehole data [a]; edaphology maps [a]
Lithology	X	X	X	X	X	X	X		Lithology maps [a]
Fracturing	X	X	X	X	X	X	X		Fissures map [a]
Unsaturated zone (depth)	X	X		X	X	X	X		DEM [b]; water table [a]
Epikarst			X		X		X	X	Dolines map [a]
Confinement			X		X				Literature review
Slope	X	X	X	X	X	X	X	X	DEM [b]
Vegetation			X		X	X	X		Land use and vegetation maps [a]
Karstification		X	X	X	X	X	X	X	Dolines/fissure maps [a]
Rainfall volume			X		X				25 years of historic data [c]
Rainfall intensity			X		X				25 years of historic data [c]
Recharge	X	X				X			Precipitation [c]
Surface features						X			Dolines and fissures maps [a]
Effective field capacity						X			Settled with minimum values
Hydraulic conductivity (soil)						X			Borehole data [a], Saxton equations
Hydraulic conductivity (aquifer)		X							Not applicable in this study.
Rock reservoir		X	X		X				Not applicable in this study.

a Data publicly available at https://www.inegi.org.mx/temas/topografia/.
b Digital Elevation Model (ASTER GDEM, 30 metres resolution) from https://earthexplorer.usgs.gov/
c Data publicly available at http://clicom-mex.cicese.mx/.

Application of the selected methods in the Yucatan karst was carried out following the methods' own guidelines as closely as possible. The goal for taking this approach was to evaluate how congruent these methods are, which were developed and validated in several karst areas in Europe and in the United States, to display agreement on groundwater vulnerability and the unique characteristics of the Yucatan karst. Nevertheless, some of the selected methods include parameters directly related with the saturated zone's behaviour, influencing the horizontal movement of a pollutant and, therefore, estimating source groundwater vulnerability.

Since this part of the study focuses solely on the evaluation of resource vulnerability, some slight modifications were made for methods that include aquifer lateral effects. For these methods, parameters characterizing the aquifer water flow were neglected and their weights were redistributed on a percentage basis (see KARSTIC description in section 3.2.1.6).

3.2.1.1   The EPIK method

EPIK is a multi-parametric system model of the point count system type. It was developed to delineate protection zones in catchment areas considering four parameters depicting karst intrinsic characteristics (Dörfliger et al., 1999). Epikarst development (E), protective cover as soil thickness (P), infiltration conditions as slope (I), and the degree of karstification (K) are analysed to define protection zones (or vulnerability classes) at catchment scale.

The EPIK indirectly characterizes epikarst development from its association with surface features like dolines and fractures. The protective cover proposes solely soil thickness as a parameter to evaluate vulnerability due to the lack of soil texture data on the EPIK area of validation. However, it does take into account the permeability of the geological sub-surface.

The depth of the vadose zone is not considered as a relevant feature since the method focuses on point infiltration catchment areas. The infiltration parameter displays a relation to the slope, in percentage, together with land cover and cultivated fields. Since the EPIK method focuses on catchment areas promoting point infiltration, it evaluates steeper slopes as promoting runoff, hence, increasing vulnerability.

The degree of karstification is defined from the size and connectivity of conduits, either from direct identification of swallow holes, dolines, and caves, or by indirect methods such as spring flow hydrographs and tracer tests. Each parameter is classified on a discrete basis in relation to its attributes, with assigned values ranging from 1 to 4 (see Appendix A1). Weighting factors are used to heighten the influence of each parameter on the travel time of a theoretical pollutant. The EPIK vulnerability index is calculated according to:

$$V_x = E_x (3) + P_x (1) + I_x (3) + K_x (2) \qquad\qquad (3)$$

where V_x is the vulnerability index of a map grid x. E_x, P_x, I_x, and K_x are the values of epikarst, protective cover, infiltration, and karstification assigned at the given grid according to the attributes' classification. The numbers inside brackets are the weights proposed by the author. Finally, vulnerability classes are assigned according to the specified ranges of the vulnerability index.

3.2.1.2   The PI method

The PI method estimates resource intrinsic vulnerability, analysing two main factors denoted as protection cover (P) and infiltration conditions (I), with each one consisting of a grouping of single parameters (Goldscheider, 2005). The P factor aims to estimate vulnerability by considering the array of elements affecting solely the vertical movement of water. Parameters influencing the vadose zone response according to this method are the effective field capacity (eFC) of the topsoil (T), soil texture (S), lithology (L), and fracturing (F).

The thickness of the soil cover and the lithology layers are elements also included in the estimation of vulnerability. Recharge (R) is classified according to established values in millimetres per year. Artesian pressure (A) is also considered; in case of occurrence, a unique value of 1,500 is assigned to this parameter.

The I factor estimates the capacity of the surface conditions to by-pass the vadose zone by generating surface flow towards karst features such as swallow holes and streams. This factor evaluates the function of the slope, soil hydraulic conductivity, and vegetation in generating surface and sub-surface runoff. For parameters in P, values are assigned from a rating point scheme while a dependent matrix system is used for those parameters forming the I factor (see Appendix A2). Vulnerability is then first estimated by the protective cover as:

$$P_x = [T_x + (\sum S_x \cdot m_x + \sum L_x \cdot F_x \cdot m_x)] \cdot R_x + A_x \tag{4}$$

where P_x is the protective function index of the map grid x; T_x is the topsoil protection value assigned according to its eFC; the S_x, L_x, and F_x are the values assigned corresponding to soil texture, lithology, and fracturing, respectively; m_x is the thickness (in metres) of each soil or lithology layer located in the vadose zone and R_x and A_x represent the values for recharge and artesian pressure. The protective function index is divided according to ranges displayed in Table 3.2 to obtain the P factor.

Table 3.2: Index of the protective function and the final P factor value. Notice that this method estimates protectiveness. Table reproduced from Goldscheider (2005).

Protective function (P_x)	Effectiveness of the protective cover	P factor
0-10	very low	1
>10-100	low	2
>100-1000	medium	3
>1000-10000	high	4
>10000	very high	5

Having defined the protection capacity of the area according to the characteristics of the vadose zone, the next step focuses on analysing to which extent these protective features can be by-passed. The score correspondent to the I factor is obtained by a continuous matrix approach as displayed in Appendix A2. This process follows an "if-then" condition to assign values for defined combinations according to slope, vegetation, and soil hydraulic conductivity. The final vulnerability index is then obtained from:

$$V_x = P_x \cdot I_x \tag{5}$$

where V_x is the vulnerability index of the map grid x; P_x is the protective factor as defined in Table 3.2 in accordance with P_x obtained from (4); I_x is the bypassing factor as estimated from the matrix approach. The vulnerability index is then divided according to ranges to select final vulnerability classes. This method does not use weights to stress the importance of parameters, instead, values of the I factor are one order of magnitude lower to highlight the importance of flow generation.

3.2.1.3 The COP method

This methodology considers three main factors to estimate intrinsic vulnerability in karst areas. Each factor corresponds to conditions concentrating flow (C), overlaying layers providing protection (O), and precipitation as an external stressor on the transport of pollutants (P). Parameters are distributed among these three groups.

The COP method evaluates vulnerability for two scenarios: sinking streams catchment areas and areas without sinking streams denoted as "rest of the area". Distinction between the two scenarios is given by the C factor (Vías et al., 2006). For scenarios with sinking streams, the evaluated parameters are slope and vegetation (Sv), distance to swallow holes (Dh), and distance to sinking streams (Ds). For the rest of the area only Sv and karst surface features (Sf) are considered.

The O factor evaluates the role of soils (S) in vulnerability from their texture and thickness. The vadose zone is classified in relation with the lithology and fracturing (L) with addition of confined conditions (Cn). Finally, the P factor discretely classifies yearly precipitation averages (Pq) and average precipitation intensity (Pi). According to the values assigned to Pq, this method considers precipitation as a medium for the transport of pollutants but also as an agent promoting pollutant dilution when precipitation volumes are high.

The COP is a multi-parameter method mostly utilizing a rating system with the exception of the soil texture-thickness, surface features, and slope-vegetation parameters, the values of which are assigned from a matrix system (see Appendix A3). This method does not use weights to stress the importance of individual parameters, however, exponential differences between the scores fulfil this purpose. Scores from the C factor range from 0 to 1, those from the O factor vary from 1 to 15, and those from the P factor fluctuate from 0.4 to 1. The COP index is obtained from:

$$V_x = (S_x + (\textstyle\sum Ly_x \cdot m_x) \cdot Cn_x) \cdot (Sv_x \cdot Dh_x \cdot Ds_x) \cdot (Pq_x \cdot Pi_x) \tag{6}$$

or

$$V_x = (S_x + (\textstyle\sum Ly_x \cdot m_x) \cdot Cn_x) \cdot (Sf_x \cdot Sv_x) \cdot (Pq_x \cdot Pi_x) \tag{7}$$

where V_x is the vulnerability index at the given grid map x; S_x is the assigned value corresponding to soils; Ly_x, m_x, and Cn_x are the values for lithology, thickness of the lithology layer (in metres), and confined conditions, respectively. Sf_x and Sv_x are surface features and slope-vegetation values. Dh_x and Ds_x are the values for distance to swallow holes and to sinking streams. Pq_x and Pi_x represent the values for precipitation quantity and intensity.

While (6) is the equation for swallow hole catchment areas, (7) is used for diffuse infiltration zones. Sv is also variable depending upon the scenario; steep slopes lead to high vulnerabilities in catchment scenarios, while the same conditions in the rest of the area decrease vulnerability. The final index is also segregated according to pre-established ranges to define vulnerability classes. This method can also assess source vulnerability by the addition of an extra factor to evaluate karstification on the phreatic zone as proposed by Andreo et al. (2009).

3.2.1.4   The PaPRIKa method

The PaPRIKa method, developed to estimate source and resource vulnerability in the French karst, is a multi-parameter point count system derived from the EPIK method (Dörfliger and Plagnes, 2009; Kavouri et al., 2011). It evaluates three parameters and one factor. PaPRIKa stands for protection of aquifers (Pa) based on an overlay protection factor (P) and parameters classifying the geological reservoir (R), infiltration conditions as slope (I), and karstification (Ka).

The P factor is composed of four single parameters denoted as catchment of sinking streams (Ca), soil layers (S), epikarst (E), and unsaturated zone conditions (UZ). The approach to define the P factor is a particularity of this method; catchment areas feeding a sinking stream will be given a value according to the characteristics of said area, as proposed by the Ca attributes, without consideration of E, S or UZ parameters. For the rest of the area, or diffuse infiltration areas, an overlapping evaluation is performed between the S, E and UZ parameters, taking the most protective value from their overlap to be considered as the P factor for that given grid map (Figure 3.9).
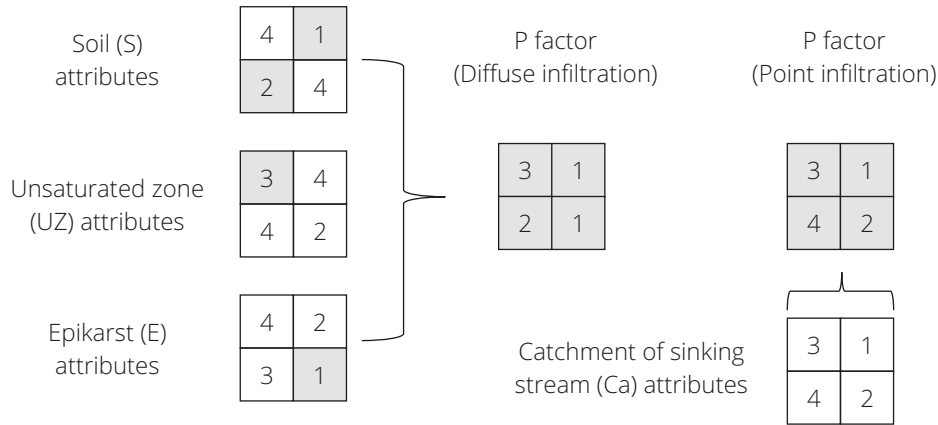
Figure 3.9: Definition of the P factor according to the PaPRIKa method. The lowest the value, the more protective is the attribute.

The R parameter represents the lithological component of the reservoir; this parameter is classified according to the lithology, degree of fracturing, or conduit development. The I parameter is analogous with the C factor from the COP method; it considers solely the slope as a protective condition. It evaluates how the slope affects the vertical infiltration, classifying steeper slopes as the most protective. However, if the area of analysis is a swallow hole catchment, no distinction regarding slope is made, assigning a unique value.

The Ka parameter focuses on the hydrological response of the area based on the karst network and draining capacity. To characterize this parameter, authors of this method based their analysis on the work of Mangin (1975), in addition to multiple analyses, such as tracer tests, hydrographs, and borehole data. Having assigned values to each attribute, vulnerability rates are obtained from a point counting equation as follows:

$$V_x = Pa_x = P_x (W_P) + R_x (W_R) + I_x (W_I) + Ka_x (W_{Ka}) \qquad (8)$$

where V_x is the vulnerability index for the map grid x (analogous to Pa_x); P_x is the assigned value for protective cover derived either from a swallow hole catchment area or taking the most protective value among soils, epikarst, or depth of the unsaturated zone parameters; R_x, I_x, and Ka_x are the values for lithology, infiltration capacity, and karstification parameters, respectively. The weights (W_P, W_R, W_I and W_{Ka}) are not fixed since this method allows the variation of weight distribution to fulfil regional application interests. However, weights must sum to a total of 1 (see Appendix A4).

Testing the PaPRIKa method, Kavouri et al. (2011) suggested a weight distribution according to the functioning characteristics of the aquifer. For the hydrological function parameters, I and Ka, the summed weights must range from 0.50 to 0.65 to represent the relevance of by-pass functions. The summed weight of the structure function parameters, P and R, must range from 35% to 50%. For this research, weights were assigned as those proposed by Marín et al. (2012), being 0.2, 0.2, 0.3, and 0.3 for W_P, W_R, W_I, and W_{Ka}, respectively. Vulnerability classes are obtained according to pre-established ranges.

3.2.1.5   The DRISTPi method

DRISTPi is a multi-parameter point count system developed to estimate detrital and karst aquifers vulnerability. It is a derivation of the DRASTIC method but eliminates the parameters directly related with the aquifer's behaviour (aquifer media and hydraulic conductivity) to focus solely on resource vulnerability (Jiménez-Madrid et al., 2013). This method proposes a new parameter for preferential infiltration (Pi), the values of which are dependent on the scenario in which it is applied (karstic or non-karstic). The proposed Pi parameter classifies areas in relation to exokarst features, such as dolines or karrenfields, promoting a fast infiltration rate. Swallow holes and dolines are evaluated as point features without considering any protective buffer. The importance of this parameter is reflected in the high weight assigned to it.

Another distinctive proposition by this method is the dissimilar classification and weighting of the parameter representing depth to groundwater (D) for karst and non-karst areas. The approach taken for the rating of this parameter in karst areas is similar to that proposed by Witkowski et al. (2003). Due to the higher likelihood of a by-pass from the surface to groundwater by karst features, the thickness of the unsaturated zone is less relevant in comparison with detrital formations. For non-karstic sub-surfaces, values and the weight of the D parameter remain as those proposed by the DRASTIC method.

Recharge (R) is also modified, as proposed by Witkowski et al. (2003), defining recharge volumes of a karst-fissured Triassic aquifer located in Poland into intervals. Soils (S) are classified according to soil texture without consideration of thickness. Lithology (I) represents the material in the vadose zone and topography (T) classifies slope in degrees of elevation change. Parameters S, L, and T are consistent in values and weights as proposed by the DRASTIC method (see Appendix A5). Vulnerability index for scenario 1, or karst areas is then calculated from:

$$V_x = D_x(2) + R_x(4) + I_x(5) + S_x(2) + T_x + Pi_x(5) \tag{9}$$

where V_x is the vulnerability index for the map grid x; D_x is the value assigned to the depth to groundwater; R_x is the value assigned to recharge; I_x is the impact of the unsaturated zone or lithology; S_x, T_x, and Pi_x are the values for soil, topography as slope, and preferential infiltration, respectively. The vulnerability index for detrital areas is also estimated from (9) but the weight of D_x is increased from two to five. Vulnerability classes are then selected from the proposed index ranges.

Similar to the PaPRIKa, the DRISTPi allows the modification of weights. Depending on the situation, parameters can be neglected and the index range to define vulnerability classes can also be modified. However, no guidelines on how to perform such modifications were found in the literature. Similarly, no literature was found regarding the application of this method in other karst areas.

3.2.1.6   The KARSTIC method

The KARSTIC method is also a multi-parameter rating point system and a derivation of the DRASTIC method. In order to estimate source groundwater vulnerability in karst areas, the DRASTIC method was modified; karstification development and fissuring were included as parameters, combined in a complex variable (Davis et al., 2002). The karstification parameter (K) is classified from swallow holes or dolines that promote point infiltration. Fractures (F) are considered to be a synergistic component of karstification. Combined, K and F display the high pollution potential derived from the easy by-pass and movement of water through fissures and cracks of considerable size. Depth to groundwater (D) is combined with the impact of the unsaturated zone parameter (I), which represents the lithology, creating a second complex variable. Recharge (R), soils (S), and topography as slope (T) are classified as proposed by the DRASTIC method (see Appendix A6).

Aquifer media (A) and aquifer hydraulic conductivity (C) are the parameters reflecting the saturated zone's influence on lateral movement. The source vulnerability index is calculated from:

$$V_x = (K_x \cdot F_x (10)) + A_x (3) + R_x (4) + S_x (2) + T_x + (I_x \cdot D_x (20)) + C_x (3) \tag{10}$$

where V_x is the vulnerability index of a given map grid x; K_x corresponds to karst development based on the hydrological function of swallow holes; F_x corresponds to fracturing degree; A_x corresponds to aquifer medium; R_x corresponds to recharge; S_x corresponds to soil texture; T_x corresponds to topography as slope; I_x corresponds to lithology of the unsaturated zone; D_x corresponds to depth to water table; C_x corresponds to the aquifer's hydraulic conductivity.

Since the scope of this research is to evaluate resource vulnerability, parameters affecting lateral flow in the aquifer were eliminated. An adjustment was performed by redistributing weights of the eliminated parameters on a percentage basis. The final equation to calculate the vulnerability index, therefore, becomes:

$$V_x = (K_x \cdot F_x (11)) + R_x (5) + S_x (3) + T_x (2) + (I_x \cdot D_x (22)) \tag{11}$$

Final vulnerability classes are archived from the vulnerability index ranges. This method can also be applied in non-karstic areas.

3.2.1.7   The RISKE method

The RISKE method arises as an improvement of the EPIK method, with many similarities in parameter classification approach with the PaPRIKa method (Petelet-Giraud et al., 2000). This method adds a parameter to characterize the lithology and fracturing of the aquifer (R). Infiltration conditions (I) is classified from the slope, in percentage of elevation change; infiltration parameter defines high slopes as less vulnerable since the possibility of vertical infiltration is decreased. Unlike the EPIK method, RISKE does not consider land use or any other parameter which could affect lateral surface flow. Soil (S) analysis is improved to include soil thickness and its effect on vulnerability, however, depth to groundwater is not part of this method. Karstification (K) is defined by degrees of fracturing and karst network development is associated with their connection with the surface. Finally, epikarst (E) characterization is defined by the zoning of surface karst expressions.

The parameters used by the RISKE method aim to describe the structure and functionality of the aquifer that, consequently, influence the behaviour of a pollutant entering the system. This multi-parameter point count system method includes fixed weights to enhance the importance of some parameters. To classify attributes, values from 1 to 4 are assigned according to Appendix A7. The vulnerability index can be then calculated from:

$$V_x = R_x (0.1) + I_x (0.4) + S_x (0.1) + K_x (0.2) + E_x (0.2) \tag{12}$$

where V_x is the vulnerability index for the map grid x; R_x represents the aquifer rock; I_x denotes the infiltration conditions by slope; S_x is the soil texture-thickness; K_x is the degree of karstification; E_x represents the epikarst. Vulnerability classes are assigned according pre-stablished index ranges.

3.2.1.8   The SA

The SA was developed in conformity with the COST Action 620 conceptual framework for assessment of vulnerability. It is considered the most complete interpretation of the European framework, adapted to fulfil the intrinsic features of karst aquifers in Slovenia. The SA estimates resource vulnerability mainly based on the COP method (Ravbar and Goldscheider, 2007).

Among the adaptations made to regionalize the methodology, modifications to the C factor stand out where the temporal variability of the swallow holes' function is considered. Also, modifications of the P factor include the integration of storm events for their influence on transport of pollutants, and a more detailed description of precipitation. Assignation of values to the parameters forming the C, O, and P factors follows the tables displayed in Appendix A8. For the calculation of vulnerability rates the equation is:

$$V_x = (Os_x + Ol_x \cdot Cn_x) \cdot (Dh_x \cdot Ds_x \cdot Sv_x + Tv_x) \cdot (Rd_x \cdot Se_x) \qquad (13)$$

or

$$V_x = (Os_x + Ol_x \cdot Cn_x) \cdot (Sv_x \cdot Sf_x) \cdot (Rd_x \cdot Se_x) \qquad (14)$$

where V_x is the vulnerability index corresponding to the map grid x; Os_x is the value for soil texture and thickness; Ol_x is the lithology and fracturing value; Cn_x represent the aquifer confinement condition; Dh_x is the value assigned to the distance to swallow hole classification; Ds_x is the value for distance to sinking stream; Sv_x represents slope and vegetation; Tv_x is the temporal variability influencing a swallow hole response; Sf_x represent surface features; Rd_x denotes rainy days; Se_x represents the extreme events values.

Equation (13) is used for swallow hole recharge areas, while (14) is used for diffuse infiltration areas denoted as "rest of the catchment". Parameters contained in brackets correspond to the O, C, and P factors, respectively. Designation of vulnerability classes from obtained indexes follows the ranges pre-stablished by the authors. This method is able to estimate source vulnerability if a parameter depicting aquifer's horizontal flow, by travel time and conduit network development, is included. Index variation among methods is displayed in Table 3.3 and Table 3.4.

Table 3.3: Variation among indexes to define final vulnerability classes. Reproduced from Moreno-Gómez et al. (2018).

Vulnerability		Original test site			
		St. Imier Springs, Switzerland	Swabian Alb, Germany	Sierra de Líbar and Torremolinos, Spain	Ouysse karst system, France
Description	Class	EPIK index	PI index	COP index	PaPRIKa index
Very low	5	N.A.	> 4	> 4	≤ 0.79
Low	4	Specific*	3.1 - 4	2.1 - 4	0.8 – 1.59
Moderate	3	> 25	2.1 - 3	1.1 - 2	1.6 – 2.39
High	2	20 - 25	1.1 - 2	0.51 - 1	2.4 – 3.19
Very high	1	≤ 19	≤ 1	≤ 0.5	> 3.19

* When conditions P4 + I3 or P4 + I4 are present (see Appendix A1).

Table 3.4: Variation among indexes to define final vulnerability classes. Table modified from Moreno-Gómez et al. (2019b).

Vulnerability		Original test site			
		Sierra de Cañete, Spain and Neblón river basin, Belgium	Rapid Creek basin, south Dakota, USA	Fontanilles and Cent Fonts karstic aquifers, France	Podstenjšek springs catchment, Slovenia
Description	Class	DRISTPi index	KARSTIC index	RISKE index	SA index
Very low	5	17 - 50	0 - 200	0 - 0.8	4 - 15
Low	4	50 - 80	200 - 350	>0.8 - 1.6	2 - 4
Moderate	3	80 - 110	350 - 600	>1.6 - 2.4	1 - 2
High	2	110 - 140	600 - 800	>2.4 - 3.2	0.5 - 1
Very high	1	>140	>800	>3.2 - 4	0 - 0.5

3.2.2 Map layers development

The geographic information system ArcGIS version 10.5 was used to prepare and manage available data and to create the necessary map layers, representing parameters, in order to obtain visual vulnerability outcomes. Since vulnerability maps classify each parameter on a discrete basis to assign values, continuous datasets, such as groundwater depth, were divided into intervals following the methods' guidelines. When necessary, point data (e.g., precipitation or borehole data) was interpolated to generate continuous rasters, which were later transformed into discrete maps, as mentioned previously.

Map layers in vector format were converted into rasters with a resolution (map grid size) of approximately 900 m^2 representing the parameters for each method here discussed. All layers were projected with the World Geodetic System (WGS) 1984, Universal Transverse Mercator (UTM) coordinates zone 16 (Mexico). Parameter value assignment was carried out according to the methodologies' guidelines, taking the map layers presented in this section as a base. The development of map layers and data processing is explained following the parameters displayed in Table 3.1. It is important to mention that besides all maps being obtained from the same base maps, they differ in the value assignment due to the different classification schemes.

Map layers representing soil texture, soil thickness, or a combination of both, were developed from the analysis of 134 boreholes with a total of 258 soil profiles obtained from INEGI through its interactive portal. Since the number of boreholes was not sufficiently representative due to the extension of the study area, an edaphology map with soil classes defined by the WRB was used as an additional variable to define a correlation between edaphology classes, soil texture, and soil thickness. In Figure 3.10, a soil map according to the German soil texture classification is displayed.
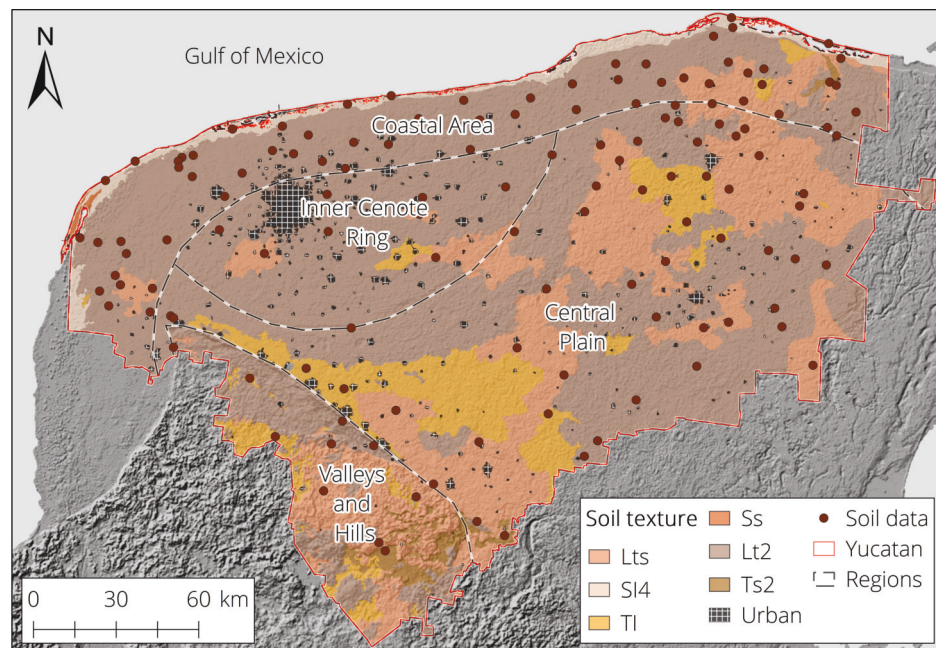
Figure 3.10: Soil texture map according to the German soil chart. As presented by the soil working group (Arbeitsgruppe BODEN, 1994), soil textures correspond to: clayey sandy loam (Lts); highly loamy sand (Sl4); loamy clay (Tl); pure sand (Ss); slightly clayey loam (Lt2); slightly sandy clay (Ts2). Map generated from edaphology datasets, publicly available from the National Institute of Statistics and Geography (INEGI, 2007).

Comparing soil texture and thickness from edaphology class definitions and those measured from borehole samples, the plausibility for such an assumption was confirmed. Borehole point data was then interpolated, using the edaphology soil type as a barrier, to generate discrete soil texture and soil thickness maps. However, a drawback of this procedure is the overestimation of soil cover, since limestone outcrops, constantly present in the Yucatan karst, are not considered.

Although all methods applied in the study area include soil as a parameter, soil textures are characterized utilizing different criteria according to the country in which the method was developed (see Table 2.7); German, French and USA standards are the basis for classifying soil texture, appearing in contrasting map layers. Therefore, soil maps used by different methods differ from each other due to their dissimilar evaluation of texture, thickness, or hydraulic response.

Dolines were subtracted from contour maps at a scale of 1:50,000 following the morphometric analysis presented by Aguilar et al. (2016). Contours defined as depressions were selected as dolines following a morphometric evaluation; depressions contours with a coefficient of circularity (Cc), also called the Gravelius coefficient (Gravelius, 1914), with a value < 1.04 and depths > 2 m were defined as dolines. Additionally, the visual inspection of high-resolution imagery, at a resolution of 0.3 m, aided the locating of dolines that are not displayed by morphometric analysis. However, dolines located under highly vegetated areas are not mapped. A total of 5,143 dolines were found in the study area, nevertheless, the number of dolines could be underestimated, as proved by a recent study presented by Moreno-Gómez et al. (2019a). For the map layer representing probable epikarst development, doline density was statistically estimated. A density of ≥ 4 dolines per km^2 was statistically defined as the higher value to classify degrees of epikarst development (Figure 3.11).
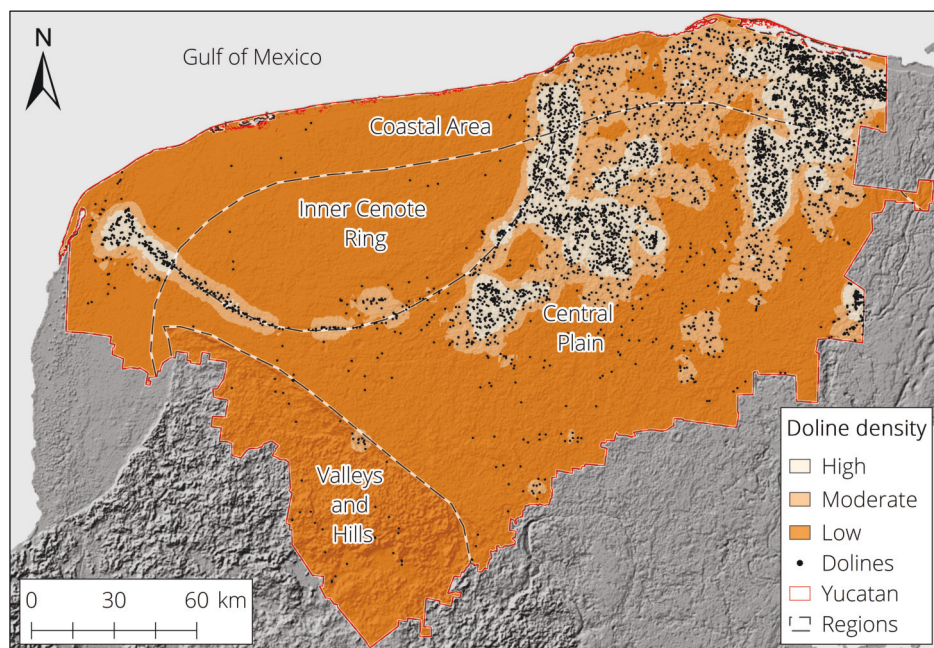
Figure 3.11: Doline density map. Map utilized to define probable epikarst development, karst surface features, and karstification. Doline map generated from topography datasets (contours) at a scale of 1:50,000, publicly available from the National Institute of Statistics and Geography (INEGI, 2015).

In the same way, statistics also helped to determine areas with high, moderate and low fracture density from fracture and fissures maps (Figure 3.12). Locations of high fissured areas match those with high doline density; this is more remarkable along the Cenote Ring and the north-eastern Central Plain. The overlapping of fracturing and doline maps served to indirectly estimate degrees of vulnerability.
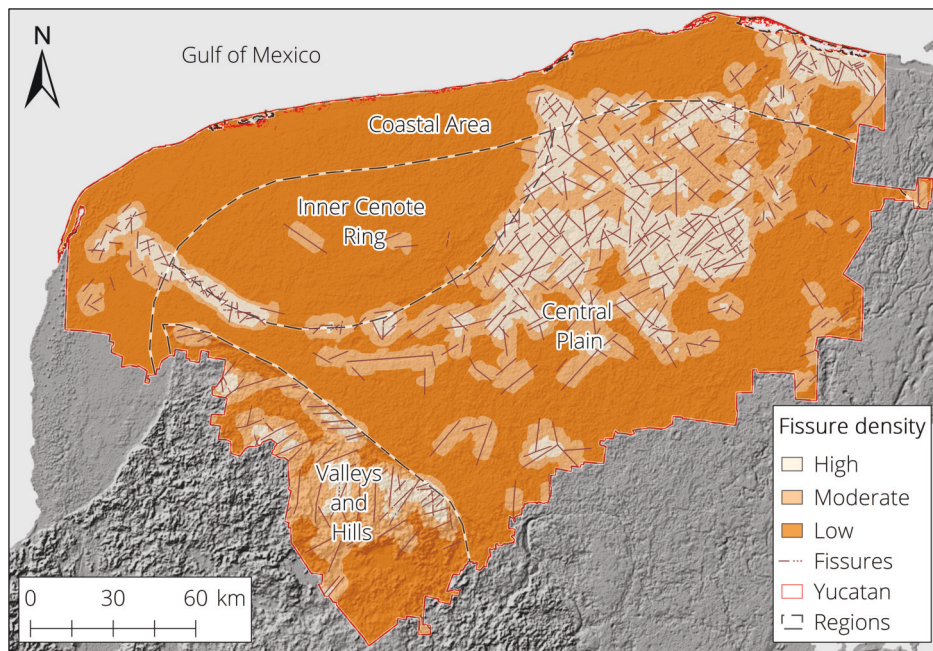
Figure 3.12: Fissure density map. Map utilized to define karstification and lithology fracturing. Map generated from geologic datasets, publicly available from the National Institute of Statistics and Geography (INEGI, 1984).

The map layer representing slope (Figure 3.13) was created based on the Advanced Space borne Thermal Emission and Reflection Radiometer (ASTER) Global Digital Elevation Model (GDEM) version 3 (NASA/METI/AIST/Japan Space systems, and U.S./Japan ASTER Science Team, 2018). This DEM at 30 m resolution was obtained from the USGS portal.
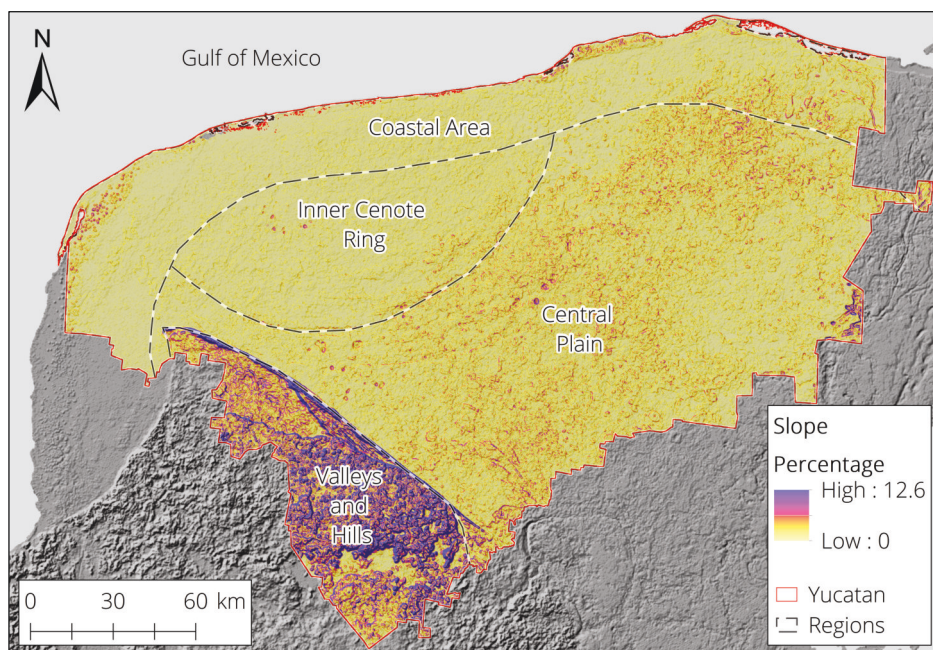
Figure 3.13: Topographic slope in Yucatan. Map generated from the ASTER-GDEM version 3, resolution of 30 m (NASA, METI, AIST, Japan Spacesystems and U.S./Japan ASTER Science Team, 2019).

Prior to the estimation of slope, the DEM was corrected to eliminate "No data" gaps utilizing a moving windows approach. The Slope tool included in ArcGIS was utilized to discretize slope, in percentages, according to the ranges proposed by the multiple vulnerability methods. The Slope tool shows a maximum elevation change of approximately 38 m from grid to grid. Despite elevation differences being displayed for the whole area, change is more apparent on the hill boundary, where a more drastic elevation change occurs.

A contour map, representing the average elevation of the groundwater table, was digitalized from a report presented by the Mexican Ministry of Agriculture and Hydraulic Resources (SARH); this map was included in the geohydrological synopsis of the state of Yucatan (SARH, 1989). Point data, obtained from multiple literature sources, served to validate results from the interpolation of the contour lines to obtain the elevation of the groundwater table in reference to sea level (see Figure 3.5). By calculating the difference between the DEM and the groundwater elevation, the unsaturated zone thickness map was obtained (Figure 3.14).
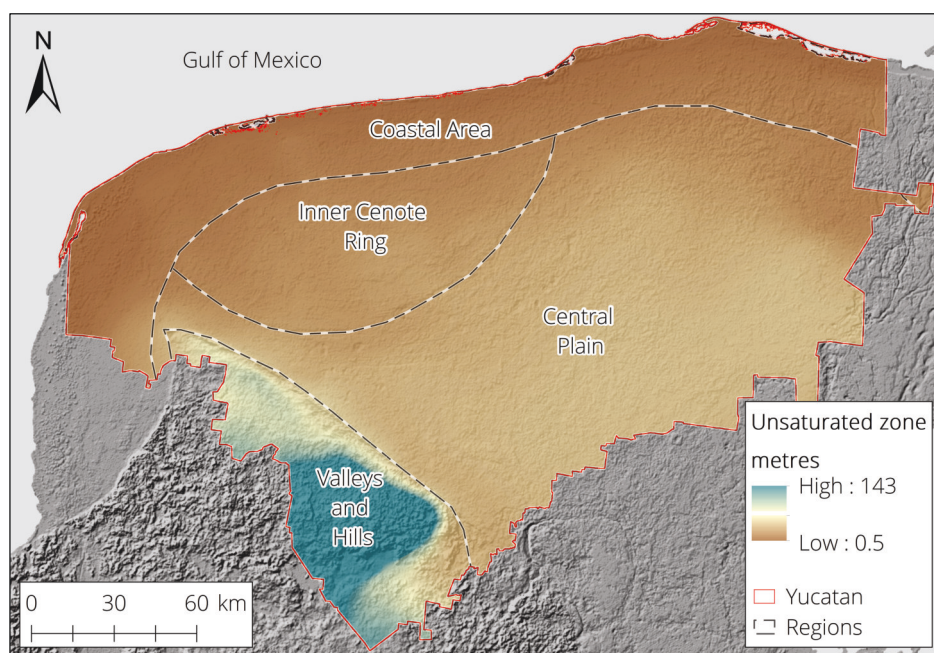
Figure 3.14: Depth to groundwater map. Map generated from water table data (contours) from SARH (1989) and the ASTER-GDEM (NASA, METI, AIST, Japan Spacesystems and U.S./Japan ASTER Science Team, 2019).

To develop maps related to precipitation, data from 65 climatic stations - part of the SMN - were gathered from its web platform (SMN, 2017). From the records, a period of 25 years (1990-2015) was analysed to obtain mean annual precipitation values, the number of precipitation days, and rainfall intensity. In this case, point data from climatic stations was interpolated using ordinary kriging to obtain precipitation-related map layers (Figure 3.15). Kriging is one of several geostatistical techniques, based on statistical models, which considers the relationships between measured points to generate an estimated surface from a scattered set of values (Ly et al., 2013).

The maps here presented are the core for other derived map layers; additional maps were also created according to the requirements of each methodology. The PI method includes soil hydraulic conductivity as an estimator for runoff generation. Using soil texture as a base, a group of mathematical formulae based on soil grain size distribution, as proposed by Saxton et al. (1986) and further improved by Saxton and Rawls (2006), were applied to obtain soil hydraulic conductivity values.
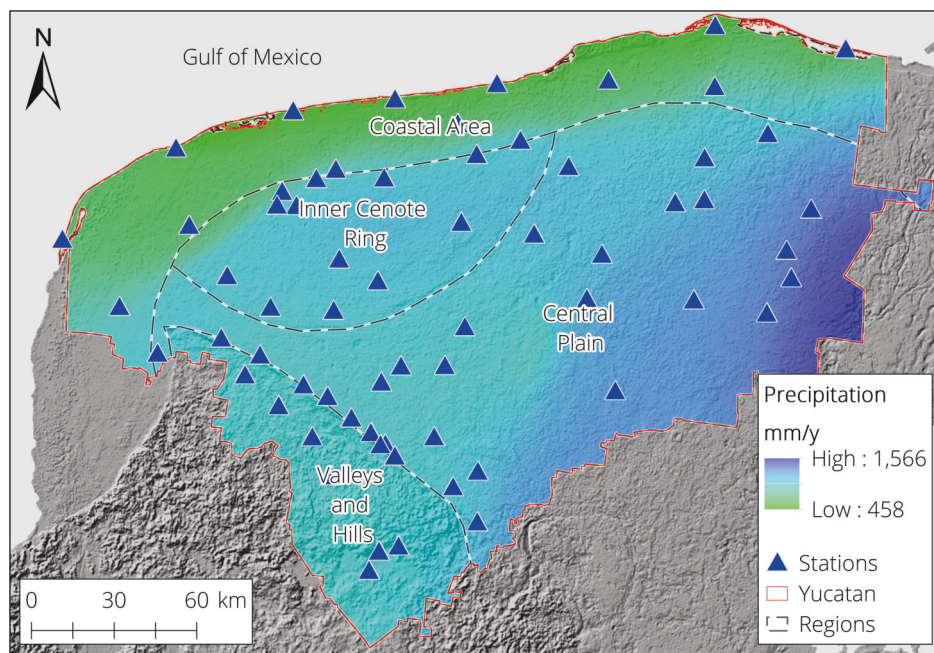
Figure 3.15: Mean annual precipitation map. Map elaborated from precipitation data from the CLICOM web platform (SMN, 2017).

The PI method also includes in its analysis the eFC as a hydraulic property of the soils. In this investigation, the eFC map was obtained setting the minimum value proposed by the method. This was done due to the complications in estimating eFC since data, such as initial water content, wetting, and redistribution changes over time, are not available.

The epikarst map was obtained directly from the doline density analysis, as proposed by the EPIK. Similarly, karstification maps were created either from doline density, fissure density, or a combination of both, as the evaluation of karstification to assign values varies among the methods. This procedure was also chosen for the creation of the surface features map.

Some methods like the COP, PI, and SA include the influence of vegetation on runoff generation. Land-use maps obtained from INEGI were classified by agricultural fields, meadows, and forest to fulfil this requirement. Due to the matrix system used by these methods to combine slope and vegetation, a binary segregation (agriculture/meadows = 1) was necessary to assign values.

A lithology map was created defining the whole study area as limestone without further discretization. However, when necessary, lithology was coupled with fissure maps as suggested by the COP method. Finally, recharge was settled as 20% of the mean annual precipitation as utilized by González-Herrera et al. (2002) in the presented regional model. Recharge spatial variability due to area characteristics was not included since no information was found in the literature. This is expected to influence outcomes of methods including this parameter. The map layers, correspondent to each method evaluated in this work, are displayed in Appendix B.

3.2.3   Congruence and sensitivity analysis

Congruence and sensitivity analysis compose an important part of this research, in order to compare outcomes regarding vulnerability classes in terms of extension match between multiple methodologies. Methods congruence analysis (MCA) estimates the degree to which vulnerability maps from the eight methods show spatial agreement among them from their overlap. This procedure was carried out utilizing the Tabulate tool included in ArcGIS.

This tool performs a cross-tabulation between two vulnerability maps, resulting in a table which summarizes the number of grids of a given vulnerability class that spatially match between the two analysed methods (Figure 3.16). From the number of map grids and their established size, this procedure aims to highlight the area percentage to which the methods are correspondent in terms of vulnerability.

Similarly, it is possible to investigate how each parameter individually influences vulnerability classes. To achieve this parameter congruence analysis (PCA), each vulnerability map is also overlapped with its own component map layers (e.g., soils, slope, lithology, etc.) to evaluate the most influential attributes in relation to vulnerability classification.

KARSTIC	RISKE					
Vulnerability	VHV	HV	MV	LV	VLV	Congruence
Very high (VHV)	4	0	1	0	0	4
High (HV)	1	2	0	0	0	2
Moderate (MV)	0	1	2	2	0	2
Low (LV)	0	0	0	1	1	1
Very low (VLV)	0	0	0	0	1	1
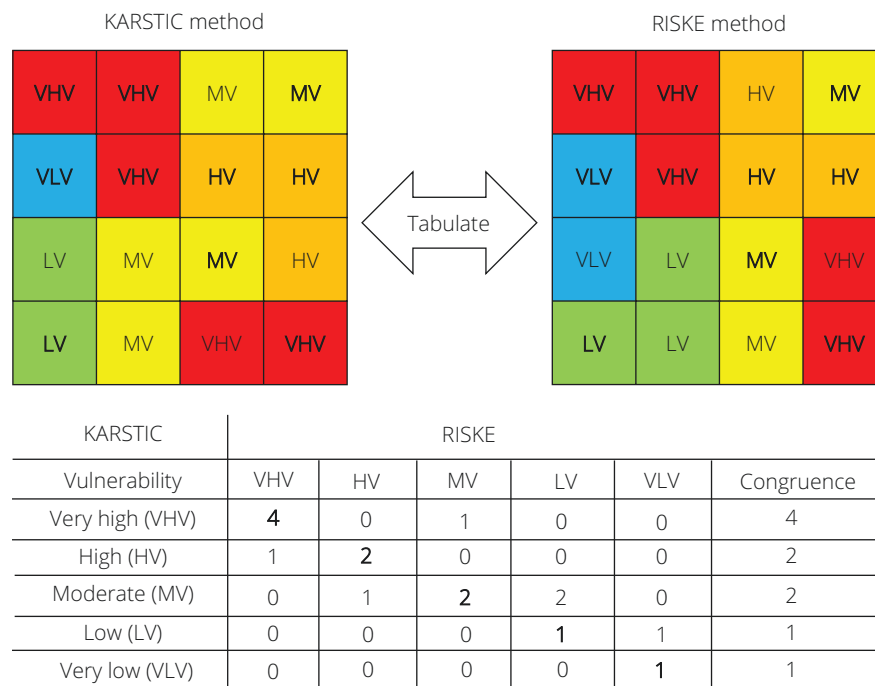
Figure 3.16: Example of the tabulate function for the MCA.

The first step before performing a sensitivity analysis is the evaluation of the multiple arrays of parameters' attributes forming a vulnerability map. This is best explained by the concept of Unique Condition Sub-area (UCS). A UCS represents a group of map grids, or a single map grid, with a unique combination of parameters in respect to their attributes. This process aims to minimize the number of grid maps, therefore, decreasing the computing time and the processing of a large number of grids during the analysis. UCSs are obtained with the Tabulate tool in ArcGIS, however, unlike the spatial analysis process, the UCS target is the vulnerability index instead of the vulnerability class (see Table 3.5).

In this work, UCSs were generated from the eight vulnerability outcomes in Yucatan. Additionally, theoretical UCSs were also created obtaining all possible combinations of parameters' attributes from each one of the eight methods with the purpose of having a solid base for comparison. While the Yucatan UCSs were computed by applying ArcGIS tools, theoretical UCSs were generated utilizing the open-source R software for statistical computing and graphics with the integrated development environment RStudio version 1.2.5019.

Table 3.5: Example of some UCSs from the DRISTPi method. Index calculated including weights.

UCS	Number of map grids forming the UCS	D value	R value	I value	S value	T value	Pi value	Index
1	7	2	6	5	7	10	3	100*
2	4	1	9	5	6	1	6	106
3	5	8	9	5	6	10	6	129
4	6	1	9	5	6	10	3	100*
5	1	6	9	5	6	10	6	125

* Notice that UCSs 1 and 4 have a similar index value; however, the combination of attributes is dissimilar, making two independent UCSs.

To evaluate the sensitivity of single parameters on vulnerability indexes, a map layer removal analysis was carried out. This was done by the removal of one map layer at a time and, then, calculating the vulnerability index with the remaining layers; through this process it is possible to assess the impact of map layers, or parameters, on final indexes (Lodwick et al., 1990). Map layer sensitivity is obtained from:

$$Si_x = |\,(Vi/N - Vi_x/(N\text{-}1))\,| \tag{15}$$

where Si_x is the sensitivity of the ith UCS from the removal of parameter x; Vi is the unaltered vulnerability index correspondent to the ith UCS; Vi_x is the vulnerability index of the ith UCS after removal of parameter x; N is the number of parameters included in the original vulnerability index calculation.

The removal of one parameter will inherently decrease the vulnerability index. Dividing the vulnerability index by the number of utilized map layers is a measure that aims to minimize the bias generated by the differences in number of maps to estimate the final index. Equation (15) solely estimates the sensitivity of an individual UCS. To evaluate sensitivity for the whole study area we apply:

$$S_x = \sum (Si_x \cdot \Delta i_x)/m \tag{16}$$

where S_x represents the mean sensitivity after the removal of parameter x for the whole study area; Si_x is the sensitivity of the ith UCS as estimated from (15); Δi_x is the percentage of the study area covered by the ith UCS and m is the number of UCS.

The index change, also referred to as effective weight, is also calculated and further compared with theoretical weights in order to adjust them to match regional characteristics. The index change is then estimated in terms of index percentage. Values can be either negative or positive and directly depend upon the vulnerability methodology's range. It is estimated from:

$$Wi_x = (Vi - Vi_x)\,/\,Vi \tag{17}$$

where Wi_x is the variation after removal of parameter x in the ith UCS; Vi is the original vulnerability index of the ith UCS; and Vi_x is the vulnerability index estimated without parameter x. Map removal sensitivity and effective weight have been constantly applied in vulnerability studies, either to evaluate the performance of a given methodology or to compare two or more methodologies (Napolitano and Fabbri, 1996; Gogu and Dassargues, 2000; Gogu et al., 2003; Kovacic and Petric, 2007; Marín et al., 2012). Although the previous sensitivity approaches being widely used, they only evaluate how sensitive to change the vulnerability index is. Looking at Table 3.3 and Table 3.4 it is easy to note that vulnerability indexes are dissimilarly divided in ranges in order to assign vulnerability classes. This means that a considerable index variation, after the removal of one parameter, does not necessarily lead to a change of vulnerability class. This is more noticeable for the DRISTPi and KARSTIC methods whose indexes show larger ranges to define vulnerability classes.

Hereinafter, vulnerability classes will be denoted as VHV for very high, HV for high, MV for moderate, LV for low, and VLV for very low. Following the methodologies, a range of colours, usually applied to distinguish vulnerability classes, are red, orange, yellow, green, and blue to categorized vulnerabilities from VHV to VLV.

3.3   Results from groundwater vulnerability mapping

3.3.1   EPIK vulnerability map

Outcomes from the EPIK method show three vulnerability classes with 12.1%, 17.3%, and 70.6% corresponding to VHV, HV, and MV, respectively. It is important to mention that the EPIK method only evaluates four vulnerability classes, in contrast to other methods that contemplate a total of five. From visual inspection it is easy to notice that VHV and HV match areas with high doline density. Since the doline density map reflects possible epikarst development with an assigned weight of 3, according to this method, it can be assumed that the leading role of this parameter is to achieve these vulnerability classes (Figure 3.17).
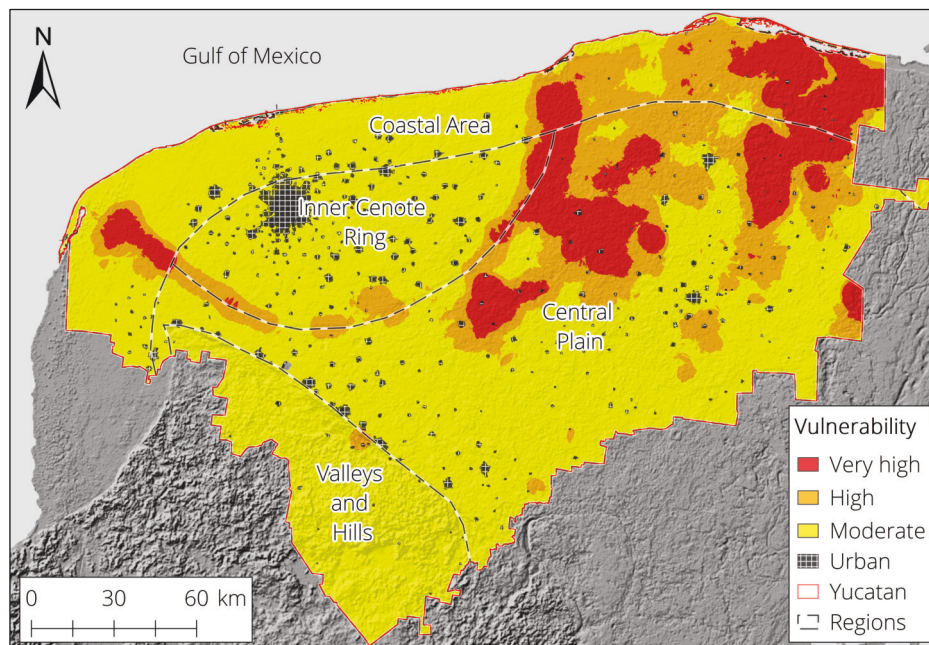
Figure 3.17: Yucatan groundwater vulnerability according to the EPIK method.

The doline density map is also the base map for karstification development, the importance of which is also relevant, holding a weight of 2. In this case, two similar map layers, obtained from the same base map, are evaluated (see Appendix B1). With epikarst and karstification layers resulting in high vulnerabilities, the rest of the area shows solely MV.

Soils do not seem to influence results as no differences are highlighted, at least visually. Although most of the area is assumed to be covered with thin soils, theoretically depicting a more vulnerable scenario, outcomes do not show differences in areas with thick soil layers (> 1 m), such as those located mostly at south. This could be a consequence of the low weight assigned to soils (weight = 1) and the consideration of soil thickness as the only evaluated feature as protective cover.

The infiltration condition was set as "rest of the area", meaning a regional diffuse infiltration; this consideration was taken due to the characteristics of the Yucatan karst where no runoff is generated. A combination of diffuse infiltration and low epikarst development (or karstification) could be the elements leading to MV in this case. The EPIK method does not include the vertical extension of the unsaturated zone because its main focus is on the possible by-pass of swallow hole catchment areas. Therefore, no differences are highlighted between the low plain, with a shallow aquifer, and the hill located in the south where depth of groundwater reaches its maximum.

3.3.2 PI vulnerability map

Vulnerability percentages, as displayed by the PI method, are 51.5%, 47.6%, and 0.9% for HV, MV, and LV, respectively (Figure 3.18). No VHV is achieved due to the fact that the I factor exhibits a homogeneous scenario for infiltration conditions, being settled as diffuse, similar to the EPIK's I parameter. The vulnerability characterization from this method relies solely on the features promoting some protection for diffuse infiltration.
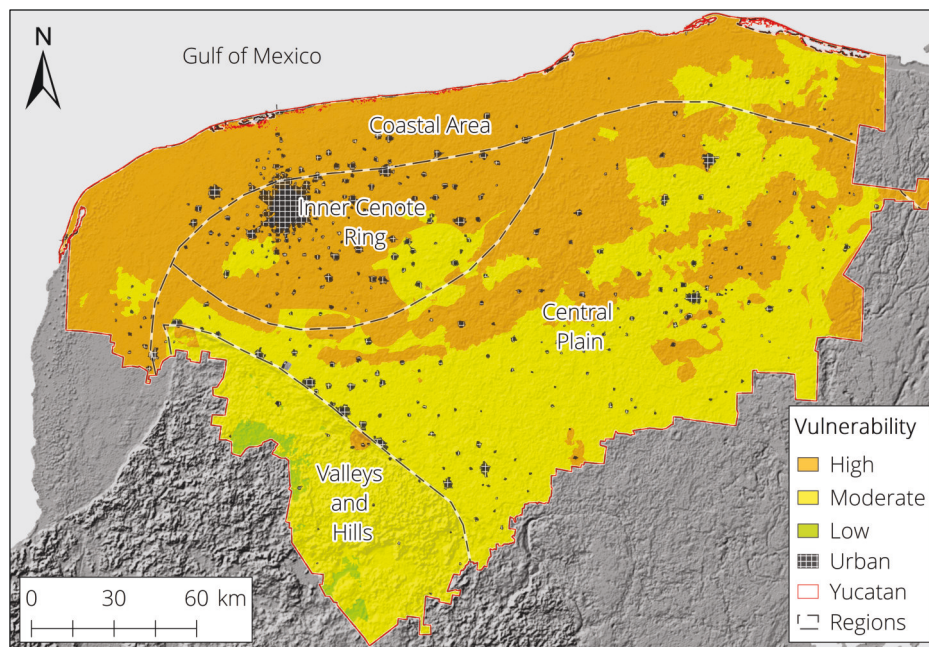
Figure 3.18: Yucatan groundwater vulnerability according to the PI method.

Results of HV seem to be triggered by the combination of high fracturing, thin soils, and a shallow water table. Despite these characteristics can be considered the most vulnerable features, a regional diffuse infiltration scenario minimizes their impact by prohibiting the achievement of VHV. Soils seem to influence MV, especially those with a thickness of > 0.3 m, however, MV is also found in areas where thin soils overlay zones where the water table is found at more than 15 m below surface. Soils with a thickness of > 1 m influence LV in the southern part of the study area, where the water table is found at its deepest.

Although this method includes the depth of the unsaturated zone in the vulnerability analysis, it does not show a relevant effect on the hill area located in the south where the water table changes drastically from 40 m to 140 m below surface. Neither recharge nor topsoil display any visible influence on results. Three map layers displayed homogeneity; topsoil, lithology, and the infiltration factor (see Appendix B2).

3.3.3 COP vulnerability map

The COP method displays a broader vulnerability scheme with VHV, HV, MV, and LV classes; the respective values are 10.6%, 37.3%, 36.2%, and 16% (Figure 3.19). Areas with a considerable karstification and a high density of karst surface features are classified with VHV, however, vulnerability in such areas decreases to HV if precipitation is low, representing an unlikely condition for the transportation of pollutants.
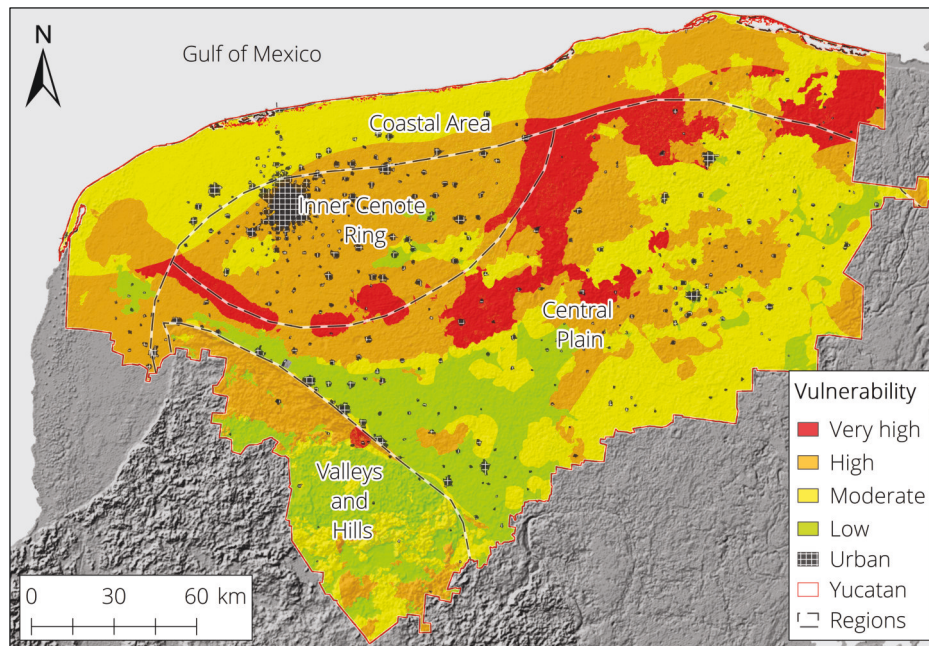
Figure 3.19: Yucatan groundwater vulnerability according to the COP method.

Since the Pi map is regionally homogeneous, Pq is the controlling parameter of the P factor and, therefore, substantially influences vulnerability discretization. This is clearly seen by the well-marked limits between VHV and HV, similar to those displayed by the mean annual precipitation map (see Appendix B3). Precipitation also induces MV at the coast due to the estimated low precipitation. Nevertheless, MV is also found in the south where precipitation volumes are higher under the assumption that high precipitation volumes induce dilution. Soils are also likely to influence MV in this zone since medium and fine textured soils, with a thickness of 0.5 m, are located here. Soils with a high content of fine particles and a thickness of > 0.5 m visually match areas categorized with LV, disregarding precipitation conditions.

Alike to the PI method, COP also includes depth of the water table as an indirect parameter linked to lithology. Nevertheless, its influence is not seen in final results since some areas on the southern hill are still categorized as MV, despite the considerable groundwater depth. The COP method evaluates two scenarios, catchment of a swallow hole and rest of the area (no point infiltration). Similar to previous methodologies, a diffuse infiltration was considered for the region, which also influences results.

3.3.4 PaPRIKa vulnerability map

Outcomes from the PaPRIKa method estimate the most vulnerable conditions for Yucatan with 29.9% of VHV, 62.2% of HV, and just 12% of MV (Figure 3.20). These vulnerability classes arise mostly due to the development of three map layers, with the doline density map as a base (see Appendix B4). Degrees of probable epikarst development, karstification, and aquifer rock characterization are directly derived from doline density, according to the PaPRIKa guidelines. This procedure does not allow further classification beyond VHV and HV in the Yucatan low plain.

Although areas with high doline density presumably contain high epikarst development, thus promoting a considerable aquifer protection, the same areas are classified as highly karstified for both the surface and sub-surface; these conditions seem to override the protective response of the epikarst acting as a perched aquifer. On the other hand, in areas where epikarst may not be well-developed, the protection is minimized because not-perched characteristics are present, resulting in an HV class.

Other parameters that are part of the P factor, such as soils and depth to groundwater, seem to have little influence as protective features. However, thick and fine textured soils match perfectly with MV in the hill area. High slopes (> 15%), mostly found in the southern hill, also promote MV since the vertical infiltration is minimized.
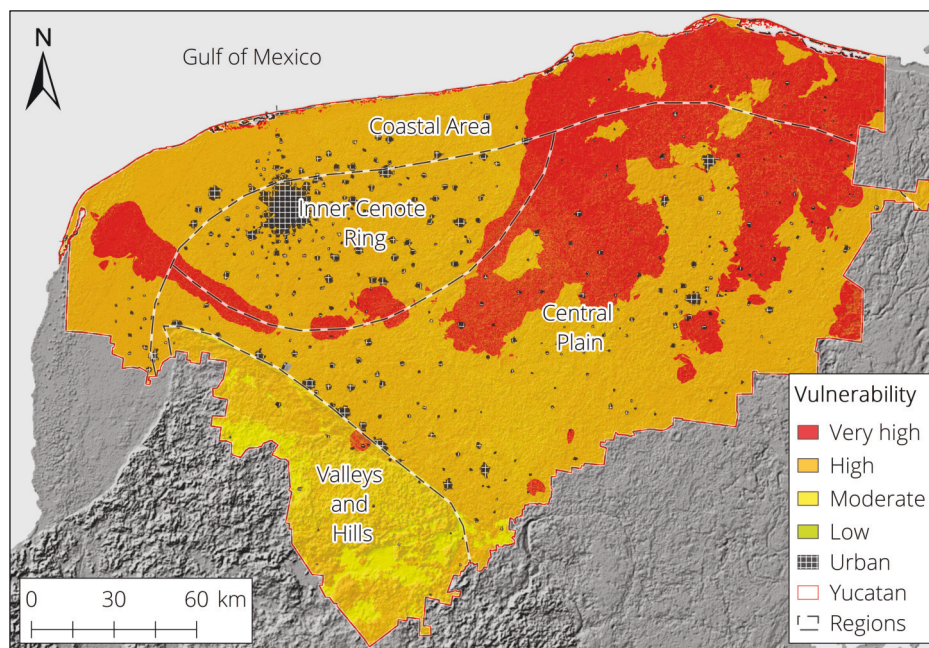
Figure 3.20: Yucatan groundwater vulnerability according to the PaPRIKa method.

It is important to consider the evaluation process that this method applies for protective layer assessment; taking the most protective function among S, E, and UZ seems to minimize the protection itself since some features delaying vertical infiltration are excluded. Although some areas in the Central Plain and Inner Cenote Ring must show some influence of thick soils, this appears not to be reflected in the final map. Thickness of the unsaturated zone seems not to affect MV in the hill area, however, this situation is unclear from visual inspection.

3.3.5   DRISTPi vulnerability map

The DRISTPi method displays VHV at 7.4%, HV at 26.8%, MV at 64.8%, and a very low 0.9% corresponds to LV (Figure 3.21). Since dolines are considered as point features without buffers in this method, preferential infiltration is solely evaluated from fracture density; this is the parameter apparently causing VHV and HV. It is difficult to define the most influential characteristics leading to MV from visual inspection.
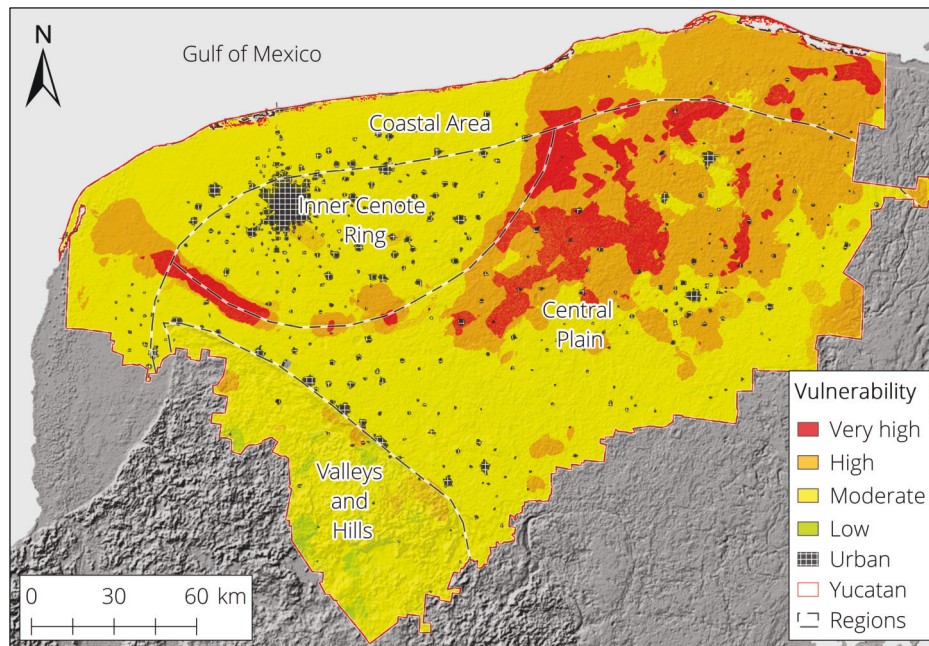
Figure 3.21: Yucatan groundwater vulnerability according to the DRISTPi method.

Even though the depth to groundwater map is divided into seven attributes, no contrast is displayed between coastal and hill areas. Neither does the recharge map, despite its division into six attributes (see Appendix B5). This method solely evaluates soil texture as protective cover, but no changes in vulnerability seem to be influenced by this map layer.

The impact of the unsaturated zone was settled with two values depicting karst limestone and limestone, the former for the area with high fracture density and the latter for the rest of the area. However, the value assigned to this parameter is high, which, together with its congruently high weighting factor, could be the argument for the elevated percentage of MV.

For areas depicted with LV it is complicated to define their influential map layers by visual comparison; a combination of slope, soil texture, and depth of the unsaturated zone could be the key characteristics depicting this class.

3.3.6   KARSTIC vulnerability map

Vulnerability classes, according to the KARSTIC method, cover 8.5%, 20.8%, 64.4%, and 6.1% for VHV, HV, MV, and LV, respectively. Some similarities with the DRISTPi method are evident since both methods are derivations of the DRASTIC method (Figure 3.22). High doline density areas match those depicting VHV, while HV is highlighted by the karstification parameter related to fissuring.
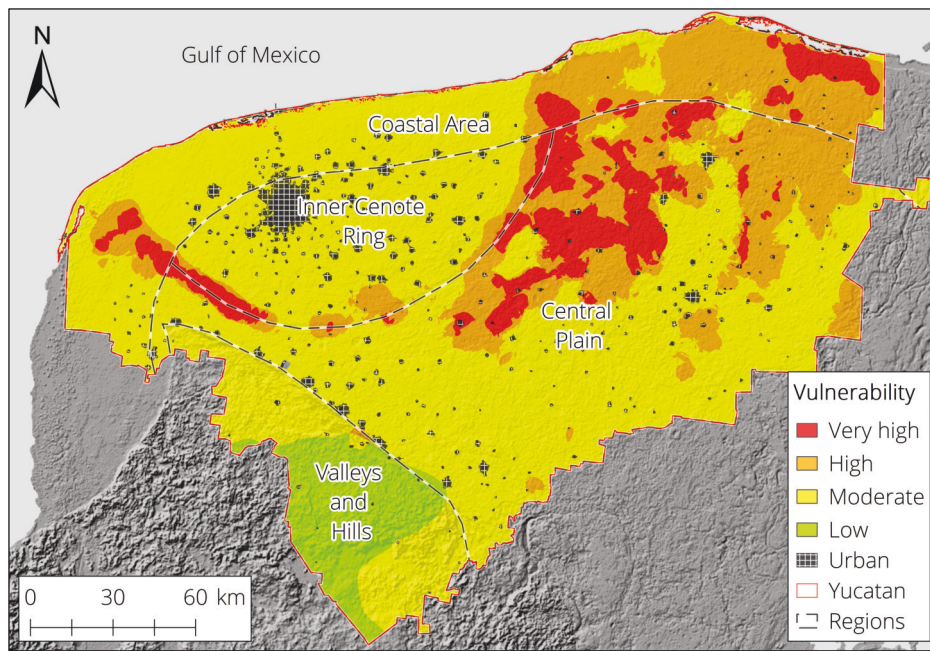
Figure 3.22: Yucatan groundwater vulnerability according to the KARSTIC method.

Similar to the DRISTPi, the impact of the unsaturated zone is divided in two zones denoted as karst limestone and limestone, however, the rates for these attributes differ from those of the DRISTPi. Areas categorized as limestone with a low karstification development display MV, however, the influence of soil texture, recharge, and topography is not visually evident.

According to the map, depth to the water table greatly influences LV in the hill area, where the thickness of the unsaturated zone is > 65 m; this parameter holds the highest weight with a value of 22. Despite this high weight, values assigned to the attributes of this map layer could be too low for the Yucatan conditions (see Appendix B6), hence not affecting the shallow water table in the Coastal Area, Inner Cenote Ring, and Central Plain.

Since this method was developed to estimate source vulnerability, its adaptation to calculate resource vulnerability, as presented in equation (11), could result in some uncertainty. However, similarities among the KARSTIC and DRISTPi methods' outcomes could indicate that the theoretical analysis can be considered accurate.

3.3.7   RISKE vulnerability map

According to the RISKE method, vulnerability classes in Yucatan are 37.4% for HV, 61.8% for MV, and 0.9% for LV (Figure 3.23). Areas categorized with HV are directly related to high epikarst and karstification development derived from a combination of doline and fissure density maps. No VHV class is reached, due to the karstification map classification scheme, which considers areas with point infiltration to be the most vulnerable scenario.

As the RISKE method is one of the methodologies from which the PaPRIKa method was developed, some considerations to assign parameter values remain similar. Similar to the PaPRIKa, a doline density map was used as a base to define epikarst and karstification parameters (see Appendix B7). As these parameters have just two values, according to the method classification scheme, MV results across a high portion of the area. However, despite the similarities, vulnerability classes differ in one class lower than those from PaPRIKa; this could be a direct consequence of epikarst analysis, which in this method is the opposite of that presented by the PaPRIKa method.
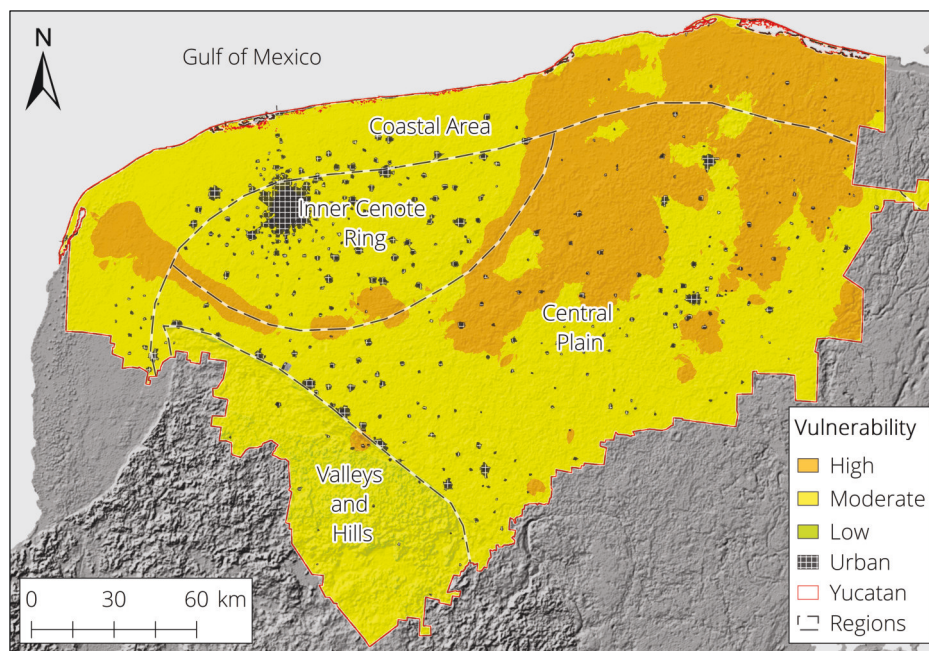
Figure 3.23: Yucatan groundwater vulnerability according to the RISKE method.

Steep slopes in the hill area play a role for the small percentage of LV since vertical infiltration in the associated map grids is minimized. Despite the infiltration parameter holding the highest weight, the low values assigned to areas with minimal elevation changes can also influence MV. Soil, discretized by texture and thickness, show no influence on vulnerability assessment.

3.3.8 SA vulnerability map

The SA is the only method which displays VLV with a low 2.9%. Other vulnerability classes are HV at 23.7%, MV at 54.9%, and LV at 18.5% (Figure 3.24). Again, high doline density areas, part of the O factor as lithology, are correlated with the HV class. As the P factor is homogeneous, it does not seem to affect changes in vulnerability, at least visually (see Appendix B8).

The slope and vegetation parameter is highly variable when separating heavily and lightly vegetated areas, however, no significant changes in vulnerability are clearly derived therefrom. Surface karst features, as part of the C factor, show a similar discretization to that of the lithology parameter; this characterizes a considerable part of the study area with no karst features at the surface as MV. Soil textures with a high content of fine particles and thickness ranging from 0.5 to 1 m seem to lead to LV classes.

Fine textured soils display VLV when their thickness overpasses 1 m. Precipitation is also included as an external stressor, however, the P factor is homogeneous and does not influence vulnerability discretization. Furthermore, depth to the unsaturated zone is linked to lithology, not showing any variation due to the low value assigned to karst limestones.

Given that the SA is a derivation of the COP, some tendencies on vulnerability classification are visually clear. Similarities for HV, MV, and LV are more evident comparing the southern areas of Yucatan from both vulnerability maps. The main differences seem to arise from the evaluation of precipitation as external stressor, directly affecting the VHV class for the COP but preventing the achievement of this class for the SA
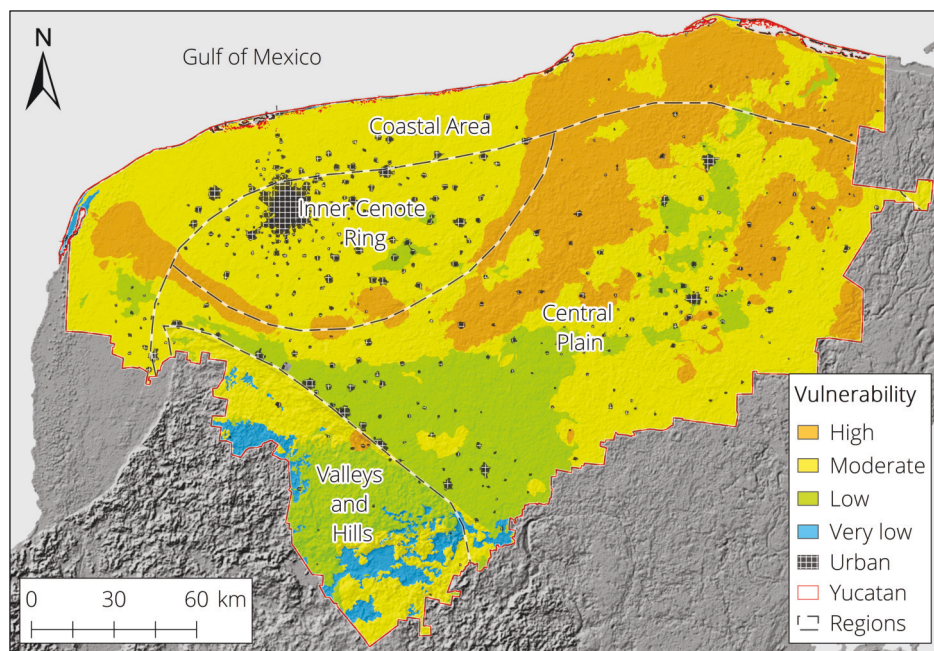
Figure 3.24: Yucatan groundwater vulnerability according to the SA.

3.4 Analysis, correlation and sensitivity

Vulnerability maps demonstrated interesting and unexpected outcomes in Yucatan. From visual inspection it was possible to highlight, with some subjectivity, some general trends on how vulnerability classes were distributed according to the theoretical base of each method applied herein. Areas where doline and fissure density are high, like the north-eastern doline field and the Cenote Ring, were classified by most of the methods either as VHV or HV zones (Figure 3.25). Variation among these two vulnerability classes is directly related to the individual discretization of the base-maps used to depict karstification and epikarst development.
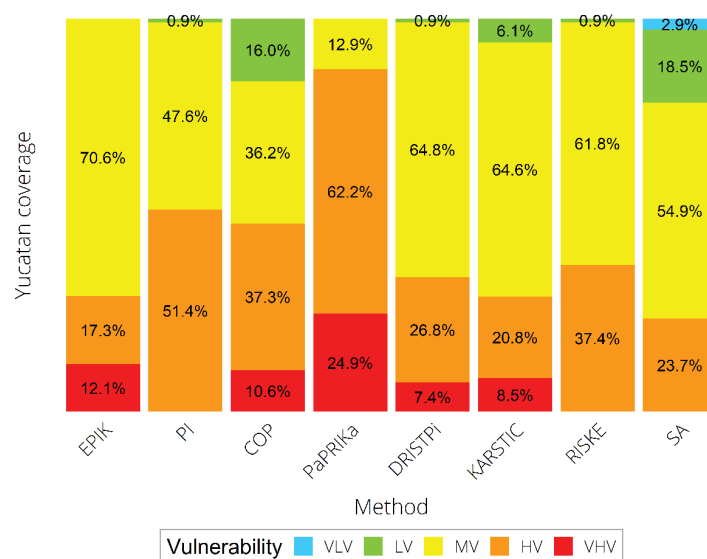
Figure 3.25: Comparative chart of vulnerability classes' percentage distribution.

A high percentage of MV was exhibited by most of the final maps, excluding that obtained from the PaPRIKa method. Six out of the eight methods, exposed areas with an LV category from which just one reached a VLV class. These classes indicate some degree of protection but did not show a clear relationship with specific characteristics, as in the case of VHV and HV, however, such areas were mainly located in the southern region where groundwater is deeper and fine-textured soils are usually present. Due to the similarities among maps, in terms of vulnerability percentage, it was necessary to evaluate the overall spatial correlation among them. An overlap analysis was performed to find the individual characteristics behind such similarities and the relevance of parameter attributes over vulnerability assignations.

Although previous studies have demonstrated contradicting vulnerability outcomes following the application of several methodologies over the same area, results in the Yucatan case revealed unexpected insights with an interesting vulnerability spatial distribution. Since some of the applied groundwater vulnerability schemes are closely related, some degree of similarity was expected from their overlap. However, the considerable spatial match percentage on vulnerability classification among most of the methods applied in Yucatan highlighted an interesting tendency that should be further investigated. The first overlap process was the MCA, performed to study the correlation in terms of vulnerability classes among multiple methods.

3.4.1   Results from the MCA

The DRISTPi and KARSTIC methods showed the highest total match on vulnerability ranks concurring across 86% of the area. This high spatial correlation was expected since these two methods apply the same scheme to classify most of their individual parameters, only varying in the process to evaluate karstification. Nevertheless, other methods like EPIK and RISKE also displayed agreement with them on vulnerability classifications with congruence values above 60%. On the other hand, the lowest congruence arose when the PaPRIKa and COP methods' vulnerability maps were included in the MCA, displaying congruence values below 30% (Figure 3.26).
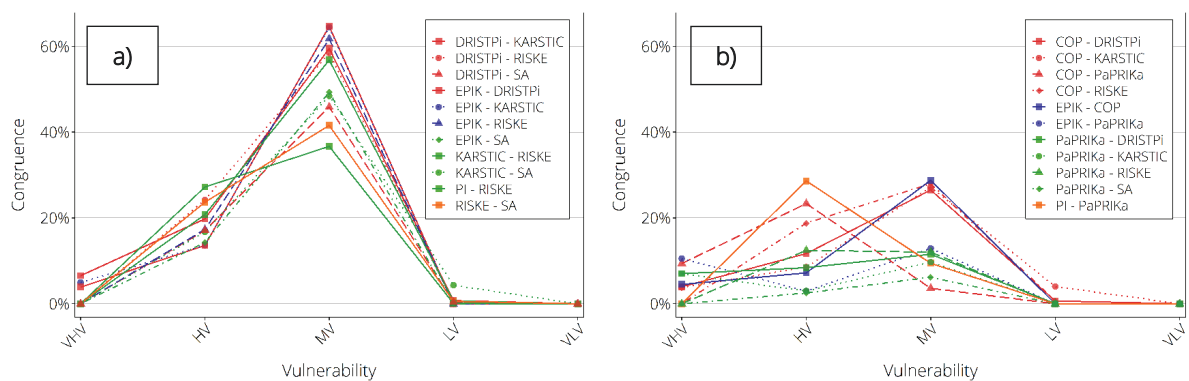
Figure 3.26: Spatial congruence on vulnerability classes according to the MCA. In a), the best correlated methods; in b), the least correlated methods.

From the overlap of 28 possible combinations, the MCA clearly demonstrated the importance of MV in methods correlation (Table 3.6). This vulnerability class resulted in the highest percentage of the total match with a mean value of 53%; the total match average increases up to 71% if the lesser correlated methods are arbitrarily excluded from the analysis. These were very interesting results as six methodologies, derived from three different base-methods (EPIK, DRASTIC, and the European framework) displayed similar tendencies on vulnerability assignments despite their unequal number of used parameters, attributes, values, and weights.

Table 3.6: Results from the MCA, discretized by vulnerability classes.

Tabulation	VHV	HV	MV	LV	Total match (%)
DRISTPi - KARSTIC	6.5	19.8	59.5	0.7	86.6
EPIK - KARSTIC	4.9	13.6	64.5	0.0	83.1
DRISTPi - RISKE	0.0	24.2	58.4	0.2	82.8
EPIK - DRISTPi	3.9	13.6	64.7	0.0	82.2
EPIK - RISKE	0.0	17.3	61.8	0.0	79.0
KARSTIC - RISKE	0.0	20.8	56.8	0.6	78.2
KARSTIC - SA	0.0	16.7	48.4	4.3	69.5
RISKE - SA	0.0	23.7	41.6	0.6	65.8
PI - RISKE	0.0	27.2	36.7	0.1	64.0
EPIK - SA	0.0	14.3	49.3	0.0	63.6
DRISTPi - SA	0.0	17.1	45.9	0.4	63.4
PI - DRISTPi	0.0	18.3	37.4	0.3	56.0
EPIK - PI	0.0	13.5	40.8	0.0	54.3
PI - COP	0.0	27.9	23.1	0.9	51.9
COP - SA	0.0	11.5	28.0	12.4	51.8
PI - KARSTIC	0.0	15.9	35.3	0.6	51.8
PI - SA	0.0	22.6	26.5	0.0	49.1
COP - RISKE	0.0	18.8	28.0	0.7	47.4
COP - KARSTIC	3.8	8.5	27.2	4.0	43.5
COP - DRISTPi	4.0	11.7	26.5	0.7	42.8
EPIK - COP	4.5	7.2	28.8	0.0	40.5
PI - PaPRIKa	0.0	28.6	9.4	0.0	38.1
COP - PaPRIKa	9.4	23.4	3.6	0.0	36.3
PaPRIKa - DRISTPi	7.0	8.4	11.5	0.0	27.0
EPIK - PaPRIKa	10.5	3.0	12.9	0.0	26.4
PaPRIKa - RISKE	0.0	12.4	12.0	0.0	24.5
PaPRIKa - KARSTIC	7.0	2.9	9.7	0.0	19.7
PaPRIKa - SA	0.0	2.5	6.2	0.0	8.7
Average match per class	2.2	15.9	34.1	0.9	53.1

Results from the MCA also highlighted an intriguing pattern; no significant differences were observable regarding VHV, LV, and VLV percentages, while a decrease of MV was directly reflected by an increment on HV. Nevertheless, at this point of the analysis, there lacked sufficient evidence to justify this inverse correlation between these two vulnerability classes.

3.4.2   Results from the PCA

To evaluate the hypotheses behind each method leading to similar results, it was necessary to extend the analysis. In order to study the relationship between parameters, attributes, and the different levels of vulnerability the PCA was performed; this was carried out by overlapping vulnerability maps with their individual map layers one by one. Similar tendencies were displayed by six methodologies (EPIK, PaPRIKa, DRISTPi, KARSTIC, RISKE, and SA) where characterization of karst-related parameters directly match the spatial distribution of VHV, HV, and MV.

Results indicated that karst-related layers such as epikarst and karstification seem to completely drive Yucatan's vulnerability spatial distribution. In all methods, vulnerability classes are strongly linked to those map layers and the way they are evaluated; the more developed the karstification (high doline-fissure density and karst surface features), the more vulnerable the area is. Therefore, the unexpected correlation between diverse methodologies was then associated with these base-maps.

For methods like PI and COP, VHV and HV arose from a combination of two or more parameters but always with a karst-related parameter as a base. In the case of the PI method, vulnerability is directly proportional to the degree of fracturing and inversely proportional to soil thickness. The COP method presented a similar association between karstification and precipitation maps influencing vulnerability classes. According to the PCA, LV is exclusively achieved when areas with minimal karstification overlap protective characteristics, such as thick or fine textured soils, deep groundwater tables, or high slopes. However, the influence of the latter on low vulnerability classes seems to depend on how the slope is characterized according to the infiltration scenario.

In Table 3.7, descriptive characteristics of influential attributes are displayed according to the vulnerability class they directly affect. Despite descriptions of attributes being used as applied by each method, those describing karstification, epikarst, or fissuring are derived from the same base maps (see section 3.2.2).

Table 3.7: Attributes of individual map layers influencing vulnerability classes.

Method	VHV	HV	MV	LV
EPIK	High epikarst and karstification development	Moderate epikarst and karstification development	Low epikarst and karstification development	Not achieved
PI	Not achieved	High fracturing and thin soils (< 0.2 m)	Moderate to low fracturing and soil thickness from 0.2 m to 1 m	Low fracturing and thick soils (> 1.5 m)
COP	High karstification and moderate precipitation	High karstification and low precipitation	Low karstification and low-high precipitation	Fine textured soil > 0.5 m of thickness
PaPRIKa	High karstification	Low karstification	Fine textured soils; steep slopes	Not displayed
DRISTPI	High preferential infiltration	Moderate preferential infiltration	Low preferential infiltration	Unclear
KARSTIC	High karstification and high fissuring	Low karstification and high fissuring	Low karstification and low fissuring	Deep water table
RISKE	Not achieved	High epikarst and karstification development	Low epikarst and karstification development	Steep slopes
SA	Not achieved	High development of karst surface features	Low development of karst surface features	Fine textured and thick soils

In a general overview, results indicated that karstification plays the leading role in assignation of vulnerability classes, independent of the evaluated scenario; protective characteristics seem to play a relevant role solely when karstification is minimal. Those parameter characteristics, highlighted as the main influence for a given vulnerability class, supported some of the early insights derived from visual inspection. Since most of the Yucatan area was classified as MV, it was very important to define the background of individual parameters creating this class. However, the PCA just pointed out descriptive characteristics influencing vulnerability. To further evaluate such influences on numerical terms, a map removal sensitivity analysis followed.

3.4.3   Map removal sensitivity analysis

While parameter congruence analysis evaluates the relationship between vulnerability classes and individual parameters according to their attributes (sands, clays, high slopes, low slopes, etc.), map removal sensitivity analysis estimates the influence of single parameters according to the rating values assigned to them and their effect on numerical vulnerability indexes. To have an analytical reference, tables of theoretical UCSs were created for each method and compared against those from the Yucatan case (Table 3.8).

Table 3.8: Numerical differences among groundwater vulnerability methods.

Method	Theoretical UCSs	Yucatan UCSs	Map layers	Attributes values	Weight range	Index range	Index-vulnerability relation*
EPIK	216	9	4	1 - 4	1 - 4	9 - 34	Inversely proportional
PI	288,800	2,304	4	0 - 750	Not applicable	0 - 5	Inversely proportional
COP	64,800	157	6	0 - 15	Not applicable	0.15 - 15	Inversely proportional
PaPRIKa	207,360	57	6	0 - 4	0.1 - 0.7	0.5 - 4	Directly proportional
DRISTPi	138,600	740	6	1 - 10	1 - 5	19 - 190	Directly proportional
KARSTIC	118,800	323	8	0.5 - 10	1 - 20	25 -1,186	Directly proportional
RISKE	8,000	43	5	0 - 4	0.1 - 0.4	0 - 3.8	Directly proportional
SA	69,120	43	6	0 - 15	Not applicable	0 - 15	Inversely proportional

* A directly proportional relation indicates that vulnerability increases as index does.

Previous studies which have performed map removal sensitivity analysis have evaluated the role of factors and their numerical influence on final indexes, such as those forming the COP method or the P factor of the PaPRIKa method. However, this procedure does not highlight the role of single parameters forming such factors, analysing in a general point of view the role of those conditions either promoting by-pass or protecting the aquifer in diffuse infiltration scenarios.

In this work, sensitivity was also evaluated for individual parameters forming a factor and not for the factor itself. For congruence with the study area characteristics, only diffuse infiltration scenarios were considered for theoretical UCSs development. For methods like PI, COP, and SA, no swallow hole catchment areas were part of the tabulation process to create UCSs. In the case of the PaPRIKa method, all possible combinations among parameters forming the P factor (soils, epikarst, and unsaturated zone) were created prior to the development of the PaPRIKa method's theoretical UCSs.

Difference in numbers among theoretical and Yucatan UCSs are outstanding. For methods which include depth to groundwater as a multiplier for parameters representing the unsaturated zone characteristics (as is the case with the PI, COP, and SA methods), the decision was taken to take five representative depths of the Yucatan area as an alternative to avoid an immense number of UCSs. Despite this measure, some methods presented considerably high numbers of UCSs since some attributes are also large in number.

As displayed in Table 3.8, values, weights, and vulnerability indexes vary by orders of magnitude among methodologies. Since the scope of the map removal analysis was to evaluate the sensitivity of individual parameters on their correspondent final index and not to compare how they differ among methodologies, no re-scaling was performed. Map layer removal sensitivity was carried out for each method for both theoretical and Yucatan UCSs.

3.4.3.1   EPIK sensitivity

For the EPIK method, sensitivity of the four parameters showed little variation on the final index for theoretical UCSs, considering the rating used by this method. Boxplots displayed similar proportionalities in the first quartile (Q_1) and the third quartile (Q_3) with respect to the median value (Q_2), demonstrating equilibrium on value assignment for theoretical UCSs (Figure 3.27).
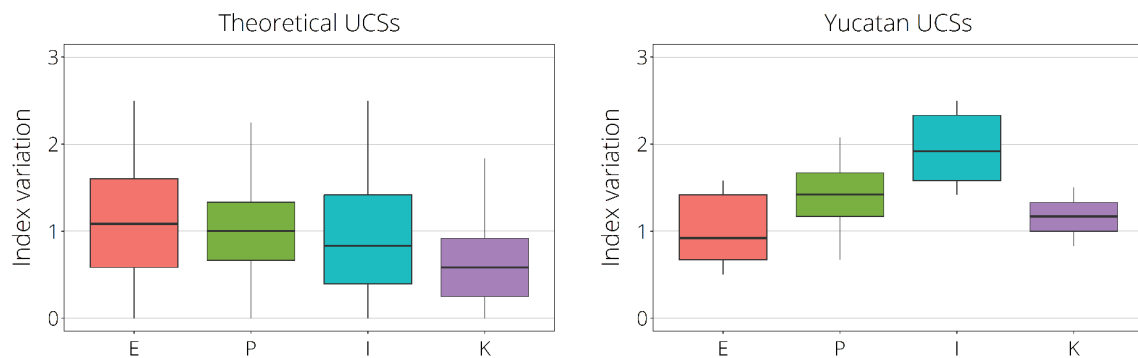
Figure 3.27: Map removal sensitivity according to the EPIK method. The evaluated parameters are: epikarst (E), protective layers by soil thickness (P), infiltration conditions by slope (I), and karstification (K).

This similarity in parameter sensitivity could be driven by the correlative rating values used to characterize each parameter attribute under the same order of magnitude. However, in the Yucatan case the highest sensitivity is driven by the infiltration layer as a result of its homogeneous characterization, representing a regionally diffuse infiltration condition. On the other hand, the lowest sensitivity is displayed by the epikarst map, meaning that there is little influence on the final vulnerability index. The index-vulnerability inverse proportionality was clear, since diffuse infiltration represents the most protective condition, while epikarst development represents the most vulnerable.

Sensitive results from the EPIK method partially support the ideas derived from the PCA. The role of epikarst was confirmed to be more influential than karstification for VHV and HV classes but the extensive MV class arises from the most protective infiltration characteristics.

3.4.3.2   PI sensitivity

Theoretical UCSs for the PI method were developed solely for the P factor. The Yucatan diffuse infiltration scenario indicates a value of one for the I factor, hence, not affecting the protective layers function according to equation (5). In conformity with the PI method theory, maps forming the P factor are similarly sensitive, indicating a well-balanced rating system influencing the vulnerability index. Although the bedrock map showed a slightly larger interquartile range (IQR), with an extended Q_3 in relation to Q_2, this was assumed to be a consequence of the unsaturated zone depth applied as an exponential factor for said map and the several lithologies evaluated in theoretical conditions (Figure 3.28).
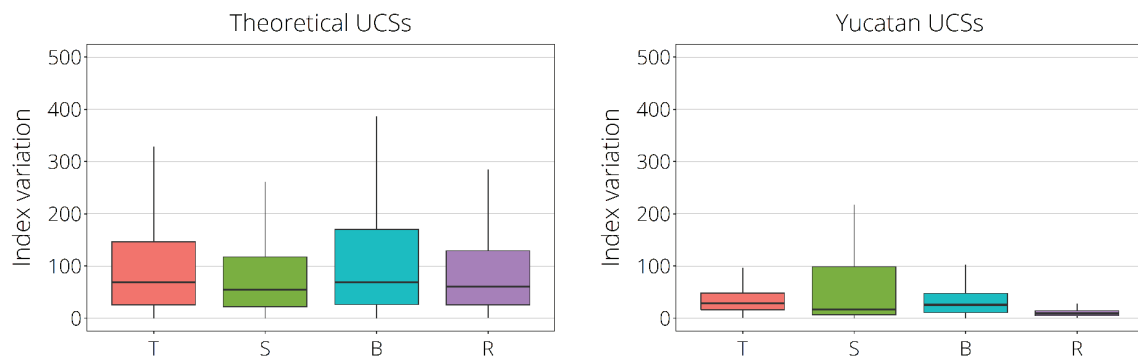
Figure 3.28: Map removal sensitivity according to the PI method. The evaluated parameters are: topsoil by its eFC (T), soils by texture (S), bedrock by lithology and fracturing (B), and recharge (R).

This sensitivity was not reflected in the Yucatan scenario where notably lower sensitivities were displayed. For Yucatan, sensitivities are, in general, lower than those displayed by theoretical predictions, as highlighted by the differences in the index range. In the Yucatan case, bedrock was settled homogeneously as limestone for the whole area, showing a fairly balanced sensitivity. However, the bedrock map is composed by lithology and fracturing development, hence, the latter being the parameter directly affecting sensitivity variation. Soils demonstrated a more variable sensitivity with a lower Q_2 value in comparison with other parameters but an extended IQR, increasing two orders of magnitude with respect to the index. Sensitivity interpretation supported the previous insights from the PCA, which noted the influence of soils on the PI vulnerability index (see Table 3.7). Despite regional heterogeneity of the recharge parameter, it shows a slight sensitivity regarding the final index.

3.4.3.3   COP sensitivity

Factors constituting the COP method were disjointed to individually evaluate the sensitivity of their forming parameters. In theoretical conditions, parameters showed low sensitivities, considering the index range as ranging from 0.15 to 15; sensitivities displayed a Q_2 of approximately 0.15, which is the minimum index value for diffuse infiltration conditions. Even with similar IQR with a skewness tendency to Q1, map layers indicate little influence on the vulnerability index. Considering the index range and its inverse relationship with vulnerability, parameters are evenly balanced with sensitivities most probably affecting VHV and HV, according to the theoretical assumptions (Figure 3.29).

Figure 3.29: Map removal sensitivity according to the COP method. The evaluated parameters are: overlying soils by texture and thickness (Os), overlying lithology (Ol), surface karst features (Sf), slope and vegetation (Sv), precipitation (Pq), and precipitation intensity (Pi).

In Yucatan, the COP method demonstrated that lithology and precipitation in terms of volume are less sensitive, with medians closer to zero. This contradicted the PCA where precipitation displayed a well-marked limit for HV and MV. The most sensitive parameters in the Yucatan case were soils and surface features indicating karstification, partially supporting results from the PCA. An alternative hypothesis to explain such results is that soils and karst-related parameters lead to index variability, while precipitation, despite its low sensitivity, is only relevant under specific conditions.

3.4.3.4   PaPRIKa sensitivity

For the PaPRIKa method, parameters forming the P factor (protective layers) were separately evaluated according to their individual sensitivity in theoretical scenarios where each one represented the most protective characteristics. Soils, lithology, and epikarst maps displayed similar sensitivities, meaning that they have an equivalent influence on the vulnerability index. The theoretical protective conditions also displayed similar sensitivities when integrated and compared with the rest of the parameters forming the PaPRIKa method. The exception is the rock type map, which showed a lower sensitivity on the vulnerability index due to the shorter rating proposed for this parameter (Figure 3.30).
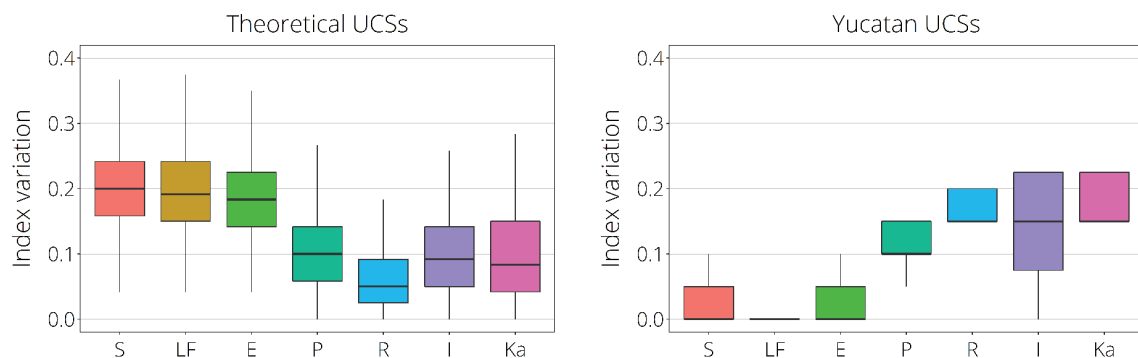
Figure 3.30: Map removal sensitivity according to the PaPRIKa method. The evaluated parameters are: Protection covers (P) formed by soils (S), lithology, (L), and epikarst (E); rock type (R), infiltration conditions by slope (I), and karstification (Ka).

Theoretical UCSs demonstrated an even sensitivity in terms of median values, indicating equilibrium among parameter ratings. A contrasting sensitivity distribution was displayed in the Yucatan scenario where protective layers were individually depicted with the lowest sensitivity, even when forming the P factor. Rock type, karstification, and infiltration conditions show similar sensitivities according to their median values. However, the infiltration parameter showed a broader IQR, indicating more variability on the final index. Comparing sensitivity outcomes with those from the PCA, it is clear that the designation of VHV and HV for the whole area is not solely a consequence of karstification related layers. Yucatan infiltration conditions and the theory behind its role on vulnerability, display an extreme situation according to the PaPRIKa method, as sustained by outcomes from sensitivity analysis.

3.4.3.5   DRISTPi sensitivity

Theoretical UCSs for the DRISTPi method indicated higher sensitivities of parameters representing the impact of the vadose zone, topography, and preferential infiltration. Most of the parameters showed equilibrated IQR, but for those depicting karstification (I and Pi) the range was broader, indicating a more variable influence. It is important to note the skewed tendency to lower sensitivities, indicating that under some conditions the parameters' sensitivity could be higher.

Sensitivity in the Yucatan case showed normality for most of the parameters but with variable medians (Figure 3.31). Results highlighted that lithology is the most sensitive parameter, greatly influencing the direct proportionality of the vulnerability index. The lowest sensitivity is represented by depth to groundwater.
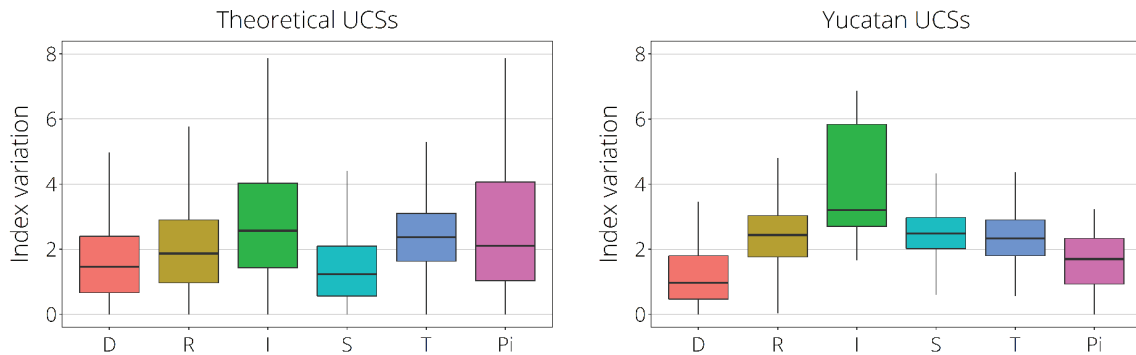
Figure 3.31: Map removal sensitivity according to the DRISTPi method. The evaluated parameters are: depth to groundwater (D), recharge (R), impact of the vadose zone by lithology (I), soils by texture (S), topography by slope (T), and preferential infiltration (Pi).

An interesting outcome is the low sensitivity displayed by preferential infiltration; this parameter hypothetically represents the most vulnerable condition; it appears not to dominate the index in the Yucatan case. However, the impact of the unsaturated zone seems to fulfil this purpose since it considers karstic and non-karstic lithology. Unlike outcomes from the PCA, which indicates the relevance of preferential infiltration for highly vulnerable areas, sensitivity indicates that the lithology parameter exerts more influence on the final index.

3.4.3.6 KARSTIC sensitivity

Unlike previous methods, the KARSTIC method's sensitivity analysis displayed dubious outcomes, surpassing the range of parameter values proposed by this method. This could be a consequence of the relatively high weights assigned to some parameters (Figure 3.32).
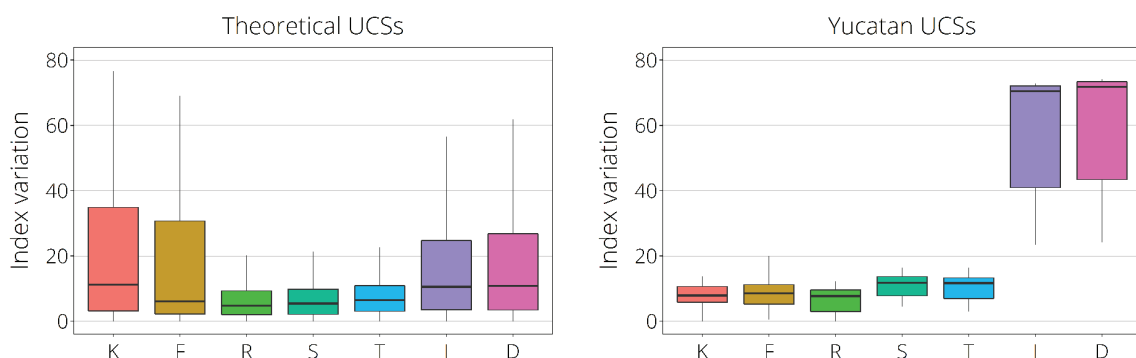
Figure 3.32: Map removal sensitivity according to the KARSTIC method. The evaluated parameters are: karstification (K), fissuring (F), recharge (R), soils by texture (S), topography by slope (T), impact of the vadose zone by lithology (I), and depth to groundwater (D).

While recharge, soils, and topography hold weights ranging from 2 to 5, the remaining parameters have weights from 11 to 22. Although equation (15) aims to minimize the role of weights to focus solely on parameters' sensitivity, such equation does not seem to be applicable when significantly contrasting weights are used. This is more noticeable in the Yucatan case where the impact of the vadose zone and depth to groundwater show the highest sensitivity with a marked tendency of Q_2 towards Q_3.

Despite the ambiguity of sensitivity outcomes, results are similar to those presented by the DRISTPi method. Lithology including karstification and depth of the unsaturated zone were the driving parameters for the vulnerability index according to sensitivity. The direct proportionality presented by this method indicates that areas with elevated vulnerability are closely related to these conditions. This is contrary to the PCA outcome, which depicted karstification exerting the most influential role.

3.4.3.7   RISKE sensitivity

Theoretically, parameters forming the RISKE method are similarly sensitive, with the exception of the infiltration parameter, which is governed by topographical differences. This hypothesizes that infiltration is of most influence for the final index, hence vulnerability. A similar trend, but with lower values, was displayed in the Yucatan case (Figure 3.33).
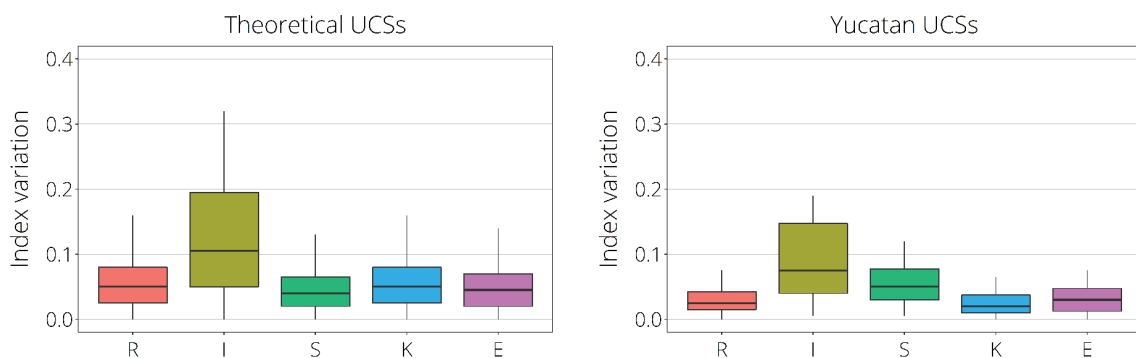
Figure 3.33: Map removal sensitivity according to the RISKE method. The evaluated parameters are: rock type (R), infiltration by slope (I), soils by texture and thickness (S), karstification (K), and epikarst (E).

Sensitivities for rock type, karstification, and epikarst were lower, in comparison with those from theoretical UCSs, by approximately half with a less pronounced IQR variability. As the method is directly proportional, sensitivity supports results from the PCA, indicating that karst-related parameters influence vulnerability outcomes. However, the infiltration parameter which includes sinkhole catchment areas, limits the vulnerability scope and does not reach VHV due to diffuse infiltration conditions despite its high sensitivity on the final index.

3.4.3.8   SA sensitivity

The SA method displayed very similar sensitivity values, in terms of the median, for most of its parameters excluding soils. This makes the SA method one of the most equilibrated methods with the index being similarly sensitive to each parameter in theoretical conditions (Figure 3.34).

Even the IQR demonstrated a balanced numerical distance from Q_2. In Yucatan, the SA method displayed a higher sensitivity for the soil parameter, followed by surface features or karstification. The rest of the parameters showed little sensitivity when removed from the analysis. This reflected the homogeneity of such parameters in the Yucatan case, as displayed in Appendix B8.
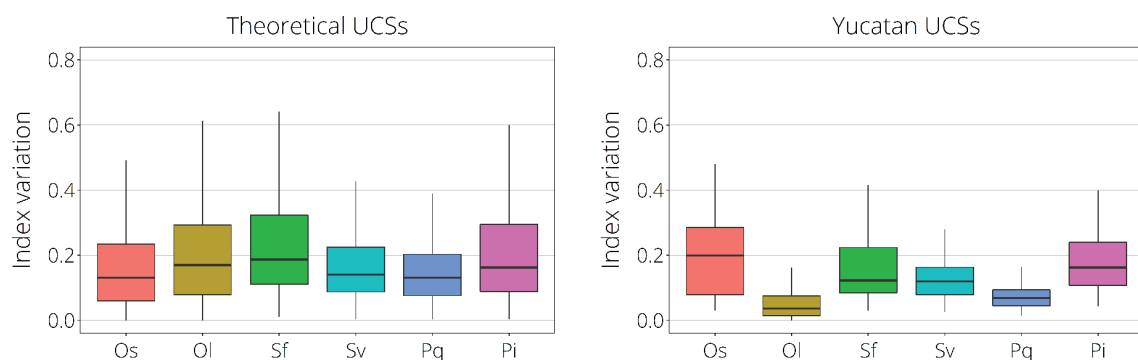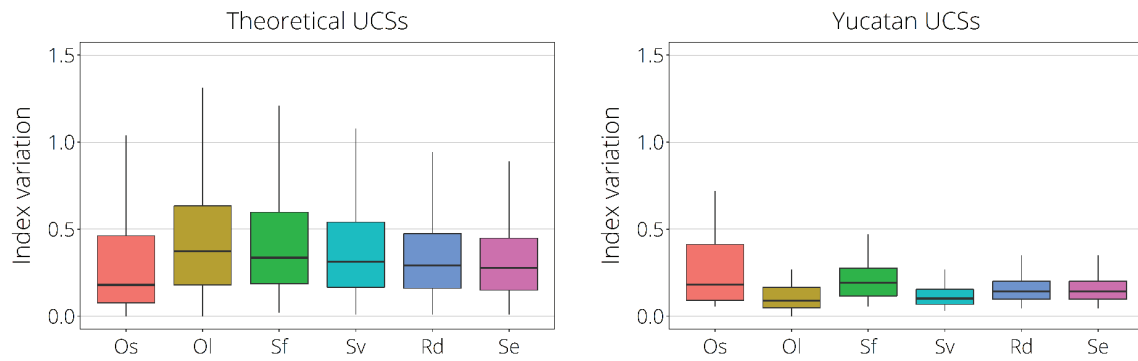
Figure 3.34: Map removal sensitivity according to the SA. The evaluated parameters are: overlying soils by texture and thickness (Os), overlying lithology (Ol), surface karst features (Sf), slope and vegetation (Sv), rainy days (Rd), and storm events (Se).

The PCA proposed that, in the case of the SA, karst-related maps (in this case surface features) are almost entirely responsible for vulnerability, with soils influencing LV solely when karstification is low. The sensitivity analysis demonstrated that this could not be the case, instead, soils could have the leading role, whilst karst-related maps only have a significant influence when some soil conditions are fulfilled.

3.4.4 Effective weight analysis

Sensitivity results helped to better identify the influence of single parameter ratings on vulnerability indexes. Some of the early outcomes from the MCA and the PCA were supported by sensitivity results. However, in some cases parameters demonstrated a more intricate role in vulnerability. Although some general trends were highlighted, the influence of weights was not included in the previous step. An additional analysis was performed for those methodologies utilizing weights according to equation (17). The goal was to establish the individual parameters hierarchy to evaluate their influence on vulnerability indexes according to their effective weight. Since the PI, COP, and SA methods do not follow such an approach, they were excluded from this analysis (Table 3.9).

Table 3.9: Parameters' rating hierarchy on vulnerability indexes including weights.

Method	Theoretical UCS	Yucatan UCS
EPIK	E > I > K > P	I > E > K > P
PaPRIKa	Ka > I > R > P	Ka > R > I > P
DRISTPi	I > PI > R > S > D > T	I > R > D > Pi > T > S
KARSTIC	K > D > I > F > R > S > T	I > D > R > K > F > T > S
RISKE	I > K > E > S > R	I > K > E > R > S

Results displayed infiltration and karstification as the most relevant and influencing parameter on vulnerability indexes in the Yucatan case. The variability induced by map layers representing those conditions, was higher in all of the weighting methods. While theoretical UCSs display a correlative hierarchy from higher to lower, according to their assigned weights, in Yucatan infiltration and karst-related maps played a more relevant role on the vulnerability indexes variability.

3.5 Discussion

Eight methodologies for intrinsic groundwater vulnerability assessment were applied in the Yucatan karst. Despite showing a considerably high agreement on the assignation of vulnerability classes, this must not be taken as indicative for the reliability of results. Methods evaluated herein displayed an arguable agreement regarding the Yucatan's intrinsic characteristics. The role of karstification and surface features, denoting a potential by-pass of pollutants towards the aquifer, are theoretically well evaluated assigning either VHV or HV on those areas where karstification is highly developed. The high weights commonly settled for karst–related maps also influence MV. Nevertheless, this vulnerability class is mostly dominated by diffuse infiltration conditions.

Given the natural characteristics of the Yucatan karst, designation of MV for most of the area is highly questionable. Although the definition of karstification as the main promotor of by-pass, hence influencing high vulnerability, can be considered theoretically correct, its effect on MV is arguable for the Yucatan case. It could be considered inaccurate to categorize areas where the groundwater table is close to the surface as MV, when analysing regional characteristics in Yucatan or any other karst landscape with shallow water tables. Even landscapes with low karstification development or low fissuring could allow pollution to infiltrate, quickly reaching near-surface phreatic levels.

Additionally, it is important to note the high subjectivity when categorizing areas as having high, moderate or low karstification. Therefore, karstification should not be considered as the leading condition with which to evaluate how fast a pollutant can reach the water table. This vulnerability misclassification is well represented in the Yucatan near-coastal areas, which theoretically represent high vulnerability conditions due to the presence of thin soils of coarse-to-medium textures, near surface phreatic levels, and fissuring.

The variability of groundwater depth is well marked in the region due to the hill area where the phreatic level is found at depths of > 100 m. Nevertheless, this area is mostly defined with MV without a significant influence of this parameter on vulnerability. According to the Yucatan characteristics, the hill area represents the most protective setting, with a combination of fine textured soils with a thickness of > 1 m, low karstification development, and the deepest groundwater table. Nevertheless, these contrasting conditions with those being displayed near the coast are not represented by any vulnerability outcome. Therefore, the high percentage of MV in Yucatan, according to the methods, can lead to some misrepresentations, also making the role of other features, such as soils and groundwater depth, which seem to have little influence on Yucatan's vulnerability outcomes according to the sensitivity analysis, irrelevant.

A moderate vulnerability class does not display congruence with the shallow water table near the coast, a regional situation that can be considered to be a naturally low protective scenario, even if these areas are not characterized as highly karstified. As a contradictory scenario, the Sierrita de Ticul is the hill area where groundwater is found at depths of > 100 m, however, it is also mostly classified with MV.

The outstanding designation of MV for most of the Yucatan area and the considerable spatial match among methodologies regarding this vulnerability class, generated more questions about the congruence of these methodologies in terms of applicability. From their spatial and sensitivity analysis it was possible to highlight some possibly misleading parameter roles in current groundwater vulnerability approaches.

It has been shown that parameters differ in range, values, and weights assigned to them, which results in differences among vulnerability outcomes. Nevertheless, in the following sections the effect of each parameter is discussed to highlight possible modifications in terms of their theoretical influence on groundwater vulnerability studies.

3.5.1 Karstification

Since high karstification increases the possibility of by-passing the unsaturated zone, thus decreasing the time for a pollutant to reach the aquifer, this parameter is also weighted as one of the most relevant. In this case, two remarks must be considered: the karstification map discretization and its overlap with other karst-related maps. No precise guidelines exist to determine how "well-karstified" an area is. Methodologies' descriptions for this map layer are based on connectivity with the surface, conduit system locations, or surface features occurrence, without a descriptive methodology to characterize said map layer as having high, moderate or low karstification.

Similarly, methods like COP and SA consider the occurrence of surface features without further descriptions to characterize such a map. Since heterogeneity in karst landscapes is high, a regional approximation is necessary in order to fulfil the study area necessities and minimize the over-/underestimation of karstification. It is important to highlight the role of karstification derived maps since overlap among them can also increase vulnerability.

Fissuring is commonly related to lithology and some methods use it to characterize epikarst or karstification degree. However, the description used to classify fissured areas is also ambiguous and not clearly defined. Terms like highly, strongly, or major fissuring are used to discretize this parameter. It is, thus, necessary to evaluate fissuring using a more descriptive approach but also in a way that is able to adapt to the regional conditions.

3.5.2 Epikarst

Epikarst is indirectly estimated either from surface features, such as dolines, or by spring flow data. In both cases, no precise definitions are provided to create a map layer of this feature. Two problems for epikarst characterization were highlighted in this work: to define their hydrologic functioning and the similarity of epikarst maps with other map layers (such as surface features or karstification maps) when estimated from doline occurrence.

Epikarst hydrologic functioning can provide some protection when acting as a perched aquifer, delaying the downward travel time of pollutants. On the other hand, it can promote a faster infiltration via shafts, connecting the base of epikarst to deeper locations below the sub-surface. However, although modelling studies have demonstrated the relationship between surface features, epikarst, and conduits development, designating epikarst functioning as protective or vulnerable solely through the occurrence of surface features, can greatly mislead groundwater vulnerability outcomes.

Additionally, epikarst estimation from the presence of dolines or fissures can overlap other map layers, which are estimated by following the same principle. In this case, vulnerability can be severely increased, thereby affecting results for the entire area and minimizing the role of other features. The integration of map layers derived from the same principle is thus proposed; unsaturated zone karstification, surface karst features, and epikarst can be merged in a unique map to avoid overestimations.

3.5.3 Lithology

Lithology map layers are classified by the material in the sub-surface according to their infiltration delaying capacity; lithology classification is variable among methods since they consider lithological profiles found in the methods' area of development. However, this is another situation causing uncertainties since the consideration of a non-existent lithology in our area of interest indirectly over/underestimates the role of this parameter in our vulnerability studies. This is clearly seen in the Yucatan case, being regionally characterized as a limestone landscape, the Yucatan lithology map does not allow further discretization.

Therefore, several lithology materials contemplated by the applied methods, such as marls, sandstones, breccias, claystone, or volcanic rocks, are inherently analysed and, therefore, influence results. This situation highlights another important case; the role of a homogeneous map layer in vulnerability studies. Since the goal of vulnerability schemes is to segregate a given area to describe locations prone to pollution, the use of a homogeneous layer will not contribute to reaching this goal.

3.5.4   Soils

Soils are settled as the least relevant feature for groundwater vulnerability; as reflected by the fact that they are always assigned with the lowest weight in all methods. A common rule among soils as a vulnerability parameter is the influence of the fine particles' percentage (clays and silts) on delaying a pollutant; the higher their percentage, the more protective the soil is. This is represented in all vulnerability methods, irrespective of the soil classification system used (USDA, German, French, etc.). However, the role of soils on vulnerability analysis needs to be re-evaluated since their theoretical hydraulic behaviour contrasts with the infiltration scenario and it is closely related to slope.

Fine textured soils can represent an important protective feature for diffuse infiltration areas since vertical infiltration would be theoretically delayed; this is the default to analyse soils' influence on groundwater vulnerability schemes. Nevertheless, fine textured soils can also increase the possibility of runoff if other conditions, such as high slopes, exist. This is not considered by the majority of the methods which analyse solely slope as the main runoff generating parameter. Therefore, inversing its role for scenarios with point infiltration, in relation with the slope parameter, is a more sensible theoretical approach for a soil texture analysis (compare scenarios in Figure 3.35).

3.5.5   Topography as slope

Slope is mostly evaluated in terms of surface flow generation; excluding DRASTIC-derived methods, a high weight is commonly assigned to slope, enhancing their relevance for point infiltration conditions. However, slope influence on vulnerability analysis must take a different point of view according to the scenario in question.

To exemplify this statement, the default rule for slope as a parameter could be taken: the higher the slope, the more likely runoff could be generated to reach a swallow hole. Despite this analysis is not considering the influence of other features on runoff generation, such as soils, vegetation cover, or even precipitation as an external factor, this evaluation regarding slope is reasonable. Nevertheless, if the study area is categorized with a diffuse infiltration condition, the theoretical role of high slopes becomes protective.

In other words, for diffuse infiltration scenarios, a high slope would promote runoff, hence, minimizing vertical infiltration in a given map grid. Not all methods take this into consideration; methodologies inversing the role of slope (COP, SA) evaluate point and diffuse infiltration collectively, thus inherently decreasing the vulnerability classification for the latter (compare scenarios in Figure 3.35).

3.5.6   Unsaturated zone

Depth to groundwater is an important parameter, which can exert a considerable influence on pollutants' travel time in diffuse infiltration areas. Nevertheless, it shows little to no influence on vulnerability outcomes in the Yucatan region according to the applied vulnerability schemes. While DRASTIC-derived methodologies include the depth of the unsaturated zone as a single parameter, those from the European approach use it as a booster for the lithology map layer.
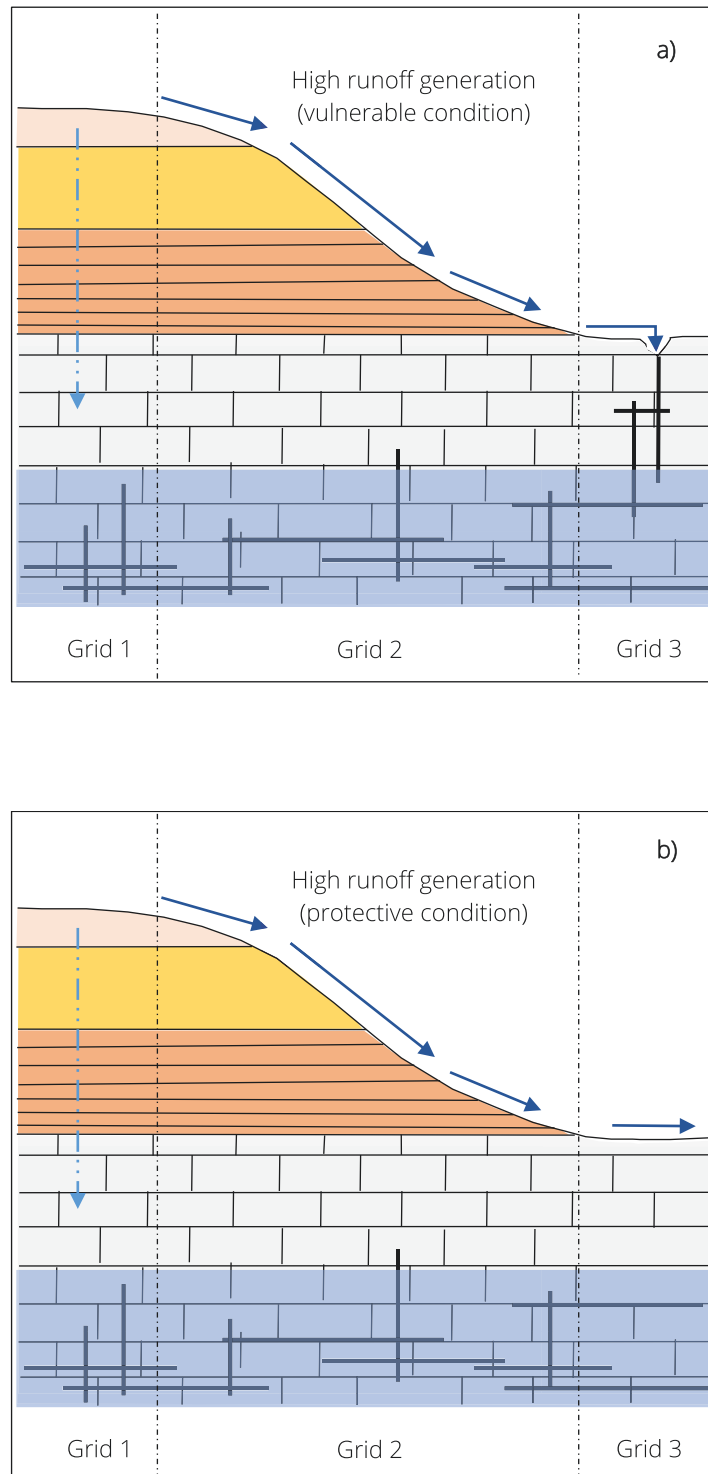
Figure 3.35: Influence of slope and soils for point and diffuse infiltration scenarios. In a), a point infiltration scenario where fine-textured soils and high slopes are likely to promote runoff towards a by-passing feature. In b), the same conditions will promote protection in a diffuse infiltration scenario since vertical infiltration could be minimized. Modified after Goldscheider (2005).

In the case of EPIK-derived methods, the depth of the unsaturated zone is irrelevant because such methods focus their main analysis on the by-pass of the unsaturated zone via karst features in catchment areas. However, if the study area is a diffuse infiltration basin, it is necessary to acknowledge the importance of this parameter, as in the Yucatan case. For the methods including EPIK, PaPRIKa, or RISKE, the description of non-feeding catchments as "rest of the area" eliminates the possibility of evaluating the depth of the unsaturated zone as a protective layer. This directly minimizes vulnerability and can lead to incorrect outcomes. Additionally, when the depth of the unsaturated zone is discretized, as proposed by some methods (KARSTIC, DRISTPi, PaPRIKa), inaccuracies in the descriptive conditions are evident, mainly for coastal karst aquifers. Therefore, methodologies including this parameter need an adaptable classification approach for the depth of the unsaturated zone to be able to incorporate regional characteristics of the studied areas.

3.5.7   Precipitation

As an external stressor, rainfall is directly evaluated by three of the methods. Either by volume, intensity, or recharge rate, precipitation can also mislead vulnerability outcomes if regional conditions are not included into the analysis. For areas where precipitation is temporal and spatially variable, the application of yearly averages as parameters for vulnerability could lead to some inaccuracies, mostly for areas with extreme conditions, well-marked precipitation regimes, or when prone to extreme events. As proposed by the COP method, precipitation can influence some dilution, nevertheless, it does have a general principle: the greater the precipitation, the greater the dilution potential. This perspective does not include the volume of solutes to be diluted, therefore, this point of view complicates the selection of precipitation boundaries when categorizing precipitation as either increasing vulnerability due to advection or decreasing vulnerability due to a dilution potential.

If precipitation is used as a vulnerability estimator, a simplistic approach must be taken to minimize misclassifications: the greater the precipitation, the greater the likeliness that the transport of pollutants will occur. Additionally, if the study area experiences considerable differences regarding precipitation regimes, a temporal vulnerability characterization would be a better approximation.

3.6   Chapter remarks and outlook

The previous discussion focuses on the most relevant vulnerability map layers, highlighting some inconsistencies regarding vulnerability evaluation. This analysis recognizes dissimilarities among methods in terms of used parameters, map layer discretization, and weight assignments. All these aspects result in contrasting outcomes when the methods are applied and compared in a given karst area. Therefore, the selection of one specific method to be applied requires some knowledge about the hydrological and geological conditions of the area as well as the vulnerability principle.

From the application of vulnerability schemes in Yucatan, a theoretical review of parameters considered for intrinsic vulnerability estimation, demonstrated a misleading analysis when scenarios (point and diffuse infiltration) are evaluated together. Despite a point infiltration scenario being theoretically more vulnerable, a joint estimation of groundwater vulnerability with both scenarios directly minimizes vulnerability classes for diffuse infiltration conditions.

This situation is remarkable in the Yucatan karst since the area is categorized as a diffuse catchment; a situation that leads to contradictions, as demonstrated in the coastal area which is classified as moderately vulnerable despite the shallow water table, coarse soils, fissuring, and low slopes. Diffuse infiltration areas can also display highly vulnerable conditions, hence, a complete segregation between point and diffuse infiltration conditions is highly recommended, where each scenario must be analysed individually. Steps to regionalize vulnerability schemes and the re-evaluation of some parameters, such as soils and slope, with respect to the scenario for which they are applied, are necessary.

The application of vulnerability methods utilizing parameter boundaries, as proposed by established methodologies, can also cause inconsistencies with regional characteristics due to the indirect evaluation of attributes not present in the study area. Another point to take into account is the heterogeneity presented by some natural characteristics. As the goal of any multi-parameter analysis is to discretize the study area in ranges according to the final goal (vulnerability, suitability, risk, etc.), homogeneous map layers may not be relevant when pursuing this goal. Therefore, when facing this situation, it is important to consider the removal of such layers and focus on those natural characteristics displaying regional or local differences.

As an example, a precipitation map layer will not help to highlight areas where advection transport is more probable if mean annual precipitation is homogeneous in the study area. However, if precipitation intensity is spatially dissimilar, a map representing this parameter could be comparatively more helpful to highlight areas prone to pollution. Even though a pre-established parameter class can be assigned to a homogeneous precipitation map (or any other invariable map layer) following guidelines of existing vulnerability methods, this situation can lead to misrepresentations, indirectly evaluating conditions that are non-existent in the area of interest. This situation also highlights the necessity of regionalization when vulnerability studies are applied.

The analysis and considerations presented in this chapter can serve as a basis for further improvements regarding intrinsic vulnerability schemes or the development of new methodologies. It is undeniable that intrinsic groundwater vulnerability approaches are important and useful for planning and protection strategies. Nevertheless, improvements for intrinsic groundwater vulnerability mapping are highly necessary in order to minimize the considerable subjectivity attached to these methods. Although an overall standardization is unlikely, given the high heterogeneity and anisotropy of karst at local and regional scales, a process to minimize the subjectivity during the mapping process would be beneficial for intrinsic groundwater vulnerability estimation. The results obtained in this chapter will be taken as a foundation from which to propose an alternative method for intrinsic vulnerability mapping, minimizing the subjectivity of the process based on specific rules and criteria for data selection, rating, and weighting system (chapter 5).

Nowadays, as demonstrated by the numerous intrinsic methodologies and study cases around the world, the role of anthropogenic influence remains excluded in vulnerability analysis. The intrinsic approach for vulnerability mapping can lead to erroneous conclusions, even if the subjectivity is minimal, if anthropogenic practices and their effect on groundwater quality are not included for actual scenarios. Therefore, it is also necessary to investigate and define representative parameters relating to activities already affecting the aquifer and their potential to be included as part of an integrated groundwater vulnerability evaluation.

For this goal, solute transport models can provide beneficial information regarding pollutant concentration or its residence time in a given point of a three-dimensional aquifer. In order to investigate what additional criteria and how to include it as part of vulnerability mapping process, a transport model was conceptualized and evaluated in the Yucatan karst. The basis, development and results of the model are explained in the next chapter.

4 Anthropogenic activities as vulnerability stressors

This chapter is based on the following research article:

As presented in the previous chapter, groundwater vulnerability in Yucatan was estimated by eight approaches that evaluate the travel time of a theoretical pollutant particle released at the surface and moving along the unsaturated zone. The methodologies applied in Yucatan were previously tested and validated on their respective areas of development, these being mostly European karst areas; outcomes from their application brought important inputs to groundwater management and protection strategies for such karst aquifers. Nevertheless, their application in the Yucatan karst highlighted the necessity to re-evaluate the role of some parameters to better display the natural characteristics of the Yucatan karst. Therefore, a regionalization process for vulnerability methods, with regard to parameter discretization, is indispensable.

In addition to the inconsistencies among methods and likely misclassification of some relevant features, anthropogenic practices, currently affecting groundwater in this region, are not included as part of the vulnerability analysis. This situation necessitates the inclusion of human-driven factors to further evaluate groundwater vulnerability, in order to expand the analysis from an intrinsic-based process into an integrated process.

Many karst aquifers, as well as detritus, undergo the effects of external stressors affecting groundwater both qualitatively and quantitatively. Leachates from dumping sites and septic tanks, large wellfields, and land-use change are some of the elements currently affecting groundwater in space and time. The application of intrinsic vulnerability methodologies is very useful to define protection areas and highlight potential areas of interest to perform further research, as demonstrated by multiple studies. However, due to the karstification process time scale, intrinsic vulnerability does not project near-future scenarios, unless the applied method utilizes land-use as an estimator. Estimation of current and future groundwater vulnerability could be performed if population growth, as well as practices related to it, are also included as vulnerability estimators. While intrinsic vulnerability considers only the natural characteristics of a given study area, inclusion of anthropogenic practices can aid in better evaluating current situations and possible changes in the future regarding groundwater vulnerability.

Since many karst areas already contain human settlements, it is sensible to acknowledge that some degree of influence over karst landscapes is already occurring. The anthropogenic factors that can be considered as stressors for groundwater are diverse. Human activities, negatively affecting groundwater, can be roughly divided according to two main characteristics: activities affecting groundwater quality or activities modifying the natural groundwater flow. The former category can include practices altering groundwater in terms of quality, such as wastewater effluents from septic tanks, leachates from waste disposal practices, or agriculture-related activities. The latter could include large extraction wellfields diverging groundwater flow due to cones of depression, hence altering this intrinsic characteristic.

The impact of the previously mentioned anthropogenic practices on groundwater resources can be estimated utilizing numerical models. By modelling, the transport and fate of a given pollutant can be predicted to focus on two important parameters: pollutant residence time and pollutant concentration. In this section, results from a solute transport model applied in a selected study area in Yucatan are discussed with a focus on vulnerability.

The aim of this chapter is to analyse which factors could be included as additional parameters to introduce a new integrated workflow in order to designate vulnerability classes. In section 3.1, the most important natural characteristics of Yucatan were presented to better understand results from intrinsic groundwater vulnerability methods. In this chapter, important anthropogenic characteristics of Yucatan, relevant for the applied model, are explained.

4.1 Anthropogenic impacts on the Yucatan karst

With around 2.1 million inhabitants, according to the 2017 census, Yucatan is the 23rd most populated of the 32 Mexican states holding 1.7% of the national population (INEGI, 2018). Yucatan is below the national average density of 61 inhabitants per square kilometre (inh/km^2), with a mean of about 53 inh/km^2. However, this number severely increases in Yucatan's densely urbanized areas.

According to data obtained from INEGI, 595 urban areas (cities and towns) currently exist in Yucatan; more than 2000 small villages with a population of less than 50 inhabitants are dispersed in the state (INEGI, 2011). The Yucatan area of approximately 39,500 km^2 is administratively divided in 106 municipalities ranging from 26 km^2 to 3,700 km^2 in extension. The Merida municipality, where the capital and largest city (also named Merida) is located, holds the highest population density reaching up to 900 inh/km^2; this is considerably high since most of the Yucatan municipalities barely reach 30 inh/km^2 (Figure 4.1).
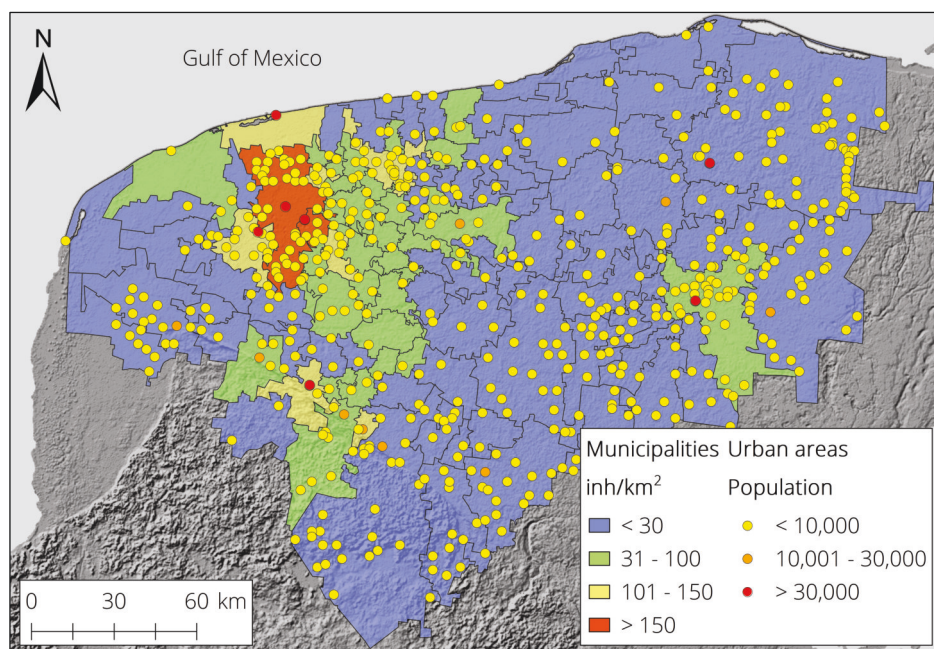
Figure 4.1: Municipal division and urban settlements of Yucatan. Small settlements with a population of less than 50 inhabitants are not displayed. Map elaborated with publicly available data from INEGI (2011).

Analysing population patterns in relation to the hydrogeological regions, the Inner Cenote Ring is the region with the most inhabitants, holding approximately 70% of Yucatan's total population; this includes part of the Coastal Area falling inside this sedimentary basin. Only seven cities in Yucatan surpass 30,000 inhabitants; such cities are regionally characterized as the most populated. The capital city, Merida, hosts the highest population number with approximately 800 thousand inhabitants. The six remaining high populated cities have a population ranging between 30,000 and 80,000 inhabitants (UADY, 2006).

During the last 70 years, Merida city has experienced rapid urbanization; from being an urbanized area of 42 km^2 in 1950, the city currently covers 270 km^2 (SEDUMA, 2010). With the Merida municipality having almost reached its maximum urban capacity, new settlements are continuously being developed on the periphery of Merida city and neighbouring municipalities. This situation is better exemplified by the municipalities of Kanasin, Uman, Conkal, Ucu, and Progreso where large housing complexes are constantly under construction (Figure 4.2).
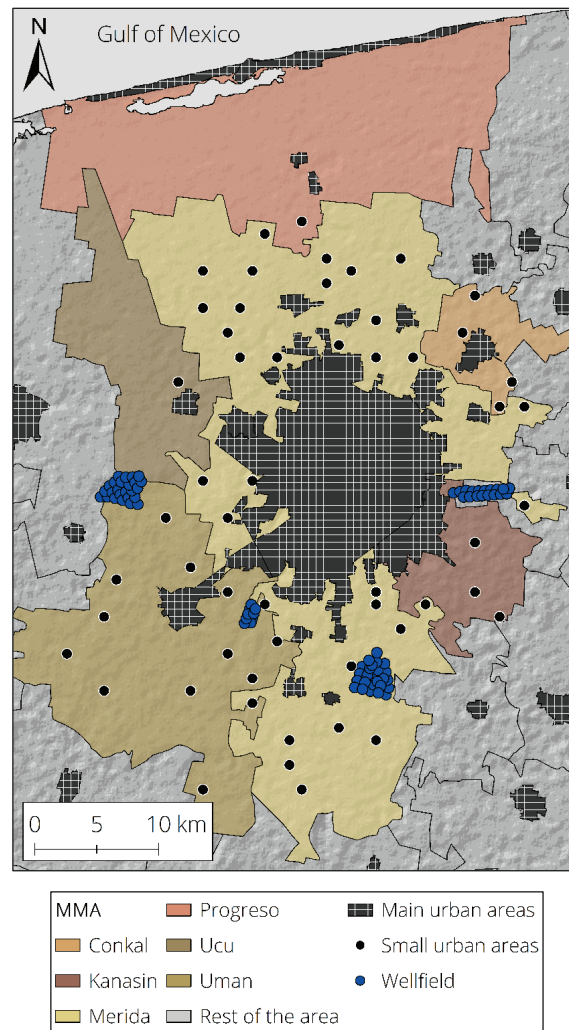
Figure 4.2: Municipalities forming the MMA and urban settlements. Map elaborated with publicly available data from INEGI (2011).

This situation highlights an important area frequently mentioned in multiple studies, the Merida metropolitan area (MMA). This urban area has become the main spot for development and economic activity, a situation which has resulted in an increase of population due to national and regional migration (Consejo estatal de planeación de Yucatán, 2013). This has turned the MMA into a highly urbanized area composed of six municipalities, which collectively hold approximately 52% of the Yucatan population (Table 4.1).

Table 4.1: Population distribution in the MMA.

Municipality	Area (km^2)	Population*	Population density (inh/km^2)	Main city
Conkal	61	9,149	150	Conkal
Kanasin	97	79,444	819	Kanasin
Ucu	152	3,447	23	Ucu
Progreso	433	53,925	125	Progreso
Merida	880	832,238	946	Merida
Uman	342	48,689	142	Uman
* Population according to the 2017 census (INEGI, 2018).				

The current urbanization trend inside the MMA represents a negative environmental and ecological impact for this region. Mean average temperatures are rising due to the extensive deforestation and further urbanization, thereby creating an urban heat island effect. Infiltration of precipitation is minimized due to impermeable surfaces, increasing evaporation and groundwater vulnerability due to the usage of shallow street-wells as rain drainage. In general, diverse anthropogenic practices like water extraction, dumping sites, and wastewater disposal among others take place in Yucatan, but are more drastic in the MMA.

4.1.1 Groundwater extraction

A positive water balance, with an approximate surplus of about 3,000 million of cubic metres per year (Mm^3/y), has been estimated for the Mexican side of the Yucatan Peninsula (CONAGUA, 2015a). For Yucatan, 80% of the mean annual precipitation is estimated as evapotranspiration, the remaining 20% is recorded as infiltration with zero runoff (Villasuso and Méndez, 2000). The estimated 80% of precipitation is intercepted by vegetation, retained in the vadose zone and returned to the atmosphere by evapotranspiration (SARH, 1989). Due to the flat topography and the considerable karstification, no surface runoff is generated and precipitating water, being unaffected by evapotranspiration, directly infiltrates, recharging the aquifer. Recharge has been estimated to range from 14% to 20% of the yearly average precipitation (Lesser, 1976; Gondwe et al., 2010; Pacheco and Cabrera, 2013). Although infiltration does not occur homogeneously, no spatial discretization for infiltration was found in the literature. Water authorities have calculated a surplus of approximately 1,360 Mm^3 as the yearly average for Yucatan (CONAGUA, 2005). This mean value was calculated from the difference between precipitation and evapotranspiration, subtracting volumes of natural discharge and estimated extraction volumes (Table 4.2).

For the Peninsula, yearly water extraction for human consumption is estimated as 1.3 Mm^3 (CONAGUA, 2015a). Distribution of groundwater extraction for regional activities is calculated as 63% for agricultural and cattle raising activities, while 30% is designated to human consumption; the remaining 7% is designated for industrial purposes. According to the regional estimations, Yucatan's groundwater extraction volume is 58% of the total Peninsula rate; this means around 758 Mm^3 on a yearly basis. Water extraction in Yucatan is carried out by wells located mostly in the north, east and south of the state, where human settlements and agricultural fields are located. Estimations describe the existence of approximately 18,400 extraction wells. However, many wells utilized for industry, irrigation, and private purposes are unregistered; this complicates a more accurate evaluation of extraction volumes (Graniel-Castro, 2010). It has been estimated that around 53% of the wells are artisanal or drilled at shallow depths, extracting water at rates ranging from 10 to 30 litres per second (lps). These water volumes are used for agricultural purposes, cattle raising, or domestic purposes. Deeper wells with an average extraction volume of 50 lps are also dispersed within the state, with depths ranging from 40 to 100 m below the surface. In Yucatan, around 57% of the water extraction volume is utilized for agricultural irrigation (CONAGUA, 2012).

Table 4.2: Comparative of the Peninsula and Yucatan water volumes. Volumes displayed in Mm^3/y.

Components	Yucatan water balance*	Peninsula water balance**
Precipitation	34,940	109,065
Evapotranspiration	27,952	87,252
Recharge	6,988	21,813
Natural discharge	4,659	14,542
Extraction	967	5,091
Surplus	1,362	3,388

* Data from CONAGUA (2005).
** Data from CONAGUA (2012).

Current extraction rates do not stress the aquifer, the recovery of which is fast due to the natural characteristics that allow fast infiltration. No records of water extraction volumes per urban settlement were found for this research. From data provided by the Yucatan Drinking Water and Sewage Council (JAPAY), a rough estimation of 0.15 cubic metres (m^3) per inhabitant can be assumed as the average for rural settlements and small cities on a daily basis. In densely populated areas, such as those inside the MMA, daily water consumption increases up to 0.28 m^3 per inhabitant. However, during spring and summer seasons when temperatures increase, consumption increases up to 0.35 m^3 per inhabitant (Diario de Yucatán, 2018).

Considering the disproportional population density by municipalities, as displayed in Figure 4.1, the extraction volume to supply the MMA is relatively high in comparison with the sum of the remaining municipalities. Around 56% of the calculated extraction volumes for human consumption takes place in the MMA; the remaining 44% is dispersed over the rest of Yucatan settlements (Figure 4.3). These estimations do not include private wells used for water supply. Despite 57% of the total extraction being assigned to agriculture, no data was found regarding the precise location of such wells or their extraction volumes. Nevertheless, the southern part of Yucatan is described as a large extraction area where agricultural fields are mostly located (SARH, 1989).
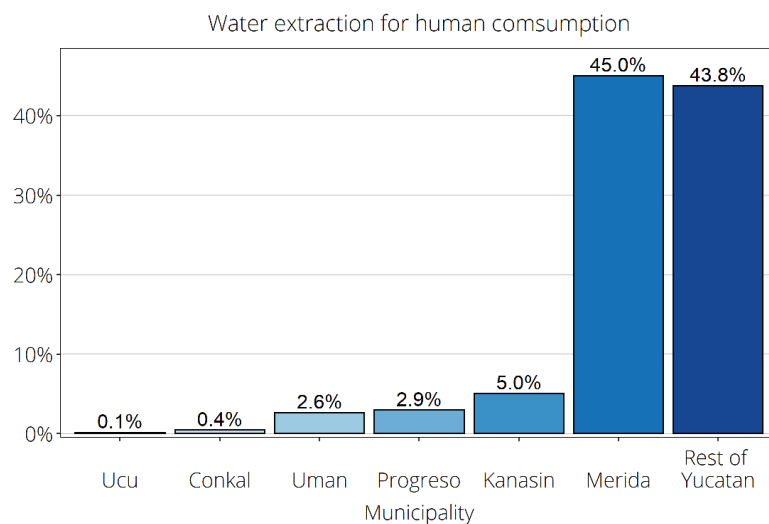
Figure 4.3: Comparative of water extraction in the MMA. Graphic elaborated based on water extraction estimates and population.

Nowadays, some small settlements exist in Yucatan where water is manually obtained directly from cenotes and used for human consumption. Due to low population rates in the majority of small towns and villages, one or two wells are commonly used for water supply, with extraction taking place for just a couple of hours per day. In bigger cities, extraction takes place in wellfields located at the periphery of the cities. Due to the large number of inhabitants and the large extension of pipelines for water distribution, extraction is constant to keep the necessary hydraulic pressure in the distribution system. Such is the case with Merida city, utilizing four wellfields with a total of 78 deep extraction wells, located outside of the city. Additionally, multiple single wells distributed inside the Merida urban area also serve supply.

As shown in Figure 4.3, the Merida municipality extraction rates are far higher than the rest of municipalities forming the MMA. The Merida city holds the highest water extraction rates in Yucatan with regard to drinking water. However, lack of maintenance and end of product service life in some sections of the Merida distribution system generate water losses of around 40% of the extraction volumes, leaking back into the aquifer (Graniel et al., 1999). Since groundwater recovery is fast due to the karstic characteristics, current water extraction volumes do not represent a risk in terms of water availability (González-Herrera et al., 2002). However, the same karstic characteristics of the area leave groundwater vulnerable to the pollution generated by multiple anthropogenic activities.

4.1.2   Main pollution sources

Reports from INEGI highlight Yucatan as a touristic area where tertiary activities (services and commerce) lead 64% of the economy (INEGI, 2016). Secondary activities (industry) follow with 32%, while primary activities (agriculture, livestock and fishing) represent only 3% of the economy. In Yucatan, the Ministry of Agriculture, Livestock, Rural Development, Fishing, and Food (SAGARPA) reported that around 1,500 km^2 of the state consists of fields used for the production of corn; approximately 3% of the Yucatan area. Other fruits and vegetables are also produced but in smaller agricultural areas. Agricultural fields are dispersed in the state, varying in size from small orchards or milpas (small to medium productive familial lands) to major cultivated areas; the latter are mostly located in the south of Yucatan.

The use of fertilizers and pesticides in agriculture helps to control and improve the production, nevertheless, it represents a problem when there exists a lack of awareness campaigns and guidance for their use. The application of Nitrogen-rich fertilizers significantly increases groundwater pollution due to the lack of a precise understanding about its purpose. This causes the application of exaggerated amounts of fertilizer with the expectation of improvements in the overall production. The excess of fertilizer, which is not being used by the crop, moves downward through irrigation, creating a leachate. No estimations, in terms of the volume of applied agrochemicals, were found in the literature for the Yucatan state. However, González-Herrera et al. (2014) presented interesting estimates regarding nutrient leaching from small agricultural areas located inside the MMA. Around 44% of the mass nutrient was calculated to leach in the study area. Leachate percentages are dependent on the type of the applied fertilizer, soil characteristics, and irrigation/precipitation patterns; this complicates the estimation of leachate volume for the whole state.

Regarding livestock production, it has been estimated that around 21% of the Yucatan area (approximately 845 km^2) is utilized for this purpose; the north-eastern Yucatan is characterized as the livestock region (Ramírez-Cancino and Rivera-Lorca, 2010). As part of livestock production, pig farming is highlighted as an increasing activity in Yucatan. Despite the economic relevance of this activity in the region, the environmental impact is high due to the volume of generated wastewater and its direct disposal without receiving any adequate pre-treatment (Vega and Romero, 1987).

No precise data regarding location, extension and production volumes were found in public databases for recent years. According to Méndez-Novelo et al. (2009), more than 450 pig farms exist dispersed throughout Yucatan, varying in size from small cooperative farms to large production complexes.

Drucker et al. (2003) reported estimations of animal wastewater volumes based on data collected from random pig farms. According to the study, wastewater volumes generated per animal range from 0.012 to 0.043 cubic metres per day (m^3/d). In general estimates for Yucatan, a total of 16,700 m^3/d of animal wastewater was calculated; from this volume, 37% is predicted to be disposed without treatment. To these volumes, those generated from bovine and poultry farming need to be added, however, no precise estimates for these activities were found in public databases.

Despite the low percentage of agriculture and livestock production as part of the Yucatan economy, such activities are two major threats to groundwater quality due to the weak environmental regulations, the extended use of agrochemicals, and the disposal of wastewater generated from pig farming. In addition to these pollution sources, the disposal of grey and black water generated in urban areas is also threatening the Yucatan karst aquifer due to the low coverage of sewer systems and plants for wastewater treatment.

In Yucatan a total of 27 plants for wastewater treatment (WWTP), located in Merida city and its surrounding areas, are currently in operation (CONAGUA, 2010). According to data digitally provided by JAPAY, approximately 56,400 houses have public sewer services connected to WWTP. This implies that around 200,000 inhabitants utilize this service or roughly 10% of the Yucatan population. The common wastewater disposal practice in Yucatan is the use of septic tanks. However, artisanal septic tanks, which are permeable, are mostly used despite the current regulations forbidding this practice. In rural and poor areas, the use of latrines or open-air defecation is still in practice.

Typically, artisanal septic tanks are pits of 2-3 m depth where black and grey water is disposed. Retention time on such pits is short; a lapse of hours, with a constant percolation into the vadose zone (Morris et al., 1994). This untreated sewage typically infiltrates rapidly into the shallow aquifer through joints, conduits, and fractures (Pacheco, 1994; Marín et al., 2000).

Estimations derived from the current WWTP's processing capacity indicate that around 80% of the supplied water for housing contributes to grey and black water volumes. Taking extraction volumes displayed in Table 4.2 as a base and excluding the estimated 57% for irrigation purposes, approximately 332 Mm^3/y of wastewater is generated in Yucatan; 45% of this volume is generated in the Merida municipality of which just 10% is treated. This situation puts additional stress on the aquifer, which acts as the only source for water supply but also as receptor of the generated wastewater. The current aquifer pollution scenario is highlighted in the sub-surface of the Merida city where the upper section of the aquifer is already being affected by a pollution plume. Below Merida city the freshwater lens has a thickness of approximately 40 m, followed by a brackish mixing zone and saline water at 60 m depth (Villasuso et al., 1984).

Marín et al. (2000) declared that the upper 15 m of the aquifer underneath Merida city are unsuitable for human consumption due to severe pollution. However, the pollution plume has recently contaminated the upper 20 m of the aquifer in some sections (L. Marín, personal communication, July 2016). This phenomenon has not yet been investigated in other highly populated areas where a similar effect is expected but at different levels. Nevertheless, the high concentration of population qualifies Merida city as the main generator of this type of pollution in Yucatan (Marín et al., 2000; Pacheco et al., 2001).

Despite the beneficial dilution effect exerted by water loss in the distribution system, the low hydraulic gradients and the constant percolation from septic tanks and pipelines have created a groundwater mound below the city (Morris et al., 1994; Marín et al., 2000). Nevertheless, the behaviour of this mound is transient, being dependent on precipitation events. High extraction volumes in the wellfields located in the Merida periphery, the groundwater mound, and the low hydraulic gradients are the current conditions possibly promoting a reversal in the groundwater flow (Figure 4.4).
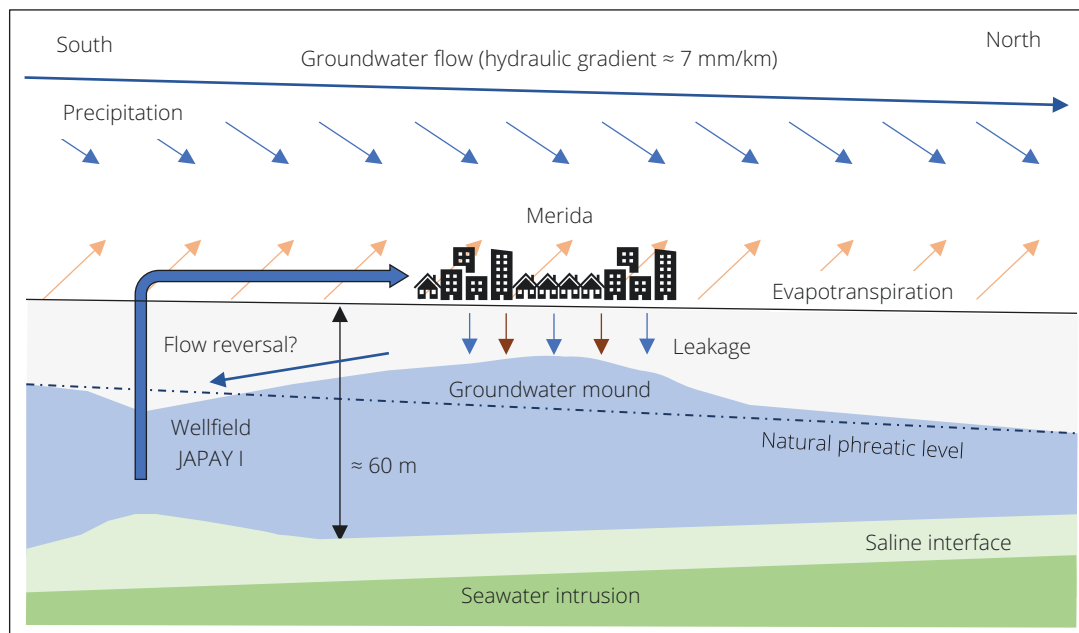
Figure 4.4: Basic hydrological conceptualization (not to scale) of the Merida city sub-surface. Leaking sources are those from septic tanks, water loss in the distribution system, and urban rainwater drains.

Estimated averaged drawdowns in the wellfield JAPAY I and further comparison with piezometric points below Merida city, suggest a groundwater movement towards this wellfield. This anthropogenic-induced flow is contrary to the natural groundwater flow (Marín et al., 2000). This situation is alarming since polluted groundwater can be redirected towards the wellfields supplying Merida city.

Similar situations are likely to occur in other large cities; this highlight how anthropogenic practices are already affecting groundwater quality in Yucatan from a resource and a source vulnerability perspective. The overall situation in Yucatan highlights wastewater generated from multiple activities such as housing, industry, and farming as the major threat affecting groundwater quality.

4.1.3   Groundwater pollution by nitrates

Pollution by nitrates stands out as a frequent topic for research in Yucatan, since nitrate (NO_3^-) concentrations, surpassing the permissible maximum for water consumption, have been reported at different locations in the state. According to the World Health Organization (WHO) the permissible maximum levels of NO_3^- must not be higher than 50 milligrams per litre (mg/L) for drinking water (World Health Organization, 1993). In Mexico, the permissible maximum is set as 45 mg/L (Diario Oficial de la Federación, 2000).

Concentrations of NO_3^- in groundwater for locations representing the 106 Yucatan municipalities were described by Pérez-Ceballos (2004). This data was gathered from several reports and extraction wells data during water sampling campaigns throughout the state (Pacheco, 2003; Pacheco, 2004; Pacheco-Ávila et al., 2004a). Results indicate that 21 out of the 106 sampling wells, located in towns representing a municipality, surpassed the permissible maximum concentration of NO_3^- for drinking water. However, no trends were found between population and the elevated NO_3^- concentrations in the localities forming this database.

This situation suggests that high NO_3^- concentrations can be a consequence of a specific activity, located at some distance from the sampling point, where a considerable source of NO_3^- is released and travels towards the extraction well. A similar situation was mentioned by Fernández et al. (1996) whose work highlighted the influence of pig farms on water quality in neighbouring localities; this exemplifies the concept of source vulnerability to pollution.

Multiple individual studies have been carried out to characterize groundwater pollution in the periphery of water supply wellfields, those supplying Merida city being the most investigated (Pacheco and Cabrera, 1997; Cabrera et al., 2002; Pacheco, 2004; Pacheco-Ávila et al., 2004b; Rojas-Fabro et al., 2015). In some cases, definition of the pollution source is a complicated task due to the multiple possible sources to be considered (González-Herrera et al., 2014). However, multiple activities threatening the Yucatan karst aquifer have also been investigated to evaluate their impact on groundwater in terms of quality (Graniel et al., 1999; Pacheco et al., 2002; Delgado et al., 2010; Febles-Patrón and Hoogesteijn, 2010; González-Herrera and Gómez-López, 2013; González-Herrera et al., 2014).

Two key investigations highlight the role of anthropogenic practices on NO_3^- pollution and the response of the natural characteristics of the Yucatan karst. A study performed by Pacheco et al. (2001) demonstrated the high impact of agriculture on groundwater pollution in southern Yucatan. As an area with a low population density but with intensive agriculture activity, high NO_3^- concentrations were defined as a consequence of the excessive use of fertilizers rich in Nitrogen. Three out of twelve monitoring wells used for this study showed NO_3^- concentrations above 45 mg/L but varying on a monthly basis. Variability of NO_3^- concentrations in this study demonstrated an inverse correlation with precipitation events where a dilution effect takes place during the rainy season.

A monitoring study performed north of Merida city also highlighted a high NO_3^- pollution scenario. Pacheco and Cabrera (1997) reported NO_3^- concentrations surpassing the permissible maximum level of 45 mg/L in shallow wells mostly utilized for water supply. From 103 water samples taken in eight long-term monitoring wells, 57 showed high NO_3^- concentrations reaching up to 223 mg/L, an alarmingly high concentration. However, the authors addressed the high variability in NO_3^- among sampling points as a relation with the area where they were taken being highly influenced by local urbanization.

Unlike the study performed in southern Yucatan, in this area NO_3^- concentrations are directly affected by precipitation with concentrations increasing subsequent to the rainy season. This could be an indirect indicator of epikarst development in this area, acting as a perched aquifer, which retains pollution being flushed during precipitation events. Nevertheless, this situation could also be derived from the lack of sewage treatment and the unregulated use of artisanal septic tanks constantly leaking into the aquifer.

Utilizing statistical and geostatistical procedures, the spatial distribution of NO_3^- in the sub-surface of Merida city was investigated by Rojas-Fabro et al. (2015). From a correlation analysis between NO_3^- and other anions, such as chloride and sulphate, agricultural activities and farming were declared as the main pollution sources affecting a wellfield (JAPAY II) located at the southern limits of the city. For several extraction wells located inside the city, permeable septic tanks were declared as the main NO_3^- source. Evidence from this study corroborates results previously presented by González-Herrera et al. (2014).

The diffuse contamination underneath Merida city by wastewater disposal from septic tanks and latrines seems to be mitigated to some degree by the constant leakage of water from the pipe distribution system, as suggested by Graniel et al. (1999). However, a groundwater reversal, due to this constant dual leakage, threatens large wellfields (see Figure 4.4). In addition to the potential of polluted water being extracted in the wellfields located in the south of Merida, small settlements located north of the city could also be affected by the pollution plume due to the natural groundwater flow. This scenario is a good example of source vulnerability where travel time from the release point to extraction wells becomes irrelevant because pollution is constant, representing a prevailing threat.

Since the MMA holds the highest population percentage and therefore the anthropogenic influence is high in terms of water extraction and wastewater generation, it was selected as the study area upon which to develop a model to investigate solute transport. Before presenting the characteristics and parameters of the study area selected for this investigation, a review of previous groundwater models and related studies in Yucatan are briefly described.

4.2 The Yucatan karst aquifer

The general model of the Yucatan aquifer is depicted as a freshwater lens of variable thickness overlying seawater (Figure 4.5). Due to geologic conditions, the Yucatan karst aquifer is unconfined. Nevertheless, an impermeable layer with a thickness ranging from 0.5 to 1.4 m is located along the coastline, covering an approximate distance of 250 km and a variable width ranging from 2 to 20 km (Perry et al., 1989). This caliche layer is impermeable with an estimated porosity of 1%, acting as a barrier between fresh and seawater.
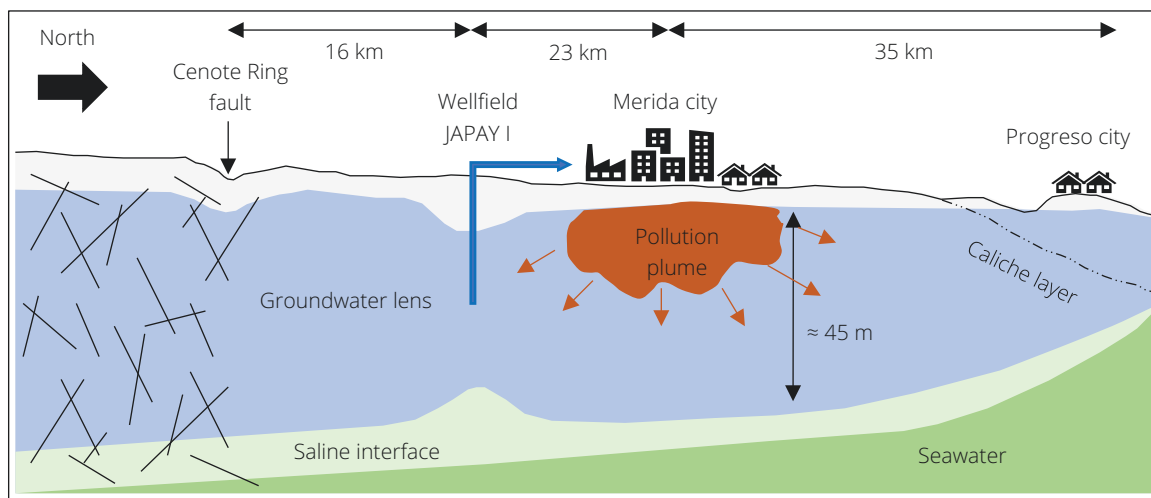
Figure 4.5: Schematic of the Inner Cenote Ring area. Image modified after Marín et al. (2000).

Several studies have investigated the extension of seawater intrusion in this coastal aquifer, which has been measured at more than 110 km inland (Perry et al., 1995; Steinich and Marín, 1996). Applying the Ghyben/Herzberg relationship, it was found that the depth of the saline interface increments radially from the coastline towards upcountry regions in the Yucatan Peninsula (Perry et al., 1989; Steinich and Marín, 1996). At the coastline the fresh-saline water interface has been measured at 18 m below sea level, in Merida city at 45 m, and at 70 m depth near the town of Abalá, which is located approximately 70 km from the coast (Steinich, 1996). Piezometric levels vary from centimetres along the coast to approximately 10 metres asl at the southern part of Yucatan, 160 km away from the coastline (SARH, 1989; Bauer-Gottwein et al., 2011).

Multiple individual studies have defined a regional groundwater flow in Yucatan mostly in a north-west direction moving from areas with high groundwater levels, located in the south due to pronounced precipitation, towards the coastline feeding coastal lagoons and mangrove areas (Lesser and Weidie, 1988). According to González-Herrera et al. (2002) no significant deviations regarding the general south-east to north-west groundwater flow have been observed. However, reports gathered by Bauer-Gottwein et al. (2011), presented as a review of the Yucatan Peninsula's characteristics, indicated some areas in Yucatan where groundwater flow does not follow this pattern. This situation is highlighted in the eastern area of Yucatan. The west-to-east and east-to-west groundwater flows reported in this zone could be a consequence of the two regional faults enclosing this area, the Cenote Ring in the west and the Holbox fault line located in the east (see Figure 3.1).

On a catchment scale, groundwater levels demonstrate low variability in the range of centimetres. Reeve and Perry (1990) reported variations in the water table ranging from 2 to 33 cm, which is influenced by precipitation volumes and tides. Pumping tests carried out by JAPAY during the construction phase of extraction and infiltration wells inside Merida and its periphery indicated a rapid recovery of groundwater levels in the lapse of a few minutes (R. Guevara, personal communication, August 2018).

Low hydraulic gradients in the nearly flat region, with values ranging from 7 to 10 mm/km, and the rapid recovery of groundwater levels, suggest a high hydraulic conductivity (Marín, 1990). However, multiple studies utilizing different techniques, have reported hydraulic conductivity values differing by several orders of magnitude. Studies performed by Buckley et al. (1994) on several locations inside Merida showed evidence of variation in electrical resistivity and water temperature at different depths, which were interpreted as horizontal dissolution channels of high permeability. These preferential flow layers were located at intervals of 11-12, 21-22 and 29-32 m below surface.

Additional pumping tests also performed by Buckley et al. (1994) highlighted the relevance of the upper high conductive layer when water is extracted from shallow wells. These secondary and tertiary porosity layers cause the high hydraulic conductivity values, which is reflected by the rapid groundwater level recovery and the low cones of depression derived from water extraction wells (Sánchez, 1999). A compilation of hydraulic conductivity values reported in the literature is displayed in Table 4.3.

Table 4.3: Reported hydraulic conductivity (K) by multiple studies. Table as presented by Sánchez (1999).

K (m/d)	Presented by	Observations
864	Back and Lesser (1981)	Estimated from a regional water balance (Peninsula).
0.1 - 432	González-Herrera (1984)	Laboratory tests of drilling cores (Merida city).
80 - 100	Andrade-Briceño (1984)	Pumping tests in the JAPAY I wellfield (south of Merida city).
22 – 44,928	Reeve and Perry (1990)	Estimated from the influence of tides on the water table (north of Merida city).
8,640 – 86,400	Marín (1990)	Estimated from a numerical model (north-western Yucatan).
0.3 - 1.21	Brewerton (1993)	Laboratory tests of drilling cores (Merida city).
12,960	Morris et al. (1994)	Estimated from a numerical model (Merida).
475 – 96,336	González-Herrera et al. (2002)	Estimated from a numerical model (Yucatan).

The Yucatan karstic aquifer has been simulated assuming an equivalent porous medium (EPM) approach due to the lack of detailed information regarding the sub-surface conduit system. However, as a measure to minimize the impact of conduits, a large representative elemental volume (REV) was utilized for the study area discretization. Some of the models that have been applied in Yucatan are briefly explained in the next section.

4.3   Previous groundwater models in Yucatan

4.3.1   Modelling the influence of the Cenote Ring

The model presented by Marín (1990) studied groundwater flow in north-western Yucatan utilizing the quasi-three-dimensional numerical finite-difference model SHARP; this model focuses on the simulation of a sharp interface between freshwater and saltwater flow in coastal aquifers (Essaid, 1990). The model simulated groundwater flow in the Inner Cenote Ring area, including the Cenote Ring as a regional feature influencing flow direction (Figure 4.6).
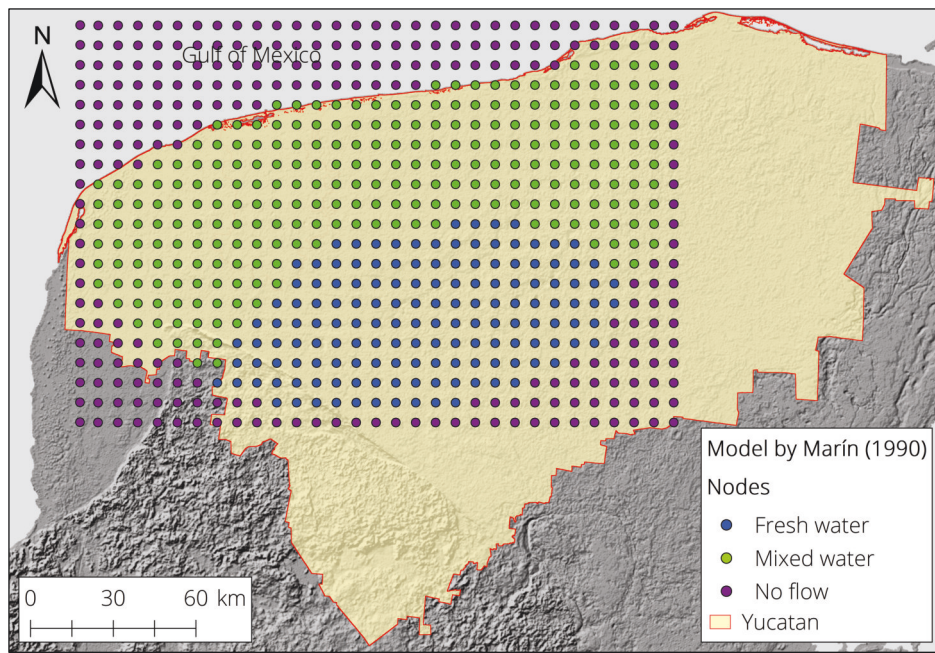
Figure 4.6: The north-west area of Yucatan modelled utilizing the SHARP code. Nodes digitalized from Marín (1990).

The area was discretized utilizing REVs of 6.3 km per side and having as boundaries the coastline in the north and the Cenote Ring in the south, east, and west. This model displayed groundwater flow occurring mostly in a south-east to north-west direction with groundwater levels declining towards the Cenote Ring. After calibration, the most sensible parameters, according to the author, were hydraulic conductivity and recharge. The best results from this model were obtained utilizing a two-layer arrangement with a low conductivity layer (50 m of thickness) overlying a high conductive layer (150 m of thickness). Hydraulic conductivities were defined as 8,640 m/d and 86,400 m/d for the upper and lower layers, respectively (Marín et al., 2003). This model emphasizes the role of the Cenote Ring acting as a groundwater divide due to the high hydraulic conductivity along this regional fault. Acting as a preferential flow path, the Cenote Ring intercepts groundwater flowing from the south, redirecting the flow towards the Cenote Ring margin and discharging at the sea.

Results obtained from this model are supported with evidence from other studies, which indirectly highlight the influence of the Cenote Ring on groundwater flow. The work of Pope et al. (1993) supports the hypothesis of the Cenote Ring acting as a preferential flow path from underwater spring discharge analysis. In locations where the Cenote Ring intercepts the coast, thermal imagery from Landsat 6 demonstrated the variability of the discharged freshwater during dry and wet seasons. An additional study, based on resistivity surveys, highlighted an area with distinctive groundwater level fluctuation. Located to the south-east of Merida city, in the periphery of the Inner Cenote Ring, this area of high variability is where the Cenote Ring diverges groundwater (Steinich and Marín, 1996; Steinich and Marín, 1997).

4.3.2   Modelling the Inner Cenote Ring area

Sánchez (1999) presented a two-dimensional groundwater flow model of the north-western area of Yucatan utilizing the code FLOWPATH. This software simulates groundwater flow for confined and unconfined aquifers with complex boundary conditions.

FLOWPATH utilizes a finite-difference method, with an Iterative Alternating Direction Implicit (IADI) algorithm, to solve non-linearity (Franz and Guiguer, 1990). The study area was simulated as homogeneous and anisotropic, including pumping rates into the model, estimated from previous studies as an external stressor of the system. The area was divided into 3,738 cells of variable size with smaller cells in the centre, corresponding to Merida city, due to the available water table data in this area. Constant head and specified head boundaries (Dirichlet condition) were considered at the coastline and the south-east limits; no flow boundaries (Neumann condition) were settled for the east and south-west boundaries (Figure 4.7).
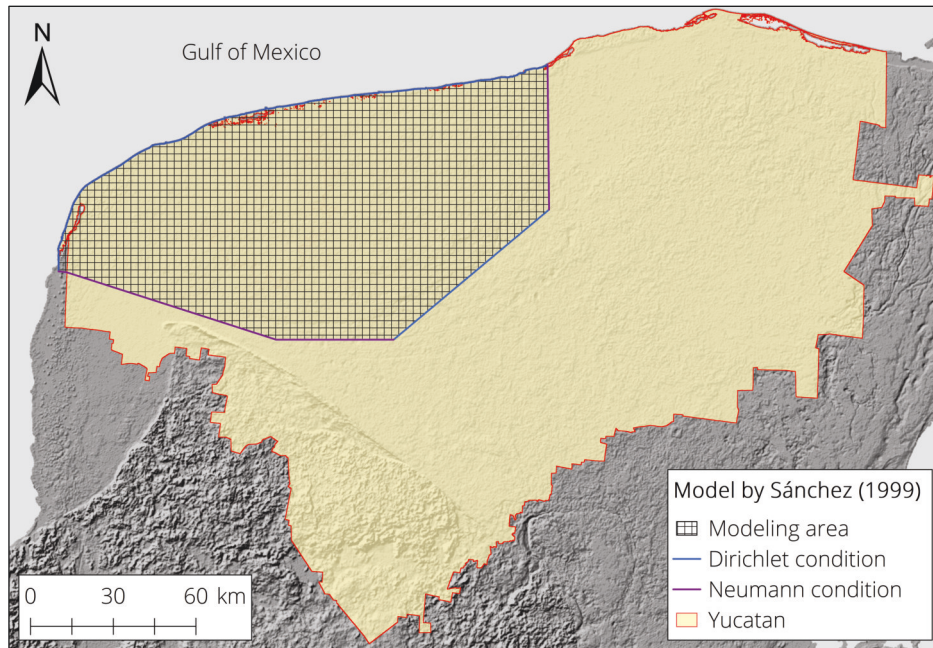
Figure 4.7: The north-west area of Yucatan modelled utilizing the FLOWPATH code. Model boundaries digitalized from Sánchez (1999).

After calibration, the best results were obtained assuming a homogeneous K value of 23,000 m/d with infiltration settled as 15% of the yearly average precipitation. This model did not include the confinement located at the coastline nor the influence of tides on the near-coastal hydraulic potential. Although the model proposed by Marín (1990) pointed out the influence of the Cenote Ring, this model showed the limited influence of this hydrogeological feature on the regional groundwater flow.

4.3.3   Modelling the Yucatan karst aquifer

The model presented by González-Herrera et al. (2002) investigated the role of physical and hydraulic settings such as karstification, the Cenote Ring, and the Sierrita de Ticul. Groundwater flow was simulated testing the different settings individually. The software AQUIFER (McLaren, 1991) was utilized for the simulations; this software solves horizontal groundwater flow utilizing a two-dimensional finite-element equation. The study area, covering the majority of the Yucatan territory, was discretized utilizing REVs varying from 3 km to 10 km of distance between nodes. Neumann and Dirichlet conditions were defined as displayed in Figure 4.8.

The best calibration was obtained utilizing two hydraulic conductivities defined as $5.5\text{x}10^{-3}$ metres per second (m/s) and 1.115 m/s for the Sierrita de Ticul and the rest of the area, respectively. With these outcomes, the authors declared the importance of the Sierrita de Ticul fault, acting as a hydraulic flow barrier with hydraulic heads decreasing in a north-easterly direction.
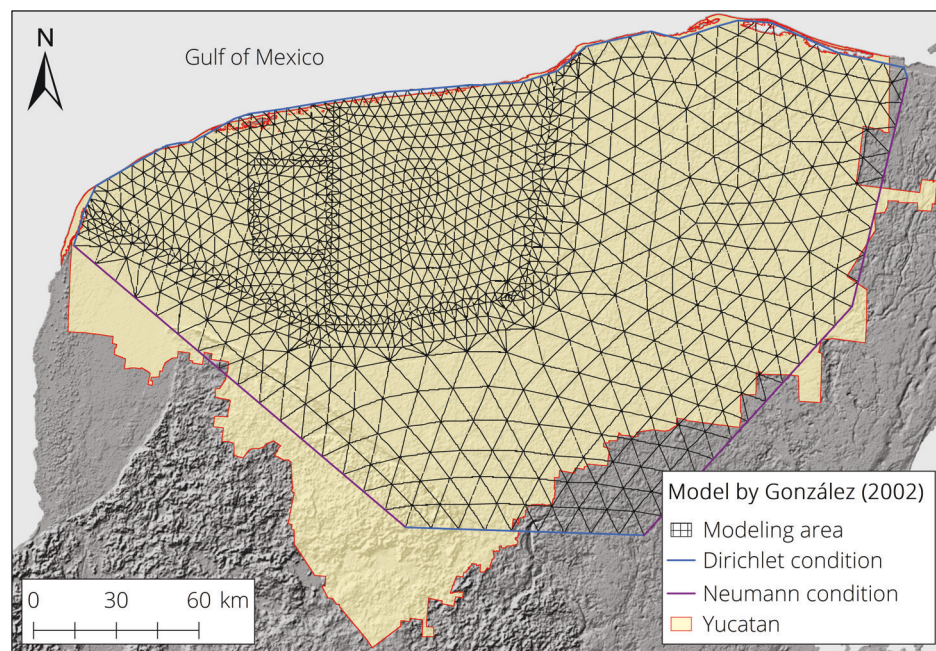
Figure 4.8: Yucatan modelled utilizing the AQUIFER code. Nodes and boundaries digitalized from González-Herrera et al. (2002).

According to the authors, the influence of the Cenote Ring and the confined aquifer along the coastline is minimal on a regional groundwater flow basis. Nevertheless, the hydrogeological functions of these characteristics respond to precipitation, affecting groundwater flow locally. Outcomes from this model indicate a groundwater flow that is regionally radial due to the Peninsula characteristics.

4.4 Material and methods

4.4.1 Study area and data

Due to the high anthropogenic impacts concentrated in this area and the available data, the MMA was selected as the study area to apply a groundwater model and investigate solute transport. The focus of the model was to investigate the behaviour of the pollution generated by the main city of each municipality forming the MMA, in terms of wastewater disposal practices and the possible negative effects on the large wellfields. A rectangular area of 50 km (east-west) and 70 km (south-north) covers the MMA and part of the surrounding municipalities (Figure 4.9).

In the model, the main city of each municipality acts as an infiltration basin due to water losses generated by the drinking water distribution system and the leakage of black and grey waters from septic tanks. The four JAPAY extraction wellfields were included for analysis as external stressors of the system because their extraction volumes are the most representative of this region. For the evaluative process, six monitoring wells, part of the CONAGUA monitoring network, were utilized. Unpublished data, digitally provided by JAPAY, was utilized to estimate water extraction volumes from the four wellfields located in the city's outer rim (Table 4.4).

Individual wells located inside the city were not included as part of the analysis due to the lack of information regarding their location, working time, extraction volumes, and depth. According to data provided by water authorities, 40% of the water extraction volumes were designated as part of the infiltration occurring in the Merida city sub-surface by distribution pipeline leakages.
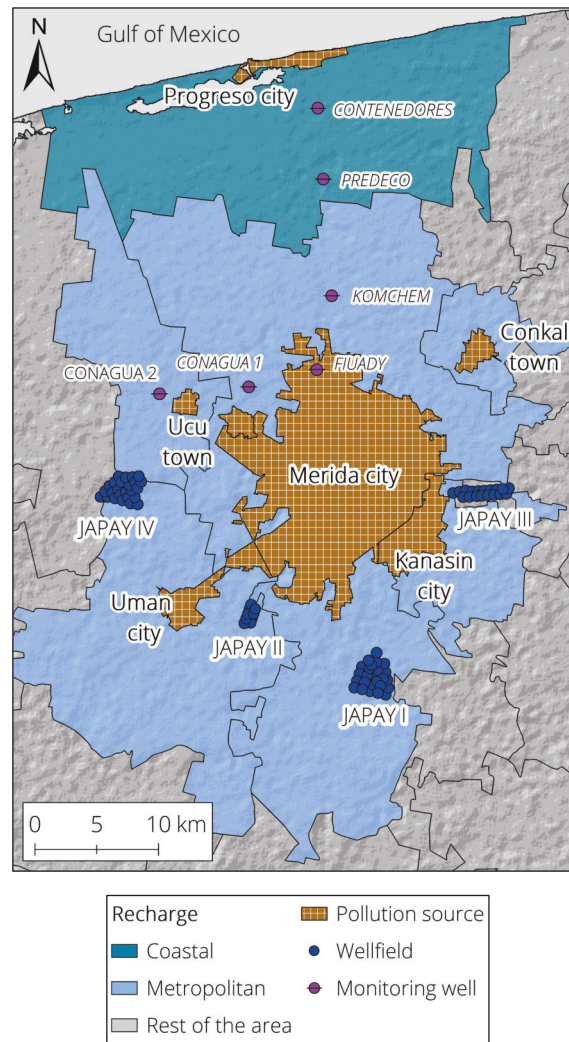
Figure 4.9: Recharge and main pollution sources in the MMA.

Table 4.4: Wellfields' extraction and wastewater volumes generated in Merida city.

Wellfield	Number of wells	Location	Total extraction	Water losses	Water supply	Wastewater
JAPAY I	25	San Ignacio Tesip (Merida municipality)	47.304	18.921	28.382	22.705
JAPAY II	9	Uman, (Uman municipality)	15.768	6.307	9.460	7.568
JAPAY III	21	Techoh, (Tixpehual municipality)	26.805	10.722	16.083	12.866
JAPAY IV	23	Oxcum, (Uman municipality)	7.884	3.153	4.730	3.784
Total	78		97.761	39.104	58.656	46.925

* Water volumes in Mm^3/y.

According to chemical and volumetric data of WWTP inflows, 80% of the water supply volume was designated as wastewater; this volume was settled as infiltrating the sub-surface from permeable septic tanks. Since large housing complexes, located in the periphery of Merida city, count with sewage and further treatment of wastewater, just the Merida city and five other main cities in the MMA were considered as infiltration basins in the model. Other settlements located inside the study area, with a presumably similar behaviour regarding water extraction, water losses, and wastewater infiltration, were not considered in the model. The necessary datasets to setup the model were obtained in multiple formats from public sources and Yucatan water authorities. Raster, vector, and point data were first evaluated and processed utilizing ArcGIS version 10.5. The same DEM utilized for intrinsic vulnerability studies was used to define the base layers for the groundwater model.

Due to the necessity of characterizing recharge according to its spatial distribution in the study area, the APLIS methodology was applied. Since traditional methods based on hydrodynamics, hydrochemical, or isotopic investigations commonly do not determine how recharge is distributed, this multi-parameter method proposed by Andreo et al. (2008) was selected to fulfil this purpose. The APLIS methodology evaluates altitude (A), protective cover by soils (P), lithology (L), infiltration landforms (I), and slope (S) to highlight areas where infiltration can be higher according to the natural conditions of the study area. Following a rating-weighting process, similar to that utilized for groundwater vulnerability estimation, APLIS estimates recharge as precipitation percentages based on the analysed natural conditions. Recharge spatial distribution was then obtained according to the array of the afore mentioned parameters utilizing shapefiles from INEGI.

Several unpublished reports and time-series of monitoring wells provided by CONAGUA were used to settle and calibrate the model. These piezometric monitoring wells were previously utilized by Martínez-Salvador (2018) as a base to calibrate a model of the Inner Cenote Ring area. Data such as lithology, hydraulic heads, water chemistry, and electrical conductivity among others was evaluated. Reports indirectly indicate the location of cavities in the sub-surface based on the variability of a drill's penetration time during the monitoring wells' drilling processes. Such information supports previous evidence in the area regarding interbedded preferential flow layers underneath Merida city.

4.4.2 Model discretization and setup

The code utilized for this work was MODFLOW, developed by the USGS to simulate groundwater flow. This model includes additional capabilities, or packages, to investigate distinctive features of a groundwater flow system, such as surface-groundwater interactions, solute transport, or variable-density flow, among others (Harbaugh et al., 2000; Langevin et al., 2017). The model divides the lithological layers of a system into grids forming rows and columns to describe hydrologic and hydrogeologic characteristics of a studied aquifer.

Layers representing the system can be defined as confined or unconfined, while individual hydrologic components, such as evapotranspiration or extraction, can be included in the simulation by subroutines and packages (Harbaugh et al., 2000). Multiple layers representing stratigraphy are discretized by rows and columns. Individual grid dimensions along the axis are denoted by Δr, Δc, and Δv; subscripts j, I, and k indicate the number of the corresponding column, row, and layer, respectively. Grids or cells can be selected as active (blue points) or inactive (white points) according to the area of interest (dotted blue line). MODFLOW utilizes a grid-centred finite-difference method to numerically represent groundwater flow (McDonald and Harbaugh, 1988). A partial differential equation based on Darcy's law is applied, assuming a porous medium and a constant density fluid represented by:

$$\partial/\partial x \, (K_{xx} \cdot \partial h/\partial x) + \partial/\partial y \, (K_{yy} \cdot \partial h/\partial y) + \partial/\partial z \, (K_{zz} \cdot \partial h/\partial z) + W = S_s \cdot \partial h/\partial t \qquad (18)$$

where K_{xx}, K_{yy}, and K_{zz} represent values of hydraulic conductivity along the x, y, and z axes; h is the potentiometric head. The volumetric flux per unit volume and the specific storage of the porous material are represented by W and S_s, respectively, and the time lapse is displayed by t.

Equation (18) is solved individually and simultaneously for each cell to numerically represent flow between them according to their hydraulic heads in the given time lapse. A basic schematic of a MODFLOW model is displayed in Figure 4.10.
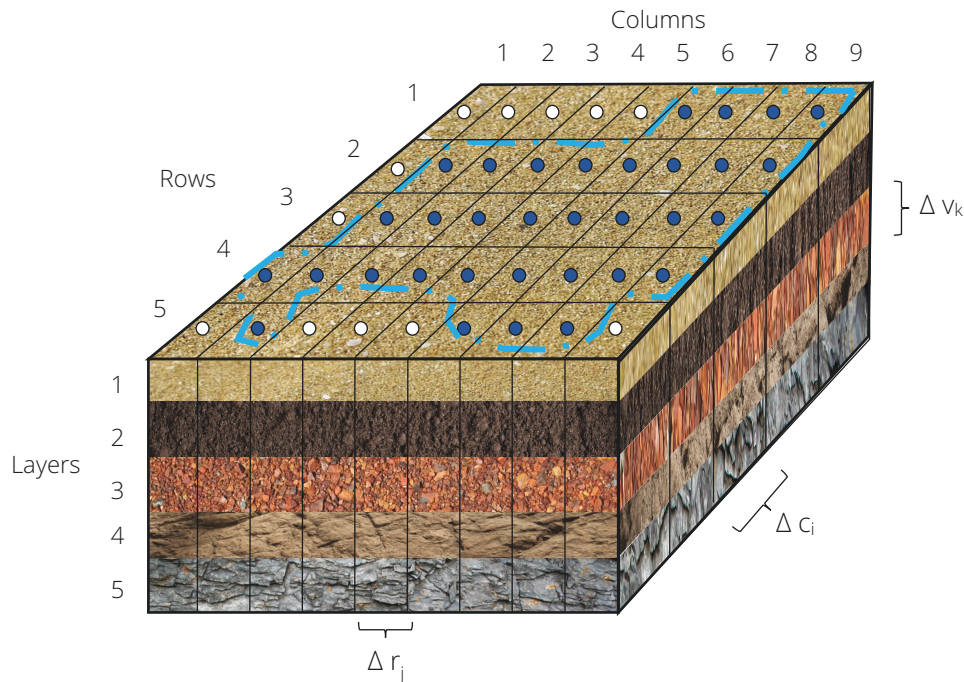
Figure 4.10: Hypothetical discretization of an aquifer system. Image digitalized from McDonald and Harbaugh (1988).

For this work MODFLOW was managed in Model Muse version 3.10.0.0 (released in March 2018). Model Muse is a graphical user interface (GUI) which facilitates the creation of input files and the temporal and spatial discretization for MODFLOW (Winston, 2009; Winston, 2019).

The study area was divided into 6,072 cells per layer, in a 66 x 92 arrangement. The two-dimensional cell size, representing the surfaces, was settled as 1 km^2. However, a smaller grid size (0.25 km^2) was defined for the Merida city and the surrounding areas. Four layers were implemented into the model following the evidence presented by previous studies (Figure 4.11).
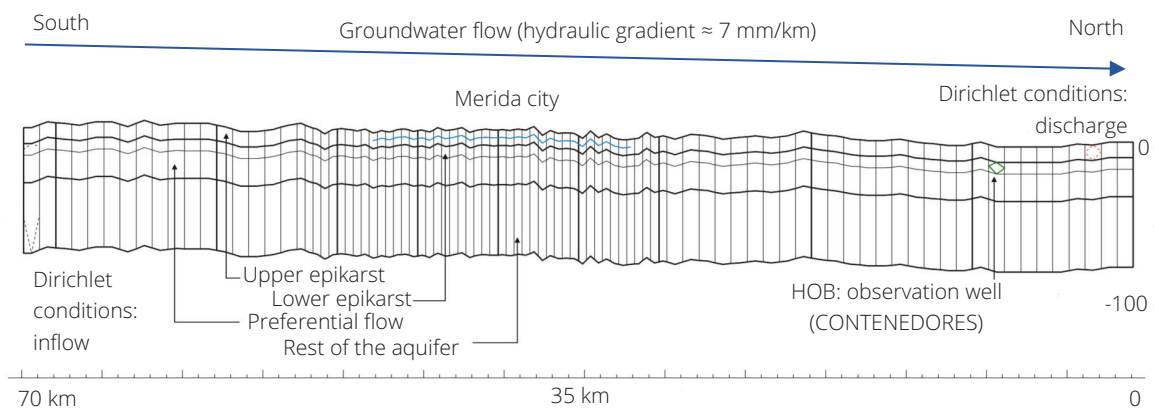
Figure 4.11: Vertical discretization of the study area. Image reproduced from Martínez-Salvador et al. (2019).

Unpublished reports of lithological profiles, obtained during the drilling works of monitoring wells, were provided by CONAGUA; these reports confirm the existence of preferential flow layers in some sections of the area, represented in the model as a preferential flow path. The discretization process was carried out utilizing ArcGIS by importing a DEM into ASCII format. The thickness of the sub-surface layers was estimated based on the top elevation depicted by the DEM, utilizing the fitted surface interpolation tool included in MODFLOW.

Based on studies defining the saline interface at approximately 60 m below the surface of Merida, the bottom of the model was defined at 80 m. As Merida is the area acting as an infiltration basin, a definition of 80 m of depth for the simulated aquifer was considered to be sufficiently representative. The assignation of initial K values for each layer was based on the estimates for the Yucatan plain area by González-Herrera et al. (2002). The higher K value was assigned to the preferential layer and a lower value assigned to the remaining layers (Table 4.5).

Table 4.5: Definition of layers and assigned K values preceding calibration.

Layer	Thickness (m)	Type	K (m/s)	Simulated karst feature
1	10	Convertible	0.1	Upper epikarst
2	7.5	Convertible	0.1	Lower epikarst
3	17.5	Convertible	1.115	Preferential layer
4	45	Confined	0.1	Rest of the aquifer

The Conduit Flow Process (CFP) model, as part of MODFLOW, simulates conditions of turbulent groundwater flow by selection of an appropriate model (Shoemaker et al., 2007; Reimann and Hill, 2009). This code was utilized to simulate the preferential flow layer (CFP Mode 2) embedded in the model, as displayed in Figure 4.11. Due to the aim of this work, a solute transport model was necessary to investigate pollution plume behaviour.

The Modular 3-Dimensional Transport model with multi-Species structure (MT3DMS) was selected for its compatibility with MODFLOW (or any other block-centred finite-difference model). This multi-species transport model simulates advection, dispersion, diffusion, and other transport phenomena (Zheng and Wang, 1999). Nevertheless, an inconvenience emerged due to the incompatibility of CFP with MT3DMS, necessitating the implementation of a two-step modelling approach:

- First, a simulation utilizing CFP was carried out utilizing MODPATH, a particle tracking model for MODFLOW (Pollock, 2016), to investigate particles' residence time and their movement in the multiple layers of the model. Analysis of particles' advection in the system also served to investigate the influence of wellfields on groundwater flow.

- Second, an EPM model was adapted with the parameters used for CFP; with these arrangements it was possible to simulate the pollution plume behaviour and NO_3^- concentrations in the study area.

4.4.3 Packages

A Time-Variant Specified Head (CHD) package defines boundaries with a defined hydraulic head. This boundary type (Dirichlet condition) allows infinite water volumes to enter or leave the system (Harbaugh et al., 2000). This boundary condition was settled in the north of the study area along the coastline; the head for this boundary was defined as zero (sea level). Similarly, a CHD was defined for the southern boundary. In this case, time series data of monitoring wells provided by CONAGUA was interpolated to estimate hydraulic heads.

The utilized data covers a period of 14 years (from 2002 to 2015) with measurements obtained in intervals of four months. For the eastern and western boundaries, a no flow boundary (Neumann condition) was set.

The Recharge (RCH) package simulates the volume of water moving through a given area in a given lapse of time (Harbaugh, 2005). Recharge derived from precipitation was estimated by applying the multi-parameter approach APLIS. Nevertheless, cities considered in the model were defined as completely impermeable due to urbanization, disallowing the occurrence of recharge from precipitation. Incidental recharge occurring under urban areas was estimated as the leaking volumes of wastewater and the water losses from the distribution systems (see Table 4.4). Recharge rates from precipitation were estimated for each month to be further applied as stress periods.

The Wells (WEL) package settles a specific flux for an individual cell. This package was used to simulate the wellfields located inside the study area. The total extraction volume from each wellfield was displayed as a sole well to be representative of each field. Extraction volumes displayed in Table 4.4 were used; extraction was kept constant during the simulation.

The Head Observation (HOB) package was used to analyse hydraulic heads in specific locations to be further compared against real measured values from time series and to calibrate the model. Each observation well is defined for a given grid, for which an observed value is assigned. Comparing real vs simulated values, residuals are computed. For this work, six monitoring wells, part of the monitoring network of CONAGUA were utilized. All packages are displayed in Figure 4.12.
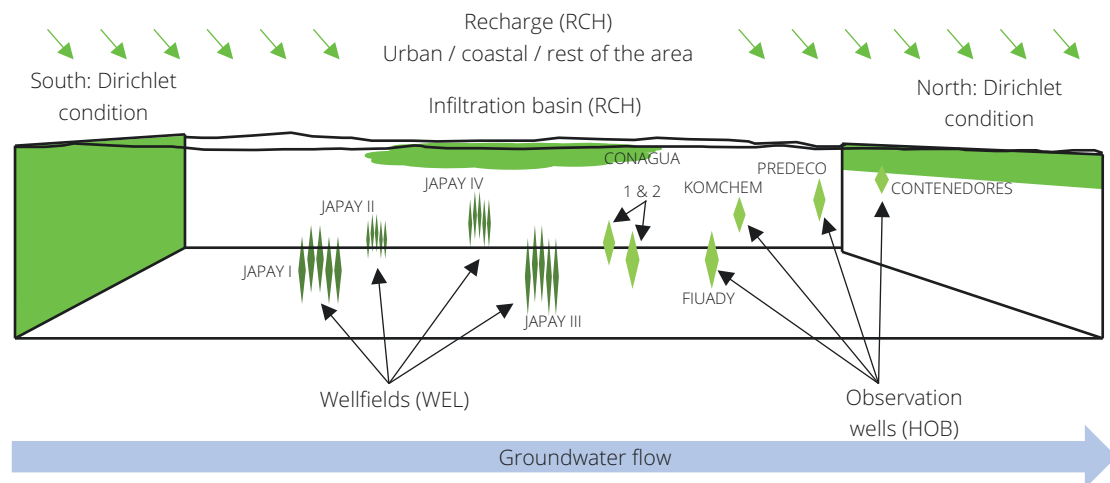
Figure 4.12: Settings and packages of the model. Image modified after Martínez-Salvador et al. (2019).

4.4.4 Generalities of the model and assumptions

For the CFP model, the mode 2 was selected. This mode simulates a preferential flow layer of turbulent flow embedded in layers simulating a laminar flow. Some pre-tests were run to define an appropriate void diameter as required by the CFP. Multiple runs, changing this value within a range from 0.5 m to 0.9 m, demonstrated no significant effects; a value of 0.9 m was chosen to run the simulations. The default Reynold's numbers were used with values of 2,000 and 4,000.

For particle tracking analysis two locations were settled as the origin, the southern boundary and the Merida city. The southern boundary was defined as the origin of particles to investigate if the wellfields exert influence on the groundwater flow, either by diverging or delaying any possible pollutant moving northwards. The Merida city was defined as the second origin of particles to investigate the direction of pollutants leaking from septic tanks in the sub-surface of this urban area.

For the EPM model, default values were selected. Regarding the MT3DMS model, the active tools to simulate mass transport were advection (ADV), transport (BTN), dispersion (DSP), sink and source mixing (SSM), and the generalized conjugate gradient solver (GCG). The simulated species was NO_3^- utilizing the finite differences solver. The initial NO_3^- concentration of 28 mg/L was defined from WWTP inflow data provided by JAPAY.

The transport model was first run for a period of one year (short term with 12 stress periods) and then for a period of 60 years (long term). For the short-term simulation, average monthly recharge was used to define 12 stress periods; the stress periods were simulated within a lapse time of one day as representatives of each month. The long-term simulation was run, applying a yearly average recharge. Stress periods from natural recharge were applied solely for non-urban areas; incidental recharge in the cities sub-surface was kept constant. In the same way, the pollutant release, in terms of volume and concentration, was kept constant during the simulation according to the values calculated from WWTP data. Some of the assumptions to describe the system and to define the model are described as follows:

- The impact of the saline interface was not considered; density and temperature were kept constant.

- The system was defined as having a steady state due to the rapid recovery and low variability of hydraulic heads.

- Cities were considered totally impermeable due to urbanization; recharge in these areas was defined from the distribution system and septic tanks leakages.

- Tidal effects were not considered as an influential factor for the model. However, a higher recharge rate was defined for near-coastal areas to compensate for this situation.

In general, the model was settled to simulate groundwater flow in an area with six pollution sources (municipalities' main cities) with variable monthly recharge rates and external stressors, such as large pumping wellfields. Having defined the basic setup of the model, the next step was the model calibration.

4.4.5 Model calibration

Calibration was carried out manually, adjusting one parameter at a time. The best calibration for each individual parameter was defined when the prediction error, according to the root mean square error (RMSE), was minimal. For this work, an RMSE of 0.25 m was designated as acceptable to stop calibrating.

During this process, hydraulic conductivity and recharge were the parameters designated for calibration; calibration started modifying hydraulic conductivity. During calibration, it was noted that changes in the vertical hydraulic conductivity (K_{zz}) were not significant in terms of variation across the model. It was then decided to utilize the proposed initial value of 1.115 m/s; although this value can be considered high, its purpose was to compensate for the fissuring of layers. Calibration of horizontal hydraulic conductivity (K_{xx} and K_{yy}) was obtained following the same principle, nevertheless, it was decided to not utilize values above the initial value of 1.115 m/s, as this value was already considered to be high. Initial and calibrated hydraulic conductivities are displayed in Table 4.6.

Slightly better RMSE values were obtained when hydraulic conductivities from upper epikarst and lower epikarst layers were inversed. However, such settings did not display the purpose of these layers acting as epikarst.

Table 4.6: Initial and calibrated hydraulic conductivity (K).

Layer	Thickness (m)	Type	Initial K (m/s)*	Final K (m/s)*	Simulated karst feature
1	10	Convertible	0.1	1	Upper epikarst
2	7.5	Convertible	0.1	0.5	Lower epikarst
3	17.5	Convertible	1.115	1.115	Preferential flow
4	45	Confined	0.1	1	Rest of the aquifer

* Values representing K_{xx} and K_{yy}; K_{zz} remained constant with a value of 1.115 m/s.

The subsequent step was to calibrate recharge. Recharge rates estimated with the APLIS method showed a notable overestimation. The average recharge for the study area according to APLIS was estimated as 56% of precipitation; this percentage was too high when compared with previous estimations ranging from 14 to 20%.

Calibration of recharge was carried out individually for each object (municipality). Calibrated recharge values are displayed in Table 4.7. In the case of the Progreso municipality, an increment of recharge was assumed, given the coarse soils and the shallowness of the water table in this coastal region; the confinement along the coast was not considered in the model.

Table 4.7: Calibrated recharge rates per municipality.

Municipality	Best calibration
Progreso	2.5 times the APLIS recharge
Merida, Conkal, Ucu, Uman and Kanasin	0.2 times the APLIS recharge
Rest of the area	0.0025 times the APLIS recharge

After calibration, the average recharge rate was 0.23 Mm^3/km^2, a slightly higher value than the 0.18 Mm^3/km^2 from previous studies. Nevertheless, simulated discharge volumes presented less than 0.1% of variability compared with those reported by CONAGUA (2012).

4.5 Results and analysis

4.5.1 CFP and particle tracking with MODPATH

For the first CFP simulation, particle tracking revealed no significant effects of the four wellfields over the particles released from the southern boundary. A slight delay on particles moving towards JAPAY IV was observed in the preferential layer, possibly as a consequence of water extraction volumes from this wellfield (Figure 4.13). However, this outcome is not conclusive.

Particles in epikarst layers remain undisturbed following the natural groundwater flow. This is an interesting outcome since other wellfields with larger extraction volumes do not display any influence on particle movement. Particles reach the southernmost well (JAPAY I) in a lapse of 2 years. A thirty years simulation indicates that particles crossing the southern boundary move northward heading towards the coast.

An average of seven years was estimated for particles to reach the coast line and eight years to reach Progreso city. Although flow paths do not differ significantly from a horizontal perspective, they do differ vertically. This is more evident when extraction wells are active, highlighting two paths concentrating particles.
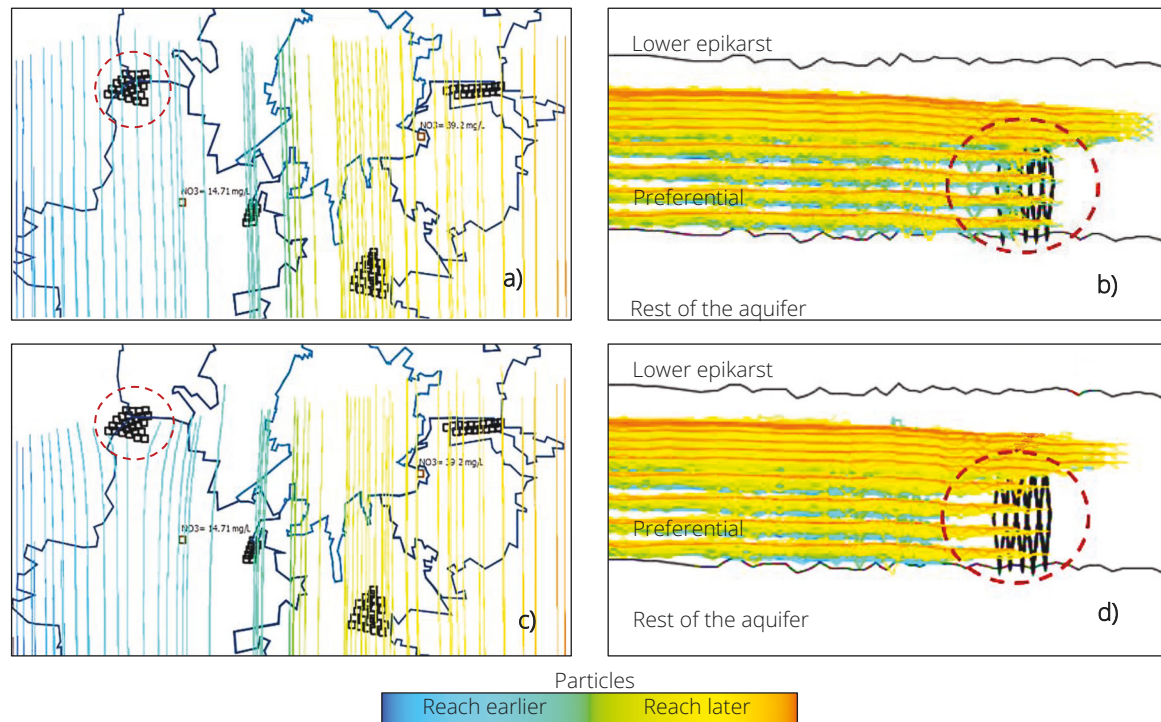
Figure 4.13: Particle tracking in the preferential flow layer. In a) and b), particles movement with inactive extraction wells. In c) and d), a minor effect on particles movement is influenced by JAPAY IV (red circle) when extraction is active. Image reproduced from Martínez-Salvador et al. (2019).

Merida city was defined as the particle release area for the second CFP simulation. A distinctive movement of particles was highlighted, moving towards the coast, influenced by the hydraulic gradient. Particles with an origin in Merida move directly towards Progreso city with an estimated travel time of approximately four years. According to the simulation, after one year, some particles have left the Merida city area, reaching the observation well FIUADY located in the northern city periphery. At the same time, some particles have barely reached the observation well KOMCHEM located approximately 15 km from the Merida centre. A distance of six km separates the FIUADY and KOMCHEM wells. Particles reaching these wells almost simultaneously are directly derived from the release point inside the Merida area. While particles reaching KOMCHEM are those being released in the northern limits of the city, those reaching FIUADY at the same time have an origin in the western limits of Merida.

Particles reached the observation wells PREDECO and CONTENEDORES, in a lapse of three years. These wells are located 26 km and 30 km away from Merida city. According to the model, a period of 5 years is necessary for a particle released in Merida to reach the coast. An average of about 8.5 km/year can be assumed from particle tracking (Figure 4.14). Results indicate a clear particle movement from Merida city towards Progreso city. This particular northward direction indicates that extraction wells supplying small communities located between these two cities could also be affected by the pollution generated in Merida.

Regarding the extraction wells located in the southern Merida periphery, no reverse flow was determined given the model setup. It is important to highlight the fact that urban areas, located between the city limits and these wellfields, were not included into the model. A similar statement applies for JAPAY III and JAPAY IV, where particles released in Merida move completely northward, without noticeable effects caused by the current extracted volumes from these wellfields.
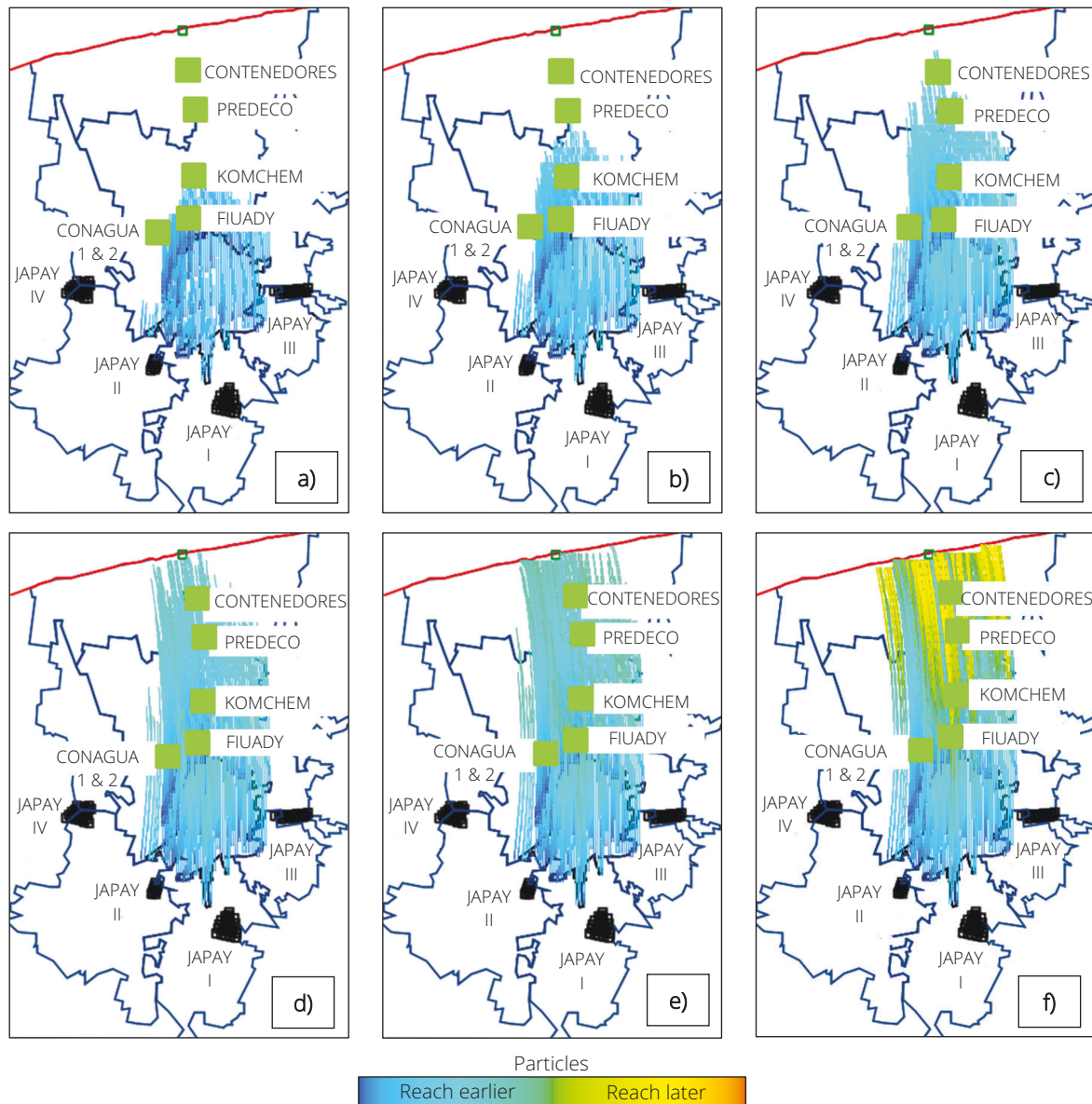
Figure 4.14: Particle tracking with Merida city as the particle release area. From a) to f), particles movement after one, two, three, four, five, and ten years, respectively. Image reproduced from Martínez-Salvador et al. (2019).

4.5.2 EPM and solute transport with MT3DMS

The pollution plume generated by septic tanks in the sub-surface of Merida displayed an interesting hydraulic behaviour, according to the model. Results indicate that pollution concentration decreases with depth. The higher concentration occurs in the upper epikarst layer where the pollution source is located (septic tanks). Concentration is also intense in the lower epikarst and the preferential layer with values ranging from 15 to 24 mg/L. The pollution plume reaches the deepest layer by diffusion where extraction takes place, nevertheless, NO_3^- concentration in this layer remains low with values below 7 mg/L. Diffusion of the pollution plume towards the east and west also occurs but with minimal concentrations (Figure 4.15). However, the pollution plume generated in Kanasin could increase, affecting JAPAY III, if there is an increase in wastewater leakage from the Kanasin municipality due to urbanization.
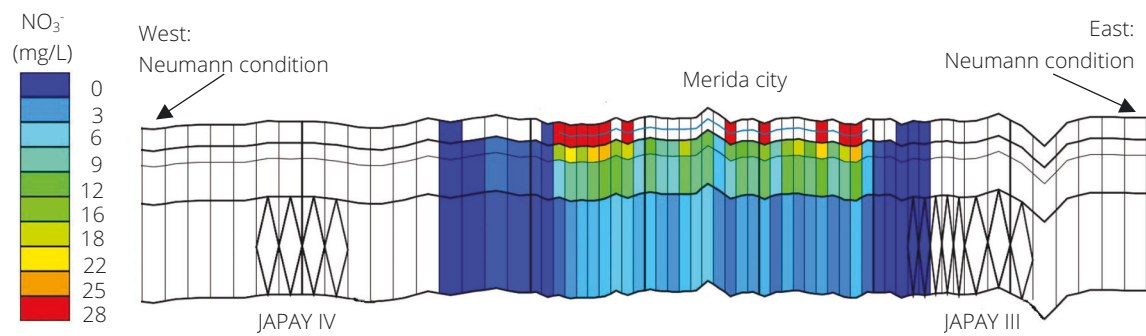
Figure 4.15: East to west view of the MT3DMS model (13th stress period). Image reproduced from Martínez-Salvador et al. (2019).

From a south-to-north trajectory, a higher NO_3^- concentration in the northern Merida sub-surface in comparison to the south is highlighted. This outcome is reasonable considering the natural groundwater flow and the model setup, which defined Merida as an impermeable surface. The north boundary of the city is the exit of the generated pollution plume, solely affected by pipe leakage (Figure 4.16).
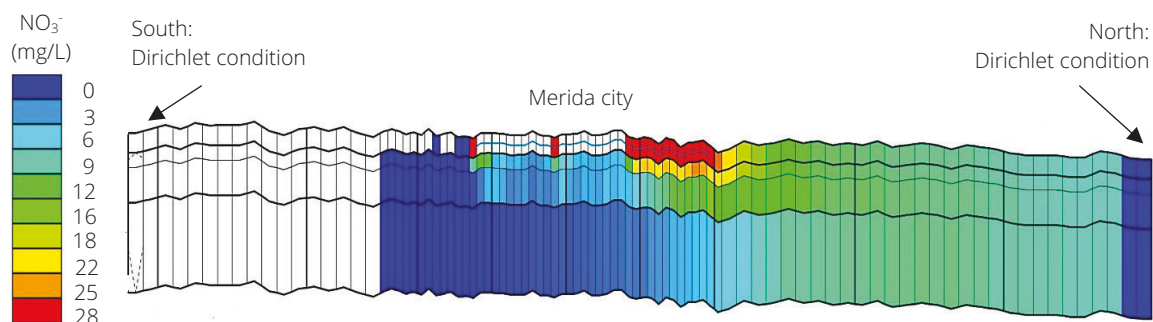
Figure 4.16: South to north view of the MT3DMS model (13th stress period). Image reproduced from Martínez-Salvador et al. (2019).

On the other hand, pollution generated nearby the southern boundary could be minimized by groundwater moving northward with the addition of the recharge generated in this area. Pollution advection occurs mostly in the horizontal axis with higher concentration in epikarst layers. Some cells of the upper epikarst below Merida remained dry and solute transport is not simulated (blank cells). Despite this inconvenience, concentrations are expected to have a similar influence as those displayed in the north of Merida sub-surface.

Given the higher hydraulic conductivity designated for the preferential flow layer, a higher concentration was predicted in this preferential flow path and expected to be the main driver for the pollution plume movement. Nevertheless, no significant effects either on velocity or concentrations seem to be induced by this layer. It is also possible to note the vertical behaviour of the plume with the concentrations in each layer decreasing towards the north. A few kilometres away from Merida city, the pollution concentration is depicted as stable with values below the permissible maximum. This stability could be driven by the higher recharge estimated for this area. The path that the pollution plume follows by advection is similar to that displayed by particle tracking, moving towards the north, heading to Progreso city. A similar pattern is better visualized in epikarst layers for the cities of Conkal, Ucu and Uman, with pollution moving northward with a minor extension (Figure 4.17).
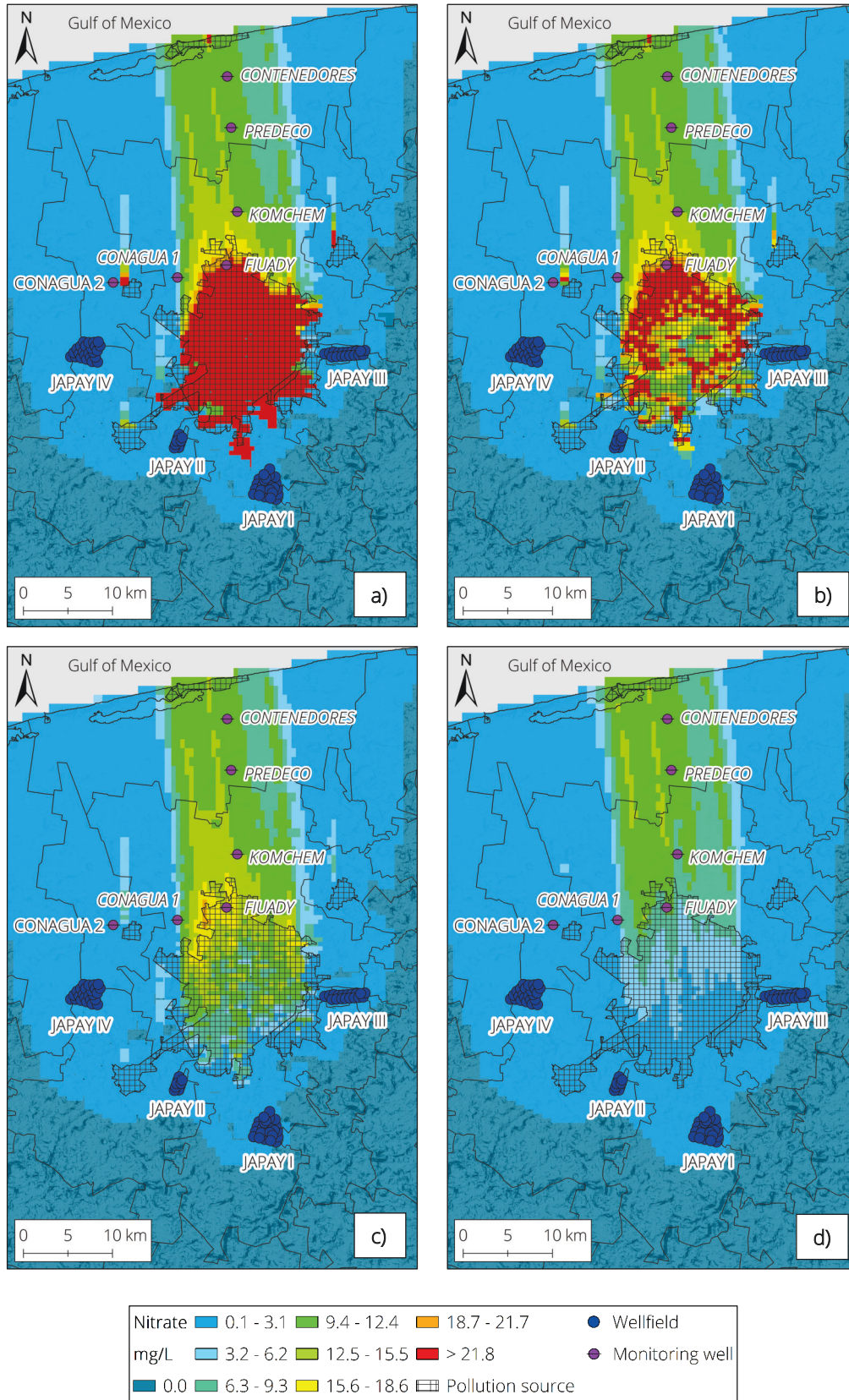
Figure 4.17: Pollution plumes in the MMA after 60 years simulation. In a), the upper epikarst layer; in b), the lower epikarst layer; in c), the preferential flow layer; in d), the rest of the aquifer.

In the case of Kanasin city the same transport direction is expected despite it is not being visually clear due to its proximity with Merida. In this case, pollution generated in Kanasin city can exert a relevant influence on NO_3^- concentrations with possible effects on the wellfield JAPAY III, as mentioned previously.

At the end of the simulation, being considered as the current situation of the MMA, the trajectory of pollution plumes is defined towards the coastline following the natural groundwater flow. No influence of large wellfields was observed. Inverse flows, as proposed by previous studies in the area, are not depicted, at least with the limitations of model setup.

4.5.3 Analysis of the results

The pollution generated by urban areas reached the extraction wells in the Merida periphery. However, this situation seems to be triggered by NO_3^- dispersion through the four layers of the model. The current evidence regarding the pollution sources affecting these wellfields is not conclusive. However, due to the proximity of specific urban areas, the pollution source can be inferred. JAPAY I could be affected by the pollution plume generated in Merida city. The wellfields JAPAY II, JAPAY III, and JAPAY IV may experience some problems from NO_3^- pollution generated in the cities of Merida, Kanasin, and Uman, respectively.

Despite the model indicating that pollution extends towards these wellfields, concentration curves do not display a serious increment of NO_3^- concentrations in any layer. During the multiple stress periods of the simulation, NO_3^- concentrations remained minimal in the wellfield's sub-surface with values lower than 0.5 mg/L. From this perspective, the gradual vertical decline of NO_3^- concentration occurring below Merida city is more noticeable, by comparison of the four layers. On the other hand, NO_3^- concentrations drastically decrease northward as they leave the Merida city area. This severe change in pollutant concentration could be driven by the assumed impermeability of the city and the recharge taking place outside of its area.

With the model it was possible to estimate the time it takes for the plume to reach the monitoring wells. Due to its proximity to Merida city, the well FIUADY displays an increment of about 15 mg/L in NO_3^- levels between 50 and 100 days after the beginning of the simulation. According to the model, NO_3^- levels are almost constant after 100 days with values around 20 mg/L. Lower concentrations, following a similar pattern, were estimated for the remaining wells but differing in approximately one year.

The general results indicate that as the distance from Merida city increases, the NO_3^- concentration decreases with a prolonged travel time. These results slightly differ from the travel times displayed by particle tracking, specifically for the FIUADY well. However, in the case of this well, dispersion is the assumed factor causing this difference. Recharge plays a very important role in the variability of NO_3^- concentration. Nevertheless, this variability is confined to the lower epikarst layer.

Pollutant concentration in deeper layers is not affected by recharge. Despite being minimal, such variability indicates how the precipitation regime affects the pollution plume providing useful insights for further analysis. A higher concentration during the dry season as well as its decline during the wet season was expected as a consequence of the additional water inflow from the surface, however, the predicted effect of recharge on dilution was partial (Figure 4.18).

The lower epikarst layer demonstrates an interesting decrease-increase pattern occurring in both dry and wet seasons. A reasonable interpretation for this variability could be linked to the low permeability of the urban area, dilution, and a flushing effect. Considering the low concentration occurring during the first months of the dry season as a starting point, it is possible to assume that the gradual increment of NO_3^- is the consequence of the pollution plume moving northward and the low recharge from the surface.
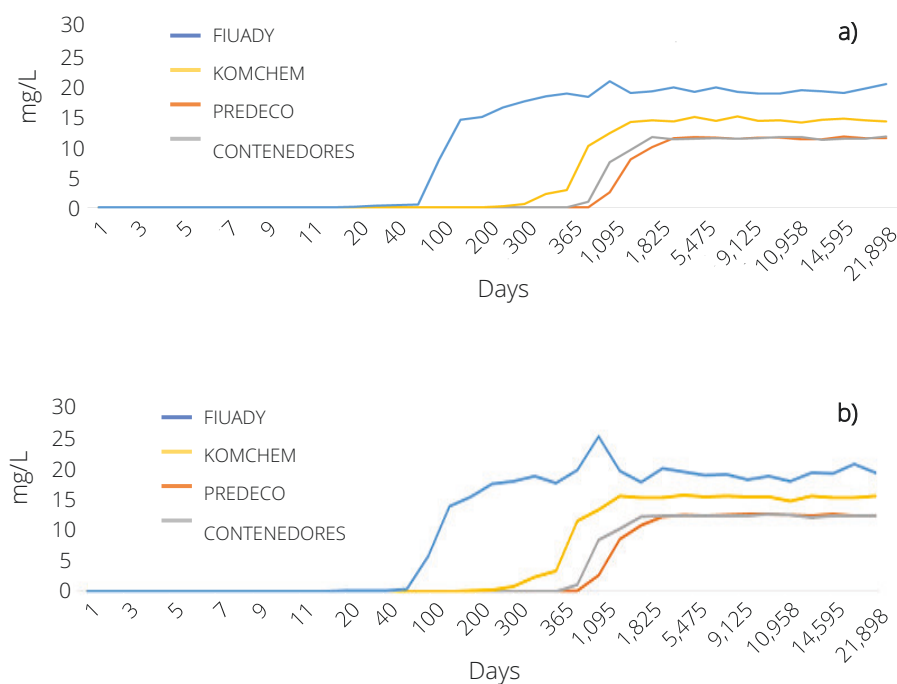
Figure 4.18: Estimates of NO$_3^-$ concentration and travel time for the northern area of Merida. In a), simulated concentrations for the upper epikarst; in b) simulated concentrations for the lower epikarst. Image reproduced from Martínez-Salvador et al. (2019).

When the wet season begins, recharge promotes a dilution effect in this area and the concentration begins to decrease. However, pollutant concentration rises again in the middle of the wet season, despite the recharge rates being higher during these months. This could be the effect of recharge taking place in the southern areas of Merida, leading to a flush effect carrying the pollution accumulated in the city sub-surface. At the end of the wet season, pollution concentration starts to decline until it reaches its lowest value; this value of approximately 12 mg/L remains stable during the first months of the dry season before it begins to increase again (Figure 4.19).
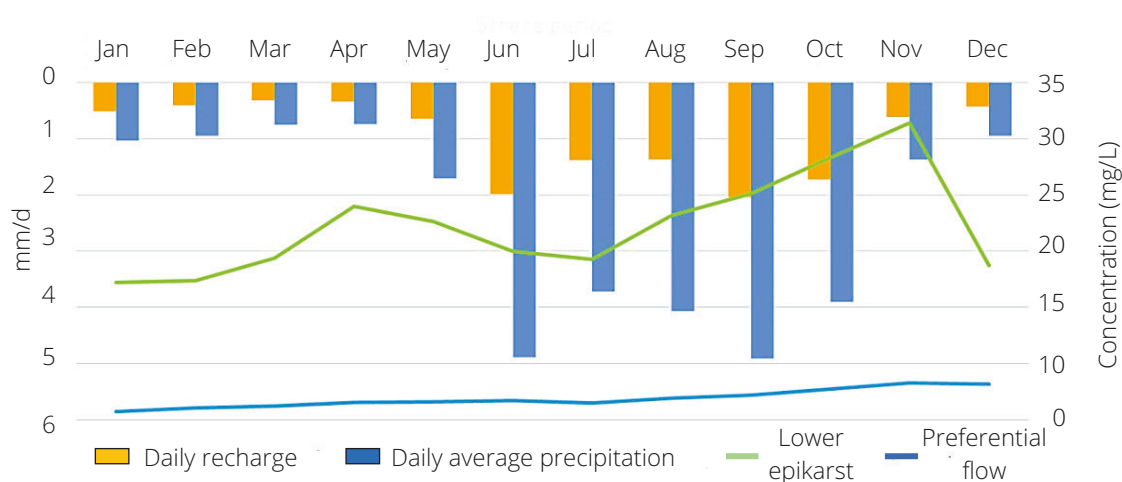
Figure 4.19: Influence of recharge patterns on NO$_3^-$ concentrations. Image reproduced from Martínez-Salvador et al. (2019).

This interesting outcome indicates that recharge can be either beneficial or unfavourable for pollution scenarios. As demonstrated by the model, recharge can be a positive factor, leading a decrease of pollutant concentration for a given area when it occurs locally. Nonetheless, recharge taking place at distant areas can induce a flush effect, increasing pollutant concentration. A summary of the simulated travel time and NO_3^- concentration is displayed in Table 4.8.

Table 4.8: Summary of pollutant travel time and NO_3^- concentrations. Table modified after Martínez-Salvador et al. (2019).

Source	Minimum estimated time	NO_3^- concentration
JAPAY wellfields	Less than one year	0.1mg/L (after 60 years of simulation)
Progreso City	Two years	11.8 mg/L (after 60 years of simulation)
Merida City	Constant	Constant concentration of 28 mg/L for the aquifer upper layers
Observation wells	FIUADY ~ 50 days KOMCHEM ~300 days PREDECO ~ 365 days CONTENEDORES ~ 730 days	Layer-dependent

Although the permissible maximum NO_3^- concentration was not simulated in any point of the study area, advection represents an interesting pattern. Areas not located along the general pollution plume paths can be affected by NO_3^-. In order to have a better evaluation of how the parameters obtained by a transport model can be integrated into a groundwater vulnerability analysis, some theoretical scenarios are presented in the following section.

4.6 Discussion

From the results obtained by modelling, it was possible to analyse the anthropogenic influence on the aquifer and to estimate factors such as the travel time, NO_3^- concentrations, and the variability exerted by the precipitation regime. With the goal of expanding the aquifer vulnerability analysis, these additional criteria could be remarkably useful, especially when outcomes from intrinsic resource vulnerability do not display a clear division of vulnerability classes. Intrinsic groundwater vulnerability analysis was conceived as a tool to aid in the decision process of water-related issues, however, it could lead to erroneous decisions under some circumstances.

As an example, let's consider a given area categorized with a homogeneous intrinsic vulnerability, where a new water extraction well is necessary to keep an optimal water supply; in this case, the water authority have no other vulnerability criteria to define the most suitable location for a new extraction well. For this illustrative scenario, a map displaying pollution paths or pollutant concentration can help to further classify an area of the aquifer as more vulnerable than others. In order to investigate the importance of evaluating anthropogenic practices and transport results influencing groundwater vulnerability, some examples from the MMA are presented and discussed. It is important to mention, that the model does not depict all the anthropogenic influences occurring in the MMA, however, it is sufficiently representative to evaluate results in terms of vulnerability.

It is very important to highlight that the goal of the vulnerability analysis of the scenarios presented herein, is not to propose a particular index scheme nor a weight assignment for such parameters; vulnerable areas are simply displayed highlighting the differences of the evaluated parameter. Therefore, the sole purpose of this section is to visualize the differences among areas that can improve decisions, for which aquifer vulnerability analysis is highly influential.

The following evaluation is carried out under the assumption that the majority of intrinsic resource vulnerability maps, presented in section 3.3, displayed a very close vulnerability scenario for Yucatan. Since the MMA is classified with an MV by the majority of the applied multi-parameter methods, additional characteristics need to be included into the vulnerability analysis in order to improve the decision process in this area.

Several tasks, such as new extraction wells, suitable areas for agriculture, and definition of source protection zones are mentioned as theoretical scenarios for which solute transport, integrated with intrinsic groundwater vulnerability mapping, can aid in the decision process. This is done to better understand the important role of additional criteria in transport modelling for aquifer vulnerability analysis and decision support.

4.6.1   Vulnerability estimation from groundwater flow

As an initial theoretical scenario, it was assumed that a new extraction well is necessary to maintain an optimal water supply in the region. Having defined this region with an MV according to intrinsic groundwater vulnerability methods, additional criteria are needed to propose the best location for the new water source. The model revealed clear NO_3^- transport northwards, triggered by the pollution generated in urban areas and the regional groundwater flow. Due to the large population differences among the evaluated cities, pollution transport is more noticeable in the northern area of Merida.

Strictly considering the negative effects of current anthropogenic practices for a vulnerability analysis, the section of the aquifer being directly affected by pollution must be avoided as a potential location for the new water source. Any well located along this pollution path can be considered as a more vulnerable source if the area is compared with other locations outside this pollution-affected aquifer section (Figure 4.20a). In general, the transport model highlights the southern areas as less vulnerable since the pollution generated in urban areas will follow the natural groundwater flow towards the coastline.

Any location, outside the pollution paths, can be considered as less vulnerable and more reliable as a new extraction well site. In this theoretical scenario, evaluating the direction of the pollution transport from existent pollution sources brings additional information, from which the aquifer can be further categorized as less or more vulnerable. Therefore, inclusion of anthropogenic impacts currently occurring in study areas is very important, since traditional groundwater vulnerability estimations, with a focus on source vulnerability, are not able to display such pollution paths.

Following this criterion, solely evaluating transport direction, a second theoretical scenario that contemplates the necessity of a new dumping site is evaluated. From this perspective, it is necessary to anticipate the possible negative influences over the existent water sources as part of the analysis. Wellfields currently in operation are classified as low vulnerable sources given their location and the low influence of the actual water extraction rates on the natural groundwater flow. However, the wellfields' southern areas must remain undisturbed to maintain a low vulnerability profile for these water sources. For the location of the new dumping site, these zones must be excluded as options.

In other words, the "protection areas" displayed in Figure 4.20a are more vulnerable for the existent water sources. From the previous basic map, it was possible to highlight two vulnerable areas (or less suitable, depending on the perspective) to improve decisions regarding two different practices; both cases are directly related to source vulnerability analysis. However, decisions are dependent on other aspects, such as those from regional development or private interests. Therefore, groundwater vulnerability analysis must be flexible as a tool to aid in the judgment of multiple scenarios.

For the third theoretical scenario it was assumed that two agricultural fields located in the south would be developed, directly in the direction of the wellfields JAPAY III and JAPAY IV. In this case, both wellfields can be considered as vulnerable from the pollution trajectory point of view. However, in order to implement protection strategies or improvements for their operation, a further classification of vulnerability is necessary.

As displayed in Figure 4.20b, both wells will be affected by agriculture activity due to the common use of fertilizer in such areas; for this scenario, pollutant travel time is added as a supplementary parameter.
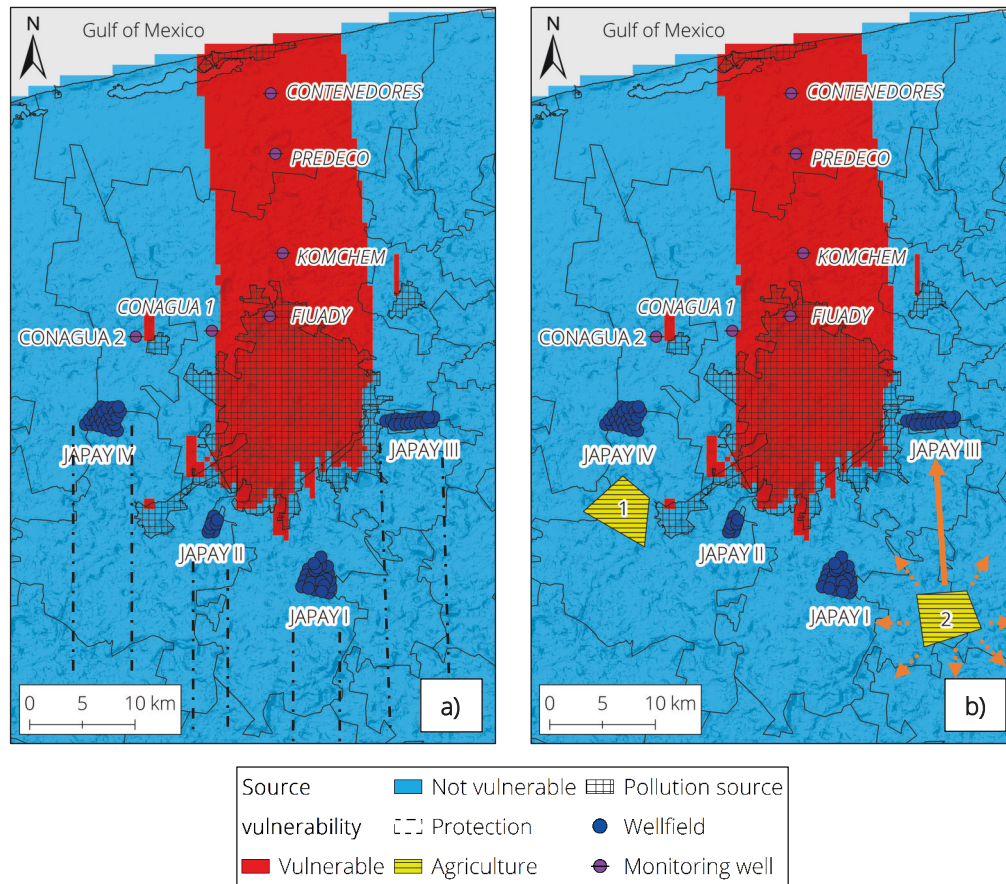
Figure 4.20: A basic example of groundwater flow to define source vulnerability. In a), representation of theoretical scenarios one and two display flow direction as indicator of vulnerability; in b), representation of theoretical scenario three to highlight the importance of diffusion for vulnerability estimation.

According to the model, the travel time it will take for a pollutant to travel from agriculture area one to JAPAY IV is approximately one year. For agriculture area two, any pollutant released here will travel towards JAPAY III in a lapse of approximately 2.5 years. This outcome designates JAPAY IV as the most vulnerable water source among all wellfields under this scenario. In this example, the source with the closest pollution source was designated as the most vulnerable, however, this is not a rule that can be applied in karst aquifers.

Up until this point, the groundwater flow model has demonstrated its utility to define vulnerable areas by taking into account anthropogenic activities. The distinctive paths that pollution follows provide important insights with which to further classify vulnerability of water sources located in a heterogeneously defined vulnerable area. However, these results solely point out vulnerability from advection and the time it takes for a pollutant to move from a release point towards a water source.

4.6.2 Vulnerability estimation from solute transport

The advantage of using a transport model as indicative of aquifer vulnerability relies in the inclusion of dispersion processes in addition to advection taking place in the aquifer. The sole use of travel time, either from groundwater flow models or by multi-parameter analysis, to define vulnerability or protection zones can misrepresent real vulnerable points in a given study area. This statement is supported by the model outcomes in Figure 4.17 where the advection-dispersion transport is clear, affecting the surrounding areas. In addition to the advection-driven pollution towards the coastline, NO_3^- concentrations were simulated to the south, east, and west of Merida city; records of NO_3^- levels in these areas are mostly driven by dispersion. Despite such low levels not representing an immediate threat for the extraction wells, this situation could change if wastewater disposal volumes increase in the future due to the inevitable urbanization.

As an additional example to highlight the importance of solute transport for aquifer vulnerability analysis, the third theoretical scenario, as displayed in Figure 4.20b, is further evaluated. The analysis of travel time, according to the groundwater flow, indicated that JAPAY IV is considered to be more vulnerable than the rest of the wellfields due to the proximity of agricultural area one. However, the inclusion of solute transport into the analysis demonstrates that JAPAY I could also be affected by agricultural area two. Although most of the NO_3^- load is expected to travel northward, reaching JAPAY III in approximately 2.5 years, solutes from this agricultural area could reach JAPAY I in a shorter period of time increasing the vulnerability of this water source. Therefore, inclusion of advection-diffusion dynamics proves to be a highly necessary step to further evaluate the influence of anthropogenic activities on groundwater vulnerability analysis.

The transport model with an initial NO_3^- load of 28 mg/L displayed that the permissible maximum NO_3^- concentration, according to the Mexican water regulations, is not surpassed at any point in the aquifer. Under these conditions, any location of the study area could be selected to build an extraction well for drinking water supply; this, of course, comes uniquely from a vulnerability point of view and according to the characteristics of the model. However, the aquifer can be subdivided in relation with the NO_3^- concentrations to display more vulnerable sections to be considered in the selection process. Taking the initial pollution concentration as the most vulnerable condition for the aquifer, additional vulnerability classes can be classified.

For illustrative purposes, the discretization was performed utilizing Jenks natural breaks (Jenks, 1967); natural breaks classification statistically creates groups of individual values (classes), minimizing the variance within a given class and maximizing the variance between classes. In Figure 4.21, areas not affected by NO_3^- are excluded from this classification since vulnerability at this stage is based purely on solute transport. The range of colours represents vulnerability classes as presented in chapter three. From the analysis of Figure 4.20, the applicability of solute transport as an indicator in vulnerability studies is well established.

The pollution path indicates that a section of the aquifer in the northern area of Merida is more vulnerable due to the pollution plume front. However, solute transport indicates that pollution travelling along this path experiences dilution. The model indicates a downgrade of more than 50% from its initial concentration in locations at seven kilometres distant from the pollutant release area. According to this classification, the urban sub-surface represents the most vulnerable area of the aquifer to drill a water extraction well; vulnerability decreases gradually following the NO_3^- concentration pattern.

Source vulnerability is estimated by intrinsic resource vulnerability methods with the addition of groundwater flow velocities. Following this definition, the extraction wells located inside Merida (not considered in the model) are then directly defined as highly vulnerable given the fact that pollution is constantly leaking from septic tanks.

This situation serves to highlight another advantage of solute transport to estimate vulnerability; if these inter-urban wells are shallow, with depths falling in the epikarst layers, as displayed by Figure 4.21a, their classification as highly vulnerable could be considered accurate. However, the deeper the inter-urban well is, the less vulnerable it must be considered, according to the model outcomes; deeper layers of the aquifer underneath Merida are less affected by pollution. In the deepest layer, located at 45 m of depth, the aquifer (or wells located at this depth) displays low and very low vulnerabilities (see Figure 4.21b).
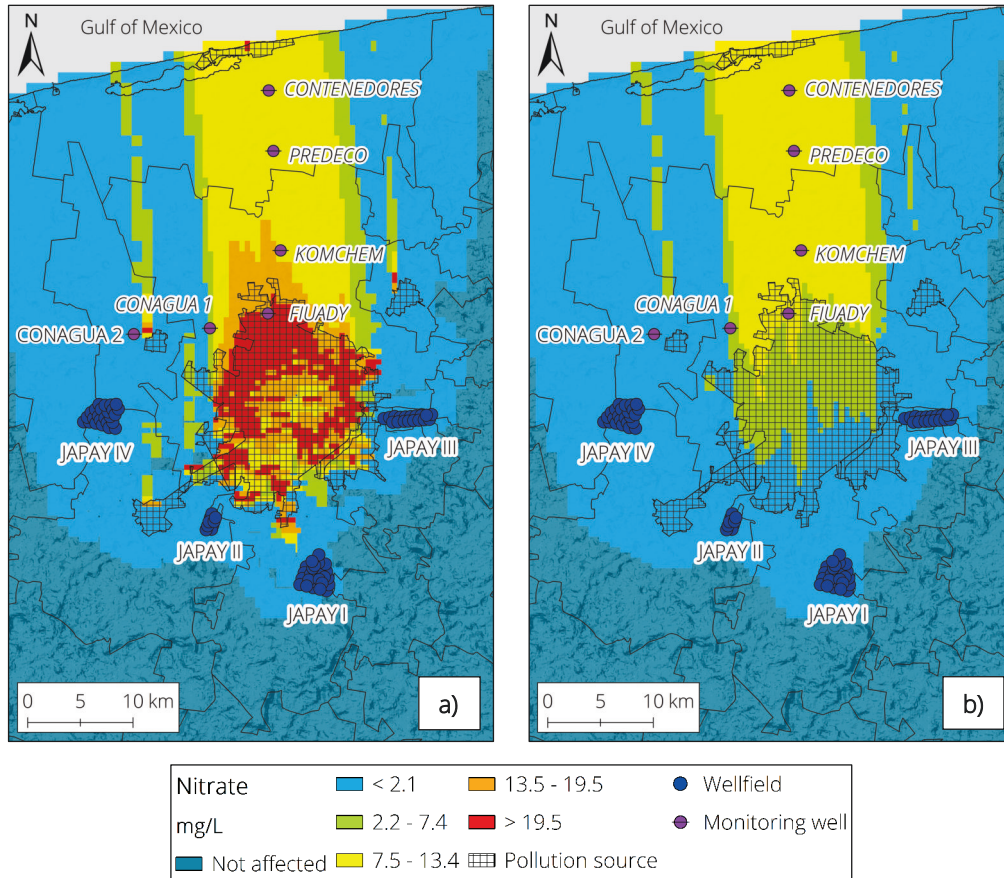
Figure 4.21: Proposed vulnerability classes based on Jenks classification. In a), simulated NO_3^- concentrations in the lower epikarst layer; in b), concentrations in the rest of the aquifer layer.

Therefore, estimation of resource and source vulnerability turns into a three-dimensional analysis, in which the depth of the water source also plays a relevant role for its classification as vulnerable or not. This is beneficial for water authorities and stakeholders since more options are available to support decisions regarding corrective or preventive measures in order to maintain optimal operative and qualitative conditions.

Vulnerability classification for water sources or aquifers sections must be dependent on water quality standards and the permissible maximum value of the pollutant being analysed; these values are variable among countries. Nevertheless, such values can provide a more solid base to categorize vulnerability classes from pollutant concentrations estimated by transport models.

For our study area, extreme values were not reached. However, vulnerability classes were defined according to the regional characteristics. From the results and examples presented in this chapter the necessity of including anthropogenic stressors and their effects via solute transport models is confirmed.

4.7 Chapter remarks and outlook

This chapter introduced a new perspective regarding groundwater vulnerability assessment, in which the anthropogenic influence, analysed by a solute transport model, highlights the importance of the inclusion of additional parameters derived from anthropogenic activities already affecting groundwater quality. Integration of such parameters expands the possibilities for the decision-making process, mostly for the areas where an intrinsic resource vulnerability map has displayed homogeneity. Additionally, this integration could change the context of the traditional two-dimensional vulnerability mapping into a three-dimensional estimation. This point of view could be helpful for scenarios where the aquifer has been categorized as highly vulnerable but continuous socio-economic development is inevitable.

The solute transport model presented in this chapter is a simplification of the current scenario in the MMA given the data availability during the model development stage. Activities such as industry, agriculture, and dumping sites affecting groundwater quality were not included. In the same way, several towns located in this area, with their respective water extraction and wastewater generation volumes, were not considered in the model. In addition to these simplifications, the unsaturated zone flow (UZF) package of MODFLOW was not included as part of the model due to the lack of necessary data to estimate processes occurring in the unsaturated zone. Despite these limitations, the model fulfilled its purpose of investigating the relevant parameters for solute transport to be considered as additional aquifer vulnerability indicators.

Nitrate was selected as the studied pollutant for this study given the data availability and the numerous studies regarding nitrate pollution in Yucatan. Vulnerability from solute transport was represented according to the simulated NO_3^- concentrations to demonstrate the benefit of its inclusion in vulnerability analysis and decision-making processes. Nevertheless, the model depicted very low NO_3^- levels in the upper part of the aquifer below Merida in comparison with those reported by previous studies. Results of the model are highly dependent on initial NO_3^- concentrations which seem to be conservative for this model. Changes in the initial contaminant load can result in drastic solute transport variations, affecting the vulnerability classification; this could be more radical if the permissible maximum levels are surpassed. However, this work does not propose nitrate as the exclusive indicator of vulnerability. Having demonstrated the necessity to include the effects of anthropogenic practices on groundwater quality, the pollutant to be evaluated by means of a solute transport model for a given study area will depend on the economic practices carried out in such areas. This supports the allowance of flexibility in groundwater vulnerability analysis and its ability to adapt to meet regional requirements.

The role of recharge in solute transport is also highlighted; from a vulnerability perspective, differences in recharge patterns have demonstrated the characteristic of being either beneficial or harmful for some areas. This provides an advantage over multi-parameter methods that evaluate precipitation (or recharge) as an external stressor solely promoting pollutant advection.

Additionally, the application of solute transport brings the opportunity to evaluate future vulnerability scenarios or extreme events. New activities, necessary for regional development, can be simulated to study the possible effects over current water sources. This can provide valuable information for more detailed urban planning, protection strategies, and environmental policies. For example, in recent years, pig farming has increased as a key economic activity in Yucatan, however, the negative effects on groundwater quality are overshadowed by the necessity of economic development. In this case, the sole use of intrinsic vulnerability methods is likely to mislead important decisions regarding the possible locations for farms if the advection-diffusion dynamics are not considered in such evaluation. Solute transport studies can bring important information to minimize the vulnerability risk of current extraction wells by analysing possible pollution scenarios.

Although nitrates were considered as the representative pollutant in the Yucatan case, the selection of the pollutant to be analysed must depend on the regional conditions and the anthropogenic activities taking place in a given study area. The inclusion of pollutant concentration as an indicator of vulnerability should be analysed in terms of water quality standards, with defined permissible maximum levels, setting a baseline to define levels of vulnerability. Additionally, the purpose of the extraction wells (drinking water supply, irrigation, industry, etc.) can serve as additional criteria to define sources as vulnerable or otherwise.

Further steps to be taken are the definition of a general process to classify vulnerability from solute transport outcomes and their integration with multi-parameter methods for intrinsic groundwater vulnerability. Given the multiple anthropogenic activities occurring in karst areas, the process of designating vulnerability classes from solute transport parameters must be flexible enough to be applicable under several hydrological, hydrogeological, and administrative conditions.

5 An integrated strategy for karst groundwater vulnerability

Intrinsic groundwater vulnerability analysis estimates the likeliness of a theoretically immutable pollutant particle reaching groundwater by advection. Disregarding the process of evaluating degrees of vulnerability (summed weight, statistical, semi-quantitative), high subjectivity is linked to each method due to the different, and sometimes contrasting, personal interpretations regarding karst features' hydrologic response, number of parameters (and attributes), and assigned rates and weights. As demonstrated by previous studies, the application of several methods in a given study area can display contrasting outcomes. However, they can also display a remarkable agreement, as in the case of Yucatan, regarding the spatial distribution of vulnerability classes. Agreement between methods is not necessarily indicative of congruence with the characteristics of the study area.

In chapter three, a detailed analysis of eight intrinsic methods and their evaluated parameters helped to infer critical considerations resulting in such outcomes, and to propose adjustments in order to improve the intrinsic vulnerability analysis (see section 3.5). Despite the proposed measures to improve the process, intrinsic groundwater vulnerability can still lead to erroneous decisions regarding groundwater prevention and protection if current anthropogenic activities, which are already affecting groundwater, are not considered as part of the vulnerability estimation. In chapter four, it was demonstrated that outcomes from a solute transport model, characterized as vulnerability indicators, can display valuable information regarding current pollution scenarios. The provision of additional parameters, such as pollutant concentration, enhances the vulnerability analysis. Even if groundwater flow is included in the evaluation of source vulnerability, flow direction must not be used as a definitive indicator when designating vulnerability classes.

In this chapter new criteria, redefinitions, and the main principles for an alternative integrated strategy to estimate groundwater vulnerability in karst are presented. This proposed methodology gathers the main outcomes from the evaluation of selected intrinsic methods, previously analysed in chapter three, and those from solute transport presented in chapter four.

5.1 Main concepts for an integrated strategy

An ideal groundwater vulnerability method must evaluate the advective nature of the saturated zone, in case of accidental pollution, and the advection-diffusion dynamics of current pollution sources generated by anthropogenic activities. Given that intrinsic vulnerability maps are theoretical approximations for the former, inclusion of solute transport can provide additional insights to improve the vulnerability analysis. An integrated karst aquifer vulnerability method of this kind will provide an upgraded analysis for the benefit of groundwater preservation strategies. This approach contradicts the current groundwater vulnerability definition of "intrinsic" since the aquifer (or source) vulnerability estimation will be also influenced by human activities. With the inclusion of anthropogenic-derived pollution to define vulnerability, some vulnerability concepts must then be further clarified in terms of occurrence.

While intrinsic vulnerability reflects an "IF" condition for a given section of the aquifer to be polluted, solute transport can display an approximation of an already existent pollution scenario. Therefore, in relation to the pollution occurrence we can subdivide the current groundwater vulnerability concept into "potential vulnerability" and "actual vulnerability". Potential aquifer vulnerability, or intrinsic vulnerability, can be redefined as:

- the potential of an incidental pollutant particle, released at the surface, to reach groundwater either by surface runoff or vertical infiltration, based on selected natural characteristics of the area. The potential is dependent on the infiltration scenario (diffuse or point infiltration) but independent of the physical or chemical characteristics of the particle.

Actual groundwater vulnerability can be defined as:

- the circumstantial contamination in a given section of the aquifer as result of a distinctive anthropogenic activity in the area. It is defined by the physical and chemical characteristics of a contaminant as well as by water regulations. Actual groundwater vulnerability can also indicate water sources operating in contaminated aquifer sections.

The term "potential vulnerability" must not be mistaken with risk analysis; risk analysis, or groundwater risk mapping, is a combination of a hazard's map (gas stations, oil pipes, industry, etc) in terms of specific pollutants, coupled with an intrinsic groundwater vulnerability map (De Ketelaere and Daly, 2003). Given the fact that potential and actual vulnerability indicate two different vulnerability conditions, it is recommended to separately evaluate each one of them according to the objectives of the integrated vulnerability analysis. A potential groundwater vulnerability map can be helpful to determine protection areas and for the planning of urban/economic development. An actual groundwater vulnerability map can be used for the development of preventative or corrective measures.

The development of a general integrated methodology with established rates and weights to characterize vulnerability, either for potential or actual pollution scenarios, is not a viable alternative; the data availability, the multiple anthropogenic practices, and the high heterogeneity of karst areas make such a goal unreliable. However, a workflow with a redefined evaluation of individual parameters, adaptable for the study areas' conditions, and integrating solute transport models can help to minimize the subjectivity of intrinsic vulnerability methods.

The proposed workflow gathers the main outcomes from the literature review and the application of eight methods in a karst area to improve the potential intrinsic vulnerability mapping. Additionally, solute transport and particle tracking outcomes are added as independent maps to improve groundwater vulnerability analysis, in order to enhance the scope of decisions regarding water management. The process forms the groundwork for an integrated karst aquifer vulnerability (IKAV) method with two independent map layers representing the potential vulnerability (IKAV-P) and actual vulnerability (IKAV-A) of groundwater.

The IKAV-P is proposed as a MCDA following a rating-weighting system. According to Carver (1991), Heywood et al. (1995), Malczewski (1999), and Malczewski (2006) a MCDA must follow certain characteristics to be able to classify the evaluated attributes. With focus on karst, the attributes are:

- Measurable – Given the fact that it is challenging to measure some attributes in karst areas, such as the degree of karstification, statistical tools can help to better define notable differences in the study area.

- Non-redundant – According to the current intrinsic vulnerability methods, some parameters can be defined utilizing the same base map (e.g., karstification and epikarst development from the EPIK). Inclusion of multiple parameters derived from the same evaluation process must be avoided to prevent vulnerability over/under estimations.

- Minimal - Considering that some degree of subjectivity is inherently attached to each evaluated characteristic, the use of an extensive number of parameters (or attributes) can complicate the process. Therefore, the number of evaluated parameters (and attributes) must be kept minimal.

- Available – The objective must be achieved with the available data from the region. Under conditions of low-resolution data, such data must be excluded, even if it has a significant influence on the objective.

From the analysis of multiple intrinsic groundwater vulnerability methods from section 3.3, it was possible to analyse and redefine additional criteria to be added to the previous aspects. In order to improve the potential intrinsic vulnerability analysis, the following characteristics must be also be considered during the evaluation process:

- Variable - Given that the goal of potential intrinsic vulnerability (or any other MCDA) is to provide a range of conditions to evaluate their relevance for a given objective, a map layer displaying homogeneity will have no purpose for the research objective. Therefore, homogeneous layers must be excluded from the analysis.

- Unambiguous – The objective must be clear and well defined. Either for point or diffuse infiltration, the characteristics influencing such processes must be considered separately; this means the assessing performance of an individual analysis for each scenario, avoiding the use of "rest of the area" conditions.

- Distinctive - The influence of some parameters is different for point and diffuse infiltration, therefore, the rates and weights assigned to individual parameters must be evaluated according to the objective. This is clear for slope and soil texture, the influence of which must be evaluated as oppositional for each scenario.

- Territorial – The number of parameters' attributes, their evaluation, and rating must be solely dependent upon the local or regional characteristics but following a rating pattern linked to the objective. Characteristics or attributes proposed by other methods but not present in the study area must be avoided as vulnerability indicators.

The previous criteria can be summarized in three main principles to apply the IKAV (Figure 5.1). The principles aim to minimize the subjectivity from pre-stablished methodologies evaluating intrinsic groundwater vulnerability, adapting the evaluation of potential and actual vulnerability conditions to be representative of the study area.
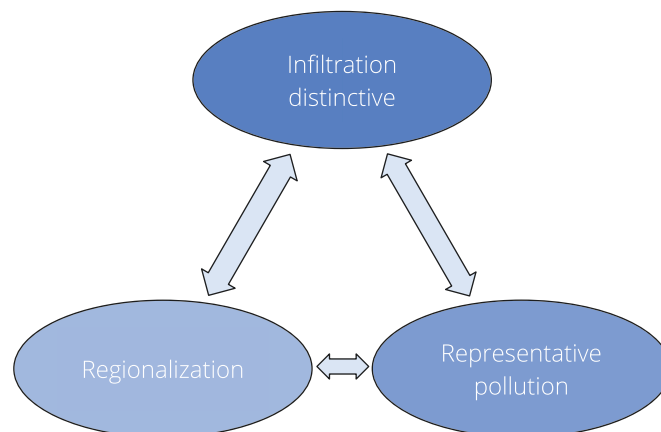
Figure 5.1: The proposed principles for an integrated evaluation of vulnerability.

In the infiltration distinctive rule, the objective is to define the goal of the analysis, settling either a point infiltration or diffuse infiltration condition; this selection dictates how some parameters will be evaluated. For example, if a point infiltration scenario is going to be investigated, high slopes and fine-textured soils will represent a more vulnerable condition due to their runoff generation capacity.

Similarly, the representative pollutant, and the activity from which it is derived, is directly linked to the infiltration condition. For example, the use of fertilizer in hillside farming could represent a more vulnerable condition for a swallow hole catchment than sewage leakage occurring simultaneously in the same study area.

Regionalization settles the individual ranges for the selected parameters; how the rates will be assigned to attributes is selected here, in congruence with the criteria from the infiltration distinctive procedure. This step aims to evaluate vulnerability according to the existing conditions in a given study area, avoiding the indirect evaluation of external characteristics proposed by current methodologies but not present in the area of interest. The link of this principle with the infiltration distinctive principle, relies on the rating scheme of some parameters and their further influence to be represented by weights.

The representative pollution defines the contaminant to be evaluated in correspondence with anthropogenic activities carried out in a given study area. Defining the most influential anthropogenic activities, a representative pollutant can be utilized for a better interpretation of groundwater (or source) vulnerability by pollution levels (permissible maximum). Activities affecting groundwater quality in karst areas are variable, as well as the pollutant derived from such activities. Therefore, the definition of actual vulnerability rates will depend on the type of pollutant, regional regulations, and the purpose of a given extraction well.

Having defined the three principles for the IKAV, a general method is presented as the groundwork to evaluate an integrated groundwater vulnerability. The process can be considered to be an improved guideline to obtain a potential groundwater vulnerability map with the addition of an actual vulnerability map, based on the regional anthropogenic activities, from solute transport.

5.2 Proposed workflow for the IKAV

The process aims to provide a more detailed guideline to estimate groundwater vulnerability conditions, but allowing for a necessary flexibility to fulfil the principles and the criteria presented previously. Flexibility is always necessary since interpretations can vary according to the data, infiltration scenario, pollutant type, and objective (Figure 5.2).

In step 1, the potential intrinsic scenario is defined either as point or diffuse infiltration. Separating each scenario helps to better define the natural characteristics and their role on groundwater vulnerability, avoiding underestimations for areas where diffuse infiltration occurs, being usually characterized as "rest of the area" conditions.

In steps 2 and 3, the available data is gathered, evaluated, and filtered according to the criteria presented in the previous section; redundant and non-variable data must be excluded from the analysis. In some cases, variability could be present in a given dataset but their relevance, either in terms of range or scale, could be minimal; the inclusion of such data into the analysis will depend on the scale of the analysis and expertise.

For step 4, depending on the data type, attributes are defined by continuous or discrete intervals; when possible, the number of attributes must be quantitatively or statistically defined, therefore, attributes can vary in number among parameters. Rates are assigned to each category according to the characteristics that influence the transport of pollutants. Independent of the number of individual parameters' attributes, a consecutive rating is recommended. The rating scheme (inverse/direct) is also herein defined in order to secure congruence among the characteristics of each parameter (see Table 3.8).

* Index partition based on statistics (e.g., Jenks classification).
** Index partition based on pollutant's permissible maximum.
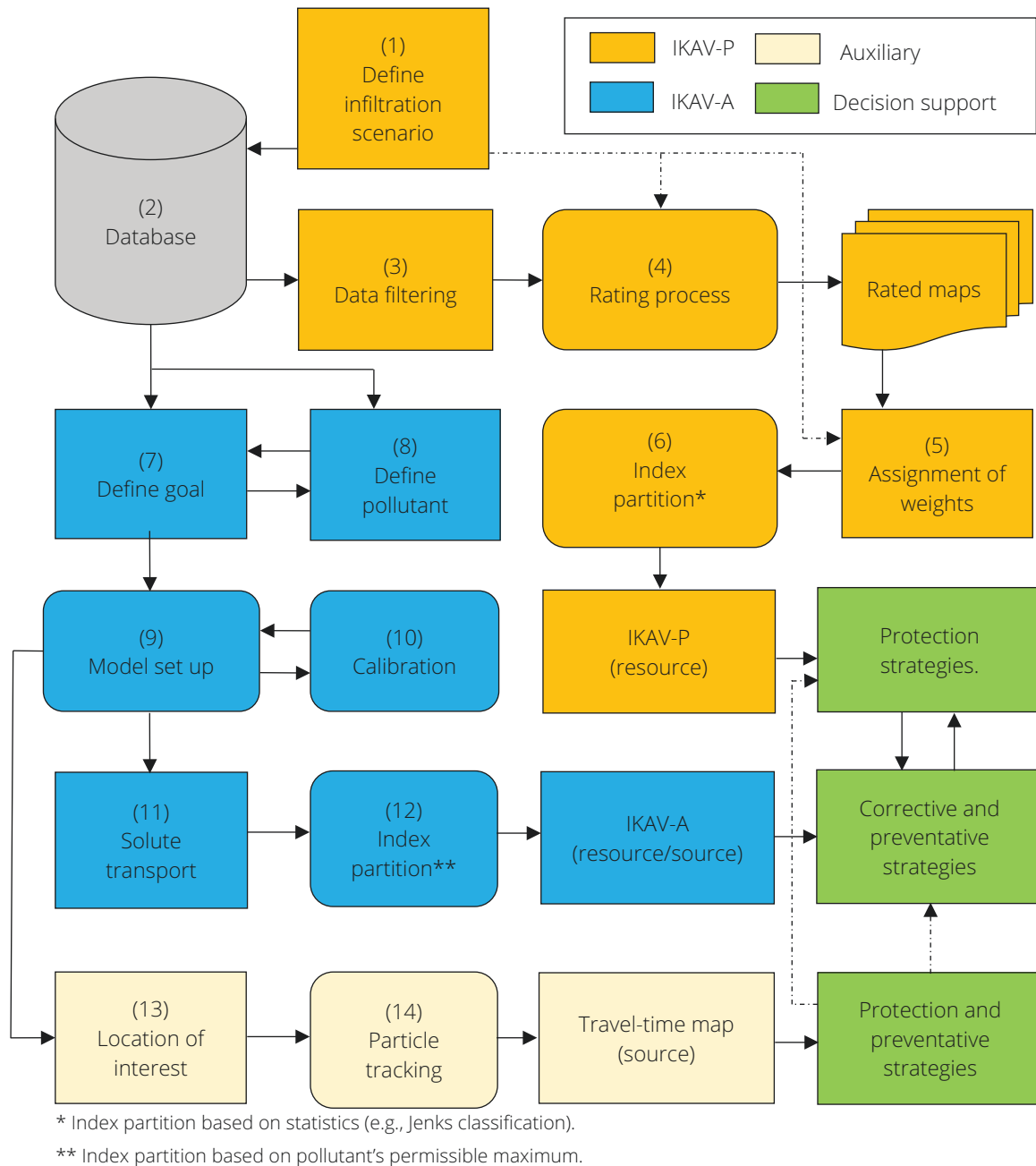
Figure 5.2: Proposed IKAV workflow.

For the definition of weights in step 5, the importance of each intrinsic feature can be highlighted by the application of a decision analysis method, such as the AHP proposed by Saaty (2008). In this step, the weights will be defined according to the selected parameters and the infiltration scenario in order to fulfil the regionalization principle. As the regionalization is one of the principles of the IKAV, proposing universal weights can lead to misrepresentations in further areas of application; independent of the number of map layers, the sum of the assigned weights must be equal to one.

With the obtention of a vulnerability index, step 6 refers to the subdivision of the calculated index to display vulnerability levels. During the method's evaluation process in section 3.3, it was noted that the Jenks optimization method divides the vulnerability index in agreeable congruence with the most relevant intrinsic characteristics of the area. Nevertheless, to achieve a congruent division of the vulnerability index, the rating process must be, as proposed, correlative and the sum of the assigned weights equalling to one.

Until this point, a potential groundwater vulnerability map can be obtained following the steps and fulfilling the criteria previously presented. The next steps are related to a solute transport model to evaluate the anthropogenic influence in terms of actual vulnerability. Steps 7 and 8 are related to data availability. In order to characterize the aquifer in terms of vulnerability, the pollutant to be evaluated and the vulnerability type (source or resource) must be defined first.

Model setup and calibration (steps 9 and 10) are highly dependent on the available data regarding aquifer characterization and anthropogenic practices (wastewater generation, agricultural areas, water extraction, livestock activities, etc.). The selected model, activated packages, calibration process, and approval will be dependent on data and expertise. The definition of ranges for pollutant concentration and the assignation of vulnerability classes can be achieved taking as a base the permissible maximum concentration of the representative pollutant (steps 11 and 12). However, in cases where the permissible maximum is not reached, vulnerability can be defined by the ratio of the maximum concentration at the source (or any three-dimensional location in the aquifer) and the initial concentration at the release point as proposed by Huan et al. (2015). The objective of the actual vulnerability analysis and expertise are also relevant for this decision; for example, if the vulnerability of a given source is being evaluated, the purpose of the well, either for drinking water or irrigation, can influence the vulnerability class assignation.

Finally, particle tracking works as an additional indicator for IKAV-P (steps 13 and 14), however, it can also be linked to IKAV-A if the natural groundwater flow is being affected by anthropogenic stressors, such as large extraction wellfields. Estimating the travel time from a given pollution release point towards a source can be very helpful to further define preventative measures. Considering that the travel time analysis requires two predefined points or cross-sections (release and source) as displayed in Figure 2.10, a regional travel time map is not suitable. Particle tracking as a vulnerability estimator must be applied for precise situations, such as the evaluation of new extraction wells or future activities in a given area.

5.3 Evaluation of the IKAV

5.3.1 Testing the IKAV-P

A potential vulnerability map as part of the IKAV was applied in Yucatan to evaluate its applicability. The steps displayed in the proposed workflow are further explained in relation to the available data and the Yucatan characteristics. For the Yucatan case, the infiltration scenario was regionally defined as diffuse, given the low relief of the area and the lack of surface streams.

Regarding data availability and filtering, Yucatan's lithology was considered homogeneous at a regional scale, therefore, no significant differences can be evaluated for our purposes, with the lithology map excluded from the process. Having defined a regionally diffuse infiltration condition, high slopes represent the most protective characteristic. Nevertheless, given the low variability displayed by the slope map and considering a regionally diffuse condition, the slope parameter was also excluded.

Due to the lack of indirect data, such as spring flow, doline density maps can be representative of karstification, epikarst or aquifer development. However, given the fact that three map layers derived from doline density could lead to over/underestimations, only the karstification parameter was selected in order to avoid redundancy.

The map representing the vadose zone, based on the depth to groundwater, was the same that was utilized in section 3.2.2, however, the discretization for the IKAV-P was carried out by natural breaks in order to highlight the shallowness of the vadose zone in the flat plain and the deeper sections in the sub-surface of the Sierrita de Ticul. Soils were evaluated based on clay content for their relationship with hydraulic conductivity. It was decided not to include soil thickness, given the extension of the study area and the low data coverage regarding this characteristic.

In total, three parameters, representing a notable variability, were selected from the data filtering step: karstification, vadose zone and soils. Parameters were rated solely in reference to their by-pass capacity (vertical advection), allowing pollutants to migrate from the surface to the water table. The most vulnerable parameters' conditions are: high karstification, shallow water tables, and soils with a low clay content. Arbitrarily, an inverse relationship was defined for rating purposes; the lower the rating, the higher the vulnerability. Following the proposed workflow, the three representative maps were discretized and rated, aiming to fulfil the infiltration and regionalization principles as displayed in Table 5.1. The representative maps utilized to obtain the IKAV-P are displayed in Appendix B9.

Table 5.1: IKAV-P selected parameters and rating.

Parameters		Attributes			
Karstification	Range	> 4 per km^2	2 - 4 per km^2	< 2 per km^2	
(Doline density)	Rating	1	2	3	
Vadose zone	Range	< 20 m	21 - 30 m	31 – 100 m	> 100 m
(Depth to groundwater)	Rating	1	2	3	4
Soils	Range	<15%	16 - 30%	31 - 40%	> 40%
(Clay content)	Rating	1	2	3	4

To define weights, a pairwise comparison was performed utilizing the AHP plugin for ArcMap. The AHP plugin automatically calculates a normalized priority vector (eigen vector) and the consistency ratio (CR) after the manual introduction of importance (judgment) values. As Yucatan is a coastal area with a shallow water table where fissures are to some degree present, it was decided to assign a similar importance for the vadose zone parameter in comparison with karstification. Soils were defined as the less important parameter in reference to karstification and the vadose zone. The selected importance values in the paired comparison matrix highlight the tendency, presented by previous methodologies, of karstification being the most relevant characteristic and the soil map being one of the least important (Table 5.2). As the order of the matrix is equal to three, the obtained CR = 0.28 was acceptable according to Saaty (2008).

Table 5.2: Assigned importance values for the selected map layers.

IKAV-P AHP			
	Karstification	Vadose zone	Soils
Karstification	1	1	5
Vadose zone	1	1	3
Soils	0.2	0.33	1
Sum	2.2	2.33	9
IKAV-P AHP normalized			
	Karstification	Vadose zone	Soils	Priority (weight)
Karstification	0.455	0.429	0.556	0.480
Vadose zone	0.455	0.429	0.333	0.406
Soils	0.091	0.142	0.111	0.115
Sum	1.00	1.00	1.00	1.00

With defined parameters, attributes, rates, and weights, an index was calculated from the multi-attribute weighting-rating process from:

$$V_x = K_x (0.480) + VZ_x (0.406) + S_x (0.115) \qquad (19)$$

were V_x is the IKAV-P vulnerability index for the grid x; K_x, VZ_x, and S_x are the rated attributes corresponding to karstification, vadose zone, and soils at the given grid x, respectively. The bracketed numbers are the calculated weights from a pairwise comparison. An index ranging from 1 to 3.5 was obtained and further divided to categorize vulnerability classes.

The Jenks natural breaks classification was directly applied in ArcMap, selecting five categories. The IKAV-P map displayed vulnerabilities percentages as 30.45, 32.07, 27.22, 7.0, and 3.25, corresponding to VHV, HV, MV, LV, and VLV, respectively (Figure 5.3).
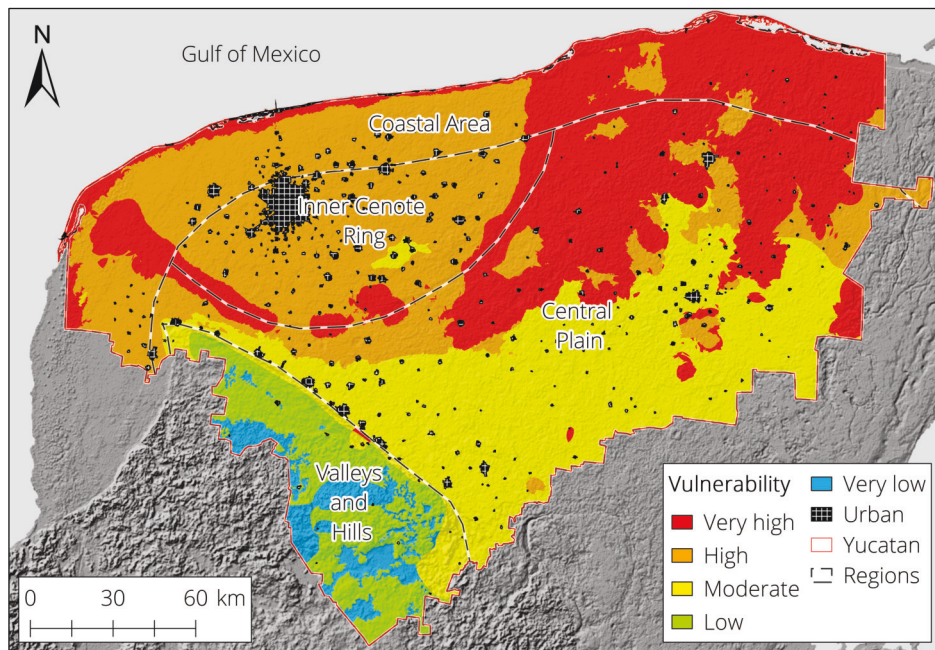
Figure 5.3: The IKAV-P map.

According to the IKAV-P, the most vulnerable sections of the aquifer are those where doline density is high, indicating advanced karstification, therefore, an incidental pollutant is more likely to reach groundwater. The IKAV-P displays a similar tendency for VHV as some of the methods in section 3.3, however, it also classifies the near coastal areas for VHV, where very shallow water tables and sands are present. Despite karstification representing the most influential characteristic, given its assigned weight, a distinctive arrangement of regional characteristics (coarse soils and a shallow water table) also indicates a highly vulnerable condition.

A vulnerability reduction pattern is displayed in relation to an increment of the vadose zone. This manifests a consistent interpretation of this coastal aquifer in relation to the contrasting conditions with respect to the flat plain and the southern hill area; both are important regional conditions that were not highlighted by the previously applied intrinsic groundwater vulnerability methods in Yucatan.

Despite the weight assigned to the soil map being the lowest, it exhibits an important role under different conditions. Soils are depicted as protective when its clay content is above 30%. In the southern area of the Inner Cenote Ring, a clay-rich soil promotes said area for MV, despite the shallow water table and fissuring.

Similarly, in the south-eastern Central Plain, clay-rich soils provide some protection in areas were karstification is at its maximum. Soils are the main promotor for VLV in the Valleys and Hills area where karstification is low and the water table is found at its deepest.

5.3.2   Testing the IKAV-A

In chapter four, the importance of including anthropogenic activities as part of the groundwater vulnerability analysis was highlighted by the application of a representative solute transport model. The analysis of multiple theoretical scenarios based on the obtained results settled the fundaments for the development of actual vulnerability mapping. However, NO_3^- concentrations in the upper section of the aquifer underneath Merida were depicted by the model as too low in comparison with those measured in previous studies. To provide a more accurate approximation using an actual groundwater vulnerability map, the original model was modified to increase the NO_3^- leaking in order to resemble measured NO_3^- concentrations in the sub-surface of Merida.

Following the proposed workflow, in step 7, the goal was to estimate the actual vulnerability of extraction wells utilized for drinking water supply inside the MMA. Septic tanks, from the six main cities in the MMA, were defined as the anthropogenic practice promoting pollution. From public datasets, 130 wells for water supply were located in the study area and added to the previous 78 wells that are part of the JAPAY extraction wellfields; the average depth of the additional wells was estimated from multiple sources and data digitally provided by JAPAY (Table 5.3).

Table 5.3: Evaluated water sources and their location in the aquifer.

Aquifer layers	Layer thickness*	Number of wells	Well average depth**
Upper epikarst	10	0	NA
Lower epikarst	7.5	98	15
Preferential	17.5	32	26
Rest of the aquifer	45	78	38

* Values in metres.
**Metres below surface.

In step 8, NO_3^- was selected as the representative pollutant. An initial concentration of 80 mg/L was defined in the pollution release areas, these being the main cities in the MMA. This value was selected to approximate the NO_3^- concentrations, reaching up to 70 mg/L in the upper aquifer, reported by Graniel et al. (1999) and Rojas-Fabro et al. (2015). Given the fact than no accurate database exists for the additional extraction wells, regarding extraction volumes nor operational schedules, no further external stressors were included in the original model. The wells were utilized as location representatives in the three-dimensional aquifer system to evaluate their actual vulnerability as individual water sources. Therefore, the setup and calibration of the model (steps 9 and 10) remained the same, as presented in section 4.4.5.

For steps 11 and 12 solute transport outcomes were analysed and classified, aiming to depict actual vulnerability rates. Nitrate concentrations were divided according to a previous groundwater pollution classification presented by Pacheco and Cabrera (1997) and Pacheco-Ávila et al. (2004a). In addition to NO_3^-, said classification evaluates chlorides, cadmium, and faecal coliforms to determine groundwater pollution according to their permissible maximum values. The ranges of NO_3^- concentration presented in the aforementioned studies were slightly modified, as displayed in Table 5.4, to depict the actual vulnerability of extraction wells.

Table 5.4: Actual vulnerability classes from NO_3^- concentrations in the MMA.

Nitrate concentration classification	
mg/L	Actual vulnerability
> 45	VHV
23 - 45	HV
10 - 22	MV
1 - 9	LV
0*	VLV

* Indicate no influence of the pollution source.

A VHV was defined for NO_3^- concentrations above 45 mg/L. Concentrations below 9 mg/L were defined with LV class suggesting a natural NO_3^- occurrence. However, this proposed minimal value is purely indicative since natural NO_3^- levels in groundwater are variable and highly dependent on natural characteristics such as geology and soils. In Yucatan, Pacheco and Cabrera (1997) estimated a concentration of 10 mg/L as a concentration base for groundwater in non-inhabited areas.

Following the proposed steps, three actual vulnerability maps, corresponding to the lower epikarst, preferential, and rest of the aquifer layers, were obtained (Figure 5.4); the upper epikarst was not considered given that no wells are located in this layer. Each map includes the wells located at the given aquifer layer to evaluate their vulnerability as drinking water sources. As expected, results display similar patterns to those from section 4.4.2 but with increased NO_3^- levels. The most relevant pollution is derived from Merida and Kanasin, moving northward with a decreasing NO_3^- concentration pattern. Pollution levels also decrease in the lower aquifer layers. No significant influence is depicted from other cities, probably due to the low population in comparison with Merida city.

Results indicate that a total of 24 wells, out of the 208 mapped, are prone to extract water with elevated NO_3^- concentrations, approximated 10% of the drinking water sources in the study area (Figure 5.5). Therefore, these water supply systems are categorized with VHV and HV given the NO_3^- concentrations, close to the permissible maximum value or exceeding it. The most vulnerable wells are located along the groundwater flow direction and neighbouring Merida city.

According to their location in the aquifer, shallow wells represent the most vulnerable conditions, with 17 out of the 98 located in the lower epikarst layer being classified as highly vulnerable. Although the number of vulnerable sources could be considered low, a more critical scenario arises when compared to the number of inhabitants being served by such sources. Rough estimations indicate that approximately 100,000 inhabitants in the study area obtain their water supply from highly vulnerable sources; according to the model, the cities of Progreso, Uman and Kanasin are the most affected.

Results of the IKAV indicate the current stress on the MMA; this highly urbanized area, with potential HV, given the natural characteristic, also experiences a high actual vulnerability derived from anthropogenic practices related to wastewater disposal (see Figure 5.4d). The joint evaluation of the two vulnerability types provides an advantage for improving decision-making processes, with a more specific approach for each condition. Therefore, in addition to the strategies to prevent incidental groundwater pollution derived from the IKAV-P, the IKAV-A can assist in developing corrective actions to maintain the water supply under the required standards for already affected drinking water sources.
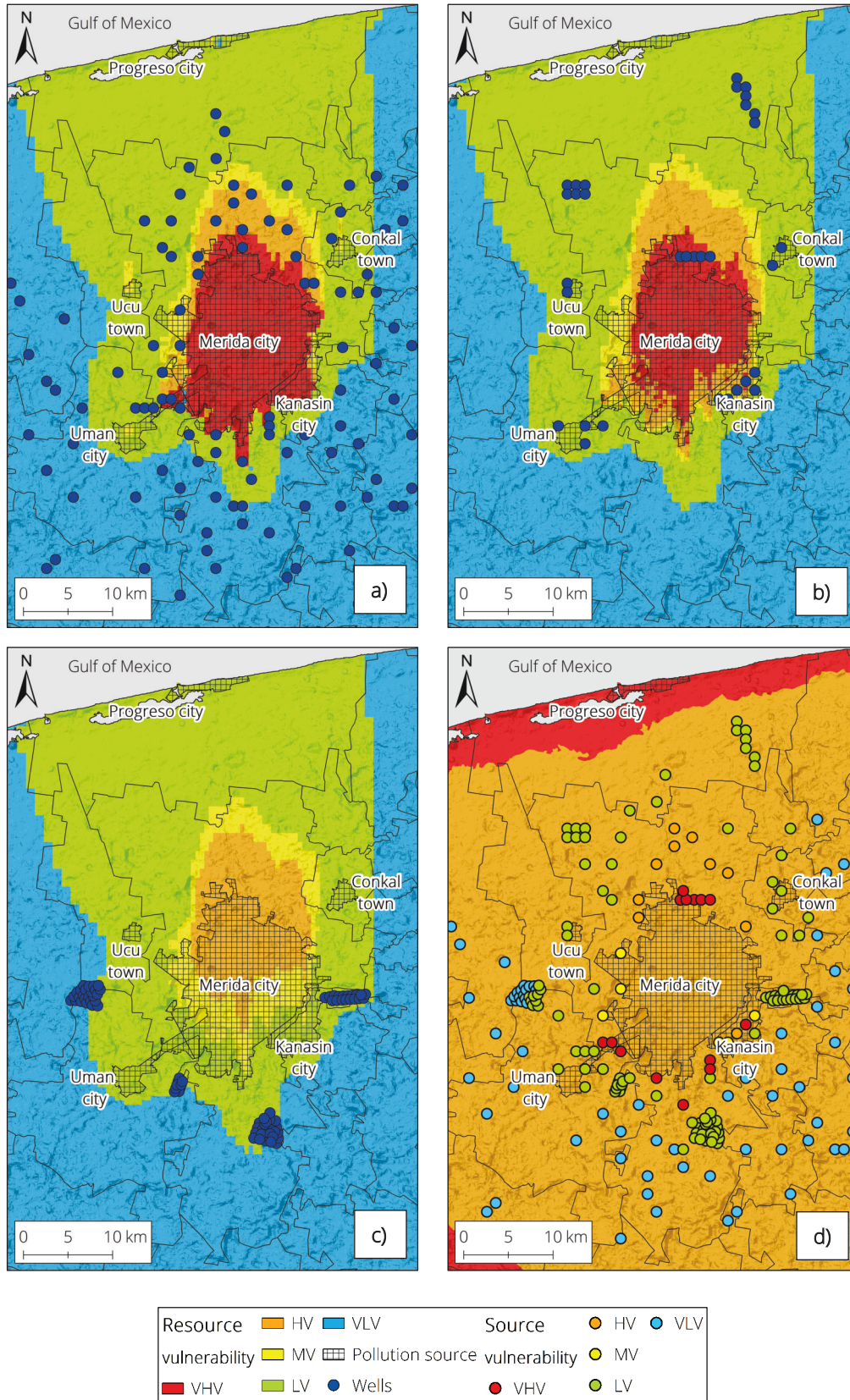
Figure 5.4: IKAV maps for source and resource vulnerability. In a), b) and c), the IKAV-A for the lower epikarst, preferential, and rest of the aquifer layers, respectively; in d), the combined IKAV-P and IKAV-A for source and resource vulnerability in the MMA.
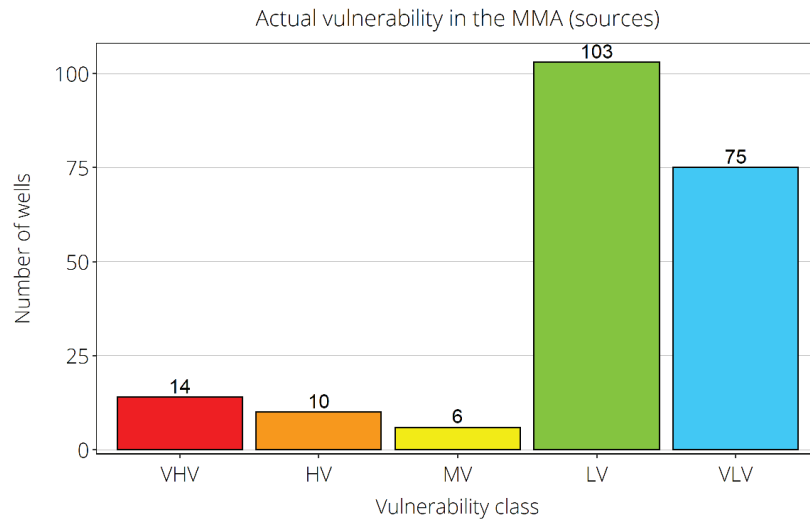
Figure 5.5: Vulnerability of water supply wells located in the study area.

5.4 Validation and discussion

Although the empirical interpretation of the IKAV showed a better approximation of the natural conditions in the Yucatan karst when compared with well-established European methodologies, a validation analysis was, nonetheless, carried out. Due to the lack of indirect data, tracer tests or water quality to validate the IKAV, the regional intrinsic vulnerability map presented by the IVAKY method was utilized to validate the IKAV-P (Figure 5.6). IVAKY stands for 'Yucatecan Karst Aquifer Vulnerability Index'; this method was presented as the local option to evaluate resource intrinsic vulnerability in the Yucatan state (Aguilar-Duarte et al., 2016).
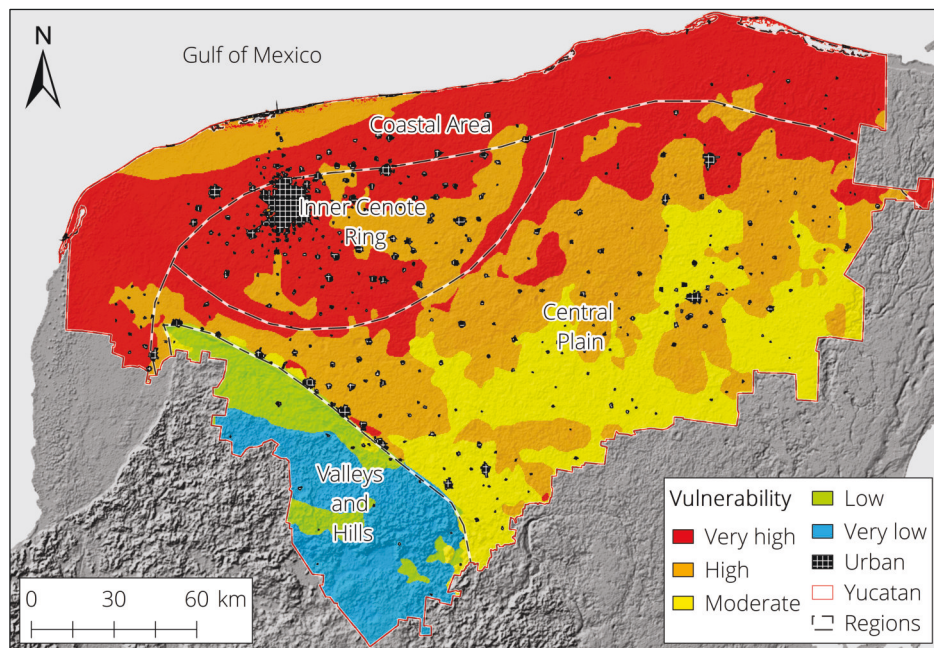
Figure 5.6: The IVAKY's Intrinsic groundwater vulnerability map. IVAKY includes an additional vulnerability class (extremely vulnerable); for comparative purposes, this class was merged with VHV. Map digitalized from Aguilar-Duarte et al. (2016).

The IVAKY method considers several interrelated parameters to estimate intrinsic resource vulnerability. The parameters are grouped into three distinctive factors according to their geomorphological, pedological, or hydrological relationship: karstic relief, edaphic, and climatic. The karstic relief factor highlights the relationship of dolines (density and type), elevation as indicative of the unsaturated zone, and recharge; the regional analysis of this factor is presented in an individual study by Aguilar et al. (2016). The edaphic factor grades the filtering aptitude of the soils based on organic matter content, clay percentage, cation exchange capacity, and thickness of the soil (Aguilar et al., 2011; Aguilar and Bautista, 2011). The climatic factor evaluates the distribution of precipitation in time and space; this factor is based on the study presented by Delgado-Carranza (2010) in which consecutive months experiencing rain events are estimated when precipitation surpasses 50% of the PET. To evaluate the IKAV-A, results from solute transport were analysed and compared to previous studies and sampling campaigns carried out in the Yucatan state.

5.4.1 Validation of the IKAV-P

Similar analyses as those utilized in section 3.4 were applied taking the IVAKY as the base for comparison. Evaluating the results from IVAKY and the IKAV-P maps, similar patterns in the distribution of vulnerabilities percentages are evident (Figure 5.7). It is clear that none of the intrinsic vulnerability maps obtained with the European methods approximates those provided by the IVAKY method. Hence, the performance of the IKAV-P provides a better evaluation of vulnerability classes for the Yucatan karst.
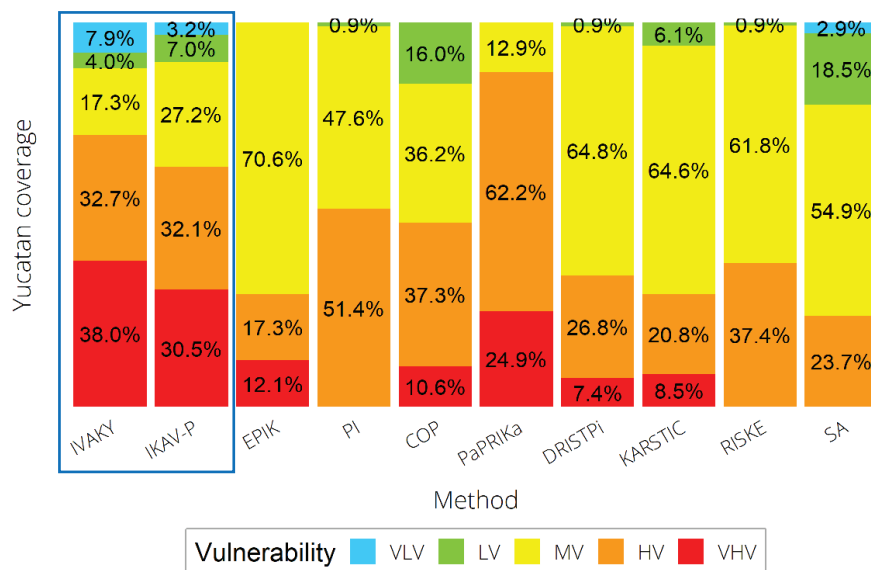
Figure 5.7: Comparison of the distribution of vulnerability classes from multiple methods.

Given that percentual similarities are not a definitive indication of spatial relationship, an MCA was performed to investigate the spatial correlation in vulnerability classes between IVAKY and IKAV-P. A remarkable total correlation with the IVAKY, above 50%, is displayed by the IKAV-P; this correspondence in the assignation of vulnerabilities is outstanding given the fact that the best correlated European methods display less than 30% of agreement with the IVAKY method (Figure 5.8).

The reliability of the IKAV-P is more significant, strictly from a methodological point of view, if its dissimilarity with the regional IVAKY method is compared. Comparing both methods, the IVAKY method evaluates three factors, with several parameters included in each; after the data availability and filtering steps, the IKAV-P method only defined three parameters to be considered (Table 5.5).
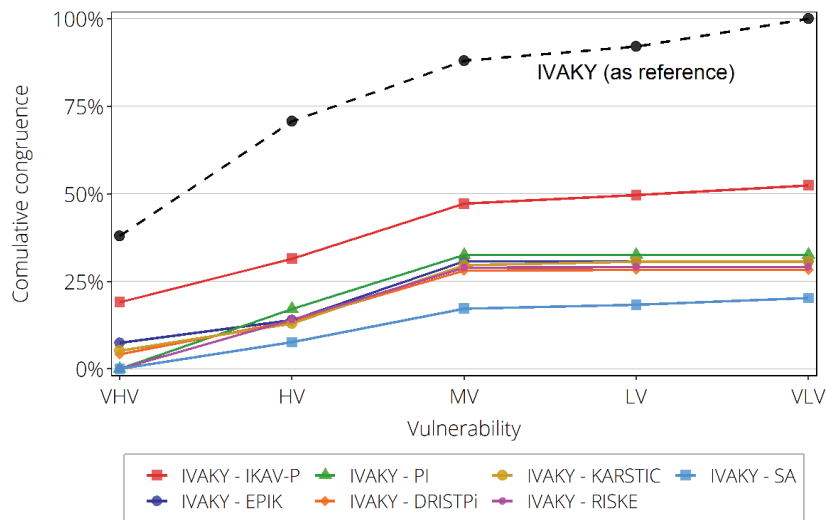
Figure 5.8: Cumulative congruence from the MCA having the IVAKY as the base.

Table 5.5: Main methodological differences between the IVAKY and IKAV-P maps.

IVAKY

Factors	Parameters	Number of attributes	Rating scheme	Rating range*	Weight
Karstic relief	Altitude	2	Directly related	1 to 9	0.655
	Depressions' density	3			
	Dominant depression type	3			
	Recharge and flow	2			
	Contact with the aquifer	2			
Edaphic	Organic matter (%)	5	Directly related	1 to 9	0.289
	Clay content (%)				
	Cation exchange capacity				
	Thickness				
	Edaphic class				
Climatic	Precipitation distribution	5	Directly related	1 to 9	0.054
	Precipitation duration (months)				
	Humidity				

* The rating is not correlative.

IKAV-P

Factors	Parameters	Number of attributes	Rating scheme	Rating range**	Weight
Not applicable	Karstification by doline density	3	Inversely related	1 to 3	0.480
	Vadose zone by depth to groundwater	5	Inversely related	1 to 5	0.406
	Soils by clay content	5	Inversely related	1 to 5	0.115

** The rating is correlative and dependent on the number of attributes.

While the IVAKY method utilizes a directly related and discontinuous rating scheme, the IKAV-P method proposes an inversely related and continuous rating for the parameters' attributes. Also, the weights proposed in both methods are different, due to the authors' personal interpretations.

It is worth mentioning that the datasets utilized for both methods (IVAKY and IKAV-P) were not the same, however, the map displaying the depth of the unsaturated zone is expected to be very similar. It is also important to note that the correlation between the IVAKY's intrinsic vulnerability map with those displayed by the European methods is mostly driven by the high percentage of MV obtained with such intrinsic schemes.

The IKAV-P map provides a better representation of the five vulnerability classes in correspondence with the natural characteristics evaluated by the IVAKY method. Therefore, by following the steps proposed by the IKAV method, it was possible to obtain a representative potential vulnerability map, highlighting the regional characteristics and their influence on the migration of accidental pollution from the surface to the water table. Therefore, the plausibility of the IKAV-P, to display potential vulnerability in accordance with the principles of regionalization and infiltration scenarios, was demonstrated.

5.4.2   Validation of the IKAV-A

Unfortunately, no water chemistry data was available to validate the IKAV-A map, based on solute transport outcomes. However, results are consistent with previous studies and water sampling campaigns that took place in Merida and in the peripheral shallow wells, mostly those located to the north of the capital city. Previous studies, explained in more detail in section 4.1.3, reported constant pollution, represented by high NO_3^- concentrations, in the upper aquifer below Merida. For shallow wells located in the north, studies indicate NO_3^- pollution conditions solely derived from local anthropogenic activities, which are variable according to the precipitation regime; NO_3^- levels in these shallow wells increase with precipitation events and decrease during the dry season.

Results from solute transport are, to some degree, consistent with the previously mentioned studies. The Merida city sub-surface experiences a continuous pollution condition, in which the upper aquifer layers seem to have a permanently high NO_3^- concentration. The pollution plume generated in Merida city moves northward according to the natural groundwater flow, temporarily increasing NO_3^- levels in northern areas during the high-rainfall season. Therefore, extraction wells located along the groundwater flow path, mostly those closer to Merida, are categorized as highly vulnerable sources.

In the case of other cities, the pollution seems to be locally generated, with highly transient NO_3^- concentration levels; this can be seen in Figure 5.4, in which the localities of Ucu and Conkal expose moderate NO_3^- concentrations in their sub-surfaces. The temporal NO_3^- variability, reported by preceding water sampling campaigns, is also demonstrated by the model (see Figure 4.19). The increment of NO_3^- levels can be associated with a flush effect, incrementing the pollution in the north of Merida city, therefore, the seasonal variations of the representative pollutant should also be considered in further protection strategies.

This complementary evaluation of potential and actual vulnerability is profoundly beneficial, expanding the scope of vulnerability studies as an important decision support tool. According to the IKAV method in the Yucatan case, the MMA is undergoing severe pollution stress given its HV, as displayed by the IKAV-P map (see Figure 5.3), and the water supply wells being categorized with VHV and HV by the IKAV-A map (see Figure 5.4). In addition to the necessary protective planning, encouraged by the IKAV-P map, the IKAV-A map serves to expand the scope of such strategies. Considering that the extraction wells to the south of Merida city demonstrate VHV, the IKAV-A map indicates that the NO_3^- levels above the permissible maximum are restrained in the upper layer of the aquifer; in this case, a deeper well can be considered as an option for corrective measures.

A contrasting condition is displayed for some extraction wells located at the northern periphery of Merida city; in this section of the aquifer, the three aquifer layers display either VHV or HV, indicating that a deeper well would not be a suitable solution. This is a perfect example of how the IKAV method not only provides indications regarding protective-corrective strategies in terms of water quality, but also how it can indicate possible solutions with a focus on environmental and cost/benefit criteria.

5.4.3   Limitations of the IKAV

One of the key rules of the IKAV is regionalization, however, the application of the IKAV on small areas could not display the necessary variability to contribute to the evaluation process of the IKAV-P. Attribute variability is an important criterion to highlight the differences and achieve the principles proposed by this method. This limitation was clear for the MMA where the three selected parameters (karstification, vadose zone and soils) display little variability, being considered practically homogeneous at this local scale. Therefore, application of the IKAV-P method is encouraged for regional analyses; its applicability for local studies will depend on the evaluated parameters and their attributes.

The application of a solute transport model to obtain the IKAV-A map is highly dependent on aquifer characterization. Considering the high heterogeneity of karst, large areas would require very extensive data collection for a more detailed model. Due to the lack of detailed information from many karst areas, regarding their conduit system, the use of an EPM with large REVs aims to reduce the significance of large cavities and underwater channels on a large scale. Nevertheless, such an approach is limited when emulating solute transport in complex karst aquifers. In addition to these constraints, the extensive efforts to gather data from non-point pollution sources in a region makes the application of the IKAV-A method impractical on a regional scale. The evaluation of actual vulnerability in selected areas, where activities threatening the aquifer are prominent and aquifer characterization work is feasible in terms of cost and time, is suggested.

5.5   Chapter remarks

The application of an integrated karst aquifer vulnerability methodology enhances the scope of the vulnerability analysis and improves its role as a decision support tool in water-related problems. A general workflow, providing additional rules and criteria, is proposed as a guide to evaluate potential and actual vulnerable conditions, either for resource or source targets. This combined analysis will serve to strengthen the development and implementation of necessary strategies, either for preventative or corrective purposes, by providing a more detailed analysis.

The proposed IKAV method is based on three important principles - infiltration distinctive, regionalization, and representative pollution - to highlight critical pollution scenarios, given both the natural and anthropogenic characteristics of karst areas. The IKAV method is presented as an alternative to deal with the high subjectivity of current (and numerous) intrinsic groundwater vulnerability methods, with problems related to data availability and further troubling decisions during the vulnerability evaluation process.

The application of the IKAV method in Yucatan displayed notable results in the mapping of potential and actual vulnerable conditions. The IKAV-P map demonstrated a remarkable congruence with regional characteristics, such as the contrasting conditions of the low relief areas and the Sierrita de Ticul. The correlation of the IKAV-P map, on the spatial distribution of vulnerability, with the regional IVAKY map, provides a clear indication of the reliability of the method to achieve a congruent relationship between regional conditions and vulnerability classes. It is important to note that these conditions were not displayed by any of the eight previously applied methodologies in Yucatan but partially.

In a highly populated area, classified with an HV by the IKAV-P map, results from the IKAV-A method indicate the necessity to develop corrective strategies for some extraction wells operating under highly vulnerable conditions. The IKAV-A map not only served to highlight vulnerable sources, it also provided very important insights to assist the evaluation of possible corrective measures.

Despite the encouraging results of the IKAV method in Yucatan, this integrated method is not proposed as a definitive solution neither for the potential nor the actual vulnerability. Its application can serve as indicative to highlight endangered sections of the aquifer and to promote further validation through field work, sampling campaigns, or monitoring projects. Given the natural characteristics of the Yucatan karst, many karst features presented in section 2.1 were not evaluated in this work. Nonetheless, despite not proposing a fixed scheme regarding the number of parameters, number of attributes or weights assignment, the IKAV method is expected to be capable of evaluating multiple karst characteristics inasmuch as the rules and criteria are achieved.

6 General conclusions

Karst groundwater has a greater exposure to pollution in comparison with detritus aquifers, given its natural characteristics, increased infiltration capacity, and flow velocities for the transport of pollutants. Intrinsic groundwater vulnerability methodologies are tools, associated with broad subjectivity, to evaluate the likeliness of a theoretical pollutant particle to reach groundwater. Given the fact that this type of evaluation focuses solely on the intrinsic conditions of a given study area under an incidental pollution scenario, this judgement process can also be referred to as "potential vulnerability analysis". This complementary definition aims to reflect the circumstantial pollution condition analysed by intrinsic vulnerability methods. Vulnerability is, thus, conditional and not a given state.

However, many karst aquifers are already being affected by multiple anthropogenic activities, representing a constant threat to water quality. Therefore, a groundwater vulnerability analysis must also consider the role of the current pollution scenarios taking place in karst aquifers. For this reason, an integrated evaluation of "potential" and "actual" aquifer vulnerability conditions is highly necessary in order to reinforce decisions regarding resource protection, reallocation of extraction wells, and other activities stressing the aquifer water quality. To propose a general structure to evaluate an integrated groundwater vulnerability, several steps were taken in this work.

In chapter two, an extensive literature review of current intrinsic vulnerability methods served to identify the scope, fundaments, and the hydrological and hydrogeological principles on which each method is based; limitations and inconsistencies among them were also highlighted. The elevated number of current intrinsic methods, with many more constantly appearing in literature, reflect the complications to evaluate this vulnerability type. The conditions promoting the constant appearance of new or adapted intrinsic methods are the high heterogeneity of karst, data availability, water regulations, and scale. Therefore, a general methodology to estimate intrinsic vulnerability must be able to reflect regional conditions with the available data for a given karst region.

In chapter three, the application of eight selected intrinsic groundwater vulnerability methods in the Yucatan karst was a key process to highlight advantages and disadvantages of some of the current methodologies. Despite an unpredictable match among multiple outcomes, vulnerability classifications were arguable in the study area, given the range of the regional conditions. Congruence analysis, among methods and individual parameters, in combination with sensitivity analysis, highlighted important considerations to improve the intrinsic groundwater vulnerability estimation.

In chapter four, the importance of including anthropogenic influence was ascertained, in order to define current groundwater vulnerability scenarios. Through the analysis of regional activities, a representative pollutant for a given area can be selected; the significance of the extension of pollution plumes and pollutant concentrations in classifying sections of the aquifer (and water sources) in terms of actual vulnerability, was demonstrated.

In chapter five, the main conclusions obtained in chapters three and four were combined, proposing an Integrated Karst Aquifer Vulnerability (IKAV) method. The IKAV method presents a detailed workflow to estimate potential vulnerability (IKAV-P) and the actual vulnerability (IKAV-A) of karst aquifers. The IKAV method was applied in Yucatan and validated with previous studies.

6.1 Improvements on vulnerability estimation

Having successfully fulfilled the objectives indicated in section 1.2, the IKAV method provides critical improvements in groundwater vulnerability studies. The important contributions of this thesis are understood to be as follows:

- The over/underestimation of the vulnerability outcomes is reduced by performing individual analyses for point and diffuse infiltration conditions (infiltration distinctive principle).

- Independent of the number of parameters or attributes, a correlative rating system is favourable for further vulnerability classification.

- The index partition is not discretional, but dependent on statistical distribution, allowing a better representation of the study area's characteristics.

- Vulnerability results are more consistent with regional characteristics when the attributes display a pronounced variability (regionalization principle).

- The evaluation of the anthropogenic influence via solute transport enhances the vulnerability analysis, depicting conditions not displayed by intrinsic methods (representative pollutant principle).

- Actual vulnerability maps can represent individual aquifer layers, providing additional criteria for cost/benefit judgements (three-dimensional vulnerability analysis).

- The IKAV method is not only a vulnerability indicator, it is capable of revealing possible solutions for endangered water sources.

In conclusion, the IKAV method is an alternative scheme to estimate potential groundwater vulnerability, integrating solute transport to evaluate an aquifer's current state of vulnerability. The IKAV method reduces the inevitable subjectivity of the MCDA by proposing a workflow with well-defined rules and systemic attributes evaluation criteria. The IKAV-P map provides decisive insights for protective-preventive procedures and the IKAV-A map focuses on presently vulnerable sections of the aquifer in order to implement corrective actions and maintain optimal groundwater quality.

Despite the presence of some limitations derived from the different scales at which the IKAV-P and IKAV-A maps can be applied, this integrated methodology is a very important groundwork to expand further vulnerability studies and their role as a decision support tools.

6.2 Further research

Since one of the main goals of the IKAV method is regionalization, evaluation of its performance in multiple karst areas is highly necessary. Testing the IKAV method in areas where current methods have been tested and validated could bring valuable information to further improve the process. Being a workflow, not establishing parameters, attributes, nor weights, the IKAV could be also applied in porous aquifers.

The proposed data filtering and rating scheme aims to minimize the subjectivity of the wide range of possible attributes and their respective rating values, indicated by multiple methodologies. However, the process to assign weights remains open. Mathematical and statistical considerations can be very helpful when defining a more objective weighting approach.

Artificial intelligence (AI) algorithms, such as deep learning and neuronal networks, could be used to introduce a fundamental weighting model using existing study results, thereby minimizing the high subjectivity of these processes. Vulnerability studies around the world utilize multiple criteria to determine the importance of certain parameters on groundwater vulnerability estimation, however, there is common agreement on how some factors are considered. This is where AI could be helpful; in developing a solid base for weighting and increase method comparability.

Literature

Aguilar, Y. and Bautista, F. (2011): 'Extrapolating the suitability of soils as natural reactors using an existing soil map: application of pedotransfer functions, spatial integration and validation procedures', Tropical and Subtropical Agroecosystems, 13(2), p. 221–232. Available at: https://www.redalyc.org/articulo.oa?id=93917767010 (accessed: 28/03/2016).

Aguilar, Y.; Bautista, F. and Díaz-Pereira, E. (2011): 'Soils as natural reactors for swine wastewater treatment', *Tropical and Subtropical Agroecosystems*, 13(2), p. 199–210. Available at: https://www.redalyc.org/articulo.oa?id=93917767008 (accessed: 28/03/2016).

Aguilar, Y.; Bautista, F.; Mendoza, M. E.; Frausto, O. and Ihl, T. (2016): 'Density of karst depressions in Yucatan State, Mexico', *Journal of Cave and Karst Studies*, 78(2), p. 51–60. DOI: 10.4311/2015ES0124.

Aguilar-Duarte, Y.; Bautista, F.; Mendoza, M. E.; Frausto, O.; Ihl, T. and Delgado, C. (2016): 'IVAKY: índice de la vulnerabilidad del acuífero kárstico yucateco a la contaminación [IVAKY: vulnerability index to pollution of the Yucatecan karst aquifer]', *Revista Mexicana de Ingeniería Química*, 15(3), p. 913–933. Available at: https://www.redalyc.org/articulo.oa?id=62048168021 (accessed: 14/01/2017).

Albinet, M. (1970): *Les cartes de vulnérabilité des nappes d'eau souterraine á la pollution [Maps of groundwater vulnerability to pollution]*. Report 70 SGN 325 HYD. Orléans, France. Bulletin du Bureau de Recherches Géologiques et Minières (BRGM), 31 p. Available at: http://infoterre.brgm.fr/rapports/70-SGN-325-HYD.pdf (accessed: 19/02/2016).

Aller, L.; Bennett, T.; Lehr, J. H.; Petty, R. J. and Hackett, G. (1987): *DRASTIC: A standardized system for evaluating ground water pollution potential using hydrogeologic settings*. Report EPA/600/287/035. Springfield, USA. US Environmental Protection Agency, 177 p. Available at: https://ntrl.ntis.gov/NTRL (accessed: 12/02/2016).

Andrade-Briceño, L. A. (1984): *Análisis de fluctuaciones y balance hídrico del acuífero de la zona de pozos de la JAPAY [Analysis of the fluctuations and the water balance of the aquifer of the JAPAY wellfields]*, Bachelor thesis, Merida, Mexico. Yucatan Autonomous University (UADY).

Andrejchuk, V. and Klimchouk, A. (2001): 'Geomicrobiology and redox geochemistry of the karstified Miocene gypsum aquifer, western Ukraine: The study from Zoloushka Cave', *Geomicrobiology Journal*, 18(3), p. 275–295. DOI: 10.1080/01490450152467796.

Andrejchuk, V. and Klimchouk, A. (2002): 'Mechanisms of karst breakdown formation in the gypsum karst of the fore-Ural region, Russia (from observations in the Kungurskaja Cave)', *International Journal of Speleology*, 31(1), p. 89–114. DOI: 10.5038/1827-806X.31.1.5.

Andreo, B.; Goldscheider, N.; Vadillo, I.; Vías, J. M.; Neukum, C.; Sinreich, M.; Jiménez, P.; Brechenmacher, J.; Carrasco, F. and Hötzl, H. (2006): 'Karst groundwater protection: First application of a Pan-European Approach to vulnerability, hazard and risk mapping in the Sierra de Líbar (Southern Spain)', *Science of the Total Environment*, 357(1–3), p. 54–73. DOI: 10.1016/j.scitotenv.2005.05.-019.

Andreo, B.; Ravbar, N. and Vías, J. M. (2009): 'Source vulnerability mapping in carbonate (karst) aquifers by extension of the COP method: application to pilot sites', *Hydrogeology Journal*, 17(3), p. 749–758. DOI: 10.1007/s10040-008-0391-1.

Andreo, B.; Vías, J.; Durán, J. J.; Jiménez, P.; López-Geta, J. A. and Carrasco, F. (2008): 'Methodology for groundwater recharge assessment in carbonate aquifers: application to pilot sites in southern Spain', *Hydrogeology Journal*, 16(5), p. 911–925. DOI: 10.1007/s10040-008-0274-5.

Aquilina, L.; Ladouche, B. and Dörfliger, N. (2006): 'Water storage and transfer in the epikarst of karstic systems during high flow periods', *Journal of Hydrology*, 327(3–4), p. 472–485. DOI: 10.1016/j.jhydrol.2005.11.054.

Arbeitsgruppe BODEN (1994): *Bodenkundliche Kartieranleitung [Soil mapping instructions]*. 5th edition. Stuttgart, Germany. Schweizerbart, 392 p. Available at: https://katalog.slub-dresden.de/id/0-18686499X (accessed: 18/11/2015).

Arthur, J. D.; Wood, H. A. R.; Baker, A. E.; Cichon, J. R. and Raines, G. L. (2007): 'Development and implementation of a Bayesian-based aquifer vulnerability assessment in Florida', *Natural Resources Research*, 16(2), p. 93–107. DOI: 10.1007/s11053-007-9038-5.

Audra, P.; Lauritzen, S. and Rochette, P. (2011): 'Speleogenesis in the hyperkarst of the Nakanai Mountains (New Britain, Papua New-Guinea) Evolution model of a juvenile system (Muruk Cave) inferred from U/Th and paleomagnetic dating', *Speleogenesis and Evolution of Karst Aquifers (SEKA)*, 10, 6 p. Available at: https://speleogenesis.com/resources/journal/issues-2003-2012/issue-10-2011/642 (accessed: 04/10/2017).

Back, W. and Lesser, J. M. (1981): 'Chemical constraints of groundwater management in the Yucatan Peninsula, Mexico', *Journal of Hydrology*, 51(1–4), p. 119–130. DOI: 10.1016/0022-1694(81)90121-9.

Bagherzadeh, S.; Kalantari, N.; Nobandegani, A. F.; Derakhshan, Z.; Conti, G. O.; Ferrante, M. and Malekahmadi, R. (2018): 'Groundwater vulnerability assessment in karstic aquifers using COP method', *Environmental Science and Pollution Research*, 25(19), p. 18960–18979. DOI: 10.1007/s11356-018-1911-8.

Bakalowicz, M. (2005): 'Karst groundwater: a challenge for new resources', *Hydrogeology Journal*, 13(1), p. 148–160. DOI: 10.1007/s10040-004-0402-9.

Bakalowicz, M.; Blavoux, B. and Mangin, A. (1974): 'Apports du tracage isotopique naturel à la connaissance du fonctionnement d'un systéme karstique-Teneurs en oxygène-18 de trois systèmes des Pyrénées, France [Contributions of natural isotopic tracing to the knowledge of how a Karst system works Oxygen-18 contents of three systems of Pyrenees, France]', *Journal of Hydrology*, 23(1–2), p. 141–158. DOI: 10.1016/0022-1694(74)90028-6.

Barrocu, G.; Muzzu, M. and Uras, G. (2007): 'Hydrogeology and vulnerability map (EPIK method) of the "Supramonte" karstic system, north-central Sardinia', *Environmental Geology*, 51(5), p. 701–706. DOI: 10.1007/s00254-006-0382-2.

Batiot, C.; Emblanch, C.; Blavoux, B.; Smiler, R. and Daniel, M. (2000): 'Organic matter in karstic aquifers: a potential tracer in the carbon cycle A small-scale', in: *Dassargues, A. (Ed). Tracers and modelling in hydrogeology. Proceedings of TraM'2000, the International Conference on Tracers and Modelling in Hydrogeology*. IAHS Publication 262. Liege, Belgium. IAHS Press, p. 459–463. Available at: https://www.researchgate.net/publication/268429197 (accessed: 28/06/2016).

Bauer, S.; Liedl, R. and Sauter, M. (2005): 'Modeling the influence of epikarst evolution on karst aquifer genesis: A time-variant recharge boundary condition for joint karst-epikarst development', *Water Resources Research*, 41, W09416. DOI: 10.1029/2004WR003321.

Bauer-Gottwein, P.; Gondwe, B. R.; Charvet, G.; Marín, L. E.; Rebolledo-Vieyra, M. and Merediz-Alonso, G. (2011): 'Review: the Yucatan Peninsula karst aquifer, Mexico', *Hydrogeology Journal*, 19(3), p. 507–524. DOI: 10.1007/s10040-010-0699-5.

Bautista, F.; Estrada-Medina, H.; Jiménez-Osornio, J. M. and González-Iturbe, J. A. (2004): 'Relación entre el relieve y unidades de suelo en zonas cársticas de Yucatán [Relationship between relief and soil units in karst areas of Yucatan]', *Terra Latinoamericana*, 22(3), p. 243–254. Available at: https://www.redalyc.org/articulo.oa?id=57322301 (accessed: 15/06/2016).

Bautista, F.; Palacio-Aponte, G.; Quintana, P. and Zinck, J. A. (2011): 'Spatial distribution and development of soils in tropical karst areas from the Peninsula of Yucatan, Mexico', *Geomorphology*, 135(3–4), p. 308–321. DOI: 10.1016/j.geomorph.2011.02.014.

Bayari, C. S.; Pekkan, E. and Ozyurt, N. N. (2009): 'Obruks, as giant collapse dolines caused by hypogenic karstification in central Anatolia, Turkey: analysis of likely formation processes', *Hydrogeology Journal*, 17(2), p. 327–345. DOI: 10.1007/s10040-008-0351-9.

van Beynen, P. E. (Ed). (2011): *Karst Management*. Heidelberg, Germany. Springer, 501 p. DOI: 10.1007/978-94-007-1207-2.

van Beynen, P.; Niedzielski, M.; Bialkowska-Jelinska, E.; Alsharif, K. and Matusick, J. (2012): 'Comparative study of specific groundwater vulnerability of a karst aquifer in central Florida', *Applied Geography*, 32(2), p. 868–877. DOI: 10.1016/j.apgeog.2011.09.005.

BGR, IAH, KIT and UNESCO (2017): *World Karst Aquifer Map*. 1 : 40,000,000. Berlin, Reading, Karlsruhe and Paris. Available at: https://www.un-igrac.org/resource/world-karst-aquifer-map-wokam (accessed: 23/04/2018).

Biondić, R.; Meaški, H. and Biondić, B. (2014): 'Vulnerability mapping of Novljanska Žrnovnica karstic spring catchment area (Croatia)', in: *Kukurić N., Stevanović Z. and Krešić N. (Eds). Proceedings of the international conference and field seminar 'Karst without boundaries'*. Trebinje, Bosnia & Herzegovina: Grafokomerc, pp. 357–363. Available at: https://bib.irb.hr/datoteka/705512 (accessed: 04/07/2017).

Bögli, A. (1980): *Karst hydrology and physical speleology*. Berlin, Germany. Springer Verlag, 284 p. DOI: 10.1007/978-3-642-67669-7.

Bonacci, O. (2014): 'Ecohydrology of karst poljes and their vulnerability', in: *Sackl P., Durst R., Kotrošan D. & Stumberger B. (Eds). Dinaric karst Poljes - Floods for Life*. Radolfzell, Germany. EuroNatur foundation, p. 25–37. Available at: https://www.euronatur.org/fileadmin/docs/docs_english-/KRASKA_POLJA.pdf (accessed: 08/05/2017).

Bonacci, O. (1987): *Karst hydrology: with special reference to the Dinaric karst*. Berlin, Germany. Springer, 184 p. DOI: 10.1007/978-3-642-83165-2.

Bonacci, O. (2013): 'Poljes, Ponors and their catchments', in: *Shroder J. F. (Ed). Treatise on Geomorphology*. Karst Geomorphology. California, USA. Elsevier, p. 112–120. DOI: 10.1016/B978-0-12-374739-6.00103-2.

Bondesan, A.; Meneghel, M. and Sauro, U. (1992): 'Morphometric Analysis of Dolines', *International Journal of Speleology*, 21, p. 1–55. DOI: 10.5038/1827-806X.21.1.1.

Bonet, F. and Butterlin, J. (1962): 'Stratigraphy of the northern part of the Yucatan Peninsula', in: *Guide book. Field trip to Peninsula of Yucatan*. New Orleans, USA. New Orleans Geological Society, p. 52–57. Available at: http://archives.datapages.com/data/nogs/data/006/006023/0052.htm (accessed: 27/10/2015).

Bonham-Carter, G. F. (1996): *Geographic information systems for geoscientists. Modelling with GIS*. 1st edition. Ontario, Canada. Elsevier, 398 p. Available at: https://katalog.slub-dresden.de/id/0-1613350384/ (accessed: 16/04/2016).

Brewerton, L. J. (1993): *Aquifer properties of samples from Merida, Yucatan, Mexico*. Report WD/93/050. British Geological Survey.

Brosig, K.; Geyer, T.; Subah, A. and Sauter, M. (2008): 'Travel-time based approach for the assessment of vulnerability of karst groundwater: the Transit Time Method', *Environmental Geology*, 54(5), p. 905–911. DOI: 10.1007/s00254-007-0898-0.

Brouyère, S. (2003): 'A quantitative point of view of the concept of vulnerability', in: *Zwahlen, F. (Ed). COST Action 620 - Vulnerability and risk mapping for the protection of carbonate (karst) aquifers*. Final report. Brussels, Belgium. European Commission, Directorate-General for Research, p. 10-15. Available at: https://op.europa.eu/en/publication-detail/-/publication/be3c99bf (accessed: 16/11/2015).

Buckley, D. K.; MacDonald, D. M. J.; Villasuso, M.; Graniel, E.; Vasquez, J. and Jimenez, M. V. (1994): *Geophysical logging of a karstic limestone aquifer for hydrogeological purposes at Merida, Yucatan, Mexico*. Report: 194/4C. British Geological Survey.

Butscher, C. and Huggenberger, P. (2008): 'Intrinsic vulnerability assessment in karst areas: a numerical modeling approach', *Water Resources Research*, 44(3). DOI: 10.1029/2007WR006277.

Butterlin, J. (1958): *Reconocimiento geologico preliminar del territorio de Quintana Roo. [Preliminary geological reconnaissance of the Quintana Roo territory]*. DF, Mexico. Asociación Mexicana de Geólogos Petroleros (AMGP), p. 631-564. Available at: http://archives.datapages.com/data/-amgp/pdf-content/1958/1958 (accessed: 09/03/2017).

Cabadas, H. V.; Solleiro, E.; Sedov, S.; Pi, T. and Alcalá, J. R. (2010): 'The complex genesis of red soils in Peninsula de Yucatan, Mexico: mineralogical, micromorphological and geochemical proxies', *Eurasian Soil Science*, 43(13), p. 1439–1457. DOI: 10.1134/S1064229310130041.

Cabrera, A.; Pacheco, J.; Cuevas, E.; Ramírez, J.; Comas, M. and Cámara, A. (2002): 'Hidrogeoquímica del agua que subyace a la JAPAY I, en Mérida, Yucatán, México [Groundwater hydrogeochemistry underlying JAPAY I in Merida, Yucatan, Mexico]', *Ingenieria*, 6(3), p. 29–40. Available at: https://www.redalyc.org/articulo.oa?id=46760303 (accessed: 31/01/2017).

Carver, S. J. (1991): 'Integrating multi-criteria evaluation with geographical information systems', *International Journal of Geographical Information System*, 5(3), p. 321–339. DOI: 10.1080/02693799108927858.

Chen, Z.; Auler, A. S.; Bakalowicz, M.; Drew, D.; Griger, F.; Hartmann, J.; Jiang, G.; Moosdorf, N.; Richts, A. and Stevanovic, Z. (2017): 'The World Karst Aquifer Mapping project: concept, mapping procedure and map of Europe', *Hydrogeology Journal*, 25(3), p. 771–785. DOI: 10.1007/s10040-016-1519-3.

Cichocki, G. and Zojer, H. (2007): 'VURAAS: vulnerability and risk assessment for Alpine aquifer system', in: *Witkowski A., Kowalczyk A. & Vrba J. (Eds). Groundwater vulnerability assessment and mapping.* International Association of Hydrogeologists selected papers, 11. London, UK. Taylor & Francis, p. 191–197. Available at: https://katalog.slub-dresden.de/id/0-1344280870#detail (accessed: 28/08/2017).

Clemens, T.; Hückinghaus, D.; Liedl, R. and Sauter, M. (1999): 'Simulation of the development of karst aquifers: role of the epikarst', *International Journal of Earth Sciences*, 88(1), p. 157–162. DOI: 10.1007/s005310050252.

Clemens, T.; Hückinghaus, D.; Sauter, M.; Liedl, R. and Teutsch, G. (1997): 'Simulation of the evolution of maze caves', in: *Jeannin P. Y. (Ed). Proceedings of the 12th International Congress of Speleology.* La Chaux-de-Fonds, Switzerland. University of Franche-Comte, Sciences & Techniques de l'Environnement, p. 65–68. Available at: https://digital.lib.usf.edu/SFS0064376/00001 (accessed: 04/05/2017).

CONAGUA (2015a): *Actualización de la disponibilidad media anual de agua en el acuífero Peninsula de Yucatán [Update of the average annual water availability of the Yucatan Peninsula aquifer].* DF, Mexico. Comisión Nacional del Agua, 23 p. Available at: https://www.gob.mx/cms/-uploads/attachment/file/103392 (accessed: 16/11/2015).

CONAGUA (2015b): *Estadísticas del agua en México, edición 2015 [Water statistics in México, 2015 edition].* DF, Mexico. Comisión Nacional del Agua, 295 p. Available at: https://agua.org.mx/biblioteca/-estadisticas-del-agua-en-mexico-edicion-2015/ (accessed: 16/11/2015).

CONAGUA (2010): *Inventario nacional de plantas municipales de potabilización y de tratamiento de aguas residuales en operación [National inventory of operational municipal drinking water and wastewater treatment plants].* DF, Mexico. Comisión Nacional del Agua, 317 p. Available at: http://www.conagua.gob.mx-/CONAGUA07/Publicaciones/Publicaciones/SGAPDS-18-11.pdf (accessed: 16/11/2015).

CONAGUA (2012): *Programa Hídrico Regional Visión 2030. Región Hidrológico-Administrativa XII Península de Yucatán [Vision 2030. Regional water agenda. Hydrological-Administrative Region XII Yucatan Peninsula].* DF, Mexico. Comisión Nacional del Agua, 135 p. Available at: http://www.conagua.gob.mx/-conagua07/publicaciones/publicaciones/12-sgp-17-12py.pdf (accessed: 16/11/2015).

CONAGUA (2005): *Síntesis de las Estadísticas del Agua en México [Synthesis of water statistics in Mexico].* 1st edition. DF, Mexico. Comisión Nacional del Agua, 100 p. Available at: http://www.conagua.gob.mx/-CONAGUA07/Publicaciones/Publicaciones/eam_junio2005.pdf (accessed: 16/11/2015).

Consejo estatal de planeación de Yucatán (2013): *Plan estatal de desarrollo 2012-2018 Yucatán [State development plan 2012-2018 Yucatan]*. Mérida, México. Gobierno del estado de Yucatán, 318 p. Available at: http://www.yucatan.gob.mx/docs/transparencia/ped/2012_2018/PED (accessed: 14/03/2017).

Couturier, B. and Fourneaux, C. (1998): 'Les relations karst-rivière dans les calcaires barrémo-bédouliens du Diois (Drôme–France) Exemple de la Gervanne [Karst-river relations in the Barremo-Bedoulian limestones of Diois (Drôme – France) Example of the Gervanne]', *Bulletin of Engineering Geology and the Environment*, 57(2), p. 207–212. DOI: 10.1007/s100640050037.

Cucchi, F. (2009): 'Kamenitzas', in: *Ginés A., Knez M., Slabe T. & Dreybrodt W. (Eds). Karst rock features. Karren sculpturing*. Carsologica. Ljubljana, Slovenia. Založba ZRC, p. 139–150. DOI: 10.3986/9789610502968.

Cvijić, J. (1893): *Das karstphänomen: Versuch einer morphologischen Monographie [The karst phenomenon: attempt of a geographic monography]*. Vienna, Austria: Hölzel. Available at: https://katalog.slub-dresden.de/id/0-1119428904 (accessed: 03/09/2016).

Daly, D.; Dassargues, A.; Drew, D.; Dunne, S.; Goldscheider, N.; Neale, S.; Popescu, I. and Zwahlen, F. (2002): 'Main concepts of the "European approach" to karst-groundwater-vulnerability assessment and mapping', *Hydrogeology Journal*, 10(2), p. 340–345. DOI: 10.1007/s10040-001-0185-1.

Davis, A.; Long, A.; Wireman, M. and Xiaodan, T. (2002): 'KARSTIC: a sensitivity method for carbonate aquifers in karst terrain', *Environmental Geology*, (42), p. 65–72. DOI: 10.1007/s00254-002-05311.

De Ketelaere, D. and Daly, D. (2003): 'Vulnerability in a Risk Framework', In: *Zwahlen, F. (Ed). COST 620 - Vulnerability and risk mapping for the protection of carbonate (karst) aquifers*. Final report. Brussels, Belgium. European Commission, Directorate-General for Research, p. 84-85. Available at: https://op.europa.eu/en/publication-detail/-/publication/be3c99bf-1a0a-4213 (accessed: 16/11/2015).

De Maio, M.; Civita, M.; Farina, M. and Zavatti, A. (2001): *Linee guida per la redazione e l'uso delle carte della vulnerabilità degli acquiferi all'inquinamento [Guidelines for the drafting and use of vulnerability cards of aquifers to pollution]*. Rome, Italy. Anpa, 99 p. Available at: https://iris.polito.it/handle/11583/2592718 (accessed: 14/11/2016).

De Waele, J.; Plan, L. and Audra, P. (2009): 'Recent developments in surface and subsurface karst geomorphology: an introduction', *Geomorphology*, 106, p. 1–8. DOI: 10.1016/j.geomorph.2008.

Delgado, C.; Pacheco, J.; Cabrera, A.; Batllori, E.; Orellana, R. and Bautista, F. (2010): 'Quality of groundwater for irrigation in tropical karst environment: The case of Yucatan, Mexico', *Agricultural Water Management*, 97(10), p. 1423–1433. DOI: 10.1016/j.agwat.2010.04.006.

Delgado-Carranza, C. (2010): *Zonificación agroecológica del estado de Yucatán con base en índices agroclimáticos y calidad agrícola del agua subterránea [Agroecological zoning of the state of Yucatan based on agroclimatic indices and agricultural quality of groundwater]*, Doctoral thesis, Merida, Mexico. Centro de Investigación Científica de Yucatán (CICY), 149 p. Available at: https://cicy.repositorioinstitucional.mx/jspui/bitstream/1003/594/1/PCBP_D_Tesis_2010_Maria_Delgado_Carranza.pdf (accessed: 27/02/2018).

Diario de Yucatán (2018): 'Se duplica el consumo de agua [water consumption duplicates]', *Diario de Yucatan*, digital edition. Website: https://www.yucatan.com.mx/merida/se-duplica-el-consumo-de-agua (accessed: 18/07/2018).

Diario Oficial de la Federación (2000): *Modificacion de la Norma NOM-127-SSA1-1994: Límites permisibles de calidad y tratamientos a que debe de someterse el agua para su potabilización [Modification of the NOM-127-SSA1-1994 Standard: Permissible quality limits and treatments to which the water must be subjected for its purification]*. Available at: https://dof.gob.mx/nota_detalle.php?codigo=-2063863&fecha=31/12/1969 (accessed: 24/07/2017).

Doehring, D. O. and Butler, J. H. (1974): 'Hydrogeologic constraints on Yucatán's development', *Science*, 186(4164), p. 591–595. DOI: 10.1126/science.186.4164.591.

Dörfliger, N.; Jeannin, P.-Y. and Zwahlen, F. (1999): 'Water vulnerability assessment in karst environments: a new method of defining protection areas using a multi-attribute approach and GIS tools (EPIK method)', *Environmental Geology*, 39(2), p. 165–176. DOI: 10.1007/s002540050446.

Dörfliger, N. and Plagnes, V. (2009): *Cartographie de la vulnérabilité des aquifères karstiques, guide méthodologique de la méthode PaPRIKa [Mapping the vulnerability of karst aquifers, methodological guide of the PaPRIKa method]*. Report: BRGM RP-57527-FR. Orléans, France. Bulletin de la Bureau de Recherches Géologiques et Minières (BRGM), 119 p. Available at: https://www.documentation.eauetbiodiversite.fr (accessed: 24/07/2017).

Drew, D. (2017): 'Karst water and human activities An overview', in: *Drew D. & Hötzl H. (Eds). Karst hydrogeology and human activities: impacts, consequences and implications*. IAH international contributions to hydrogeology, 20. Rotterdam, Netherlands. Balkema, 322 p. Available at: https://katalog.slub-dresden.de/id/0-269932690/ (accessed: 13/05/2018).

Drucker, A. G.; Escalante-Semerena, R.; Gómez-González, V. and Magaña-Rueda, S. (2003): 'La industria porcina en Yucatán: un análisis de la generación de aguas residuales [Pig farming industry in Yucatan: an analysis of wastewater generation]', *Problemas del Desarrollo. Revista Latinoamericana de Economia*, 34(135), p. 105–124. DOI: 10.22201/iiec.20078951e.2003.-135.7505.

Dunne, S. (2004): *Vulnerability mapping for the protection of karst aquifers in England and Wales*, Doctoral thesis, Dublin, Ireland. Trinity College, Dublin University. Available at: http://www.tara.tcd.ie/-handle/2262/78365 (accessed: 05/07/2017).

Emblanch, C.; Blavoux, B.; Puig, J. and Mudry, J. (1998): 'Dissolved organic carbon of infiltration within the autogenic karst hydrosystem', *Geophysical Research Letters*, 25(9), p. 1459–1462. DOI: 10.1029/98GL01056.

Escolero, O. A.; Marín, L. E.; Steinich, B.; Pacheco, J.; Cabrera, S. A. and Alcocer, J. (2002): 'Development of a protection strategy of karst limestone aquifers: the Merida Yucatan, Mexico case study', *Water Resources Management*, 16(5), p. 351–367. DOI: 10.1023/A:1021967909293.

Essaid, H. I. (1990): *The computer model SHARP, a quasi-three-dimensional finite-difference model to simulate freshwater and saltwater flow in layered coastal aquifer systems*. Water-Resources Investigations Report: 90-4130. California, USA. U.S. Geological Survey, 181 p. DOI: 10.3133/wri904130.

Estrada-Medina, H.; Canto-Canché, B. B.; De los Santos-Briones, C. and O'Connor-Sánchez, A. (2016): 'Yucatan in black and red: Linking edaphic analysis and pyrosequencing-based assessment of bacterial and fungal community structures in the two main kinds of soil of Yucatan State', *Microbiological Research*, 188, p. 23–33. DOI: 10.1016/j.micres.2016.04.007.

Farfán-González, H. and Plagnes, V. (2013): 'First Outcomes in the Application of PaPRIKa Method to Assess Aquifer Vulnerability in Tropical Karst Mountain: Santo Tomás Watershed: Viñales National Park, Cuba', in: *Farfán González H., Corvea Porras J., de Bustamente Gutiérrez I. & LaMoreaux J. (Eds). Management of Water Resources in Protected Areas*. Berlin, Germany. Springer, p. 95–101. DOI: 10.1007/978-3-642-16330-2_11.

Febles-Patrón, J. L. and Hoogesteijn, A. (2010): 'Evaluación preliminar de la eficiencia en las lagunas de oxidación de la ciudad de Mérida, Yucatán [Preliminary evaluation of the efficiency in the oxidation lagoons of the city of Merida, Yucatan]', *Ingeniería*, 14(2), p. 127–137. Available at: https://www.redalyc.org/articulo.oa?id=46715068006 (accessed: 06/09/2016).

Fernández, C.; de la Torre, A.; Carsonell, G.; Muñoz, M. and Tarazona, J. (1996): 'Evaluación toxicológica del riesgo ambiental ligado al vertido de los purines (excretas) de cerdo [Toxicological evaluation of the environmental risk linked to pig slurry discharge]', *Desarrollo Porcícola*, (35), p. 18–20.

Fleury, S. (2009): *Land use policy and practice on karst terrains: Living on limestone*. Dordrecht, Netherlands. Springer, 187 p. DOI: 10.1007/978-1-4020-9670-9.

Florea, L. J. (2015): 'Carbon flux and landscape evolution in epigenic karst aquifers modeled from geochemical mass balance', *Earth Surface Processes and Landforms*, 40(8), p. 1072–1087. DOI: 10.1002/esp.3709.

Ford, D. C. and Williams, P. D. (2007): *Karst hydrogeology and geomorphology*. Chichester, UK. Wiley, 553 p. DOI: 10.1002/9781118684986.

Foster, S. (1987): 'Fundamental concepts in aquifer vulnerability, pollution risk and protection strategy', in: *van Duijvenbooden W. & van Waegeningh H. G. (Eds). Vulnerability of soil and groundwater to pollutants*. The Hague, Netherlands. TNO Committee on Hydrological Research, p. 69–86. Available at: http://pascal-francis.inist.fr/vibad/index.php?action=getRecordDetail&idt=7424-894 (accessed: 17/06/2016).

Foster, S. S. D. and Hirata, R. C. A. (1988): *Groundwater pollution risk assessment; a methodology using available data*. Lima, Perú. Pan American Centre for Sanitation, Engineering and Environmental Sciences (CEPIS), 81 p. World Health Organization.

Franz, T. and Guiguer, N. (1990): FLOWPATH version 3.0. Two-dimensional horizontal aquifer simulation model, User's manual, Waterloo, Canada. Waterloo Hydrogeologic Software, 72 p. Available at: https://semspub.epa.gov/work/05/41145.pdf (accessed: 21/05/2018).

Freeze, R. A. and Cherry, J. A. (1979): *Groundwater*. New Jersey, USA. Prentice-Hall, 604 p. Available at: https://katalog.slub-dresden.de/id/0-1611347637 (accessed: 12/10/2015).

Frumkin, A. (1994): 'Hydrology and denudation rates of halite karst', *Journal of Hydrology*, 162(1–2), p. 171–189. DOI: 10.1016/0022-1694(94)90010-8.

Gams, I. (1978): 'The polje: the problem of definition', *Zeitschrift für Geomorphologie*, (22), p. 170–181.

Gaona-Vizcayno, S.; Gordillo-de Anda, T. and Villasuso-Pino, M. (1980): 'Cenotes, karst característico: mecanismos de formación [Cenotes, characteristic karst: formation mechanisms]', *Revista Mexicana de Ciencias Geológicas*, 4(1), p. 32–36. Available at: https://dialnet.unirioja.es/servlet/-articulo?codigo=2231580 (accessed: 13/11/17).

Ginés, A. (2004): 'Karren', in: *Gunn J. (Ed). Encyclopedia of Caves and Karst Science*. London, UK. Fitzroy Dearborn, p. 1010–1016. DOI: 10.4324/9780203483855.

Ginés, A. (2009a): 'Karrenfield landscapes and karren landforms', in: *Ginés A., Knez M., Slabe T. & Dreybrodt W. (Eds). Karst rock features. Karren sculpturing*. Carsologica. Ljubljana, Slovenia. Založba ZRC, p. 13–24. DOI: 10.3986/9789610502968.

Ginés, A. (2009b): 'Trittkarren', in: *Ginés A., Knez M., Slabe T. & Dreybrodt W. (Eds). Karst rock features. Karren sculpturing*. Carsologica. Ljubljana, Slovenia. Založba ZRC, p. 151–160. DOI: 10.3986/9789610502968.

Ginés, A. and Lundwerg, J. (2009): 'Rainpits', in: *Ginés A., Knez M,. Slabe T. & Dreybrodt W. (Eds). Karst rock features. Karren sculpturing*. Carsologica. Ljubljana, Slovenia. Založba ZRC, p. 169–184. DOI: 10.3986/9789610502968.

Glew, J. R. and Ford, D. C. (1980): 'A simulation study of the development of rillenkarren', *Earth Surface Processes*, 5(1), p. 25–36. DOI: 10.1002/esp.3760050104.

Gogu, R. C. and Dassargues, A. (2000): 'Sensitivity analysis for the EPIK method of vulnerability assessment in a small karstic aquifer, southern Belgium', *Hydrogeology Journal*, 8(3), p. 337–345. DOI: 10.1007/s100400050019.

Gogu, R. C.; Hallet, V. and Dassargues, A. (2003): 'Comparison of aquifer vulnerability assessment techniques Application to the Néblon river basin (Belgium)', *Environmental Geology*, 44(8), p. 881–892. DOI: 10.1007/s00254-003-0842-x.

Goldie, H. S. (2009): 'Kluftkarren or grikes as fundamental karstic phenomena', in: *Ginés A., Knez M,. Slabe T. & Dreybrodt W. (Eds). Karst rock features. Karren sculpturing*. Carsologica. Ljubljana, Slovenia. Založba ZRC, p. 89–102. DOI: 10.3986/9789610502968.

Goldscheider, N. (2002): *Hydrogeology and vulnerability of karst systems: examples from the Northern Alps and the Swabian Alb*, Doctoral thesis, Karlsruhe, Germany. Universität Karlsruhe. Available at: https://publikationen.bibliothek.kit.edu/1812002 (accessed: 08/10/2015).

Goldscheider, N. (2003): 'The concept of groundwater vulnerability'. In: *Zwahlen, F. (Ed). COST Action 620-Vulnerability and risk mapping for the protection of carbonate (karst) aquifers*. Final report. Brussels, Belgium. European Commission, Directorate-General for Research, p. 5-9. Available at: https://op.europa.eu/en/publication-detail/-/publication/be3c99bf (accessed: 16/11/2015).

Goldscheider, N. (2005): 'Karst groundwater vulnerability mapping: application of a new method in the Swabian Alb, Germany', *Hydrogeology Journal*, 13, p. 555–564. DOI: 10.1007/s10040-003-0291-3.

Goldscheider, N. (2015): 'Overview of methods applied in karst hydrogeology', in: *Stevanović Z. (Ed). Karst Aquifers - Characterization and Engineering*. Professional Practice in Earth Sciences Series. Sophia, Bulgaria. Springer, p. 127–145. DOI: 10.1007/978-3-319-12850-4.

Goldscheider, N. and Popescu, I. C. (2003): 'The European approach', In: *Zwahlen, F. (Ed). COST 620 - Vulnerability and risk mapping for the protection of carbonate (karst) aquifers.* Final report. Brussels, Belgium. European Commission, Directorate-General for Research, p. 17-21. Available at: https://op.europa.eu/en/publication-detail/-/publication/be3c99bf-1a0a-4213 (accessed: 16/11/2015).

Gondwe, B. R. N.; Hong, S.-H.; Wdowinski, S. and Bauer-Gottwein, P. (2010): 'Hydrologic dynamics of the ground-water-dependent Sian Ka'an wetlands, Mexico, derived from InSAR and SAR data', *Wetlands*, 30(1), p. 1–13. DOI: 10.1007/s13157-009-0016-z.

González-Herrera, R. (1984): *Correlación de Muestras de Roca en Pozos de la Ciudad de Mérida [Rock samples correlation in wells of Mérida city].* Bachelor Thesis. Merida, Mexico. Yucatan Autonomous University (UADY).

González-Herrera, R. and Gómez-López, R. (2013): 'Two in one leachate plume in a karstic aquifer', *Environmental Earth Sciences*, 68(7), p. 1945–1953. DOI: 10.1007/s12665-012-1882-x.

González-Herrera, R.; Martínez-Santibañez, E.; Pacheco-Avila, J. and Cabrera-Sansores, A. (2014): 'Leaching and dilution of fertilizers in the Yucatan karstic aquifer', *Environmental Earth Sciences*, 72(8), p. 2879–2886. DOI: 10.1007/s12665-014-3192-y.

González-Herrera, R.; Sánchez-y-Pinto, I. and Gamboa-Vargas, J. (2002): 'Groundwater-flow modeling in the Yucatan karstic aquifer, Mexico', *Hydrogeology Journal*, 10(5), p. 539–552. DOI: 10.1007/s10040-002-0216-6.

Gracia, F. J.; Gutiérrez, F. and Gutiérrez, M. (2003): 'The Jiloca karst polje-tectonic graben (Iberian Range, NE Spain)', *Geomorphology*, 52(3–4), p. 215–231. DOI: 10.1016/S0169-555X(02)00257-X.

Graniel, E. (2010): 'Capítulo 1. Contexto físico. Hidrología [Chapter 1. Physical context. Hydrology]', in: *Durán, R. & Méndez, M. (Eds). Biodiversidad y desarrollo humano en Yucatán [Biodiversity and human development in Yucatan].* Merida, Mexico. CICY-CONABIO-SEDUMA, p. 12-13. Available at: https://bibliotecasibe.ecosur.mx/sibe/book/000050517 (accessed: 15/04/2017).

Graniel, E.; Morris, L. B. and Carrillo-Rivera, J. J. (1999): 'Effects of urbanization on groundwater resources of Merida, Yucatan, Mexico', *Environmental Geology*, 37(4), p. 303–312. DOI: 10.1007/s002540050388.

Gravelius, H. (1914): *Grundriss der gesamten Gewässerkunde [Basis of the overall hydrology].* Berlin, Germany. Göschen, 179 p. Available at: https://katalog.slub-dresden.de/id/0-1188663771 (accessed: 14/11/2017).

Guo, Y.; Zhai, Y.; Wu, Q.; Teng, Y.; Jiang, G.; Wang, J.; Guo, F.; Tang, Q. and Liu, S. (2016): 'Proposed APLIE method for groundwater vulnerability assessment in karst-phreatic aquifer, Shandong Province, China: a case study', *Environmental Earth Sciences*, 75:112, p. 1-14. DOI: 10.1007/s12665-015-4903-8.

Gutiérrez, F.; Cooper, A. H. and Johnson, K. S. (2008): 'Identification, prediction, and mitigation of sinkhole hazards in evaporite karst areas', *Environmental Geology*, 53(5), p. 1007–1022. DOI: 10.1007/s00254-007-0728-4.

Gutiérrez, F.; Fabregat, I.; Roqué, C.; Carbonel, D.; Zarroca, M.; Linares, R.; Yechieli, Y.; García-Arnay, Á. and Sevil, J. (2019): 'Sinkholes in hypogene versus epigene karst systems, illustrated with the hypogene gypsum karst of the Sant Miquel de Campmajor Valley, NE Spain', *Geomorphology*, 328, p. 57–78. DOI: 10.1016/j.geomorph.2018.12.003.

Hall, F. G. (1936): 'Physical and chemical survey of cenotes of Yucatan', in: *The cenotes of Yucatan : a zoological and hydrographic survey*. Washington, USA. Carnegie Institution of Washington, p. 5–16. Available at: https://babel.hathitrust.org/cgi/pt?-id=mdp.39015013434280 (accessed: 14/09/2017).

Hanshaw, B. B. and Back, W. (1980): 'Chemical Mass-Wasting of the Northern Yucatan Peninsula by Groundwater Dissolution', *Geology* 8(5), p. 222–224. DOI: 10.1130/0091-7613(1980)8<222:-CMOTNY->2.0.CO;2.

Harbaugh, A. W. (2005): *MODFLOW-2005, the US Geological Survey modular ground-water model: the ground-water flow process*. Report. Techniques and Methods 6-A16. Reston, USA. US Geological Survey, 253 p. DOI: https://doi.org/10.3133/tm6A16.

Harbaugh, A. W.; Banta, E. R.; Hill, M. C. and McDonald, M. G. (2000): *MODFLOW-2000, The U. S. Geological Survey Modular Ground-Water Model-User Guide to Modularization Concepts and the Ground-Water Flow Process*. Open-File Report 2000-92. Reston, USA. US Geological Survey, 121 p. DOI: 10.3133/ofr200092.

Healy, R. W.; Winter, T. C.; LaBaugh, J. W. and Franke, O. L. (2007): *Water budgets: foundations for effective water-resources and environmental management*. Circular 1308. Reston, USA. US Geological Survey, 90 p. Available at: https://pubs.usgs.gov/circ/2007/1308/ (accessed: 06/04/2017).

Herak, M. and Burdon, D. (1984): 'Outlets', in: *LaMoreaux P. E., Wilson B. M. & Memon B. A. (Eds). Guide to the hydrology of carbonate rocks*. Studies and Reports in Hydrology, 41. Mayenne, France. UNESCO, 343 p. Available at: https://hydrologie.org/BIB/Publ_UNESCO/SR_041_1984.pdf (accessed: 15/09/2015).

Heywood, I.; Oliver, J. and Tomlinson, S. (1995): 'Building an exploratory multi-criteria modelling environment for spatial decision support', in: *Fischer P. (Ed). Innovations in GIS*. London, UK. Taylor & Francis, p. 127–136. Available at: https://katalog.slub-dresden.de/id/0-1645085481 (accessed: 27/04/2016).

Hildebrand, A. R.; Pilkington, M.; Connors, M.; Ortíz-Alemán, C. and Chávez, R. E. (1995): 'Size and structure of the Chicxulub crater revealed by horizontal gravity gradients and cenotes', *Nature*, 376(6539), p. 415-417. DOI: 10.1038/376415a0.

Hölting, B.; Haertlé, T.; Hohberger, K.-H.; Nachtigall, K. H.; Villinger, E.; Weinzierl, W. and Wrobel, J.-P. (1995): *Konzept zur Ermittlung der Schutzfunktion der Grundwasserüberdeckung [Concepts to determine the protective function of the groundwater cover]*. Stuttgart, Germany. Schweizerbart, 65 p. Available at: https://katalog.slub-dresden.de/id/0-1117363759 (accessed: 16/10/2015).

Hong, L.; Teng, M.; Xiucheng, T.; Wei, Z.; Guang, H.; Di, X.; Bing, L.; Shujiao, S. and Chengpeng, S. (2016): 'Origin of structurally controlled hydrothermal dolomite in epigenetic karst system during shallow burial: An example from Middle Permian Maokou Formation, central Sichuan Basin, SW China', *Petroleum Exploration and Development*, 43(6), p. 1000–1012. DOI: 10.1016/S1876-3804(16)30117-3.

Howard, A. D. (1963): 'The development of karst features', *Bulletin of the National Speleological Society*, 25, p. 45–65. Available at: https://erode.evsc.virginia.edu/papers/howard_karst_63.pdf (accessed: 21/11/2016).

Huan, H.; Wang, J.; Lai, D.; Teng, Y. and Zhai, Y. (2015): 'Assessment of well vulnerability for groundwater source protection based on a solute transport model: a case study from Jilin City, northeast China', *Hydrogeology Journal*, 23(3), p. 581–596. DOI: 10.1007/s10040-014-1211-4.

Huneau, F.; Jaunat, J.; Kavouri, K.; Plagnes, V.; Rey, F. and Dörfliger, N. (2013): 'Intrinsic vulnerability mapping for small mountainous karst aquifers, implementation of the new PaPRIKa method to Western Pyrenees (France)', *Engineering Geology*, 161, p. 81–93. DOI: 10.1016/j.enggeo.20-13.03.028.

INEGI (2013): 'Conjunto de datos vectoriales de la carta de Uso del suelo y Vegetación, serie V [Vegetation and land-use chart; vector data set, series V]'. Datasets. Available at: https://www.inegi.org.mx/temas/usosuelo/ (accessed: 31/01/2016).

INEGI (2007): 'Conjunto de datos vectoriales edafológicos serie II [Edaphology vector dataset series II]'. Datasets. Available at: https://www.inegi.org.mx/temas/edafologia/ (accessed: 31/01/2016).

INEGI (1984): 'Conjunto de datos vectoriales geológicos serie I [Geology vector data set series I]'. Datasets. Available at: https://www.inegi.org.mx/temas/geologia/ (accessed: 31/01/2016).

INEGI (2015): 'Conjunto de datos vectoriales topográficos serie III [Topography vector dataset series III]'. Datasets. Available at: https://www.inegi.org.mx/app/mapas/ (accessed: 31/01/2016).

INEGI (2016): 'Directorio Estadístico Nacional de Unidades Económicas (DENUE) [National statistical directory of economic units]'. Datasets. Available at: https://en.www.inegi.org.mx/app/-mapa/denue/ (accessed: 31/01/2016).

INEGI (2018): 'Informacion por entidad, Yucatán [Information by region, Yucatan]'. Website: cuentame.inegi.org.mx/monografias/informacion/yuc/default.aspx (accessed: 17/02/2018).

INEGI (2011): Panorama sociodemográfico de Yucatán [Social-demographic panorama of Yucatan]. Report. DF, Mexico. Instituto Nacional de Estadística y Geografia (INEGI), 234 p. Available at: https://www.inegi.org.mx/app/biblioteca/ficha.html?upc=702825 (accessed: 12/10/2015).

Isphording, W. C. (1975): 'The physical geology of Yucatan', *GCAGS Transactions. American Association of Petroleum Geologists (AAPG)*, 25, p. 231–262. Available at: https://archives.datapages.com/data-/gcags/data/025/025001/0231.htm (accessed: 23/09/2017).

IUSS Working Group WRB (2015): *World Reference Base for soil resources 2014. International soil classification system for naming soils and creating legends for soil maps. Update 2015*. World Soil Resources Reports No. 106. Rome, Italy. FAO, 192 p. Available at: http://www.fao.org/3/a-i3794en.pdf (accessed: 12/10/2017).

Iván, V. and Mádl-Szőnyi, J. (2017): 'State of the art of karst vulnerability assessment: overview, evaluation and outlook', *Environmental Earth Sciences*, 76:112, p. 1-25. DOI: 10.1007/s12665-017-6422-2.

Jeannin, P. Y.; Cornaton, F. and Zwahlen, F. (2001): 'VULK: a tool for intrinsic vulnerability assessment and validation', in: *Zwahlen, F. & Mudry, J. (Eds). Proceedings of the 7th Conference on Limestone Hydrology and Fissured Media*. Besançon, France. Sciences et techniques de l'environnement, p. 185–188.

Jenks, G. F. (1967): 'The Data Model Concept in Statistical Mapping', *International Yearbook of Cartography*, 7, p. 186–190.

Jennings, J. N. (1975): 'Doline morphometry as a morphogenetic tool: New Zealand examples', *New Zealand Geographer*, 31(1), p. 6–28. DOI: 10.1111/j.1745-7939.1975.tb00793.x.

Jennings, J. N. (1971): *Karst*. An introduction to systematic geomorphology, volume 7. Canberra, Australia. Australian National University Press, 252 p. Available at: https://openresearch-repository.anu.edu.au/bitstream/1885/114685/2/b13527940.pdf (accessed: 12/06/2017).

Jianhua, C.; Daoxian, Y.; Groves, C.; Fen, H.; Hui, Y. and Qian, L. (2012): 'Carbon fluxes and sinks: the consumption of atmospheric and soil CO_2 by carbonate rock dissolution', *Acta Geologica Sinica*, 86(4), p. 963–972. DOI: 10.1111/j.1755-6724.2012.00720.x.

Jiménez-Madrid, A.; Carrasco, F.; Martínez, C. and Gogu, R. (2013): 'DRISTPI, a new groundwater vulnerability mapping method for use in karstic and non-karstic aquifers', *Quarterly Journal of Engineering Geology and Hydrogeology*, 46(2), p. 245–255. DOI: 10.1144/qjegh2012-038.

Jones, W. K.; Culver, D. C. and Herman, J. S. (Eds). (2004): *Epikarst. Special Publication 9*. Proceedings of the 2003 Epikarst Symposium. Leesburg, USA. Karst Waters Institute, 160 p. Available at: https://karstwaters.org/publications/sp9-epikarst/ (accessed: 13/01/2018).

Kavouri, K.; Plagnes, V.; Tremoulet, J.; Dörfliger, N.; Rejiba, F. and Marchet, P. (2011): 'PaPRIKa: a method for estimating karst resource and source vulnerability - application to the Ouysse karst system (southwest France)', 19(2), p. 339–353. DOI: 10.1007/s10040-010-0688-8.

Kavousi, A.; Javadi, S.; Kardan Moghadam, H. and Mirarabi, A. (2018): 'Evaluation of Water Resources Exploitation in a Karst Region Using Intrinsic Vulnerability Assessment', *Water Harvesting Research*, 3(1 & 2), p. 53–68. DOI: 10.22077/JWHR.2019.1055.

Király, L. (1975): 'Rapport sur l'état actuel des connaissances dans le domaine des caractères physiques des roches karstiques [Report on the present knowledge on the physical characteristics of kartic rocks]', in: *Burger A. & Dubertret L. (Eds). Hydrogéologie des terrains karstiques*. Series B, no. 3. International Union of Geological Sciences, p. 53–67. Available at: https://doc.rero.ch-/record/260622 (accessed: 06/12/2015).

Klimchouk, A. (1995): 'Karst morphogenesis in the epikarstic zone', *Cave and Karst Science*, 21(2), p. 45–50. Available at: https://www.researchgate.net/publication/2927767 (accessed: 16/05/-2017).

Klimchouk, A. (1996): 'The dissolution and conversion of gypsum and anhydrite', *International Journal of Speleology*, 25(3), p. 21-36. DOI: 10.5038/1827-806X.25.3.2.

Klimchouk, A. (2000): 'The formation of epikarst and its role in vadose speleogenesis', in: *Klimchouk A., Ford D., Palmer A. & Dreybrodt, W. (Eds). Speleogenesis: evolution of karst aquifers*. Huntsville, USA. National Speleological Society, p. 91–99. Available at: https://katalog.slub-dresden.de/id/0-097730866 (accessed: 13/02/2016).

Klimchouk, A. (2004): 'Towards defining, delimiting and classifying epikarst: Its origin, processes and variants of geomorphic evolution', in: *Jones W. K., Culver D. C. & Herman J. S. (Eds). Epikarst. Special Publication 9*. Proceedings of the 2003 Epikarst Symposium. Leesburg, USA. Karst Waters Institute, p. 23–35. Available at: https://karstwaters.org/publications/sp9-epikarst/ (accessed: 13/01/2018).

Klimchouk, A. (2017): 'Types and settings of hypogene karst', in: *Klimchouk A., Palmer A. N., De Waele J., Auler A. S. & Audra P. (Eds). Hypogene karst regions and caves of the world*. Cave and Karst Systems of the World. Cham, Switzerland. Springer, p. 1–39. DOI: 10.1007/978-3-319-53348-3_1.

Klimchouk, A. and Ford, D. (2000): 'Types of karst and evolution of hydrogeologic settings', in: *Klimchouk A., Ford D., Palmer A. & Dreybrodt, W. (Eds). Speleogenesis: evolution of karst aquifers*. Huntsville, USA. National Speleological Society, p. 45–53. Available at: https://katalog.slub-dresden.de/id/0-097730866 (accessed: 13/02/2016).

Koutsi, R. and Stournaras, G. (2011): 'Groundwater vulnerability assessment in the Loussi polje area, N Peloponessus: the PRESK method', in: *Lambrakis N., Stournaras G. & Katsanou K. (Eds). Advances in the research of aquatic environment*. Berlin, Germany. Springer, p. 335–342. DOI: 10.1007/978-3-642-24076-8_39.

Kovacic, G. and Petric, M. (2007): 'Karst aquifer intrinsic vulnerability mapping in the Orehek area (SW Slovenia) using the EPIK method', in: *Witkowski A. J., Kowalczyk A. & Vrba J. (Eds). Groundwater vulnerability assessment and mapping. Selected papers from the groundwater vulnerability assessment and mapping international conference, Ustroń, Poland, 2004*. IAH-Selected Papers. London, UK. Taylor & Francis, p. 213–221. Available at: https://katalog.slub-dresden.de/id/0-1344280870 (accessed: 28/08/2017).

Kovács, A.; Perrochet, P.; Király, L. and Jeannin, P.-Y. (2005): 'A quantitative method for the characterisation of karst aquifers based on spring hydrograph analysis', *Journal of Hydrology*, 303(1–4), p. 152–164. DOI: 10.1016/j.jhydrol.2004.08.023.

Kralik, M. and Keimel, T. (2003): 'Time-input, an innovative groundwater-vulnerability assessment scheme: application to an alpine test site', *Environmental Geology*, 44(6), p. 679–686. DOI: 10.1007/s00254-003-0809-y.

Kresic, N. and Bonacci, O. (2009): ' Spring discharge hydrograph', in: *Kresic, N. & Stevanović, Z. (Eds). Groundwater hydrology of springs. Engineering, theory, management and sustainability*. Burlington, USA. Butterworth-Heinemann, p. 129-163. DOI: 10.1016/B978-1-85617-502-9.00004-9.

Krogulec, E. and Trzeciak, J. (2017): 'DRASTIC assessment of groundwater vulnerability to pollution in the Vistula floodplain in central Poland', *Hydrology Research*, 48(4), p. 1088–1099. DOI: 10.2166/nh.2016.259.

Langevin, C. D.; Hughes, J. D.; Banta, E. R.; Niswonger, R. G.; Panday, S. and Provost, A. M. (2017): *Documentation for the MODFLOW 6 groundwater flow model*. Techniques and Methods, book 6, chap. A55. Reston, USA. US Geological Survey, 197 p. DOI: 10.3133/tm6A55.

Laudermilk, J. D. and Woodford, A. O. (1932): 'Concerning rillensteine', *American Journal of Science*, (134), p. 135–154. DOI: 10.2475/ajs.s5-23.134.135.

LeGrand, H. E. (1983): 'Perspective on karst hydrology', *Journal of Hydrology*, 61(1–3), p. 343–355. DOI: 10.1016/0022-1694(83)90257-3.

Lesser, J. M. (1976): *Resumen del estudio hidrogeológico e hidrogeoquímico de la Peninsula de Yucatán [Summary of the hydrogeological and hydrochemical study of the Yucatan Peninsula]*. Secretaría de Recursos Hidráulicos (SRH) Bulletin no. 10. Available at: http://www.lesser.com.mx/files/76-4-Resumen-Estudio-Geohidrologico-Yucatan.pdf (accessed: 12/11/2016).

Lesser, J. M. and Weidie, A. E. (1988): 'Region 25, Yucatan Peninsula', in: *Back W., Rosenhein J. S. & Seaber P. R. (Eds). Hydrogeology. The Geology of North America.* Boulder, USA. Geological Society of North America, p. 237–241. DOI: 10.1130/DNAG-GNA-O2.

Leyland, R. C. and Witthüser, K. T. (2010): 'VUKA: a modified COP vulnerability mapping method for karst terrains in South Africa', *Quarterly Journal of Engineering Geology and Hydrogeology*, 43(1), p. 107–116. DOI: 10.1144/1470-9236/08-075.

Liedl, R.; Sauter, M.; Hückinghaus, D.; Clemens, T. and Teutsch, G. (2003): 'Simulation of the development of karst aquifers using a coupled continuum pipe flow model', *Water Resources Research*, 39(3). DOI: 10.1029/2001WR001206.

Lodwick, W. A.; Monson, W. and Svoboda, L. (1990): 'Attribute error and sensitivity analysis of map operations in geographical informations systems: suitability analysis', *International Journal of Geographical Information System*, 4(4), p. 413–428. DOI: 10.1080/02693799008941556.

Loehnert, E. P. and Papakonstantinou, A. (1988): 'Relationship between karst and porous aquifers on the Chalkidiki Peninsula, Greece', in: *Proceedings of the 21st Congress of the IAH. Karst Hydrogeology and Karst Environment Protection*. Guilin, China. IAHS Press, p. 321–326. Available at: http://hydrologie.org/redbooks/a176/iahs_176_0321.pdf (accessed: 02/04/2017).

López-Ramos, E. (1975): 'Geological summary of the Yucatan Peninsula', in: *Nair, A. & Stehli F. G. (Eds). The Gulf of Mexico and the Caribbean*. The ocean basins and margins. Boston, USA. Springer, p. 257–282. DOI: 10.1007/978-1-4684-8535-6_7.

Lugo-Hubp, J.; Aceves-Quesado, J. F. and Espinosa-Pereño, R. (1992): 'Rasgos geomorfológicos mayores de la península de Yucatán [Major geomorphological features of the Yucatan peninsula]', *Revista Mexicana de Ciencias Geológicas*, 10(2), p. 143–150. Available at: https://dialnet.unirioja.es/servlet/articulo?codigo=2231919 (accessed: 28/06/2017).

Lugo-Hubp, J. and García, M. (1999): 'El relieve de la península de Yucatán [The Yucatan Peninsula relief]', in: *Atlas de procesos territoriales de Yucatán*. Merida, Mexico. Facultad de Arquitectura, Universidad Autonoma de Yucatan (UADY), p. 159–162.

Lvovitch, M. I. (1973), 'The global water balance', Eos Trans. AGU, 54 (1), p. 28–53. DOI:10.1029/EO054i001-p00028.

Ly, S.; Charles, C. and Degré, A. (2013): 'Different methods for spatial interpolation of rainfall data for operational hydrology and hydrological modeling at watershed scale: a review', *Biotechnologie, Agronomie, Société et Environnement*, 17(2), p. 392–406. Available at: http://hdl.handle.net/2268/136084 (accessed: 04/03/2017).

Magiera, P. (2000): 'Methoden zur Abschätzung der Verschmutzungsempfindlichkeit des Grundwassers [Methods for estimating the sensitivity of groundwater to pollution]', *Grundwasser*, 5(3), p. 103–114. DOI: 10.1007/s767-000-8357-1.

Malczewski, J. (1999): *GIS and multicriteria decision analysis*. New York, USA. Wiley, 392 p. Available at: https://katalog.slub-dresden.de/id/0-249746727 (accessed: 11/07/2016).

Malczewski, J. (2006): 'GIS-based multicriteria decision analysis: a survey of the literature', *International Journal of Geographical Information Science*, 20(7), p. 703–726. DOI: 10.1080/1365881060066-1508.

Malík, P. and Švasta, J. (1999): 'REKS: an alternative method of karst groundwater vulnerability estimation', in: *Fendekova M. and Fendek M. (Eds). Hydrogeology and Land Use Management*. Proceeding of the XXIX Congress of the International Association of Hydrogeologists. Bratislava, Slovakia. p. 79–85. DOI: 10.13140/2.1.2919.7766

Mangin, A. (1975): *Contribution à l'étude hydrodynamique des aquifères karstiques [Contributions to the hydrodynamics of karst aquifers]*, Doctoral thesis, Dijon, France. Université Dijon, 268 p. Available at: https://hal.archives-ouvertes.fr/tel-01575806 (accessed: 07/08/2017).

Marín, A.; Dörfliger, N. and Andreo, B. (2012): 'Comparative application of two methods (COP and PaPRIKa) for groundwater vulnerability mapping in Mediterranean karst aquifers (France and Spain)', *Environmental Earth Sciences*, 65(8), p. 2407–2421. DOI: 10.1007/s12665-011-1056-2.

Marín, L. E. (1990): *Field investigations and numerical simulation of groundwater flow in the karstic aquifer of northwestern Yucatan, Mexico.* Doctoral thesis, Dekalb, USA. Northern Illinois University.

Marín, L. E.; Perry, E. C.; Essaid, H. I. and Steinich, B. (2003): 'Hydrogeological investigations and numerical simulation of groundwater flow in the karstic aquifer of northwestern Yucatan, Mexico', in: *Cheng A. H-D. & Ouazar D. (Eds). Coastal aquifer management. Monitoring, modeling, and case studies*. Boca Raton, USA. CRC Press, p. 257–275. DOI: 10.1201/9780203493496.

Marín, L. E.; Steinich, B.; Pacheco, J. and Escolero, O. A. (2000): 'Hydrogeology of a contaminated sole-source karst aquifer, Mérida, Yucatán, Mexico', *Geofísica Internacional*, 39(4), p. 359–365. Available at: https://www.redalyc.org/articulo.oa?id=56839406 (accessed: 22/10/2017).

Marker, M. E. and Swart, P. G. (1995): 'Pseudokarst in the Western Cape, South Africa: its paleoenvironmental significance', in: *Gunn J. & Lowe D. (Eds). Cave and Karst Science. The Transactions of the British Cave Research Association*, 22(1), p. 31–38. Available at: https://bcra.org.uk/pub/candks/catalogue.html (accessed:05/10/2017).

Martínez-Salvador, C. (2018): *Estimation of pollutant residence time and its inclusion in vulnerability assessment approaches for the Yucatan karst system in Mexico*, Master thesis, Dresden, Germany. Dresden University of Technology.

Martínez-Salvador, C.; Moreno-Gómez, M. and Liedl, R. (2019): 'Estimating pollutant residence time and NO_3^- concentrations in the Yucatan karst aquifer; considerations for an integrated karst aquifer vulnerability methodology', *Water*, 11(7). DOI: 10.3390/w11071431.

McDonald, M. C. and Harbaugh, A. W. (1988): *A modular three-dimensional finite difference groundwater flow model*. Techniques of Water-Resources Investigations 06-A1. Washington, USA. US Geological Survey, 586 p. DOI: 10.3133/twri06A1.

McLaren, R. (1991): *Program Aquifer 2-D aquifer model*. Software, FORTRAN source code. Waterloo, Canada. Waterloo Center for Groundwater Research.

Méndez-Novelo, R.; Castillo-Borges, E.; Vázquez-Borges, E.; Briceño-Pérez, O.; Coronado-Peraza, V.; Pat-Canul, R. and Garrido-Vivas, P. (2009): 'Estimación del potencial contaminante de las granjas porcinas y avícolas del estado de Yucatán [Estimation of the polluting potential from pig and poultry farms in the Yucatan state]', *Ingeniería*, 13(2), p. 13–21. Available at: https://www.redalyc.org/articulo.oa?id=46713053002 (accessed: 12/11/2017).

Mihevc, A. and Prelovšek, M. (2010): in: *Mihevc, A.; Prelovšek, M. and Hajna, S. H. (Eds). Introduction to the Dinaric Karst*. Pstonija, Slovenia. Karst Research Institute at ZRC SAZU. Available at: https://www.researchgate.net/publication/261884078 (accessed: 24/10/2017).

Milanović, P. (2004a): 'Dinaride Poljes', in: *Gunn J. (Ed). Encyclopedia of Caves and Karst Science*. London, UK. Fitzroy Dearborn, p. 599–603. DOI: 10.4324/9780203483855.

Milanović, P. (2004b): *Water resources engineering in karst*. Boca Raton, USA. CRC press, 328 p. DOI: 10.1201/9780203499443.

Milanović, S.; Stevanović, Z.; Đurić, D.; Petrović, T. and Milovanović, M. (2010): 'Regionalni pristup izradi karte ugroženosti podzemnih voda Srbije – nova metoda "IZDAN" [Regional approach in creating groundwater vulnerability map of Serbia – a new method „IZDAN"]', in: *Proceedings of XV Geological Congress of Serbia*. Belgrade, Serbia. Serbian Geological Society, p. 585–590.

Mimi, Z. A.; Mahmoud, N. and Madi, M. A. (2012): 'Modified DRASTIC assessment for intrinsic vulnerability mapping of karst aquifers: a case study', *Environmental Earth Sciences*, 66(2), p. 447–456. DOI: 10.1007/s12665-011-1252-0.

Moreno-Gómez, M.; Liedl, R. and Stefan, C. (2019a): 'A New GIS-Based Model for Karst Dolines Mapping Using LiDAR; Application of a Multidepth Threshold Approach in the Yucatan Karst, Mexico', *Remote Sensing*, 11:1147, 14 p. DOI: 10.3390/rs11101147.

Moreno-Gómez, M.; Martínez-Salvador, C.; Moulahoum, A.-W.; Liedl, R.; Stefan, C. and Pacheco, J. (2019b): 'First Steps into an Integrated Karst Aquifer Vulnerability Approach (IKAV) Intrinsic Groundwater Vulnerability Analysis of the Yucatan Karst, Mexico', *Water*, 11(8),1610. 18 p. DOI: 10.3390/w11081610.

Moreno-Gómez, M.; Pacheco, J.; Liedl, R. and Stefan, C. (2018): 'Evaluating the applicability of European karst vulnerability assessment methods to the Yucatan karst, Mexico', *Environmental Earth Sciences*, 77:682. 13 p. DOI: 10.1007/s12665-018-7869-5.

Morris, B. L.; Lawrence, A. R. and Stuart, M. E. (1994): *The impact of urbanisation on groundwater quality (project summary report)*. Technical Report: WC 94/56. Nottingham, UK. British Geological Survey, 54 p. Available at: http://nora.nerc.ac.uk/id/eprint/502681/1/WC_94_56.pdf.

Napolitano, P. and Fabbri, A. (1996): 'Single-parameter sensitivity analysis for aquifer vulnerability assessment using DRASTIC and SINTACS', in: *Kovar K. & Nachtnebel H. P. (Eds). Application of geographic information systems in hydrology and water resources management*. Proceedings of the HydroGIS 96 Conference. Vienna, Austria. IAHS, p. 559–566. Available at: http://hydrologie.org/redbooks/a235/iahs_235_0559.pdf (accessed: 18/06/2016).

NASA JPL (2013): *NASA Shuttle Radar Topography Mission Global 1 arc second [Data set]*. NASA EOSDIS Land Processes DAAC. DOI: 10.5067/MEaSUREs/SRTM/SRTMGL1.003.

NASA, METI, AIST, Japan Spacesystems and U.S./Japan ASTER Science Team (2019): *ASTER Global Digital Elevation Model V003 [data set]*. NASA EOSDIS Land Processes DAAC. DOI: 10.5067/ASTER/ASTGTM.003.

National Research Council (1993): *Ground water vulnerability assessment: Predicting relative contamination potential under conditions of uncertainty*. Washington, USA. National Academy Press, 224 p. DOI: 10.17226/2050.

Nguyet, V. T. M. and Goldscheider, N. (2006): 'A simplified methodology for mapping groundwater vulnerability and contamination risk, and its first application in a tropical karst area, Vietnam', *Hydrogeology Journal*, 14(8), p. 1666–1675. DOI: 10.1007/s10040-006-0069-5.

Pacheco, J. (2004): Delimitación de una zona de reserva hidrogeológica para el abastecimiento de agua potable a la ciudad de Mérida [Delimitation of a hydrogeological reserve area for the supply of drinking water to the city of Mérida]. *Ingeniería* 8(1), p. 7-16. Available at: https://www.revista.ingenieria.uady.mx/volumen8/-delineacion.pdf (accessed: 15/09/2016).

Pacheco, J. (2003): *Determinación y prueba de un índice de contaminación por nitratos en el acuífero cárstico de Yucatán, México [Determination and testing of a nitrate contamination index in the Yucatan krast aquifer, Mexico]*. Technical report. Merida, Mexico. Yucatan Autonomous University.

Pacheco, J. (1994): *Impacto del uso del suelo en las concentraciones de nitratos del agua subterránea en el estado de Yucatán [Impact of land use on nitrate concentrations in groundwater in the Yucatan State]*. Technical report. Merida, Mexico. Yucatan Autonomous University.

Pacheco, J. and Cabrera, A. (1997): 'Groundwater contamination by nitrates in the Yucatan Peninsula, Mexico', *Hydrogeology Journal*, 5(2), p. 47–53. DOI: 10.1007/s100400050113.

Pacheco, J.; Cabrera, A.; Steinich, B.; Frías, J.; Coronado, V. and Vázquez, J. (2002): 'Efecto de la aplicación agrícola de la excreta porcina en la calidad del agua subterránea [Effect of agricultural application of porcine excreta on groundwater quality]', *Ingeniería*, 6(3), p. 7–17. Available at: https://www.redalyc.org/articulo.oa?id=46760301 (accessed: 16/09/2016).

Pacheco, J. and Cabrera, S. (2013): *Calidad del agua subterranea en el estado de Yucatán después del huracán Isidore (2002) [Groundwater quality in the state of Yucatan after Hurricane Isidore (2002)]*. Mérida, México. Fondo Mixto de Fomento a la Investigación Científica y Tecnológica CONACYT-Gobierno del Estado de Yucatán (FOMIX) Convocatoria 2002-01.

Pacheco, J.; Marín, L.; Cabrera, A.; Steinich, B. and Escolero, O. (2001): 'Nitrate temporal and spatial patterns in 12 water-supply wells, Yucatan, Mexico', *Environmental Geology*, 40(6), p. 708–715. DOI: 10.1007/s002540000180.

Pacheco-Ávila, J.; Cabrera-Sansores, A. and Pérez-Ceballos, R. (2004a): 'Diagnóstico de la calidad del agua subterránea en los sistemas municipales de abastecimiento en el Estado de Yucatán, México [Diagnosis of groundwater quality from municipal supply systems in the State of Yucatan, Mexico]', *Ingeniería*, 8(2), p. 165–179. Available at: https://www.revista.ingenieria.-uady.mx/-volumen8/diagnostico.pdf (accessed: 16/09/2016).

Pacheco-Ávila, J.; Calderón-Rocher, L. and Cabrera-Sansores, A. (2004b): 'Delineación de la zona de protección hidrogeológica para el campo de pozos de la planta Mérida I, en la ciudad de Mérida, Yucatán, México [Delineation of the hydrogeological protection zone for the well field "Mérida I", in the city of Mérida, Yucatán, México]', *Ingeniería*, 8(1), p. 7–16. Available at: https://www.revista.ingenieria.uady.mx/volumen8/delineacion.pdf (accessed: 16/09/2016).

Palmer, A. N. (1991): 'Origin and morphology of limestone caves', *Geological Society of America Bulletin*, 103(1), p. 1–21. DOI: 10.1130/0016-7606(1991)103%3c0001:OAMOLC%3e2.3.CO;2.

Palmer, A. N. and Palmer, M. V. (1995): 'The Kaskaskia paleokarst of the northern Rocky Mountains and Black Hills, northwestern USA', *Carbonates and Evaporites*, 10(2), p. 148-160. DOI: 10.1007/BF03175400.

Panagopoulos, G. P.; Antonakos, A. K. and Lambrakis, N. J. (2006): 'Optimization of the DRASTIC method for groundwater vulnerability assessment via the use of simple statistical methods and GIS', *Hydrogeology Journal*, 14(6), p. 894–911. DOI: 10.1007/s10040-005-0008-x.

Parise, M.; Qiriazi, P. and Sala, S. (2008): 'Evaporite karst of Albania: main features and cases of environmental degradation', *Enviromental Geology*, 53, p. 967–974. DOI: 10.1007/s00254-007-0722-x.

Parise, M.; Qiriazi, P. and Sala, S. (2004): 'Natural and anthropogenic hazards in karst areas of Albania', *Natural Hazards and Earth System Sciences*, 4, p. 569–581. DOI: 10.5194/nhess-4-569-2004.

Peel, M.; Finlayson, P. L. and McMahon, T. A. (2007): 'Updated world map of the Köppen-Geiger climate classification', *Hydrology and Earth System Sciences*, 11, p. 1633–1644. DOI: 10.5194/hess-11-1633-2007.

Péntek, K.; Veress, M. and Lóczy, D. (2007): 'A morphometric classification of solution dolines', *Zeitschrift für Geomorphologie*, 51(1), p. 19–30. DOI: 10.1127/0372-8854/2007/0051-0019.

Pérez-Ceballos, R. (2004): *Vulnerabilidad del agua subterránea a la contaminación de nitratos en el estado de Yucatán [Groundwater vulnerability to Nitrate pollution in the Yucatan State]*, Master thesis, Merida, Mexico. Yucatan Autonomous University.

Perrin, J.; Jeannin, P.-Y. and Zwahlen, F. (2003): 'Epikarst storage in a karst aquifer: a conceptual model based on isotopic data, Milandre test site, Switzerland', *Journal of Hydrology*, 279(1–4), p. 106–124. DOI: 10.1016/S0022-1694(03)00171-9.

Perry, E.; Marín, L. E.; McClain, J. and Velázquez, G. (1995): 'Ring of cenotes (sinkholes), northwest Yucatan, Mexico: its hydrogeologic characteristics and possible association with the Chicxulub impact crater', *Geology*, 23(1), p. 17–20. DOI: 10.1130/0091-7613(1995)023<0017:ROCSNY>2.3.CO;2.

Perry, E.; Swift, J.; Gamboa, J.; Reeve, A.; Sanborn, R.; Marín, L. and Villasuso, M. (1989): 'Environmental aspects of surface cementation, north coast, Yucatan, Mexico', *Geology*, 17, p. 818–821. DOI: 10.1130/0091-7613(1989)017<0818:GAEAOS>2.3.CO;2.

Petelet-Giraud, E.; Doerfliger, N. and Crochet, P. (2000): 'RISKE: Méthode d'évaluation multicritère de la vulnérabilité des aquifères karstiques Application aux systèmes des Fontanilles et Cent-Fonts (Hérault, Sud de la France) [RISKE: multicriteria assessment of karstic aquifer vulnerability mapping Application to the Fontanilles and Cent-Fonts karstic aquifers (Herault, S France)]', *Hydrogéologie*, (4), p. 71–88. Available at: https://www.researchgate.net/publication/280984851 (accessed: 06/09/2016).

Plagnes, V.; Théry, S.; Fontaine, L.; Bakalowicz, M. and Dörfliger, N. (2005): 'Karst vulnerability mapping: improvement of the RISKE method', in: *Water resources and environmental problems in Karst*. Proceedings of the International conference and field seminars, Belgrade/Kotor, Serbia and Montenegro, 13-19 September 2005. Belgrade, Serbia. Faculty of Mining and Geology, Institute of Hydrogeology, p. 123–140.

Pollock, D. (2016): *User guide for MODPATH Version 7. A particle-tracking model for MODFLOW*. Open-File Report 2016-1086. Reston, USA. U.S. Geological Survey, 35 p. DOI: 10.3133/ofr20161086.

Pope, K. O.; Ocampo, A. C. and Duller, C. E. (1991): 'Mexican site for K/T impact crater?', *Nature*, 351(6322), p. 105–105. DOI: 10.1038/351105a0.

Pope, K. O.; Ocampo, A. C. and Duller, C. E. (1993): 'Surficial geology of the Chicxulub impact crater, Yucatan, Mexico', *Earth, Moon, and Planets*, 63(2), p. 93–104. DOI: 10.1007/BF00575099.

Quinlan, J. F. (1978): *Types of karst with emphasis on cover beds in their classification and development*, Doctoral thesis, Austin, USA. University of Texas.

Raines, G. L.; Bonham-Carter, G. F. and Kemp, L. (2000): 'Predictive probabilistic modeling using ArcView GIS', *ArcUser*, 3(2), p. 45–48. Available at: https://www.esri.com/news/arcuser/0400/apjn2000 (accessed: 18.03.2016).

Ramírez-Cancino, L. and Rivera-Lorca, J. A. (2010): 'La ganadería en el contexto de la biodiversidad [Livestock farming in a biodiversity context]', in: *Durán-García R. & Méndez-González M. E. (Eds). Biodiversidad y desarrollo humano en Yucatán [Biodiversity and human development in Yucatan]*. Merida, Mexico. CICY-CONABIO-SEDUMA, p. 106–108. Available at: https://bibliotecasibe.ecosur.mx/sibe/book/000050517 (accessed: 15/04/2017).

Ravbar, N. and Goldscheider, N. (2009): 'Comparative application of four methods of groundwater vulnerability mapping in a Slovene karst catchment', *Hydrogeology Journal*, 17(3), p. 725–733. DOI: 10.1007/s10040-008-0368-0.

Ravbar, N. and Goldscheider, N. (2007): 'Proposed methodology of vulnerability and contamination risk mapping for the protection of karst aquifers in Slovenia', *Acta Carsologica*, 36(3), p. 397–411. DOI: 10.3986/ac.v36i3.174.

Redondo-Vega, J. M.; Alonso-Herrero, E.; Santos-González, J.; González-Gutiérrez, R. B. and Gómez-Villar, A. (2015): 'La Balouta exhumed karst: a Roman gold-mine-derived landscape within the Las Médulas UNESCO World Heritage Site (Spain)', *International Journal of Speleology*, 44(3), p. 267–276. DOI: 10.5038/1827-806X.44.3.5.

Reeve, A. and Perry, E. C. (1990): 'Aspects and tidal analysis along the western north coast of the Yucatan Peninsula, Mexico', in: AWRA International Symposium on Tropical Hydrogeology, San Juan, Puerto Rico.

Reimann, T. and Hill, M. E. (2009): 'MODFLOW-CFP: A new conduit flow process for MODFLOW–2005', *Groundwater*, 47(3), p. 321–325. DOI: 10.1111/j.1745-6584.2009.00561.x.

Roglic, J. (1964): '"Karst Valleys" in the Dinaric Karst', *Erdkunde*, p. 113–116. Available at: https://www.jstor.org/stable/25640118 (accessed: 13/05/2016).

Rojas-Fabro, A. Y.; Pacheco-Ávila, J. G.; Esteller-Alberich, M. V.; Cabrera-Sansores, S. A. and Camargo-Valero, M. A. (2015): 'Spatial distribution of nitrate health risk associated with groundwater use as drinking water in Merida, Mexico', *Applied Geography*, 65, p. 49–57. DOI: 10.1016/j.apgeog.2015.10.004.

Różkowski, J. (2007): 'Evaluation of intrinsic vulnerability of an Upper Jurassic karst-fissured aquifer in the Jura Krakowska (southern Poland) to anthropogenic pollution using the DRASTIC method', *Geological Quarterly*, 51(1), p. 17–26. available at: https://moam.info/geol-quart-51-1-ostat-1_5b9af8d2097c477c588b471c.html (accessed: 03/04/2017).

Saaty, T. L. (2008): 'Decision making with the analytic hierarchy process', *International Journal of Services Sciences*, 1(1), p. 83–98. DOI: 10.1504/IJSSci.2008.01759.

Sackl, P.; Dervović, I.; Kotrošan, D.; Topić, G.; Drocić, S.; Šarac, M.; Sarajlić, N.; Durst, R. and Stumberger, B. (2014): 'The distribution and population numbers of Corncrakes Crex crex in the karst poljes of Bosnia-Herzegovina Rresults of a large-scale survey in 2012 and 2013', in: *Sackl P., Durst R., Kotrošan D. & Stumberger B. (Eds). Dinaric karst Poljes - Floods for Life*. Radolfzell, Germany. EuroNatur foundation, p. 91–103. Available at: https://www.euronatur.org/fileadmin/-docs/docs_english/KRASKA_POLJA.pdf (accessed: 08/05/2017).

Salathé, T. (2014): 'Wetlands in drylands: the global importance of Karst poljes', in: *Sackl P., Durst R., Kotrošan D. & Stumberger B. (Eds). Dinaric karst Poljes - Floods for Life*. Radolfzell, Germany. EuroNatur foundation, p. 11–15. Available at: https://www.euronatur.org/fileadmin/docs/-docs_english/KRASKA_POLJA.pdf (accessed: 08/05/2017).

Salomon, J. N.; Pomel, S. and Nicod, J. (1995): 'L'évolution des cryptokarst: comparaison entre le Périgord-Quercy (France) et le Franken Alb (Allemagne) [The evolution of cryptokarst: comparison between Périgord-Quercy (France) and Franken Alb (Germany)]', *Zeitschrift für Geomorphologie*, 39(3), p. 381–409. DOI: 10.1127/zfg/39/1995/381.

Sánchez, I. (1999): *Modelo numérico del flujo subterráneo de la porción acuífera N-NW del Estado de Yucatán: implicaciones hidrogeológicas [Groundwater flow numerical model of the N-NW aquifer sector of the state of Yucatan: hydrogeological implications]*, Master thesis, Chihuahua, México. Chihuahua Autonomous University.

SARH (1989): *Sinópsis Geohidrológica del Estado de Yucatán [Geohydrologic synopsis of the State of Yucatan]*. DF, Mexico. Secretaría de Agricultura y Recursos Hidráulicos. Subsecretaría de Infraestructura Hidráulica. Dirección General de Administración y Control de Sistemas Hidrológicos.

Sauro, U. (2016): 'Dolines and sinkholes: aspects of evolution and problems of classification', *Acta Carsologica*, 32(2), p. 41–52. DOI: 10.3986/ac.v32i2.335.

Saxton, K. and Rawls, W. (2006): 'Soil water characteristic estimates by texture and organic matter for hydrologic solutions', *Soil Science Society of America Journal*, 70(5), p. 1569–1578. DOI: 10.2136/sssaj2005.0117.

Saxton, K.; Rawls, W.; Romberger, J. and Papendick, R. (1986): 'Estimating generalized soil-water characteristics from texture', *Soil Science Society of America Journal*, 50(4), p. 1031–1036. DOI: 10.2136/sssaj1986.03615995005000040039x.

Schneider, S. H., Root, T. L. and Mastrandrea, M. D. (Eds) (2011): *Encyclopedia of climate and weather 2nd Edition*. New York, USA. Oxford University Press, 1488 p. DOI: 10.1093/acref/9780199765324.-001.0001.

Schürch, M. and Buckley, D. (2002): 'Integrating geophysical and hydrochemical borehole-log measurements to characterize the Chalk aquifer, Berkshire, United Kingdom', *Hydrogeology Journal*, 10(6), p. 610–627. DOI: 10.1007/s10040-002-0220-x.

SEDUMA (2010): *Zona metropolitana de Merida [Merida metropolitan area]*. Report. Secretaría de Desarrollo Urbano y Medio Ambiente (SEDUMA), 54 p. Gobierno del Estado de Yucatán. Available at: http://acervo.-yucatan.gob.mx/contenidos/ZonaMetropolitaadeMerida.pdf (accessed: 14/11/2015).

Shiklomanov, I. A. (1993): 'World freshwater resources', in: *Gleick P. H. (Ed). Water in crisis: A guide to the world's freshwater resources*. New York, USA. Oxford University Press, p. 13–24. Available at: https://katalog.slub-dresden.de/id/0-110445007 (accessed: 27/03/2018).

Shoemaker, W. B.; Kuniansky, E. L.; Birk, S.; Bauer, S. and Swain, E. D. (2007): *Documentation of a conduit flow process (CFP) for MODFLOW-2005*. Techniques and Methods 6-A24. Reston, USA. US Geological Survey, 50 p. DOI: 10.3133/tm6A24.

Şimşek, C.; Kaya, B.; Alkan, A.; Büyüktopçu, F.; Türk, N. and Arisoy, Y. (2015): 'Hydrology and hydrochemistry of marble aquifer with point recharge from two deep sinkholes, Menderes Massive, western Turkey', *Acta Carsologica*, 44(2), p. 205-214. DOI: 10.3986/ac.v44i2.673.

Slabe, T. and Liu, H. (2009): 'Significant subsoil rock forms', in: *Ginés A., Knez M., Slabe T. & Dreybrodt W. (Eds). Karst rock features. Karren sculpturing*. Carsologica. Ljubljana, Slovenia. Založba ZRC, p. 123–137. DOI: 10.3986/9789610502968.

SMN (2017): 'Datos climáticos diarios del CLICOM del SMN a través de su plataforma web del CICESE [Daily climate data from the CLICOM of the SMN through its CICESE web platform]'. Datasets. Website: http://clicom-mex.cicese.mx (accessed: 06/10/2017).

Sotornikova, R. and Vrba, J. (1987): 'Some remarks on the concept of vulnerability maps', in: *van Duijvenbooden W. & van Waegeningh H. G. (Eds). Vulnerability of soil and groundwater to pollutants*. The Hague, Netherlands. TNO committee on hydrological research, p. 39–43.

Steinich, B. (1996): *Investigaciones geofísicas e hidrogeológicas en el noroeste de la Península de Yucatán, México [Geophysical and hydrogeological investigations in the northwest peninsula of Yucatan, Mexico]*. Doctoral Thesis, DF, Mexico. National Autonomous University of Mexico (UNAM).

Steinich, B. and Marín, L. (1996): 'Hydrogeological investigations in northwestern Yucatan, Mexico, using resistivity surveys', *Groundwater*, 34(4), p. 640–646. DOI: 10.1111/j.1745-6584.1996.tb02051.x.

Steinich, B. and Marín, L. E. (1997): 'Determination of flow characteristics in the aquifer of the Northwestern Peninsula of Yucatan, Mexico', *Journal of Hydrology*, 191(1–4), p. 315–331. DOI: 10.1016/S0022-1694(96)03038-7.

Stevanović, Z. (2015): 'Characterization of Karst Aquifer', in: *Stevanović, Z. (Ed). Karst aquifers-characterization and engineering*. Professional Practice in Earth Sciences Series. Sophia, Bulgaria. Springer, p. 47-125. DOI: 10.1007/978-3-319-12850-4_3.

Stevanović, Z.; Ristić-Vakanjac, V.; Milanović, S.; Vasić, L.; Petrović, B. and Čokorilo-Ilić, M. (2015): 'Karstification depth and storativity as main factors of karst aquifer regimes: some examples from southern Alpine branches (SE Europe and Middle East)', *Environmental Earth Sciences*, 74(1), p. 227–240. DOI: 10.1007/s12665-015-4046-y.

Stokes, T.; Griffiths, P. and Ramsey, C. (2010): 'Karst geomorphology, hydrology, and management', in: *Pike R. G., Redding T. E., Moore R. D., Winkler R. D. & Bladon K. D. (Eds). Compendium of forest hydrology and geomorphology in British Columbia, Vol. 1*. Land Management Handbook 66. British Columbia. Government Publications Services, p. 373–400. Available at: https://www.for.gov.bc.ca/hfd/pubs/Docs/Lmh/Lmh66.htm (accessed: 23/07/2016).

Taheri, K.; Taheri, M. and Mohsenipour, F. (2015): 'LEPT, a simplified approach for assessing karst vulnerability in regions by sparse data: a case in Kermanshah province, Iran', in: *Doctor D. H., Land L. & Stephenson J. B. (Eds). Sinkholes and the engineering and environmental impacts of karst: proceedings of the 14th multidisciplinary conference*. Carlsbad, USA. National Cave and Karst Research Institute, p. 483–492. Available at: https://digital.lib.usf.edu/SFS0053749/00001 (accessed: 28/03/2017).

Taviani, M.; Angeletti, L.; Campiani, E.; Ceregato, A.; Foglini, F.; Maselli, V.; Morsilli, M.; Parise, M. and Trincardi, F. (2012): 'Drowned karst landscape offshore the Apulian margin (southern Adriatic Sea, Italy)', *Journal of Cave and Karst Studies*, 74(2), p. 197-212. DOI: 10.4311/2011JCKS0204.

Tayer, T. de C. and Velásques, L. N. M. (2017): 'Assessment of intrinsic vulnerability to the contamination of karst aquifer using the COP method in the Carste Lagoa Santa Environmental Protection Unit, Brazil', *Environmental Earth Sciences*, 76:445, p. 1-13. DOI: 10.1007/s12665-017-6760-0.

Theilen-Willige, B.; Malek, A. H.; Charif, A.; El Bchari, F. and Chaïbi, M. (2014): 'Remote sensing and GIS contribution to the investigation of karst landscapes in NW-Morocco', *Geosciences*, 4(2), p. 50–72. DOI: 10.3390/geosciences4020050.

UADY (2006): *Fase 1. Caracterización del Municipio de Mérida [Phase 1. characterization of the Merida municipality]*. Technical report. Merida, Mexico. Yucatan Autonomous University (UADY), 241 p. Available at: http://bitacoraordenamiento.yucatan.gob.mx/archivos/2007020637 (accessed: 02/05/2016).

Vega, F. and Romero, H. L. (1987): 'Daños y soluciones ecológicas en las granjas porcinas [Damage and ecological solutions in pig farms]', *Porcirama*, II(131), p. 62–67.

Veress, M. (2010): *Karst environments: karren formation in high mountains*. Dordrecht, Netherlands. Springer, 230 p. DOI: 10.1007/978-90-481-3550-9.

Veress, M. (2009): 'Wandkarren', in: *Ginés A., Knez M., Slabe T. & Dreybrodt W. (Eds). Karst rock features. Karren sculpturing*. Carsologica. Ljubljana, Slovenia. Založba ZRC, p. 237–248. DOI: 10.3986/9789610502968.

Veress, M.; Samu, S. and Mitre, Z. (2015): 'The effect of slope angle on the development of type a and type b channels of rinnenkarren with field and laboratory measurements', *Geomorphology*, 228, p. 60–70. DOI: 10.1016/j.geomorph.2014.08.014.

Veress, M. and Tóth, G. (2004): 'Types of meandering karren', *Zeitschrift für Geomorphologie*, 48(1), p. 53–77. DOI: 10.1127/zfg/48/2004/53.

Vías, J. M.; Andreo, B.; Perles, M. J. and Carrasco, F. (2005): 'A comparative study of four schemes for groundwater vulnerability mapping in a diffuse flow carbonate aquifer under Mediterranean climatic conditions', *Environmental Geology*, 47(4), p. 586–595. DOI: 10.1007/s00254-004-1185.

Vías, J. M.; Andreo, B.; Perles, M. J.; Carrasco, F.; Vadillo, I. and Jiménez, P. (2006): 'Proposed method for groundwater vulnerability mapping in carbonate (karstic) aquifers: the COP method', *Hydrogeology Journal*, 14(6), p. 912–925. DOI: 10.1007/s10040-006-0023-6.

Viles, H. (2009): 'Biokarstic processes associated with karren development', in: *Ginés A., Knez M., Slabe T. & Dreybrodt W. (Eds). Karst rock features. Karren sculpturing*. Carsologica. Ljubljana, Slovenia. Založba ZRC, p. 37–46. DOI: 10.3986/9789610502968 .

Villasuso, M.; González, R.; Sánchez, I. and Frias, J. (1984): 'Alteración de la interfase salina por pruebas de inyección en Yucatán [Alteration of the saline interface due to injection tests in Yucatan]'. *Revista de Agua Potable*. pp. 79–84.

Villasuso, M. J. and Méndez, R. (2000): 'A conceptual model of the aquifer of the Yucatan Peninsula', in: *Lutz W., Prieto L. & Sanderson W. (Eds). Population, development, and Environment on the Yucatan Peninsula: from ancient Maya to 2030*. Research reports. Laxenburg, Austria. International Institute for Applied Systems Analysis, p. 120–139. Available at: http://pure.iiasa.ac.at/id/eprint-/6110/1/RR-00-014.pdf (accessed: 14/05/2017).

Villumsen, A.; Jacobsen, O. S. and Sonderskov, C. (1982): 'Mapping the vulnerability of groundwater reservoirs with regard to surface pollution', in: *Geological Survey of Denmark Yearbook*. Copenhagen, Denmark. Geological Survey of Denmark, p. 17–38. Available at: https://www.researchgate.net/publication/318006720 (accessed: 14/05/2016).

Vinson, G. L. (1962): 'Upper Cretaceous and tertiary stratigraphy of Guatemala', *Bulletin of the American Association of Petroleum Geologists (AAPG)*, 46(4), p. 425–456. DOI: 10.1306/BC743835-16BE-11D7-8645000102C1865D.

Vrba, J. and Zaporožec, A. (1994): *Guidebook on Mapping Groundwater Vulnerability*. Hannover, Germany. Heise, 131 p. Available at: https://agris.fao.org/agris-search/search.do?recordID=US201-300287789 (accessed: 09/10/2015).

Waltham, T. and Lu, Z. (2007): 'Natural and anthropogenic rock collapse over open caves', in: *Natural and Anthropogenic Hazards in Karst Areas: Recognition, Analysis and Mitigation*. Special Publications. London, UK. Geological Society of London, p. 13–21. DOI: 10.1144/SP279.3.

Weidie, A. E. (1985): 'Geology of Yucatan Platform', in: *Ward W. C., Weidie A. E. & Back, W. (Eds). Geology and hydrogeology of the Yucatan and Quaternary geology of northeastern Yucatan Peninsula*. New Orleans, USA. New Orleans Geological Society, p. 1–19. Available at: http://archives.-datapages.com/data/nogs/data/006/006007/0001 (accessed: 13/11/2015).

White, W. B. (2007): 'A brief history of karst hydrogeology: contributions of the NSS', *Journal of Cave and Karst Studies*, 69(1), p. 13–26. Available at: http://citeseerx.ist.psu.edu/viewdoc/summary?-doi=10.1.1.539.6022 (accessed: 03/08/2016).

White, W. B. (1988): *Geomorphology and hydrology of karst terrains*. New York, USA. Oxford University Press. 464 p. Available at: https://openlibrary.org/books/OL220588 (accessed: 02/11/2016).

Williams, P. W. (1972a): 'Morphometric analysis of polygonal karst in New Guinea', *Geological Society of America Bulletin*, 83(3), p. 761–796. DOI: 10.1130/0016-7606(1972)83%5b761.

Williams, P. W. (1972b): 'The analysis of spatial characteristics of karst terrains', in: *Chorley R. J. (Ed). Spatial analysis in geomorphology*. London, UK. Routledge, p. 135–163. DOI: 10.4324/9780429273346-5.

Williams, P. W. (2008): 'The role of the epikarst in karst and cave hydrogeology: a review', *International Journal of Speleology*, 37(1), p. 1–10. DOI: 10.5038/1827-806X.37.1.1.

Williams, P. W. (1983): 'The role of the subcutaneous zone in karst hydrology', *Journal of Hydrology*, 61(1–3), p. 45–67. DOI: 10.1016/0022-1694(83)90234-2.

Winston, R. B. (2009): *ModelMuse: a graphical user interface for MODFLOW-2005 and PHAST*. Techniques and Methods 6–A29. Reston, USA. US Geological Survey, 52 p. Available at: https://pubs.usgs.gov/tm/tm6A29/ (accessed: 16/01/2020).

Winston, R. B. (2019): *ModelMuse Version 4: A Graphical User Interface for MODFLOW 6*. Scientific Investigations Report 2019-5036. Reston, USA. US Geological Survey, 10 p. DOI: 10.3133/sir20195036.

Witkowski, A. J.; Rubin, K.; Kowalczyk, A.; Różkowski, A. and Wróbel, J. (2003): 'Groundwater vulnerability map of the Chrzanów karst-fissured Triassic aquifer (Poland)', *Environmental Geology*, 44(1), p. 59–67. DOI: 10.1007/s00254-002-0735-4.

World Health Organization (1993): *Guidelines for drinking-water quality*. 4th edition. Geneva, Switzerland. WHO Press, 541 p. Available at: https://katalog.slub-dresden.de/id/0-1612657532 (accessed: 03/08/2017).

Worthington, S. R. (2009): 'Diagnostic hydrogeologic characteristics of a karst aquifer (Kentucky, USA)', *Hydrogeology Journal*, 17(7), p. 1665-1678. DOI: 10.1007/s10040-009-0489-0.

Worthington, S. R. H. (2004): 'Hydraulic and geological factors influencing conduit flow depth', *Cave and Karst Science*, 31(3), p. 123-134. available at: https://www.researchgate.net/publication/283832-825 (accessed: 12/10/2016).

Zaporožec, A. (Ed). (1985): *Groundwater protection principles and alternatives for Rock County, Wisconsin. Special report 8*. Madison, USA. Wisconsin Geological and Natural History Survey, 73 p. Available at: https://wgnhs.wisc.edu/pubs/sr08/ (accessed: 21/09/2016).

Zhang, F.; Qi, J.; Lu, Y.; Zhang, S. and Yin, M. (2013): 'Mechanism of karst formation in sulfate rocks', *Procedia Earth and Planetary Science*, 7, p. 944–947. DOI: 10.1016/j.proeps.2013.03.148.

Zheng, C. and Wang, P. P. (1999): *MT3DMS: a modular three-dimensional multispecies transport model for simulation of advection, dispersion, and chemical reactions of contaminants in groundwater systems; documentation and user's guide*. Report SERDP-99-1. Vicksburg, USA. US Army Engineer Research and Development Center, 202 p. Available at: https://hydro.geo.ua.edu-/mt3d/index.htm (accessed: 07/04/2018).

Zwahlen, F.; Goldscheider, N. and Neale, S. (2003): 'Introduction', In: *Zwahlen, F. (Ed). COST 620 - Vulnerability and risk mapping for the protection of carbonate (karst) aquifers*. Final report. Brussels, Belgium. European Commission, Directorate-General for Research, p. 1-4. Available at: https://op.europa.eu/en/publication-detail/-/publication/be3c99bf-1a0a-4213 (accessed: 16/11/2015).

Appendix A

Rating tables of intrinsic groundwater vulnerability methods

Appendix A1

EPIK method rating tables

Epikarst (E)			Value
Karst morphology observed (pertaining to epikarst)	E1	Caves, swallow holes, dolines, karrenfields, mine-like relief, cuestas	1
	E2	Intermediate zones situated along doline alignments, uvalas, dry valleys, canyons, poljes	3
Karst morphology absent	E3	The rest of the catchment	4

Protective cover (P)		Case A *	Case B **	Value
Low protective cover	P1	0 – 20 cm of soil	Not applicable	1
	P2	20 – 100 cm of soil	20 - l00 cm of soil and low hydraulic conductivity formations	2
	P3	> 1 meter of soil	> 1 m of soil and low hydraulic conductivity formations	3
Protective cover important	P4	Not applicable	> 8 m of very low hydraulic conductivity formations or > 6 m of very low hydraulic conductivity formations with > 1 m of soil	4
* Soil overlying limestone formations or detrital formations with very high hydraulic conductivity. ** Soil overlying on > 20 cm of low hydraulic conductivity geological formations. Examples: silts, clays.				

Infiltration conditions (I)			Value
Concentrated infiltration	I1	Perennial or temporary swallow hole - banks and bed of temporary or permanent stream supplying a swallow hole, infiltrating surficial flow – areas of the water course catchment containing artificial drainage	1
	I2	Areas of a water course catchment which are not artificially drained and where the slope is greater than 10% for ploughed (cultivated) areas and greater than 25% for meadows and pastures	2
	I3	Areas of a water course catchment which are not artificially drained and where the slope is less than 10% for ploughed areas and less than 25% for meadows and pastures. Outside the catchment of a surface watercourse: bases of slopes and steep slopes (greater than 10% for ploughed areas and greater than 25% for meadows and pastures) where runoff water infiltrates	3
Diffuse infiltration	I4	The rest of the catchment	4

Karstification (K)			Value
Well-developed karst network	K1	Well-developed karst network with decimetres to meters sized conduits with little fill and well interconnected	1
Poorly developed karst network	K2	Poorly developed karst network with poorly interconnected or infilled drains or conduits, or conduits of decimetres or smaller size	2
Mixed or fissured aquifer	K3	Porous media discharge zone with a possible protective influence - fissured non-karstic aquifer	3

Appendix A2

PI method rating tables

Topsoil (T)	
eFC [mm] up to 1 m depth	*Value*
> 250	750
> 200-250	500
> 140-200	250
> 90-140	125
> 50-90	50
0-50	10

Recharge (R)	
Recharge [mm/y]	*Value*
0-100	1.75
>100-200	1.50
>200-300	1.25
>300-400	1.00
>400	0.75

Soil (s)			
Type of subsoil (grain size distribution)	*Value*	*Type of subsoil (grain size distribution)*	*Value*
Clay	500	Very clayey sand, clayey sand, loamy silty sand	140
Loamy clay, slightly silty clay	400		
Slightly sandy clay	350	Sandy silt, very loamy sand	120
Silty clay, clayey silty loam	320	Loamy sand, very silty sand	90
Clayey loam	300	Slightly clayey sand, silty sand, sandy clayey gravel	75
Very silty clay, sandy clay	270		
Very loamy silt	250	Slightly loamy sand, sandy silty gravel	60
Slightly clayey loam, clayey silty loam	240	Slightly silty sand, slightly silty sand with gravel	50
Very clayey silt, silty loam	220	Sand	25
Very sandy clay, sandy silty loam, slightly sandy loam, loamy silt, clayey silt	200	Sand with gravel, sandy gravel	10
		Gravel, gravel with breccia	5
Sandy loam, slightly loamy silt	180	Non-lithified volcanic material (pyroclastic)	200
Slightly clayey silt, sandy loamy silt, silt, very sandy loam	160	Peat	400
		Sapropel	300

Lithology (L) and fracturing (F)			
Lithology	Value	Fracturing	Value
Claystone, slate, marl, siltstone	20	Non-jointed	25
Sandstone, quartzite, volcanic rock, plutonite, metamorphite	15	Slightly jointed	4
Porous sandstone, porous volcanic rock (e.g., tuff)	10	Moderately jointed, slightly karstified or karst features completely sealed	1
Conglomerate, breccia, limestone, dolomitic rock, gypsum rock	5	Moderately karstic or karst features mostly sealed	0.5
		Strongly fractured or strongly karstified and not sealed	0.3
		Epikarst strongly developed, not sealed	0
		Not known	1

PI method rating tables (continue)

I.- Determination of soil properties for the I factor			
Saturated hydraulic conductivity (m/s)	Depth to low permeable layer		
	< 30 cm	30 - 100 cm	> 100 cm
> 10^{-4}	Type D	Type C	Type A
10^{-5}-10^{-4}		Type B	
10^{-6}-10^{-5}	Type E		
< 10^{-6}	Type F		

II.- Determination of the slope and vegetation conditions for the I factor							
Land use: Forest				Land use: Field/Meadow/Pasture			
Soil properties	Slope			Soil properties	Slope		
	< 3.5 %	3.5 - 27 %	> 27 %		< 3.5 %	3.5 - 27 %	> 27 %
Type A	1.0	1.0	1.0	Type A	1.0	1.0	0.8
Type B	1.0	0.8	0.6	Type B	1.0	0.6	0.4
Type C	1.0	0.6	0.4	Type C	1.0	0.4	0.2
Type D	0.8	0.6	0.4	Type D	0.6	0.4	0.2
Type E	1.0	0.6	0.4	Type E	0.8	0.4	0.2
Type F	0.4	0.4	0.2	Type F	0.6	0.2	0.0

III.- Determination of the I factor						
Surface Catchment Map	Values from II					
	0	0.2	0.4	0.6	0.8	1
Swallow hole, sinking stream, 10 m buffer	0.0	0.0	0.0	0.0	0.0	0.0
Swallow hole, sinking stream 100 m buffer	0.0	0.2	0.4	0.6	0.8	1
Catchment of sinking stream	0.2	0.4	0.6	0.8	1	1
Rest of the area	0.4	0.6	0.8	1	1	1

Appendix A3

COP method rating tables

Overlying soils (Os)				
Soil thickness	Soil texture			
	Clay	*Silt*	*Loam*	*Sand*
> 1 metre	5	4	3	2
0.51 – 1 metre	4	3	2	1
< 0.5 metres	3	2	1	0

Soil texture classification	
Clay	> 30% clay
Silt	> 70% silt
Sand	> 70% sand and ≤ 15% clay
Loam	Rest

Layer index (ΣLy · m)	Value
0-250	1
251-1000	2
1001-2500	3
2501-10000	4
> 10000	5

Lithology and fracturing (Ly)	Value
Clays	1500
Silts	1200
Marls, non-fissured metapelites and igneous rocks	1000
Marly limestones	500
Fissured metapelites and igneous rocks	400
Cemented or non-fissured conglomerates and breccias	100
Sandstones	50
Scarcely cemented or fissured conglomerates and breccias	40
Sands and gravels	10
Permeable basalts	5
Fissured carbonate rocks	3
Karstic rocks	1

Confined condition (Cn)	Value
Confined	2
Semi-confined	1.5
Not confined	1

O Factor	Protection
1	Very low
2	Low
2.1-4	Moderate
4.1-8	High
8.1-15	Very high

Slope & vegetation, Scenario 1 (Sv1)		
Slope (%)	Vegetation	Value
≤ 8	---	1
8.1-31	Yes	0.95
	No	0.9
31.1-76	Yes	0.85
	No	0.8
> 76	---	0.75

Slope & vegetation, Scenario 2 (Sv2)		
Slope (%)	Vegetation	Value
≤ 8	---	0.75
8.1-31	Yes	0.8
	No	0.85
31.1-76	Yes	0.9
	No	0.95
> 76	---	1

COP method rating tables (continue)

Distance to swallow hole in meters (Dh)	Value
≤ 500	0
501-1000	0.1
1001-1500	0.2
1501-2000	0.3
2001-2500	0.4
2501-3000	0.5
3001-3500	0.6
3501-4000	0.7
4001-4500	0.8
4501-5000	0.9
> 5000	1

Surface features (Sf)			
Karst features	Surface conditions		
	Absence	Permeable	Impermeable
Developed karst	0.25	0.5	0.75
Scarcely developed or dissolution features	0.5	0.75	1
Fissured karst	0.75	0.75	1
Absence of karst features	1	1	1

Distance to sinking streams (Ds)	Value
< 10	0
11-100	0.5
> 100	1

C Factor	Protection
0 - 0.2	Very low
0.3 – 0.4	Low
0.5 – 0.6	Moderate
0.7 – 0.8	High
0.8 - 1	Very high

Precipitation in mm/y (Pq)	Value
> 1600	0.4
1201 - 1600	0.3
801 - 1200	0.2
400 - 800	0.3
≤ 400	0.4

Precipitation intensity in mm/day (Pi)	Value
≤ 10	0.6
10 - 20	0.4
> 20	0.2

P Factor	Protection
0.4 – 0.5	Very low
0.6	Low
0.7	Moderate
0.8	High
0.9 - 1	Very high

Appendix A4

PaPRIKa method rating tables

Sinking stream catchment area (Ca)	
Characteristics	Value
Highly permeable formations: sand, gravels	1
Moderately permeable formations: altered granites, karst limestones	2
Low permeability formations: sandstone, conglomerates, magmatic and metamorphic rocks	3
Very low permeability formations: marls and clays. Areas around temporary streams	4

Soil texture and gravel content			
Gravel content (%)	Clays	Loams	Sand
0 - 15	S1	S1	S2
16 - 60	S1	S2	S3
> 60	S2	S3	S3

Soil (S)				
Soil thickness in centimetres	Soil texture and gravel content			
	Unknown	S1	S2	S3
> 500	1	1	1	2
100 - 500	1	1	2	3
60 - 99	2	2	3	4
30 - 59	3	3	4	4
0 - 29	4	4	4	4
Note: For impervious formations a value of zero is assigned				

Lithology	
Characteristics	Value
Thick layers of clay	1
Clay, marl, marly limestone (25–35% of clay minerals)	2
Marly limestone (10–25% of clay minerals), limestone in small blocks	3
Massive limestone and dolomite	4

Unsaturated zone lithology, fracturing and thickness (UZ)			
Fracturing	Unsaturated zone thickness in meters		
	< 15	16 – 60	> 60
Low to moderate	Lithology value + 1	Lithology value	Lithology value
Significant	Lithology value + 1	Lithology value + 1	Lithology value
Tectonic faults	4	4	4

Epikarst (E)	
Characteristics	Value
Perched aquifer, with productive boreholes and high piezometric level	1
Epikarstic aquifer, laterally continuous with temporary springs characterized by a flow rate of about 1 l/s or more, capacitive function verified	2
Epikarstic aquifer with perched springs of low flow rate and limited lateral continuity; limited delay effect	3
No epikarst	4

PaPRIKa method rating tables (continue)

Rock reservoir (R)	
Characteristics	Value
Low influence on vulnerability*: marly limestones (25–35% of clay minerals) and chalk with a low fracturing degree	1
Moderate influence on vulnerability: marly limestones (10–25% of clay minerals), highly fractured chalk, limestones and dolomites affected by homogeneous fracturing, limestones	2
High influence on vulnerability: karstic and fractured massive limestones/dolomites, thick layers of limestones/dolomites with a dip higher than 45° enhancing flow towards the spring	3
Very high influence on vulnerability*: karstic networks (drains and cavities) that are well known, fault zones when playing a role in the underground flow	4
* Low influence on vulnerability means that this index will convey protection of the resource.	

Infiltration conditions (I)	
Characteristics	Value
Slopes higher than 50% inducing major runoff and a negligible infiltration	0
High slopes (15–50%) in favour of runoff	1
Moderate slopes (5–15%) + areas where the runoff is limited in carbonate terrains (dry valleys, karrenfields)	2
Low slopes (0–5%) where infiltration dominates the runoff + dolines and poljes + karrenfields with high vertical development (cracks of meter size)	3
Swallow holes and sinkholes with concentrated infiltration because of stream losses + their catchment areas	4

Karstification degree (Ka)	
Characteristics	Value
Catchments <10 km^2 with low mean annual discharge where the karst system is characterized by a low functionality behaviour (low variability of hydrograph and chemographs); absence of indications of fast groundwater flow	0
Catchments >10 km^2 without water losses, having low functional behaviour or a limited catchment around a borehole intercepting fissured media + complex karst systems such as classified by Mangin	1
Catchments >10 km^2 or limited catchment around a borehole intercepting fissured media. Karst systems with high level of functionality which do not present water losses; or karst systems with low level of functionality which present water losses. The underground drainage network is well developed with a presence of a moderate network connected to the surface. Fast transit velocity demonstrated with tracer tests (50–100 m/h). Domain 2 of Mangin's classification	2
Catchments < or > 10 km^2+karst systems with water losses. Underground drainage network very well developed with the presence of large conduits connected to the surface. High level of functionality. Very fast transit velocities demonstrated with tracing tests (> 100 m/h). Domains 3 or 4 of Mangin's classification	3

Appendix A5

DRISTPi method rating tables

Depth to groundwater (D)		
Scenario 1 (karst)	Scenario 2 (non-karst)	Value
≤ 5	≤ 1.5	10
5.1 - 15	1.6 - 5	9
15.1 - 30	5.1 - 10	7
30.1 - 50	10.1 – 16.6	5
50.1 - 75	16.6 - 25	3
75.1 - 100	25.1 – 33.3	2
> 100	> 33.3	1
Depth in metres		

Recharge (R)	
mm/y	Value
≤ 20	1
21 - 50	2
50 - 100	4
101 - 150	6
151 - 200	7
201 - 250	8
251 - 300	9
> 300	10

Impact of the vadose zone (I)	
Lithology	Value
Silt or clay	1
Shale	3
Limestone	6
Sandstone	6
Bedded limestone, sandstone or shale	6
Sand and gravel with significant content of silt and clay	6
Metamorphic or igneous rock	4
Sand or gravel	8
Basalt	9
Karst limestone	10

Soil media (S)	
Texture	Value
Thin or absent	10
Gravel	10
Sand	9
Peat	8
Shrinking or aggregated clay	7
Sandy loam	6
Loam	5
Silty loam	4
Clay loam	3
Muck	2
Non-shrinking or non-aggregated clay	1

Topography as slope percentage (T)	
Slope	Value
≤ 2	10
3 - 6	9
7 - 12	5
13 - 18	3
> 18	1

Preferential infiltration (Pi)		
Scenario	Characteristics	Value
Scenario 1 karstic landforms	Swallow hole, doline, polje, lapiaz	10
	River	10
	Artificial quarry	9
	Canyon, gorge, narrow pass	7
Scenario 1 non-karstic landforms	Swallow hole recharge area	10
	High fissured zone	6
	Low fissured zone	3
	Rest of the area	1
Scenario 2, infiltration zones	Swallow hole recharge area	10
	River, lake	10
	Artificial quarry	7
	Lagoon	5

Appendix A6

KARSTIC method rating tables

Karstification (K)	
Karstification development	Value
Major sinkhole losses	10
Minor sinkhole losses	5
No visible sinkhole losses	1

Aquifer media (A)	
Rock type	Value
Massive shale	2
Metamorphic/igneous	3
Weathered metamorphic/igneous	4
Glacial till	5
Bedded sandstone, limestone and shale	6
Massive sandstone	6
Massive limestone	6
Sand and gravel	8
Basalt	9
Karst limestone	10
Massive gypsum with karst development	10
Interbedded gypsum and shale (no karst)	5

Fissuring (F)	
Fissuring development	Value
Major fissures and structure	5
Minor fissures and structure	3
No significant development	1

Recharge (R)	
mm/y	Value
≤ 50	1
51 - 101	3
102 - 178	6
179 - 254	8
> 254	9

Soil media (S)	
Texture	Value
Thin or absent	10
Gravel	10
Sand	9
Peat	8
Shrinking or aggregated clay	7
Sandy loam	6
Loam	5
Silty loam	4
Clay loam	3
Muck	2
Non-shrinking or non-aggregated clay	1

Topography as slope percentage (T)	
Slope	Value
≤ 2	10
3 - 6	9
7 - 12	5
13 - 18	3
> 18	1

Depth to groundwater (D)	
Depth (m)	Value
≤ 65	5
65.1 - 164	3
164.1 - 328	1.5
> 328	0.5

Impact of the vadose zone (I)	
Lithology	Value
Confining layer	0.5
Silt or clay	1.5
Shale	1.5
Limestone	3
Sandstone	3
Bedded limestone, sandstone or shale	3
Metamorphic or igneous rock	2
Sand or gravel	4
Basalt	4.5
Karst limestone	5
Massive Gypsum with karst development	5
Interbedded Gypsum without karst development	2.5

Appendix A7

RISKE method rating tables

Rock reservoir (R)	
Characteristics	Value
Marls	0
Calcareous marl	1
Marly limestone	2
Massive limestones and dolomite in large unfractured banks; limestones in small banks with homogeneous fracturing	3
Limestone in massive fractured benches	4

Infiltration condition as slope (I)	
Characteristics	Value
Very steep slope (> 50%)	0
Steep slope (from 15% to 50%)	1
Average slope (from 5% to 15%)	2
Low slopes (< 15%); cultivates zones (furrows) perpendicular to the slope	3
Catchment area feeding a swallow hole	4

Soil texture and gravel content			
Gravel content (%)	Clays	Loams	Sand
0 - 15	S1	S1	S2
16 - 60	S1	S2	S3
> 60	S2	S3	S3

Soil protective cover (S)								
Over geology with high hydraulic conductivity				Over geology with low hydraulic conductivity				Value
Soil type				Soil type				
Unknown	S1	S2	S3	Unknown	S1	S2	S3	
---	---	---	---	Geology > 5 metres (with or without soil cover)				0
depth > 100 cm	depth > 100 cm	---	---	Geology < 5 meters or > 1meter with soil (unknown or type 1) > 20cm				1
depth 20 – 100 cm	depth 20 – 100 cm	depth > 100 cm	---	depth < 20 cm	depth < 20 cm	depth < 20 cm		2
depth 0 – 20 cm	depth 0 – 20 cm	depth 20 – 100 cm	depth > 100 cm	Absent soil	Absent soil	depth < 20 cm	depth 20 – 100 cm	3
Absent soil	Absent soil	depth 0 – 20 cm	depth 0 – 20 cm	---	---	---	---	4

Karstification condition (K)	
Characteristics	Value
Low fracturing or unfractured aquifer	0
Not karstified fractured aquifer	1
Roughly karstified network or bad connection with the surface	2
Well-developed network; presence of a small collecting drain (or presumed big) connected with the surface	3
Well-developed network; presence of a big collector connected with the surface	4

Epikarst development (E)	
Characteristics	Value
Zone without identified karstic morphology	0
Zone without a net karstic morphology	1
Lapiaz (karrenfields), dry valleys + feeding catchment	2
Dolines and uvalas	3
Avens (swallow holes)	4

Appendix A8

SA rating tables

Overlying soils (Os)		
Soil thickness	*Soil texture*	
	Loamy/silty	*Clayey/sandy*
> 1 meter	5	5
0.51 – 1 meter	3	2
0.2 - 0.5 meters	1	0
< 0.2 meters	0	0

Lithology and fracturing (Ly)	Value
Clays	1500
Silts	1200
Marls, non-fissured metapelites and igneous rocks	1000
Marly limestones	500
Fissured metapelites and igneous rocks	400
Cemented or non-fissured conglomerates and breccias	100
Sandstones	60
Scarcely cemented or fissured conglomerates and breccias	40
Sands and gravels	10
Permeable basalts	5
Fissured carbonate rocks	3
Karstic rocks	1
Extremely karstified areas	0.2

Layer index ($\Sigma Ly \cdot m$)	Value
0-250	1
251-1000	2
1001-2500	3
2501-10000	4
> 10000	5

Confined condition (Cn)	Value
Confined	2
Semi-confined	1.5
Not confined	1

O Factor	Protection
1	Very low
2	Low
2.1-4	Moderate
4.1-8	High
8.1-15	Very high

Distance to swallow hole in meters (Dh)	Value
≤ 10	0
11-100	0.2
101-500	0.4
501-1000	0.6
1001-5000	0.8
> 5000	1

Distance to sinking streams in meters (Ds)	Value
≤ 10	0
11-100	0.5
> 100	0.75

Slope & vegetation (Sv)				
Slope (%)	Vegetation cover			
	Impermeable surface		Permeable surface	
	Less dense	Dense	Less dense	Dense
≤ 8	0.7	0.8	1	1
8.1-31	0.6	0.7	0.95	1
> 31	0.5	0.6	0.9	0.95

SA rating tables (continue)

Surface features (Sf)			
Karstic features	Subsoil layers		
	Absence	*Permeable*	*Impermeable*
Developed karst features	0.25	0.5	0.75
Scarcely developed or dissolution features	0.5	0.75	1
Fissured karst	0.75	0.75	1
Absence of karstic features	1	1	1

C Factor	Protection
0 - 0.2	Very low
0.3 – 0.4	Low
0.5 – 0.6	Moderate
0.7 – 0.8	High
0.8 - 1	Very high

Rainy days (Rd) with average intensity ranging from 20 to 80 mm/day	Value
≤ 10	1
11 - 20	0.9
20 – 50	0.8
> 50	0.6

Storm events (Pi) with average intensity > 80 mm/day	Value
1	1
2 - 5	0.8
> 5	0.6

P Factor	Protection
0.36 – 0.5	Very low
0.51 – 0.6	Low
0.61 - 0.7	Moderate
0.71 - 0.8	High
0.81 - 1	Very high

Appendix B

Map layers for groundwater vulnerability methods

Appendix B1

The EPIK method
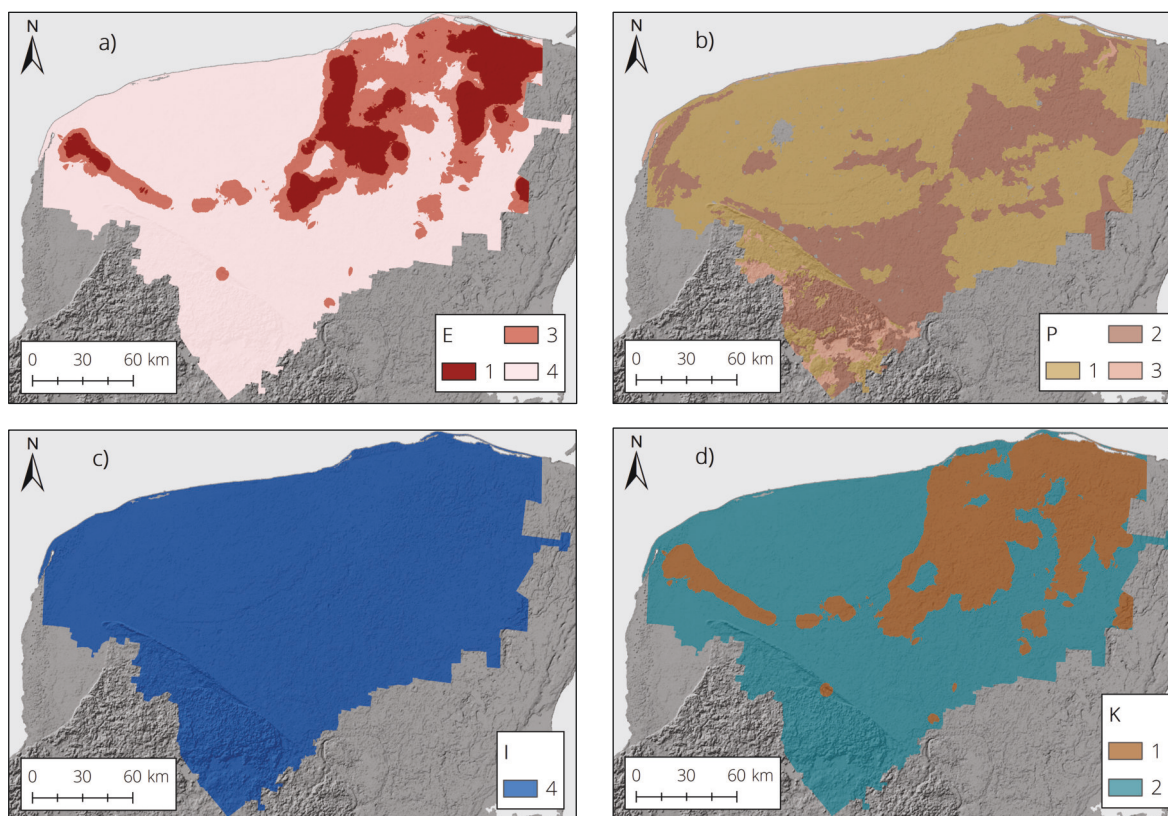
Figure B1: The EPIK method's map layers and attibutes rating. In a), epikarst (E); in b), protective cover by soil thickness (P); in c), infiltration conditions by slope and vegetation (I); in d), karstification by surface features (K).
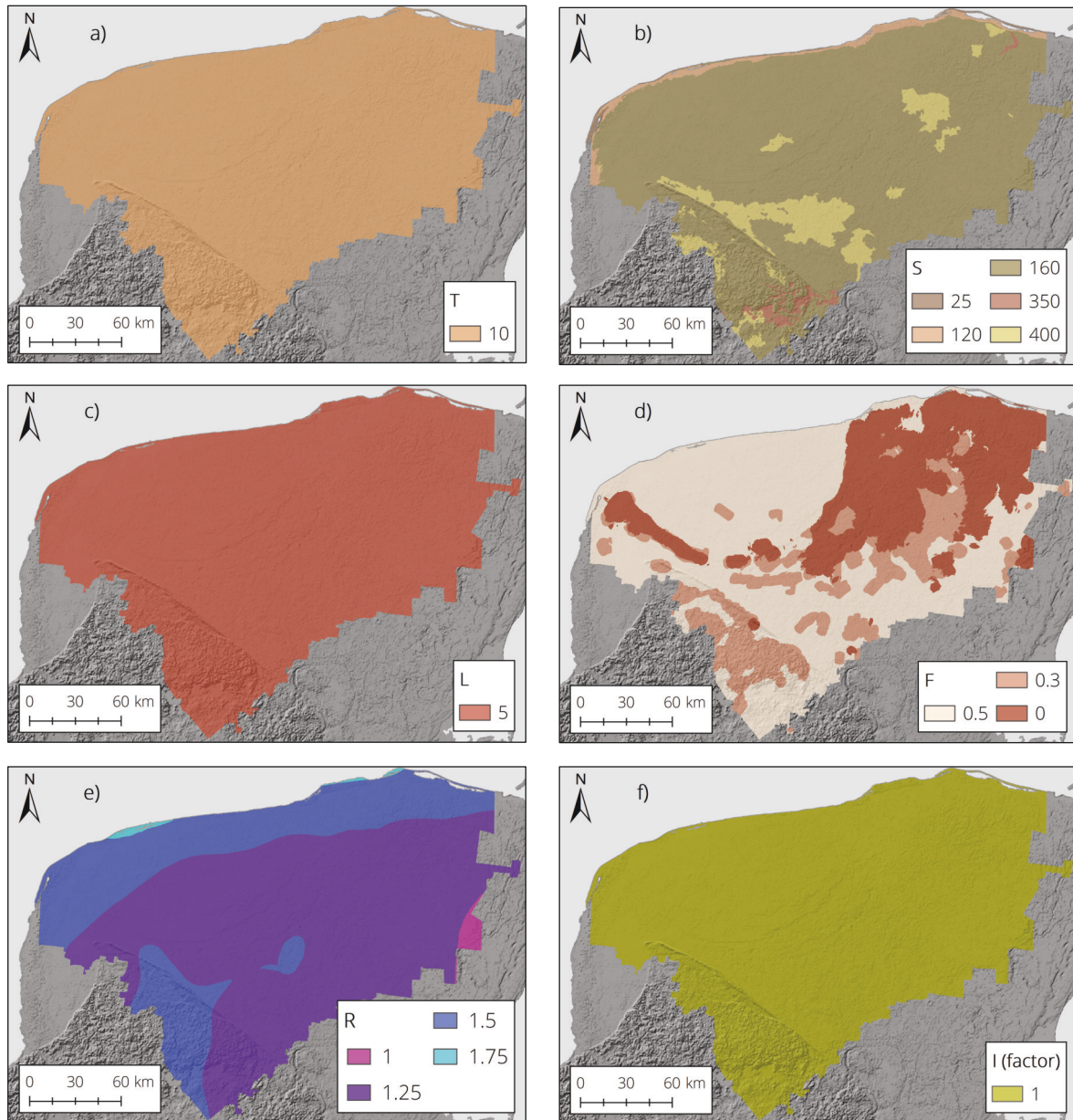
Appendix B2

The PI method

Figure B2: The PI method's map layers and attributes rating. In a), topsoil by its eFC (T); in b), soils by texture and thickness (S); in c), lithology (L); in d), fracturing (F); in e), recharge (R); in f), the infiltration factor (I).

Appendix B3

The COP method
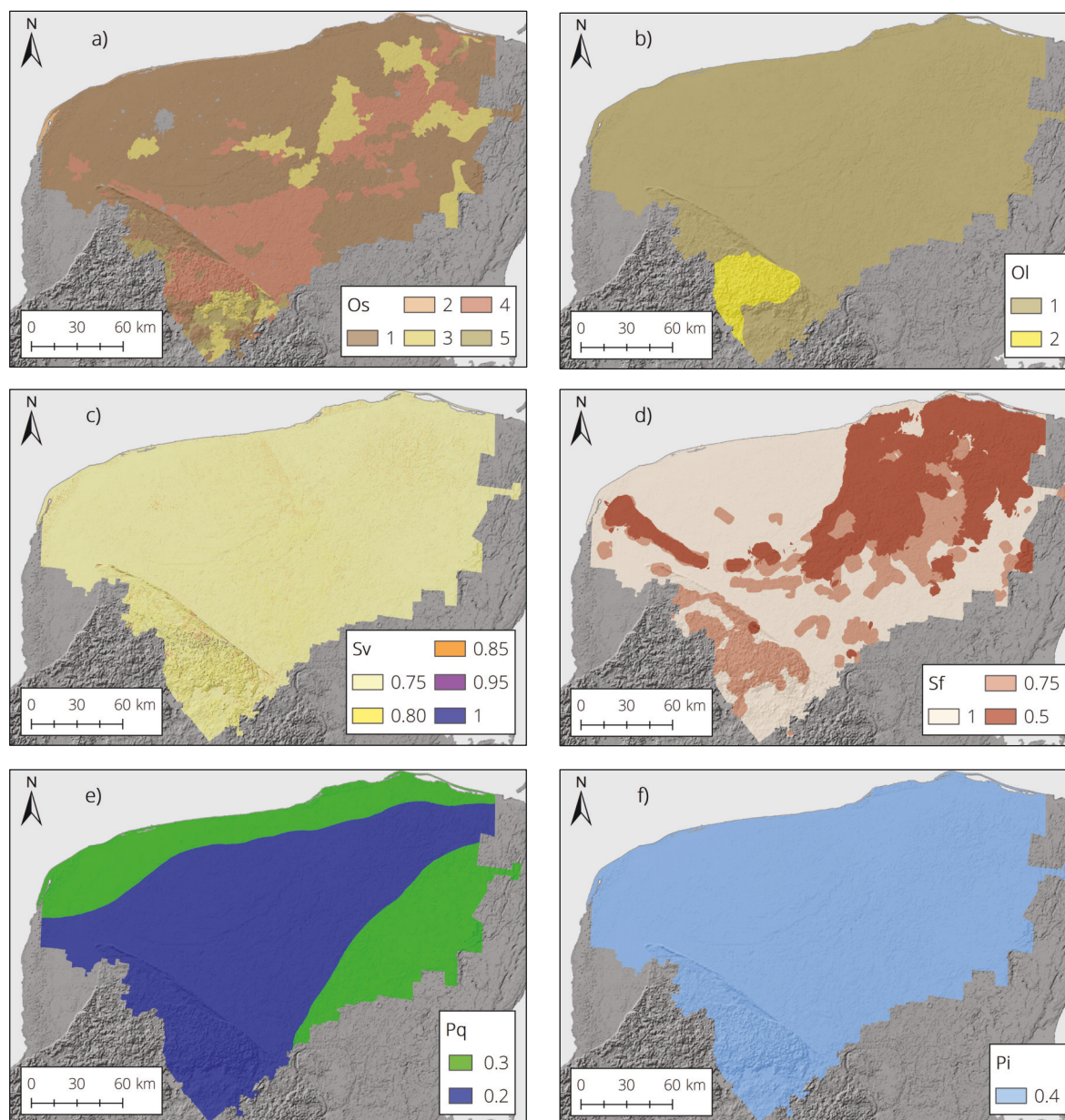
Figure B3: The COP method's map layers and attributes rating. In a), overlying soils by texture and thickness (Os); in b), overlying lithology and thickness (Ol); in c), slope and vegetation for scenario 2 (Sv); in d), surface features (Sf); in e), precipitation volume (Pv); in f), precipitation intensity (Pi).

Appendix B4

The PaPRIKA method
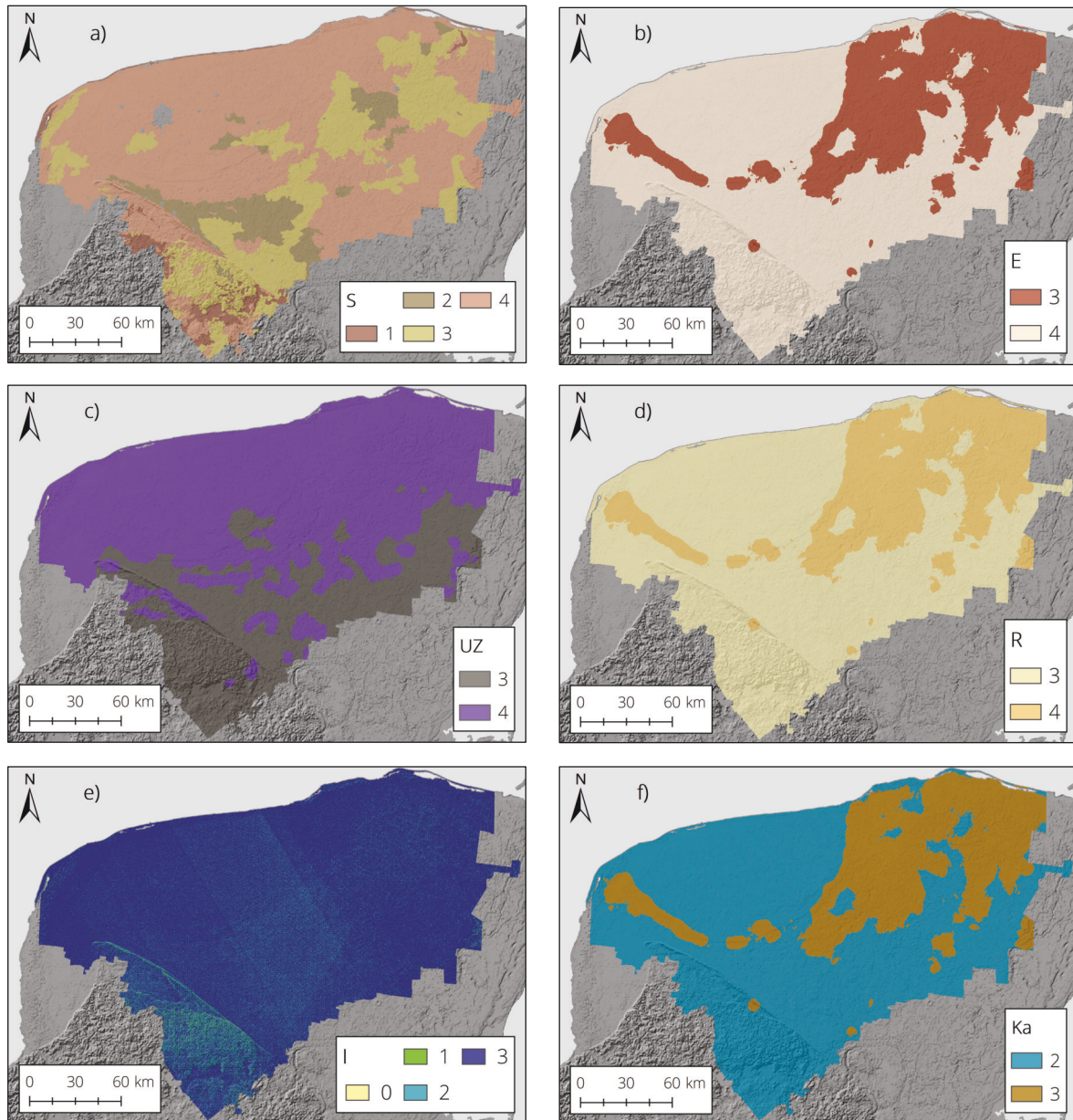
Figure B4. The PaPRIKa method's map layers and attributes rating. In a), soils by texture and thickness (S); in b), epikarst probability by surface features (E); in c), unsaturated zone by lithology, thickness, and fracturing (UZ); in d), rock reservoir (R); in e), infiltration by slope (I); in f), karstification (Ka).
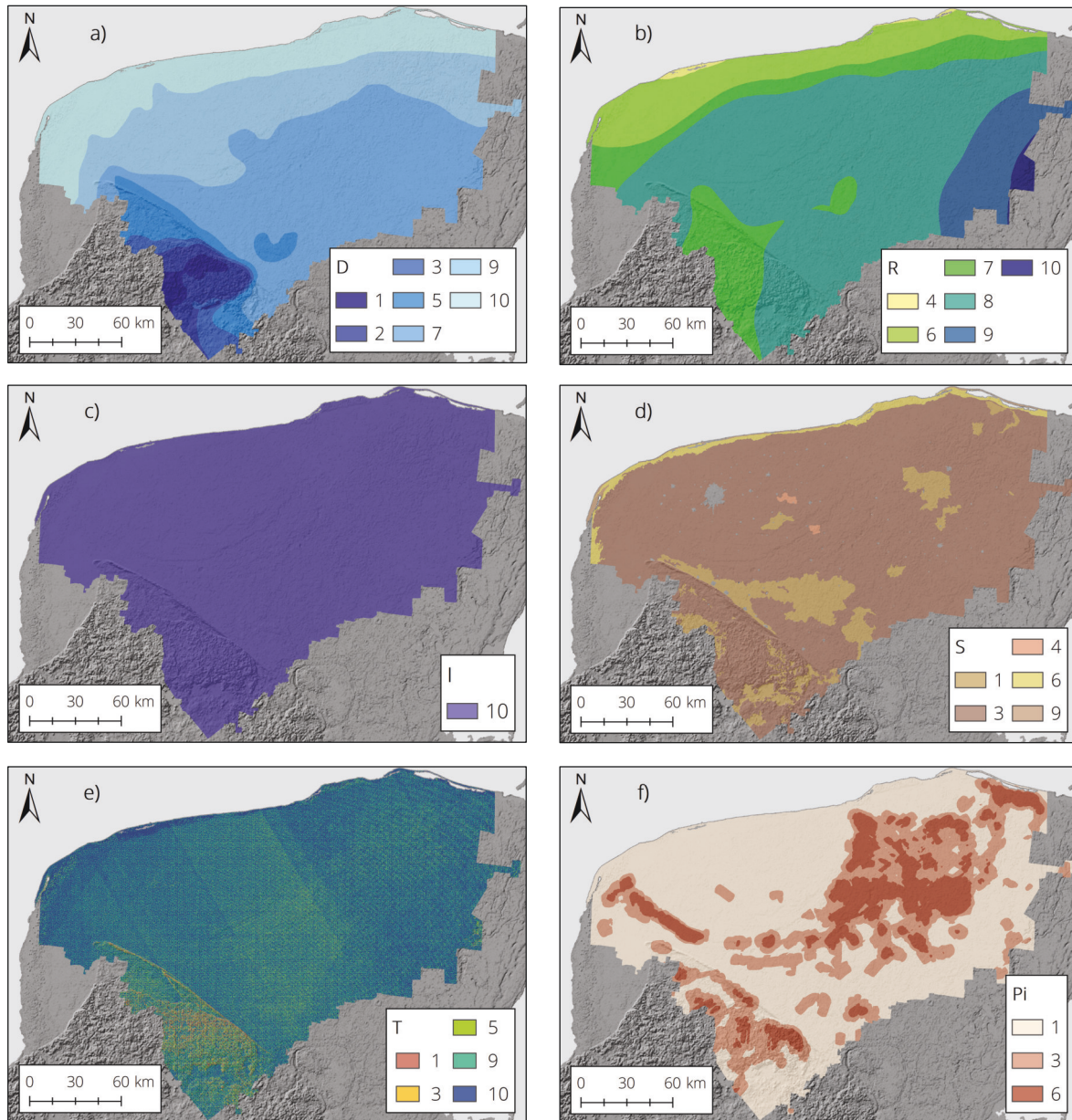
Appendix B5

The DRISTPi method

Figure B5: The DRISTPi method's map layers and attributes rating. In a), depth to groundwater (D); in b), recharge (R); in c), impact of the vadose zone by lithology (I); in d), soils by texture (S); in e), topography by slope (T); in f), preferential infiltration by fissuring (Pi).
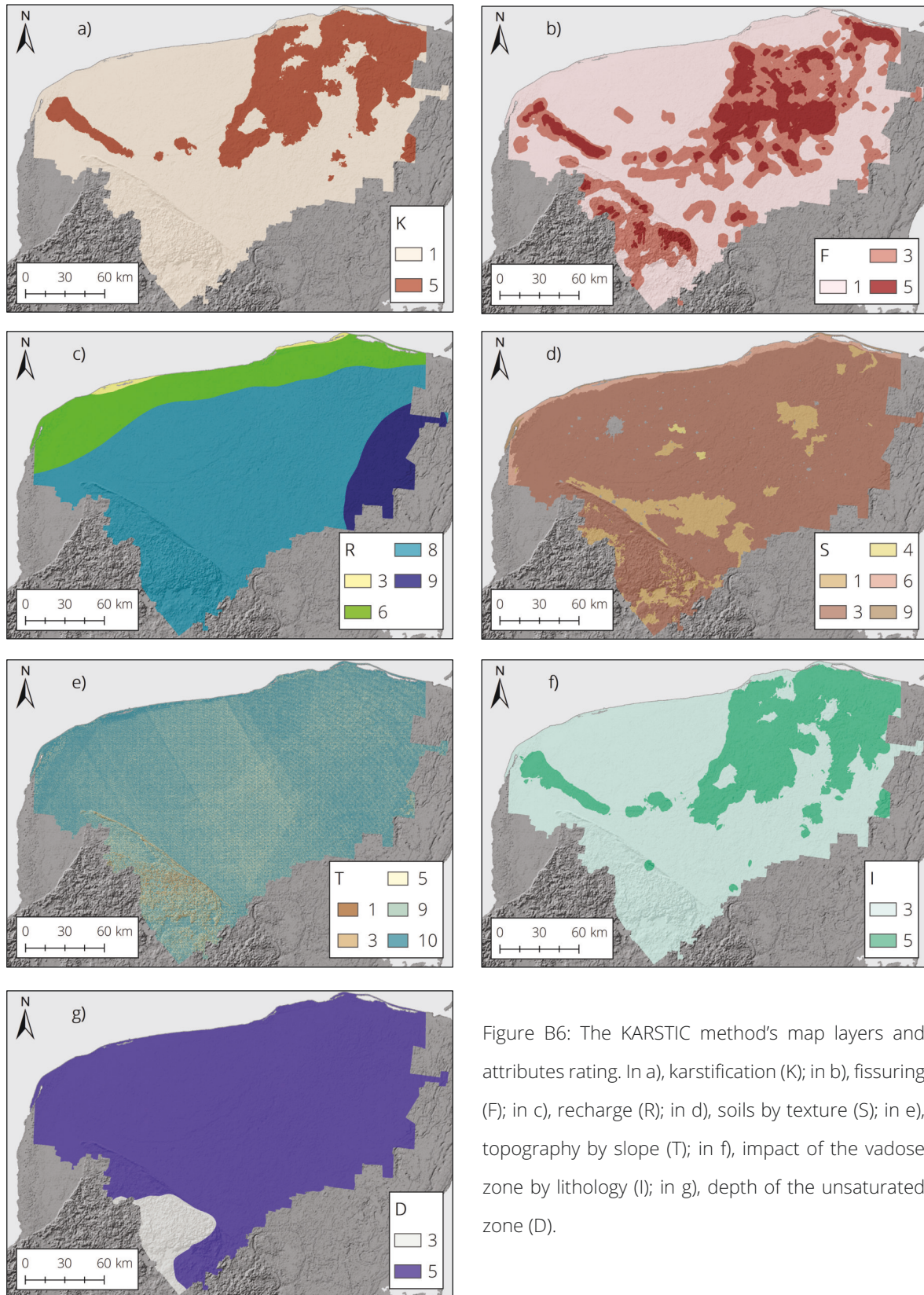
Appendix B6

The KARSTIC method

Figure B6: The KARSTIC method's map layers and attributes rating. In a), karstification (K); in b), fissuring (F); in c), recharge (R); in d), soils by texture (S); in e), topography by slope (T); in f), impact of the vadose zone by lithology (I); in g), depth of the unsaturated zone (D).
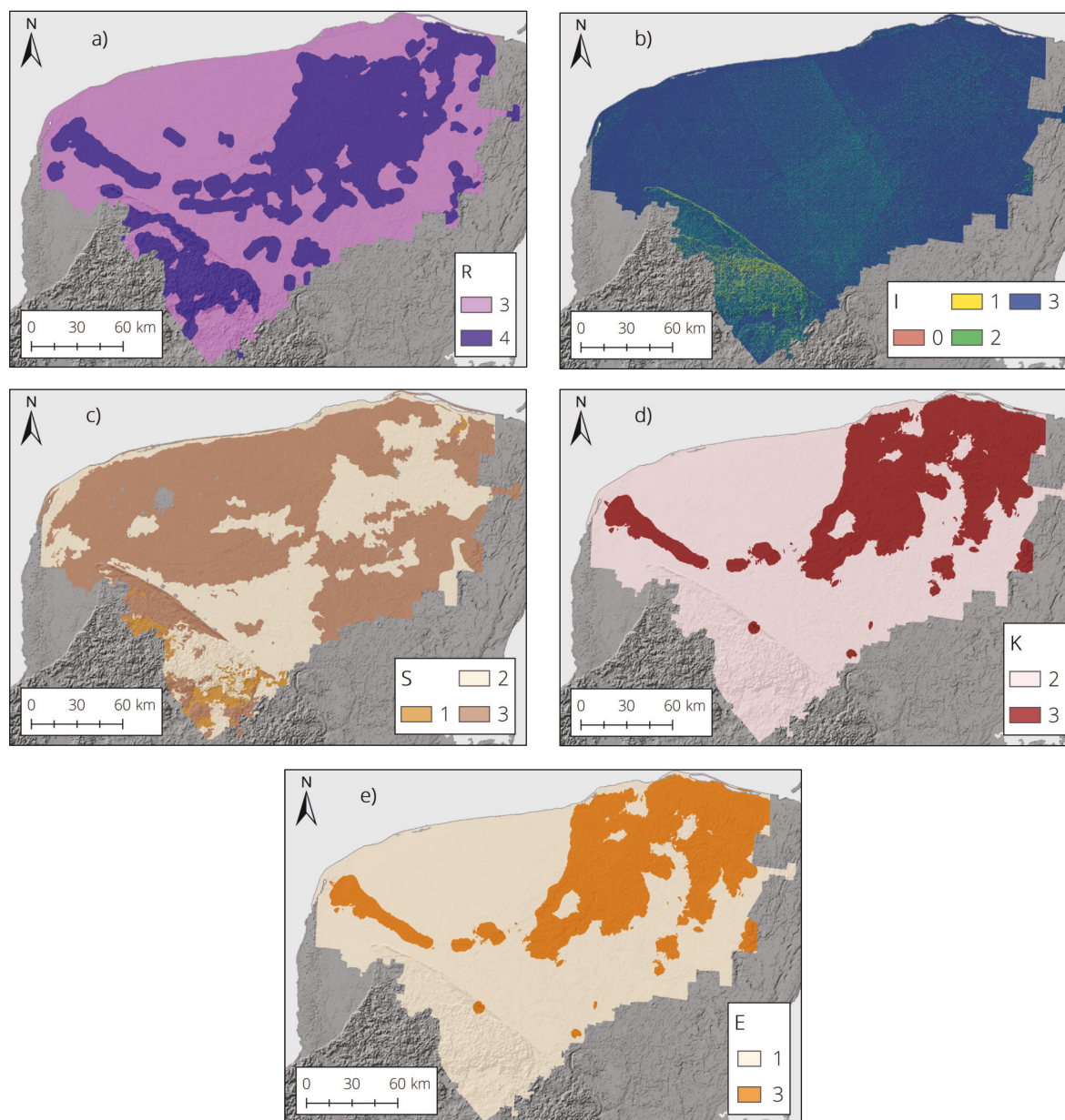
Appendix B7

The RISKE method

Figure B7: The RISKE method's map layers and attributes rating. In a), rocks by lithology and fissuring (R); in b), infiltration by slope (I); in c), soils by texture (S); in d), karstification (K); in e), epikarst (E).
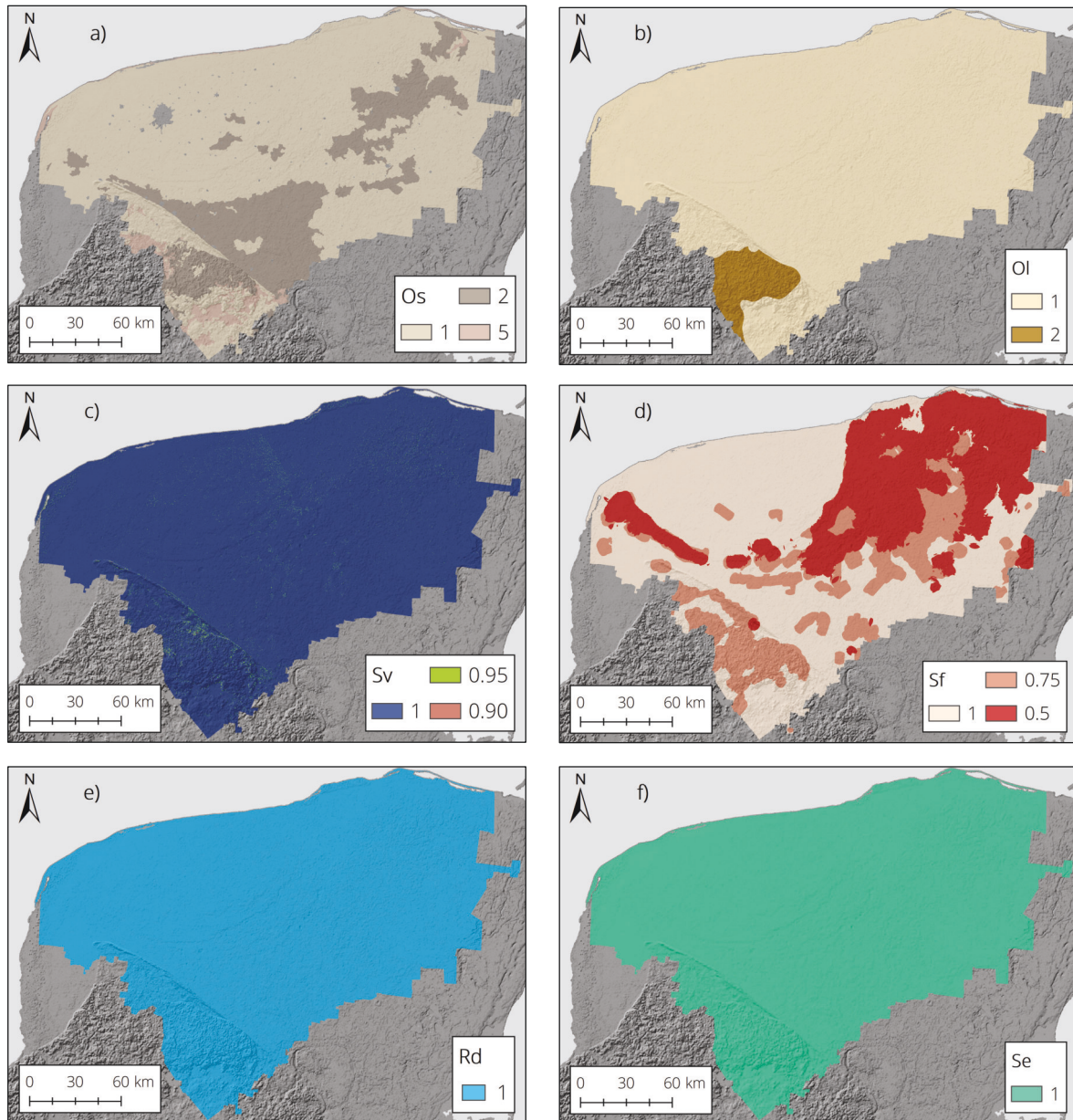
Appendix B8

The SA

Figure B8: The SA map layers and attributes rating. In a), overlying soils by texture and thickness (Os); in b), overlying lithology (Ol); in c), slope and vegetation (Sv); in d), surface karst features (Sf); in e), rainy days (Rd); in f), storm events (Se).
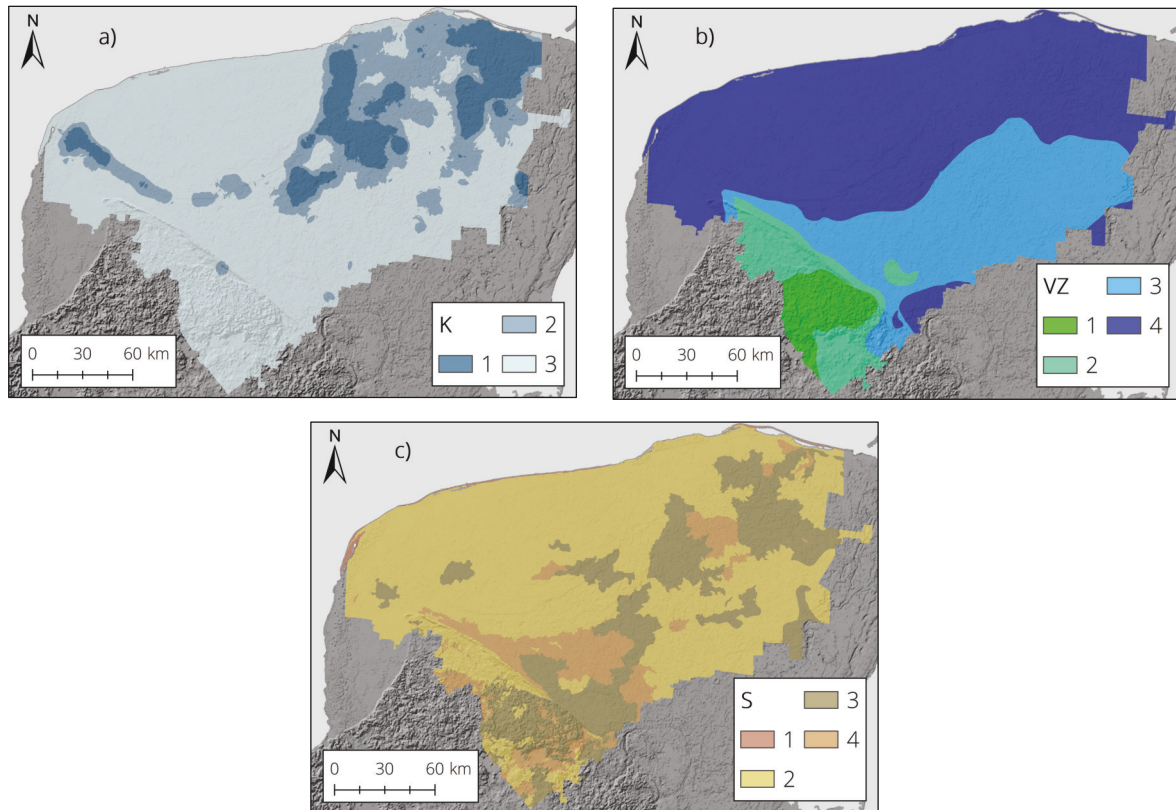
Appendix B9

The IKAV-P

Figure B9: The IKAV-P map layers and attributes rating. In a), karstification by doline density (K); in b), vadose zone by depth to groundwater (VZ); in c), soils by clay content (S).

Appendix C

List of publications

Appendix C1

List of publications

- **Moreno-Gómez, M.**; Martínez-Salvador, C., Moulahoum, A-W., Liedl, R., Stefan, C. & Pacheco, J. (2019) "First Steps into an Integrated Karst Aquifer Vulnerability Approach (IKAV). Intrinsic Groundwater Vulnerability Analysis of the Yucatan Karst, Mexico". Water 2019, 11, 1610. https://doi.org/10.3390/w11081610.

- Martínez-Salvador, C.; **Moreno-Gómez, M**. & Liedl, R. (2019) "Estimating Pollutant Residence Time and NO_3^- Concentrations in the Yucatan Karst Aquifer. Considerations for an Integrated Karst Aquifer Vulnerability Methodology". Water 2019, 11, 1431. https://doi.org/10.3390/w11071431.

- **Moreno-Gómez, M**.; Liedl, R. & Stefan, C. (2019) "A New GIS-Based Model for Karst Dolines Mapping Using LiDAR; Application of a Multi-depth Threshold Approach in the Yucatan Karst, Mexico". Remote Sensing. 2019, 11, 1147. https://doi.org/10.3390/rs11101147.

- **Moreno-Gómez, M**., Pacheco, J., Stefan, C. & Liedl, R. (2018) "Evaluating the applicability of European karst vulnerability assessment methods to the Yucatan karst, Mexico" Environmental Earth Sciences (2018) 77: 682. https://doi.org/10.1007/s12665-018-7869-5.

Appendix C2

List of conference proceedings (only first author)

- **Moreno-Gómez, M**., Pacheco, J., Stefan, C. & Liedl, R. (2017). "Evaluation and congruence of European karst vulnerability methodologies from their application on the Yucatan Karst, Mexico". Presentation at international Scientific meeting "Man and Karst". Zadar, Croatia, June 26-29, 2017.

- **Moreno-Gómez, M**., Stefan, C. & Liedl, R. (2016). "Characterization of the Yucatan karst aquifer: intrinsic vulnerability scenarios and possible solutions". Poster presented at 9th International Symposium on Managed Aquifer Recharge. Mexico City, Mexico, June 20-24, 2016.